

Extension of the Reference atmospheres and Vibrational Temperatures (WP9220)

Support to MIPAS Level 2 product validation (MIPAS L2).

ESA ESRIN Contract No 21719/08/I-OL

M. López-Puertas, Bernd Funke, Maya García-Comas, Diego Bermejo
(Instituto de Astrofísica de Andalucía, Granada, Spain)

Martin Kaufmann
(FZ Jülich, Jülich, Germany)

Anu Dudhia
(Oxford University, UK)

Issue 2.0
6th November 2009

Abstract

We report here on the description of the extension of the abundances (vmr) of the IG profiles above 60 km and on the vibrational temperatures calculated for the update of the evaluation of the non-LTE errors spectra. This is the first part of the study. With these vibrational temperatures, non-LTE spectra will be calculated and non-LTE errors will then be derived.

The major findings can be summarized as:

- CO₂, O₃, and NO₂(00v₃) vibrational temperatures have changed significantly, although not for all levels.
 - CO: small (but significant) changes in vibrational temperatures and in the spectra.
 - H₂O-CH₄ vibrational temperatures show some minor changes (although the rates for the involved processes have changed significantly).
 - CH₄ high-energy levels have largely changed (due to more accurate radiative transfer) but limited to the non-LTE region. We expect small changes in the spectra.
 - N₂O and HNO₃ VTs have significantly changed because of the more accurate radiative transfer but limited to the non-LTE region (at high altitudes). We expect small changes in the spectra.
 - NO exhibits very small changes.
 - OH also exhibits very small changes, only those introduced by the IG O₃ and H profiles.
 - A new model has been developed for HCN. The predicted non-LTE effects for the (010-000) band, used for HCN retrieval, below 80 km is negligible. The higher energy levels exhibit large deviations from LTE during illuminated conditions but do not have any impact on the HCN retrieval and the effects on the spectra are expected to be very small.

Contents

1	Introduction	1
2	The 5 Reference Atmospheres	1
3	Vibrational temperatures for the 5 reference atmospheres	15
3.1	General Improvements	15
3.2	H ₂ O and O ₂	17
3.3	CO ₂	31
3.4	O ₃	67
3.5	N ₂ O	98
3.6	CO	109
3.7	CH ₄	117
3.8	NO	128
3.9	NO ₂	136
3.10	HNO ₃	147
3.11	OH	153
3.12	HCN	156
4	Summary and Conclusions	164

1 Introduction

This report describes the revision and upgrade of the vibrational temperatures climatology that was calculated before in this project, basically described in *López-Puertas et al.* (2002) and with an subsequent upgrade of the NO₂ vibrational temperatures (*López-Puertas et al.*, 2004).

Since this is an upgrade and extension to previous vibrational temperatures, we describe here only the major updates and the major differences with respect to those formerly calculated. This description then is based on the reports mentioned above and on the models described in López-Puertas and Taylor (2001).

The vibrational temperatures have been calculated for the 5 reference atmospheres compiled in previous studies (see Table 1). The description of these reference atmospheres are given in the next section, and the upgrade and discussion of the new vibrational temperatures are given in the subsequent sections.

2 The 5 Reference Atmospheres

The five reference atmospheres used for computing the vibrational temperatures comprise profiles for the kinetic temperature, pressure, and many species abundances, and cover typical and extreme atmospheric conditions for which the potential non-LTE effects vary from weakest to moderate to strongest. The reference atmospheres for the calculation of the non-LTE populations have been set up from 0 to 120 km using a grid of 1 km, except for NO, which are extended up to 200 km.

Table 1: Reference Atmospheres

Ref. Atm.	Season/Latitude	Solar Illumination
1	Mid-latitude	Day, SZA=30°
2	Mid-latitude	Night
3	Polar Summer	Day, SZA=45°
4	Polar Winter	Night
5	Equator	Day, SZA=30°

Some changes have been introduced in these IG reference atmospheres in order to correctly compute the non-LTE populations. They fall generally within three categories: a) to include correctly the chemical or photochemical constraints for certain species (NO, NO₂, O, O₃) (mainly between 60 and 120 km); b) the extension in altitude for some species (up to 200 km); and c) the extension of the reference atmospheres to other species, some of them electronically and vibrationally excited, which are needed for the non-LTE calculations (e.g., O(¹D), O, H, N(⁴S), and OH(v)).

Below 120 km, we have modified the vmrs of the following species O₃, NO, NO₂ and H (see Figs. 6–10). The CO₂ vmr profile is also slightly changed (not noticeable in the scale). For calculating the NLTE error spectra we can use either the CO₂ in the IG climatology or that included here. However, we have to be consistent including the same CO₂ profile in both the LTE and NLTE spectra.

For those species whose vmrs have been significantly changed we have to use the modified abundances in both the LTE and NLTE spectra because they should be consistent with the calculated vibrational temperatures. However, for the species that we do not provide vibrational temperatures, e.g. SO₂, CFCs, etc., their abundances have to be taken from the IG, since they are not included in the modified set. Note that O, O(¹D), H and N(⁴S) are not used in the spectra calculation.

Table 2 describes the reference atmospheres used in the generation of the vibrational temperatures and Table 3 the data sources. Those atmospheres were constructed taken as a basis the IG. The tables then summarize the changes introduced in the profiles in the 0-120 km region, and their extension above 200 km. The major processes taken into account in the revision in the 60-120 km range are:

- NO, NO₂, O and O₃ due to the reactions NO₂ + O → NO + O₂ (important excitation mechanism for NO(v)), and NO + O₃ → NO₂ + O₂ (important excitation mechanism of NO₂($\nu_3 > 1$)).
- O, O₂ and O₃ due to O + O₂ + M → O₃ (important excitation mechanism for O₃(v)).
- H and O₃ due to H + O₃ → OH + O₂ (important excitation mechanism for OH(v)).
- For N₂, O₂, O, Ar, H₂O in order to satisfy that the sum of all vmr is equal to 1.

The O_x (=O₃+O) and NO_x (=NO₂+NO) abundances above 60 km are taken from the Garcia and Salomon 2D model. They were incorporated into the reference atmospheres by interpolating in pressure levels. The partitioning of these families, into O₃ and O for the O_x family, and NO₂ and NO for the NO_x family, was readjusted to the local time of MIPAS overpasses (i.e. 10 am and 10 pm) by applying a simple photochemical box model included in the IAA/IMK a priori generation tool. The chemical scheme employed by this box model is based on the JPL 2007 (Sander et al., 2006) recommendation. Photolysis rates are calculated with the TUV model (Madronich and Flocke, 1998).

The abundances of all species for which vibrational temperatures were calculated as well as of those necessary for computing them are shown in Figs. 1–5 for the 5 reference atmospheres. In addition, the differences in the abundances (w.r.t. the current IG) are shown in Figs. 6–10.

Table 2: Summary of the changes introduced in the IG reference atmospheres.

Gas	Hitran ID	Data source
Pressure		IG: 0-120 km; Hydrostatic: 120-200 km
T _k		IG: 0-120 km; NRLMSIS-00: 120-200 km
H ₂ O	1	IG: 0-120 km; vmr(200 km) = 10 ^{-4†}
CO ₂	2	Old IG [vmr(z=0 km)=373.9 ppmv]: 0-120 km; vmr(200 km) = 2.0
O ₃	3	IG: 0-60 km; GS [‡] : 60-120 km; vmr(200 km) = 10 ⁻⁶
N ₂ O	4	IG: 0-120 km; vmr(200 km) = 10 ⁻⁶
CO	5	IG: 0-120 km; vmr(200 km) = 1.0
CH ₄	6	IG: 0-120 km; vmr(200 km) = 10 ⁻⁵
O ₂	7	IG: 0-75 km; NRLMSIS-00: 75-200 km
NO ₂	10	IG: 0-75 km; GS [‡] : 75-100 km with diurnal correction applied using the NOx from Garcia & Solomon and the NO ₂ /NO partitioning from the IAA box model; vmr(200 km) = 5.0 × 10 ⁻¹⁰
NO	8	IG: 0-70 km; GS [‡] : 70-100 km with diurnal variation as for NO ₂ ; NOEM: 100-150 km; constant: 150-200 km
HNO ₃	12	IG: 0-120 km; vmr(200 km) = 10 ⁻¹⁷
OH	13	Garcia and Solomon: 0-120 km; vmr(200 km) = 10 ⁻¹²
N ₂	22	vmr(N ₂) = 1 - \sum_i vmr _i (remaining gases, including Ar)
O [•]	34	Garcia and Solomon [‡] : 0-80 km; NRLMSIS-00: 80-200 km
N	152*	IAA/IMK box model: 0-85 km; NRLMSIS-00: 85-200 km
H	154*	Garcia and Solomon: 0-120 km; vmr(200 km) = 10 ⁻²

*Not in HITRAN, KOPRA internal reference. [†]All vmr values are in ppmv. [‡]Garcia and Solomon but including diurnal variation to obtain profiles at LT=10 and 22 hours for day and night. *For the O₃ VTs calculation, however, the O was obtained from the photochemical equilibrium with O₃.

Table 3: Data source for the reference atmospheres.

Model		Reference
NRLMSIS-00:	day 45°N, 10 LT, 1 April: Ap=25, F10.7=155 ngt 45°N, 22 LT, 1 April: Ap=25, F10.7=155 AP=10 sum 75°S, 10 LT, 1 Jan 2003, Ap=35, F10.7=130 win 75°N, 22 LT, 1 Jan 2003, Ap=35, F10.7=130 equ same as day	Picone et al. (2002)
GS:	Garcia and Solomon chemical transport model run for 2006	Garcia and Solomon (1994)
NOEM model		Marsh et al. (2004)
IAA/IMK photochemical box model. It uses J_{NO} from Minschwaner and Siskind (1993) and the NO_2 and O_3 photolysis rates from TUV v4.3 (Madronich and Flocke, 1998)	Unpublished	

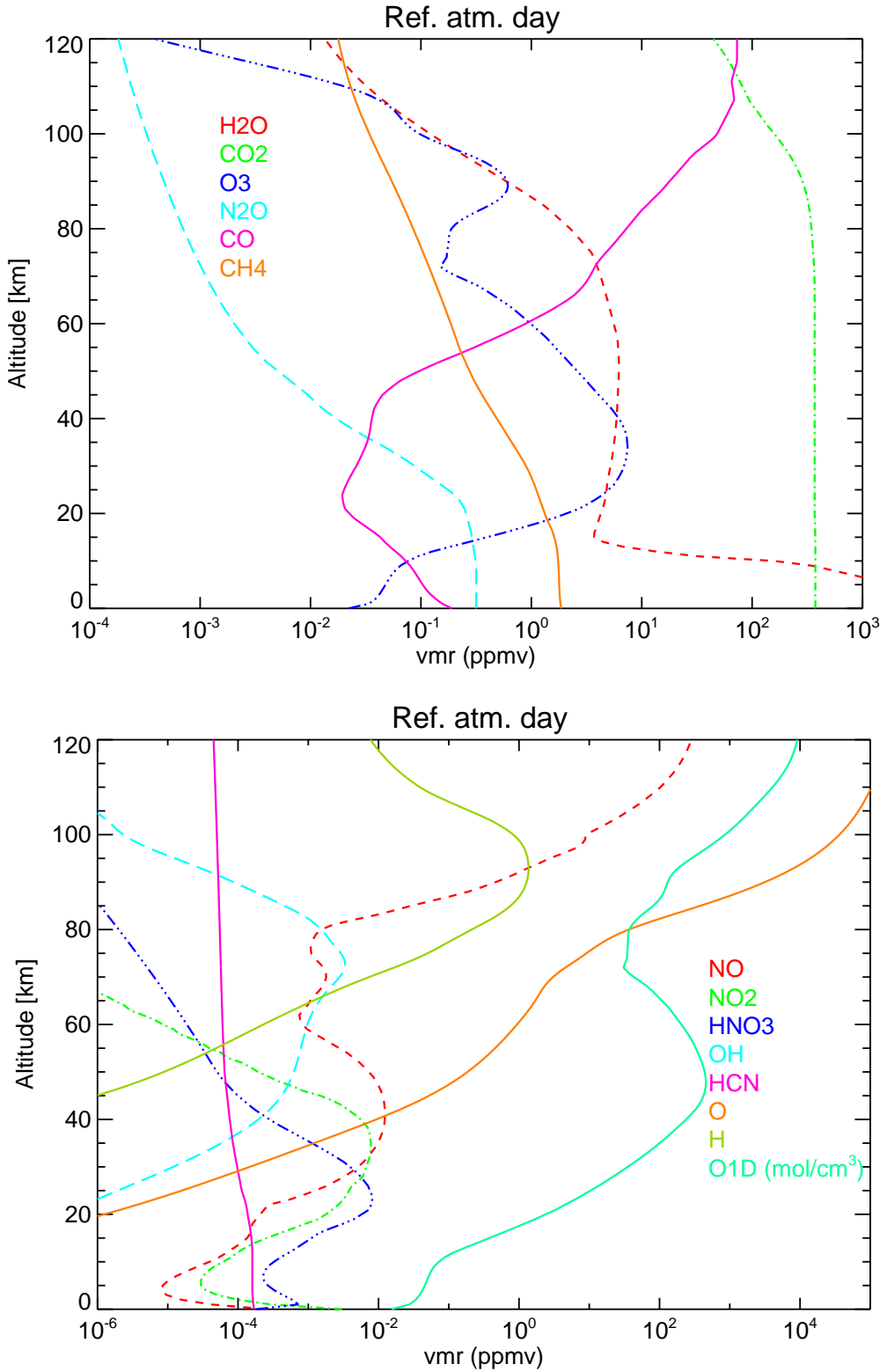


Figure 1: Volume mixing ratios (ppmv) (except for O^{1D} in mol/cm³) for the specified species for reference atmosphere #1, day (see Table 1).

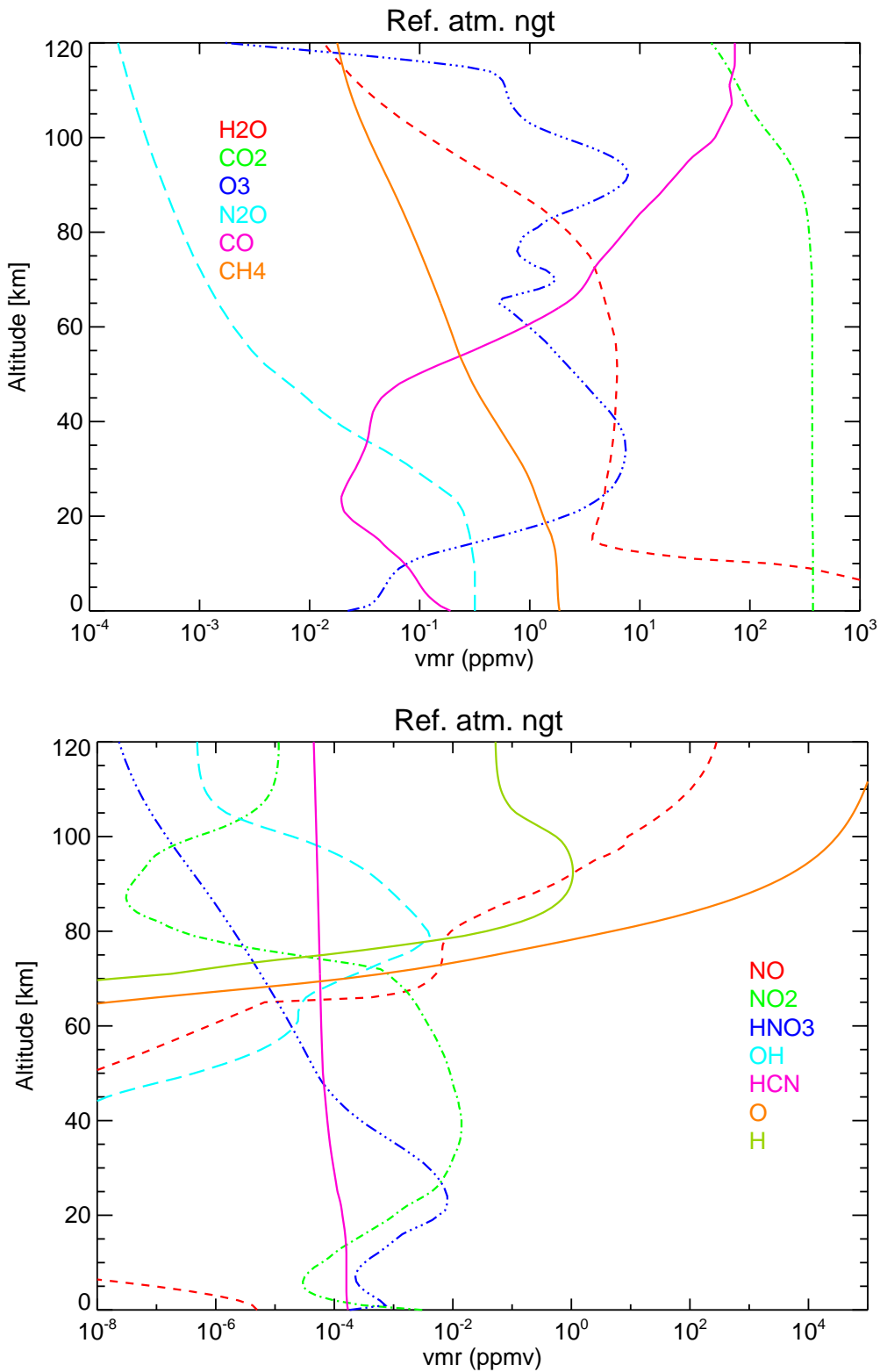


Figure 2: Volume mixing ratios (ppmv) for the specified species for reference atmosphere #2, night (see Table 1).

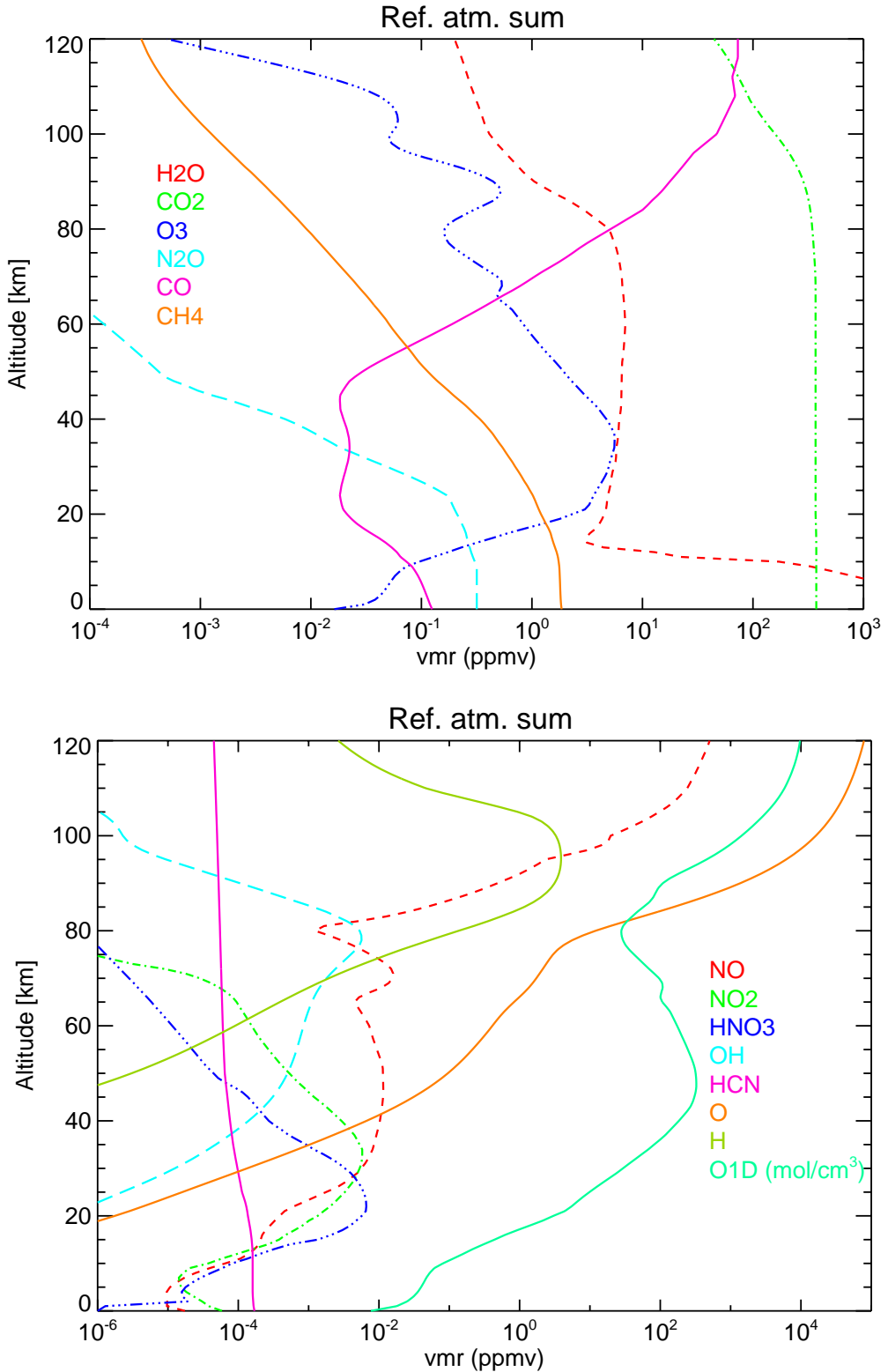


Figure 3: Volume mixing ratios (ppmv) (except for $O^{1}D$ in mol/cm^3) for the specified species for reference atmosphere #3, summer (see Table 1).

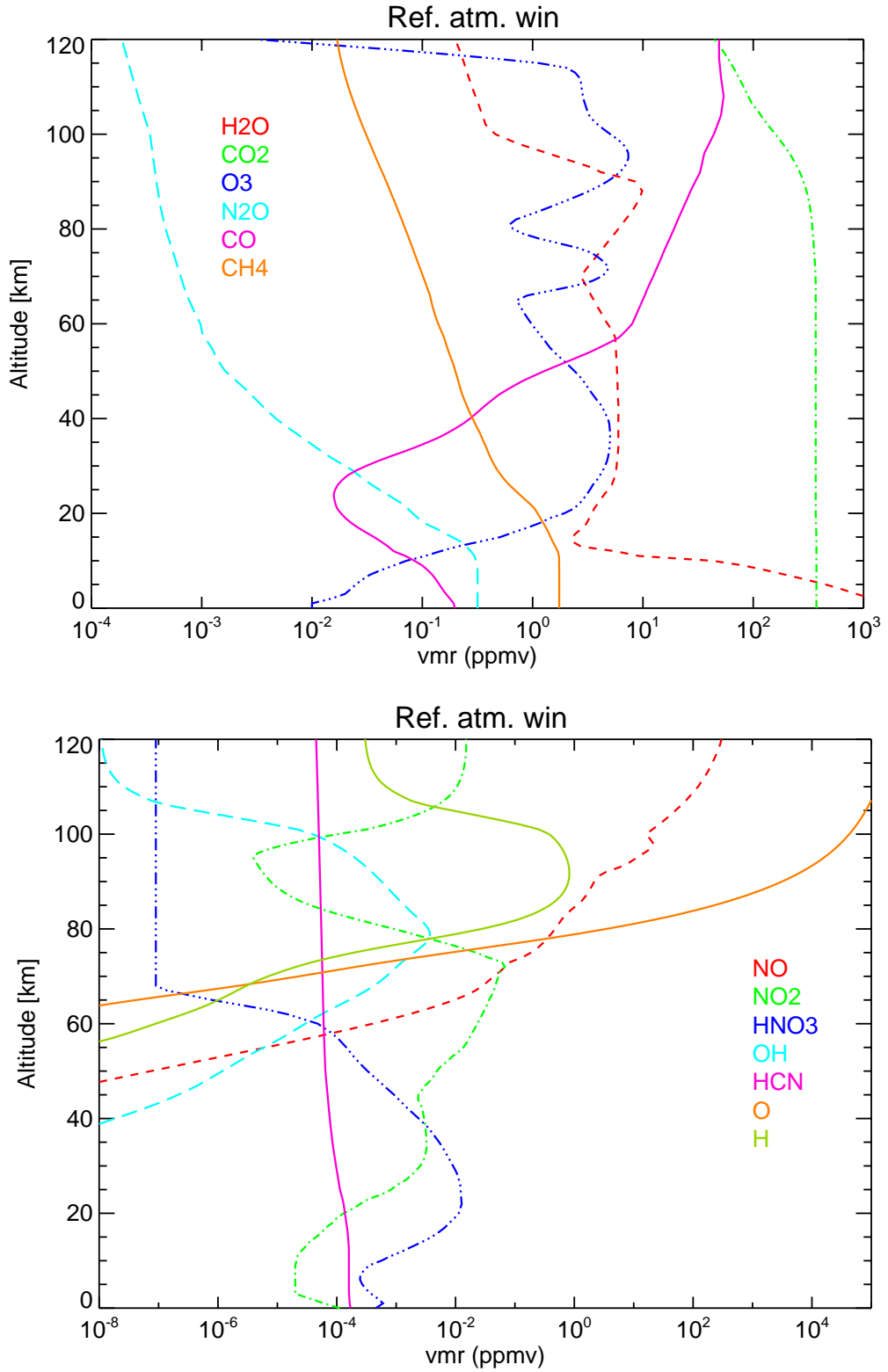


Figure 4: Volume mixing ratios (ppmv) for the specified species for reference atmosphere #4, winter (see Table 1).

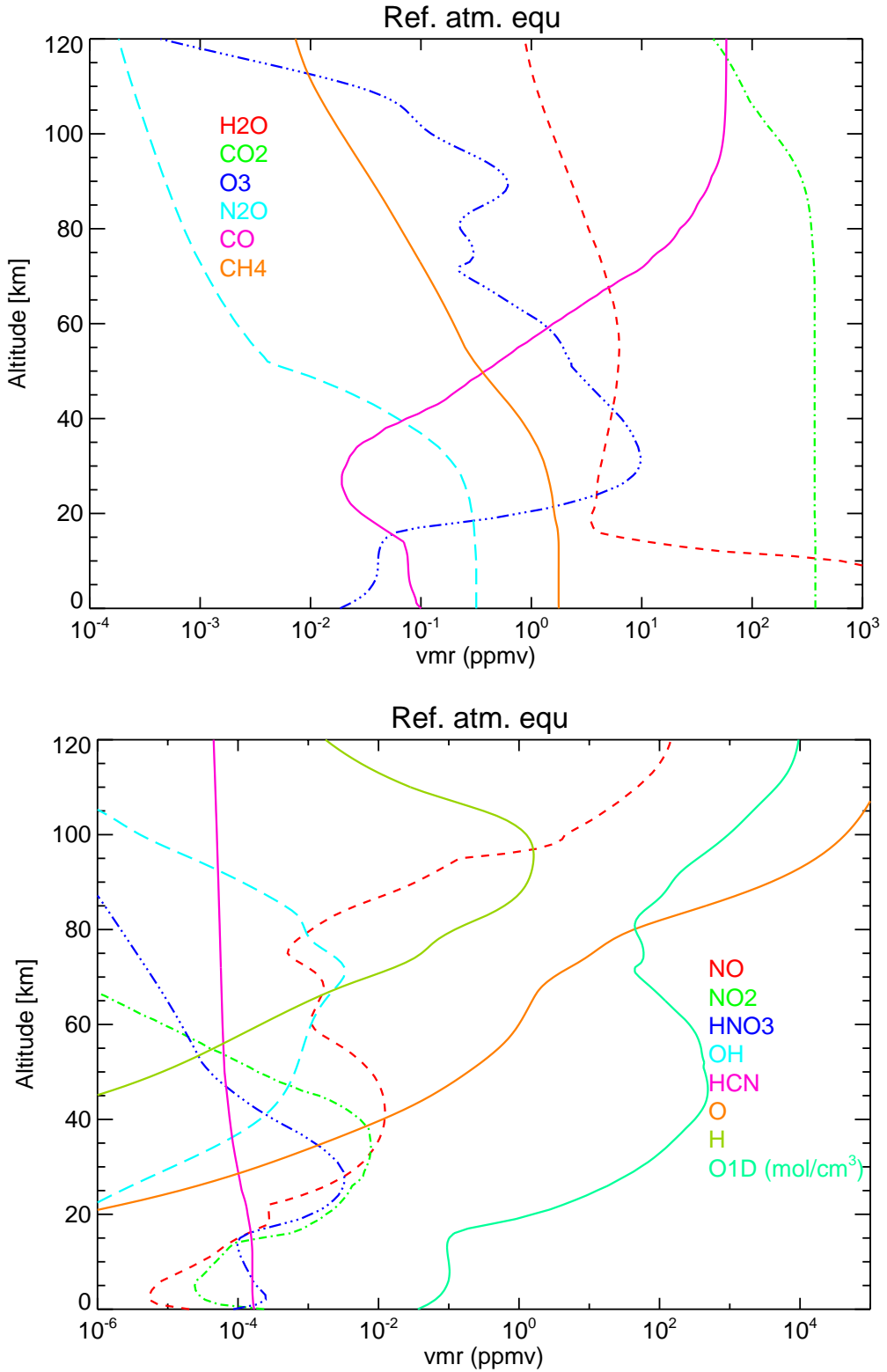


Figure 5: Volume mixing ratios (ppmv) (except for O¹D in mol/cm³) for the specified species for reference atmosphere #5, equator (see Table 1).

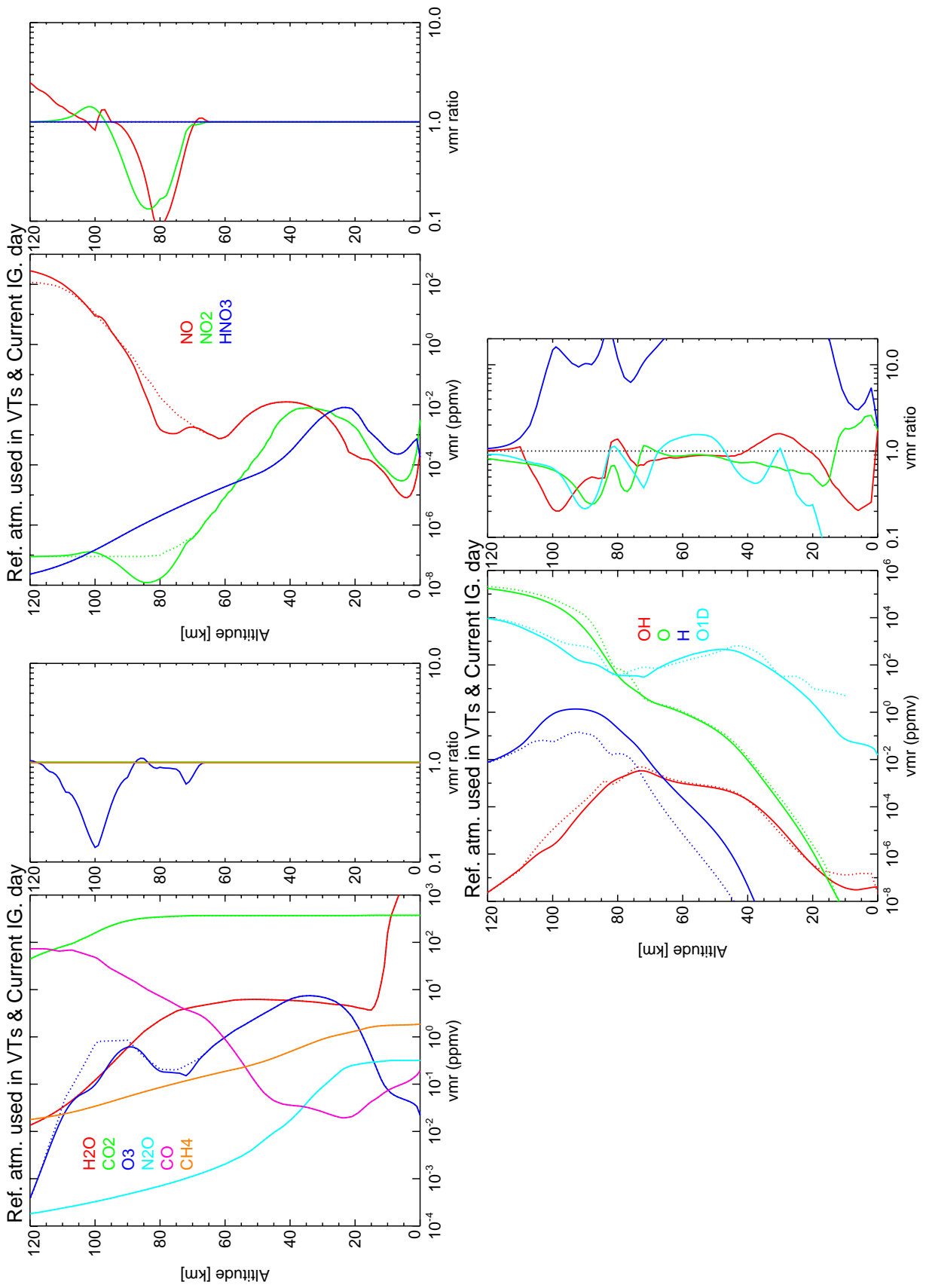


Figure 6: Species abundances used in the calculation of the vibrational temperatures and in the current IG for reference atmosphere day.
 Solid: this study; Dash: current IG. Right panel: this study/current IG.

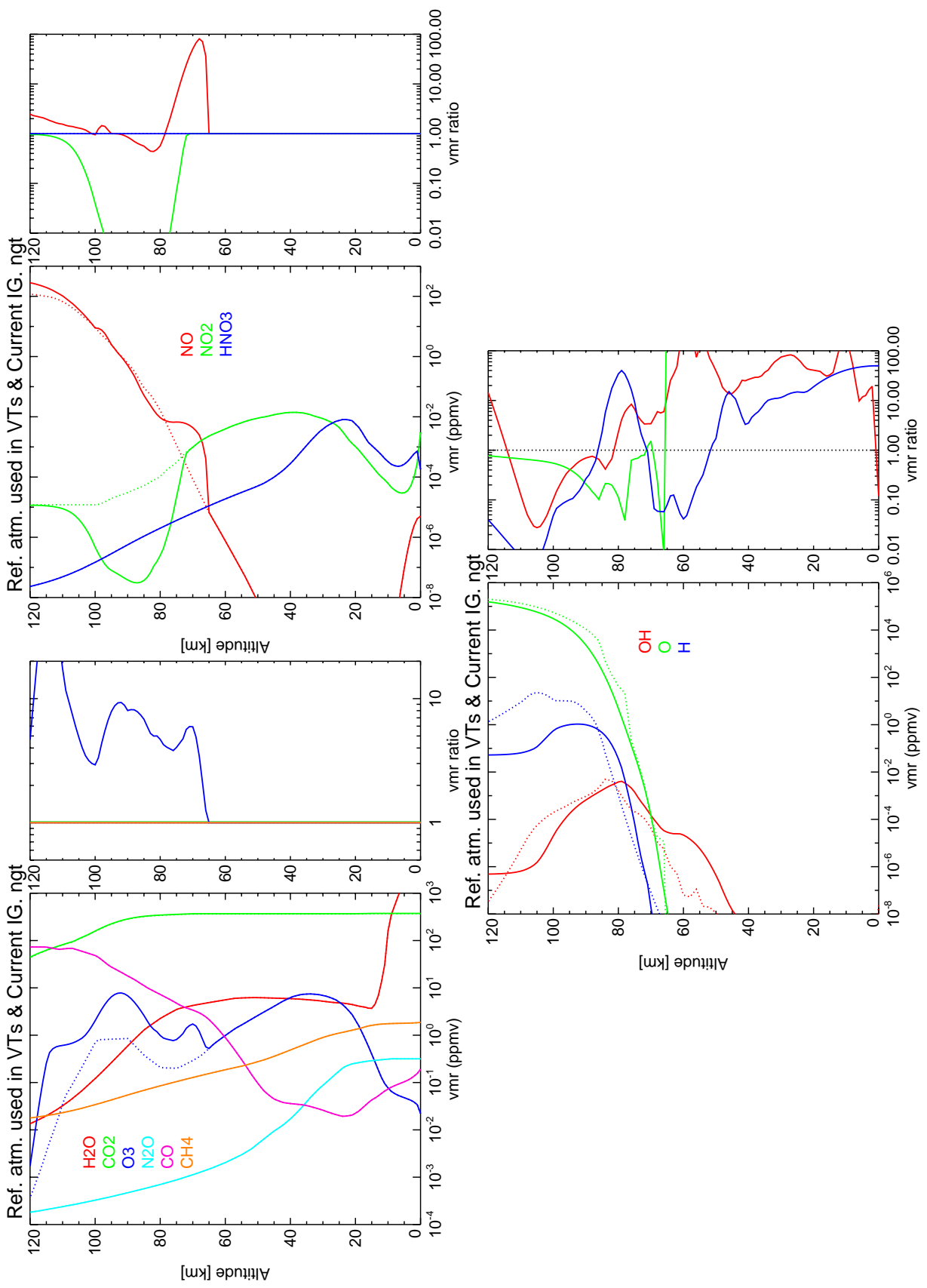


Figure 7: Species abundances used in the calculation of the vibrational temperatures and in the current IG for reference atmosphere night. Solid: this study; Dash: current IG. Right panel: this study/current IG.

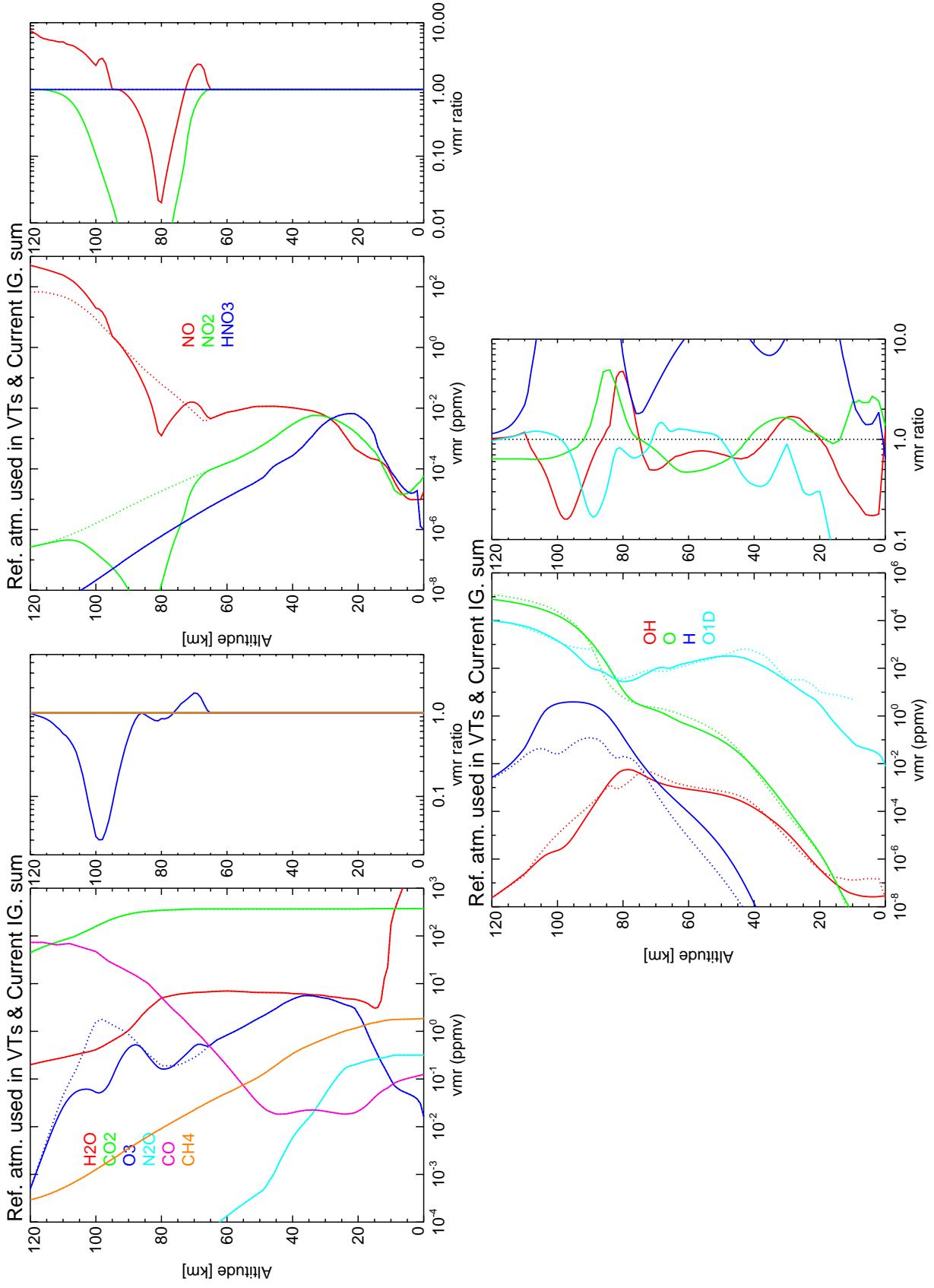


Figure 8: Species abundances used in the calculation of the vibrational temperatures and in the current IG for reference atmosphere summer. Solid: this study; Dash: current IG. Right panel: this study/current IG.

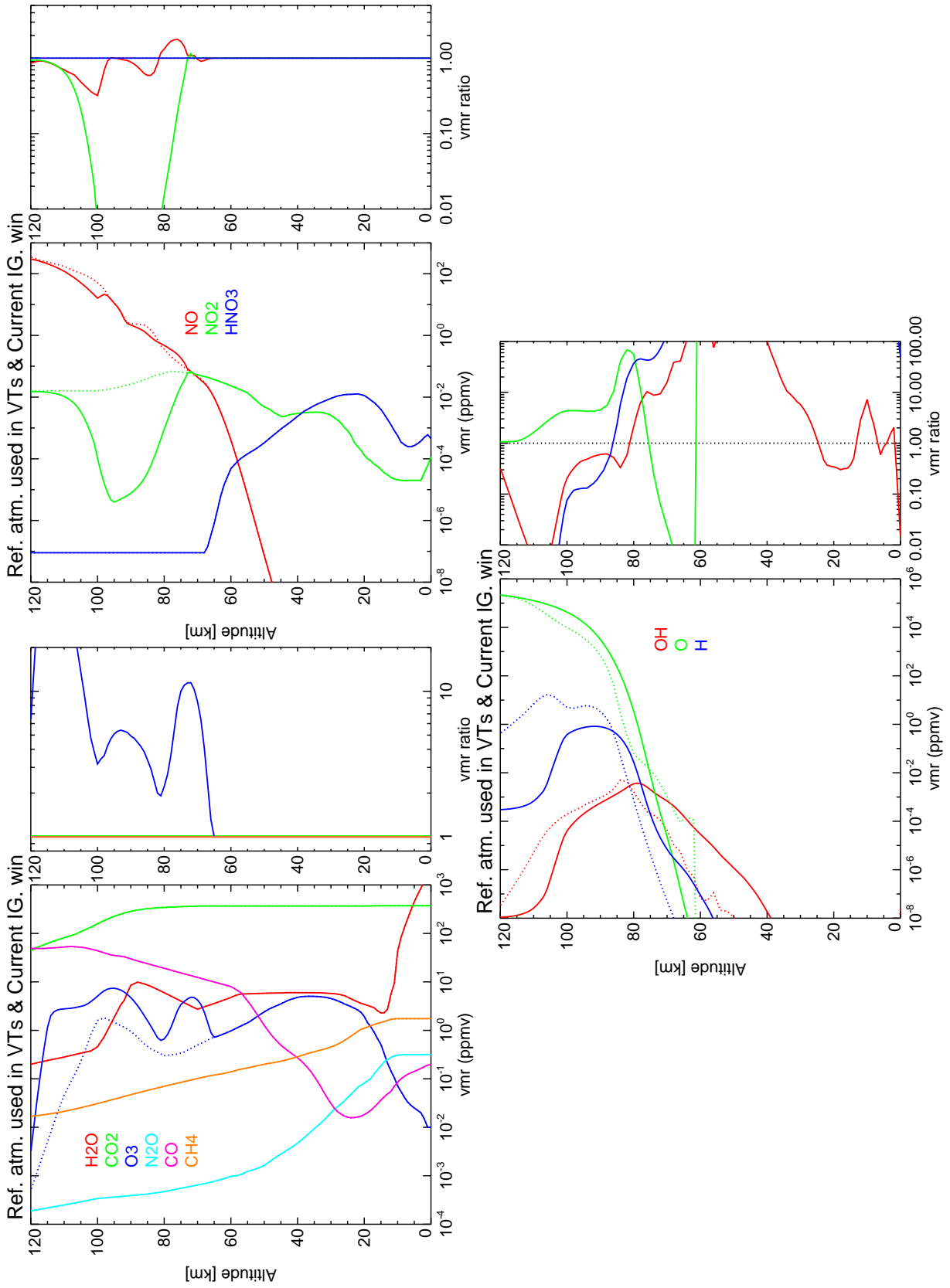


Figure 9: Species abundances used in the calculation of the vibrational temperatures and in the current IG for reference atmosphere winter. Solid: this study; Dash: current IG. Right panel: this study/current IG.

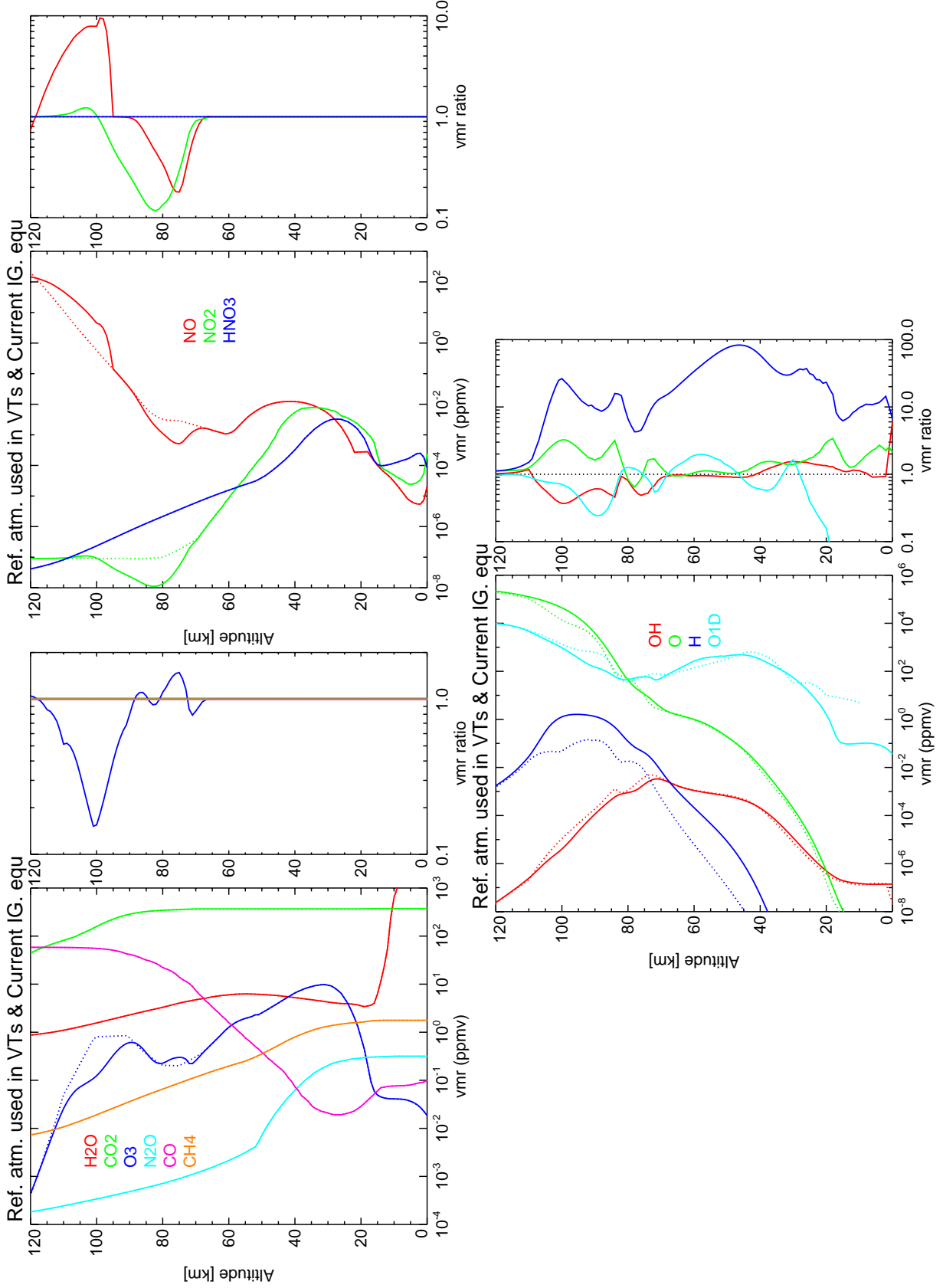


Figure 10: Species abundances used in the calculation of the vibrational temperatures and in the current IG for reference atmosphere equator. Solid: this study; Dash: current IG. Right panel: this study/current IG.

3 Vibrational temperatures for the 5 reference atmospheres

This climatology of vibrational temperatures includes calculations for the 5 reference atmospheres and conditions described above for the following species and vibrational levels:

1. H₂O: 21 + 19 O₂ levels (previously 6 and 1 respectively), emitting around 6.3 and 4.7 μm .
2. CO₂: 129 (previously 56) vibrational levels, emitting at 15, 10, and 4.3 μm , and the N₂(1) level.
3. O₃: 104 levels (previously 249), emitting around 14.6, 10 and 4.8 μm . We do not provide now vibrational temperatures for the very energetic vibrational levels of O₃, whose contribution to MIPAS spectra is entirely negligible.
4. N₂O: 41 levels originating the 8.6, 7.8, 4.5, 4.0, 3.6, and 3.0 μm bands.
5. CO: 4 levels (previously 1) with transitions near 4.6 μm and 2.0 μm .
6. CH₄: 12 levels, emitting around 7.6 and 6.5 μm .
7. NO: 10 levels (previously 6) emitting near 5.3 μm .
8. NO₂: 7 (0,0, v_3) levels, originating the ν_3 fundamental and hot bands in the 6.2–7.0 μm interval.
9. HNO₃: 8 levels, originating the 5.9, 7.5, 11, and 22 μm bands.
10. OH: 18 (previously 9) vibrational levels.
11. HCN: 25 energy levels (all new levels).

The vibrational temperatures are given at 1 km grid from 0 to 120 km, except nitric oxide (NO) which is given up to 200 km. The vibrational temperatures have been written in the KOPRA format and are available at <http://www.iaa.es/~puertas/qwg.html>. The files are named as aaa/vt_mm.kop, where aaa is the reference atmosphere (day, ngt, sum, win, equ), and mm is the molecule (H₂O, CO₂, ...).

In the next section we summarize the major upgrades which are common for most of the vibrational temperatures of the species and in the following sections we detail the specific changes included for the vibrational temperatures of the different gases.

3.1 General Improvements

We discuss in this section a number of improvements in the calculation of the vibrational temperatures which are common to many species. These include:

1. For most of the molecules we use new non-LTE models developed from the Generic RAdiative traNsfer AnD non-LTE population Algorithm (GRANADA) (Funke et al., 2002). This model has several advantages as:

- (a) Calculation of rotational and vibrational populations and their derivatives w.r.t. the NLTE retrieval parameters.
 - (b) The model uses a generalized scheme. That is the same algorithm is used for calculating the populations of all molecules.
 - (c) The model characteristics are "user-defined". That is, the user defines the states and transitions to be considered, the altitude range, the iteration strategies, the non-LTE processes to be included, etc.)
 - (d) The model is capable of calculating rotational (and spin-orbit) non-LTE populations, and line-by-line and line independent radiative transfer calculations, which are implemented using KOPRA (Stiller et al., 2002).
 - (e) The inversion of the system of multilevel steady state equations can be performed by either using the Lambda-iteration or the Curtis matrix formalisms.
2. For many molecules, the number of vibrational levels has been significantly increased. The vibrational levels of HCN have been included for the first time.
 3. New spectroscopic line data has been included, in particular for CO₂ and H₂O from HITEMP (Rothman et al., 1995). For N₂O, vibrational energy levels and *A* Einstein coefficients have been calculated from HITRAN 2004 and GEISA (<http://ara.lmd.polytechnique.fr/htdocs-public/products/GEISA/HTML-GEISA>) line lists. Additional energy levels not included in both spectroscopic data sets have been determined by means of least squares fitting of spectroscopic constants. *A* Einstein coefficients for these bands have been estimated by scaling of data for available vibrational levels.
 4. Solar fluxes in the IR and near-IR have been taken from SOLAR 2000 (Tobiska et al., 2000), taking into account seasonal variations related to the Sun-Earth distance.

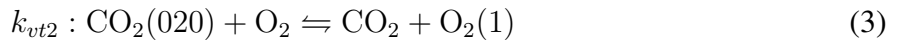
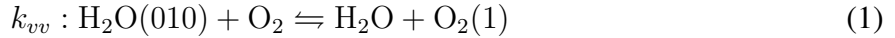
As in the previous climatology we retain a number of improvements which are very important for the accurate calculation of vibrational temperatures. Among the most important are:

1. The species abundances are physically and chemically consistent. E.g.,
 - Consistent O₃ and O for the calculation of the vibrational temperatures of O₃ and H₂O
 - Consistent NO and NO₂ for the calculation of the vibrational temperatures of NO and NO₂
 - Consistent NO and O₃ for the calculation of the vibrational temperatures of NO₂ and
 - Consistent O₃ and H for OH vibrational temperatures.
2. Some vibrational temperatures depend on the volume mixing ratio (vmr) of the species considered, e.g., O₃, NO₂, NO and OH. This implies that, for estimating non-LTE effects correctly, the same abundances used in the calculation of their vibrational temperatures should be used in the forward model when computing the atmospheric radiance. This might lead to incorrect retrieved quantities for some species if the vibrational temperatures are not recalculated within the retrieval scheme.

3.2 H₂O and O₂

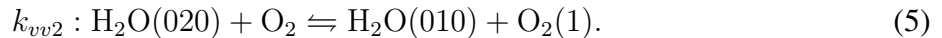
The non-LTE model for H₂O has been upgraded in several ways. First, from the analysis of MIPAS spectra in the region of the H₂O fundamental and first hot bands, and from the region of CH₄ v_4 band (López-Puertas et al., 2005; Fischer et al., 2008). Second, from the most recent measurements of the collisional deactivation of O₂(1) by O carried out by the SRI group (Kalogerakis et al., 2005; Copeland et al., 2009). In addition, we have now developed a full non-LTE model for O₂, including 19 vibrational levels.

The most important rates that affects the population of H₂O(010) in the Earth's mesosphere are:



With respect to reaction (1), the analysis of the ISAMS, CRISTA and CIRRIS measurements (Zaragoza et al., 1998; Edwards et al., 2000; Zhou et al., 1999) show that the values are limited to the range $0.9\text{--}3.1 \times 10^{-12} \text{ cm}^3\text{s}^{-1}$. The rate in the previous version of VTs is $1.68 \times 10^{-12} \text{ cm}^3\text{s}^{-1}$.

The analysis of MIPAS spectra (not yet published), suggests a value of $2.0 \times 10^{-12} \text{ cm}^3\text{s}^{-1}$ for the rate



Assuming the harmonic oscillator approach, which predicts $k_{vv2} = 2 \times k_{vv}$, gives a value of $1.0 \times 10^{-12} \text{ cm}^3\text{s}^{-1}$ for the rate of reaction (1). The value for k_{vv2} is derived with an uncertainty of about 10%. However, the value derived for k_{vv} , carries along also the uncertainty of assuming the harmonic oscillator approach.

In this study we used the value recently derived from MIPAS, $1.0 \times 10^{-12} \text{ cm}^3\text{s}^{-1}$, which is also consistent with previous values derived from ISAMS, CRISTA and CIRRIS measurements. About temperature dependence, in absence of measurements, we continue with a temperature-independent rate.

The rate of process (2), k_{vt} , has been recently measured by Kalogerakis et al. (2005) with a value of $3.2 \times 10^{-12} \text{ cm}^3\text{s}^{-1}$ at 315 K. This is about three times larger than the value of $1.3 \times 10^{-12} \times (T/300)$ which has been used in several non-LTE models until recently (see Fig. 11). In addition, Kalogerakis et al. (2005) also discussed the temperature dependence of this rate and, based on the experiments and theoretical calculations of the temperature dependence of the isotope exchange reaction (Anderson et al., 1985), they suggested a value of $4.16 \times 10^{-12} \text{ cm}^3\text{s}^{-1}$ at 230 K. This implies an inverse temperature dependence of this rate at low temperatures (see Fig. 11). This, however, gives an even larger value at low temperatures, which does not agree well with MIPAS CH₄ non-LTE analysis. Besides, more recently, measurements taken by Copeland et al. (2009) also reject the inverse temperature dependence. Thus, we use a \sqrt{T} -law, which gives $k_{vt} = 3.2 \times 10^{-12} \sqrt{T/315}$. Note that this rate is significantly larger than that used in the previous version (see Fig. 11).

In the previous version, we used a rate of $k_{vt2}=9.1 \times 10^{-15} \sqrt{T} \exp(-56.7/\sqrt{T})$, which has both a \sqrt{T} and an exponential temperature dependence. Bass (1973) measured this rate in the temperature range of 300–600 K, with a rather large error at 300 K. That expression for k_{vt2} was derived

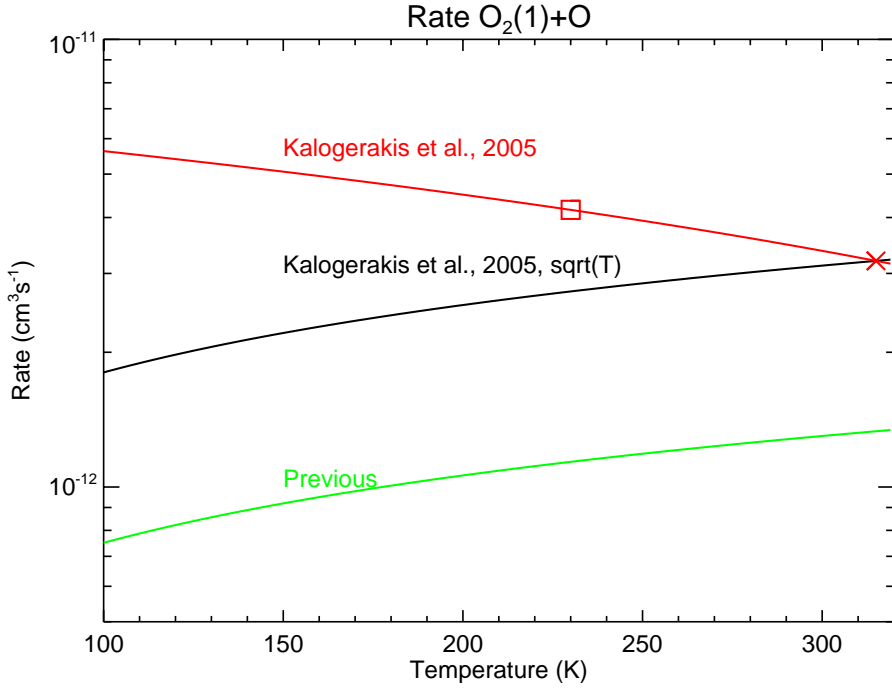


Figure 11: Rates for the relaxation of $\text{O}_2(1)$ by O , k_{vt} .

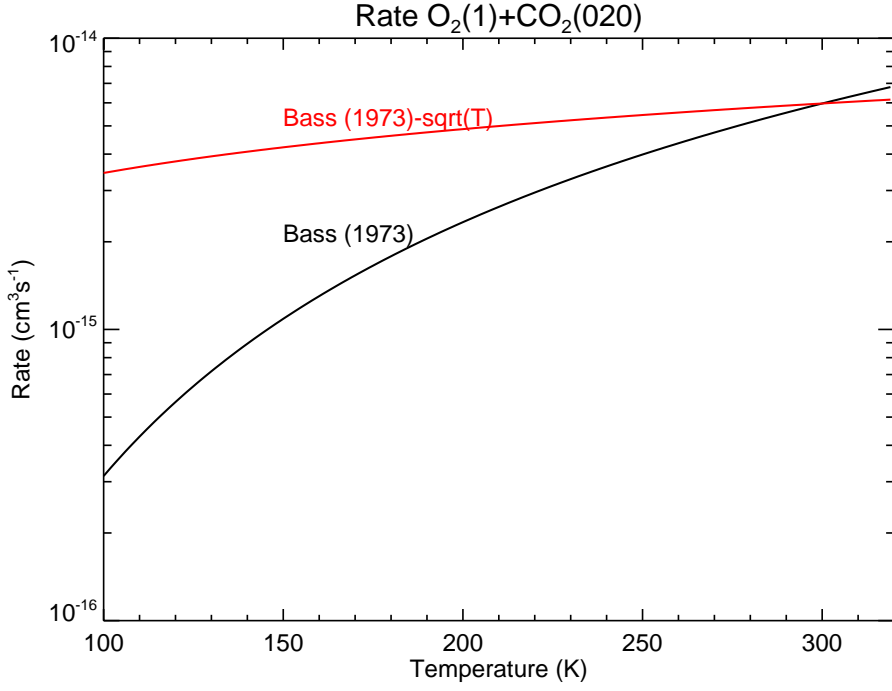


Figure 12: Rates for VV exchange between $\text{CO}_2(020)$ and $\text{O}_2(1)$, k_{vt2} .

for the 300-600 K range. However, it gives very low values when extrapolated at low temperatures (see Fig. 12). Hence, we use a \sqrt{T} dependence, which is very similar to the dependence used for the collisional deactivation of $\text{CO}_2(010)$ by atomic oxygen.

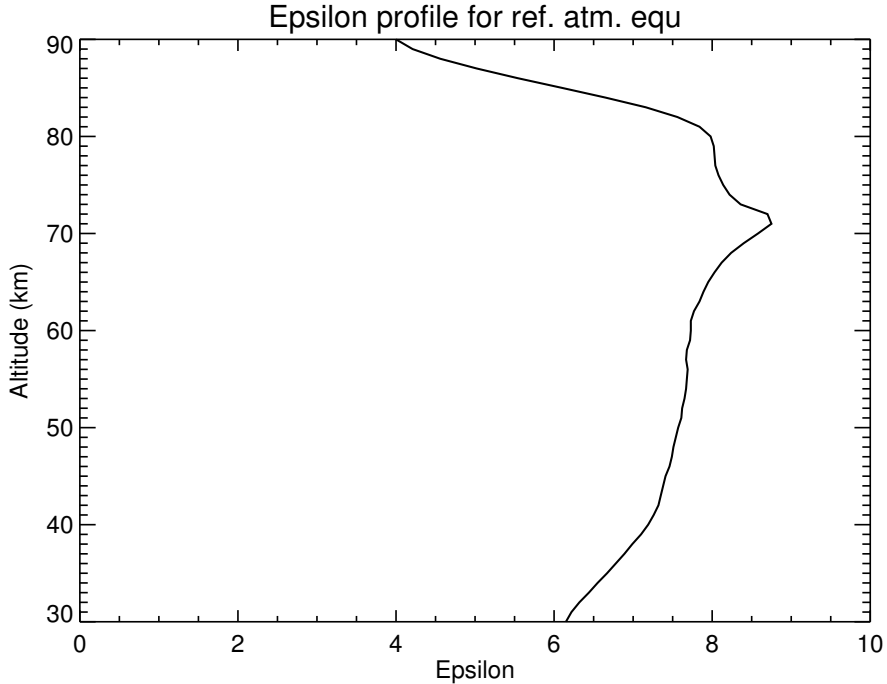


Figure 13: Profile of ϵ calculated in the new O₂ model for the “equator” (#5) reference atmosphere.

In the previous version, we used an excitation of O₂(1) from O₃ photodissociation of $\epsilon=4$. Instead of using an altitude-constant ϵ , we have now implemented an O₂(v) non-LTE model and include the most important electronic-vibrational levels of O₂. The scheme of the electronic-vibrational kinetics implemented is based on Yankovsky and Manuilova (2006). The result of the O₃ photolysis on the O₂(1) excitation is analogous to include an ϵ that depends on altitude, on the atmospheric conditions and, obviously, is more accurate. The values of ϵ thus obtained are significantly higher than before ($\epsilon = 6-8$) in the lower mesosphere (see Fig. 13).

Furthermore, a most recent measurement of the rate of V-V collisional exchange between CH₄(v₂) and O₂(1) has been included (Boursier et al., 2007). This affects the population of O₂(1) and since this is coupled to that of H₂O(010) (see Fig. 108), it also affects to the population of H₂O(010).

The non-LTE parameters used in the current version for the H₂O vibrational temperatures are summarized in Table 4 and compared to the previous values.

Table 4: H₂O non-LTE parameters.

Parameter	Previous value	Current value
$k_{vv}, \times 10^{-12}$, H ₂ O(010)-O ₂ (1)	1.7	1.0
$k_{vt}, \times 10^{-12}$, O ₂ (1)+O	1.3	3.2
ϵ , O ₃ +hν → O ₂ (1)	4	(6-8, see Fig. 13)

The vibrational temperatures for the H₂O and O₂(1) levels for the 5 reference atmospheres are shown in Figs. 14–18. The right panels of the corresponding vibrational temperatures show their deviation from the kinetic temperature, which inform us about the departure from LTE. The vibrational temperatures are plotted for the corresponding energy levels, using the same color, which are identified by the HITRAN notation. The first digit correspond to the molecule HITRAN ID (1 for H₂O, 2 for CO₂, etc.), the second digit is for the isotope ID (1 is the main isotope, 2 is the second most abundant, and so on), and the rest of the digits are the HITRAN notation for the level in question.

Instead of discussing the VT's for all energy levels and reference atmospheres, we will mainly discuss the differences with the previous version (AMIL2DA), which are plotted in Figs. 19–23 for H₂O. For some species we include vibrational temperatures for new levels. In those cases we briefly discuss their behaviour.

Figure 19 shows the differences in the VT's for H₂O for the day atmosphere. We see that the Tv of H₂O(010) has not changed up to above 70 km. Around 70 km it is smaller because of the larger O₂(1)-O rate of Kalogerakis et al. (2005) introduced now. This effect is larger, and extends to higher altitudes (85 km), in the summer case (Fig. 21). Above 70 km, the Tv is larger because of the slower k_{vv} rate included now, which makes H₂O(010) to decouple from O₂(1) and hence having larger population because it is largely pumped by absorption of radiation from below (López-Puertas and Taylor, 2001). The Tv of the (010) level of the minor isotopes exhibit a similar behaviour.

The Tv of the H₂O(020) level is generally larger now in the mesosphere because of the slower k_{vv2} rate, which makes it to be closer to the larger populations of the (100) and (001) levels which are solar pumped. The other levels do not change significantly.

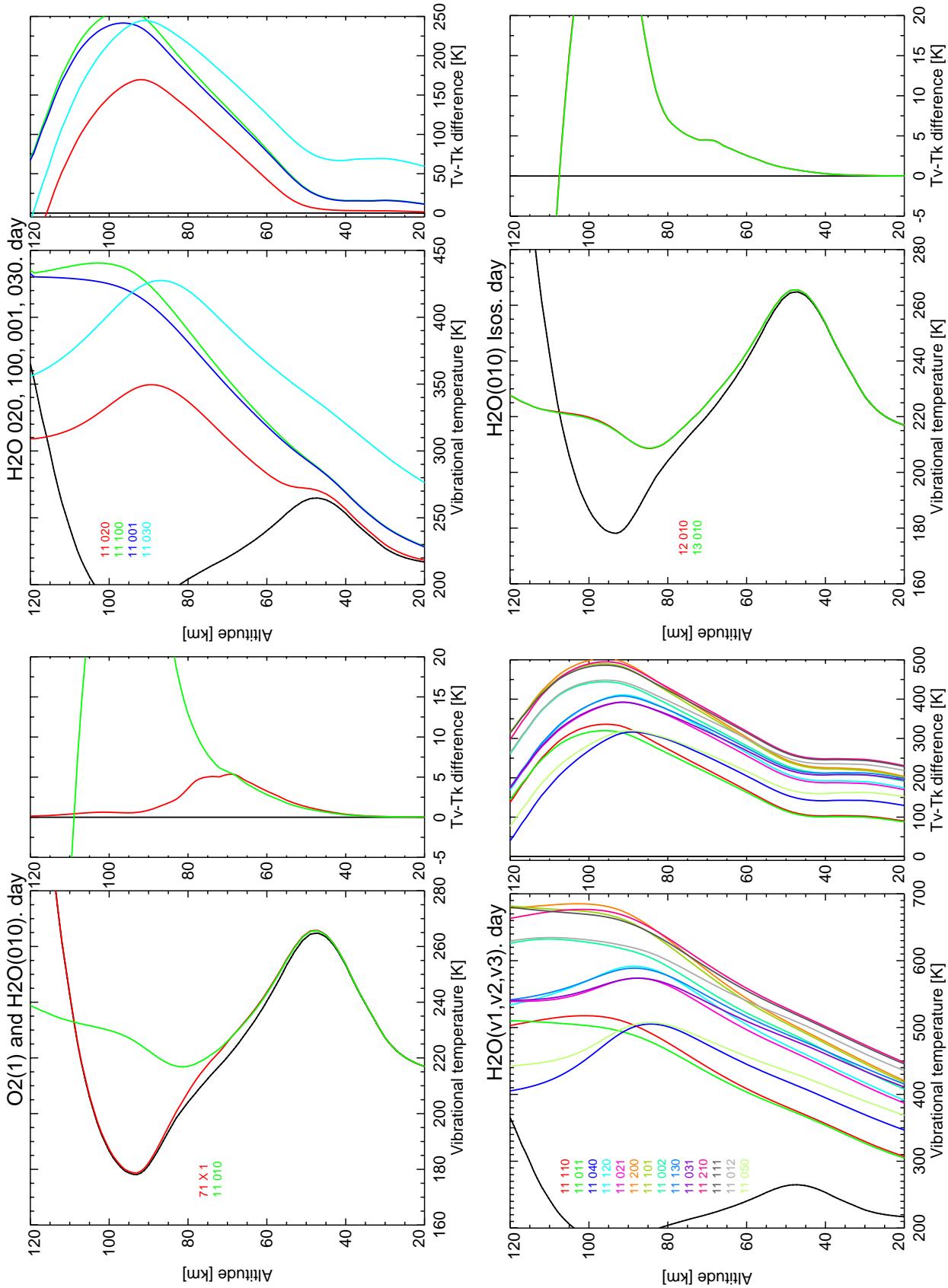


Figure 14: Vibrational temperatures for H_2O and $\text{O}_2(1)$ levels, for reference atmosphere #1, day.

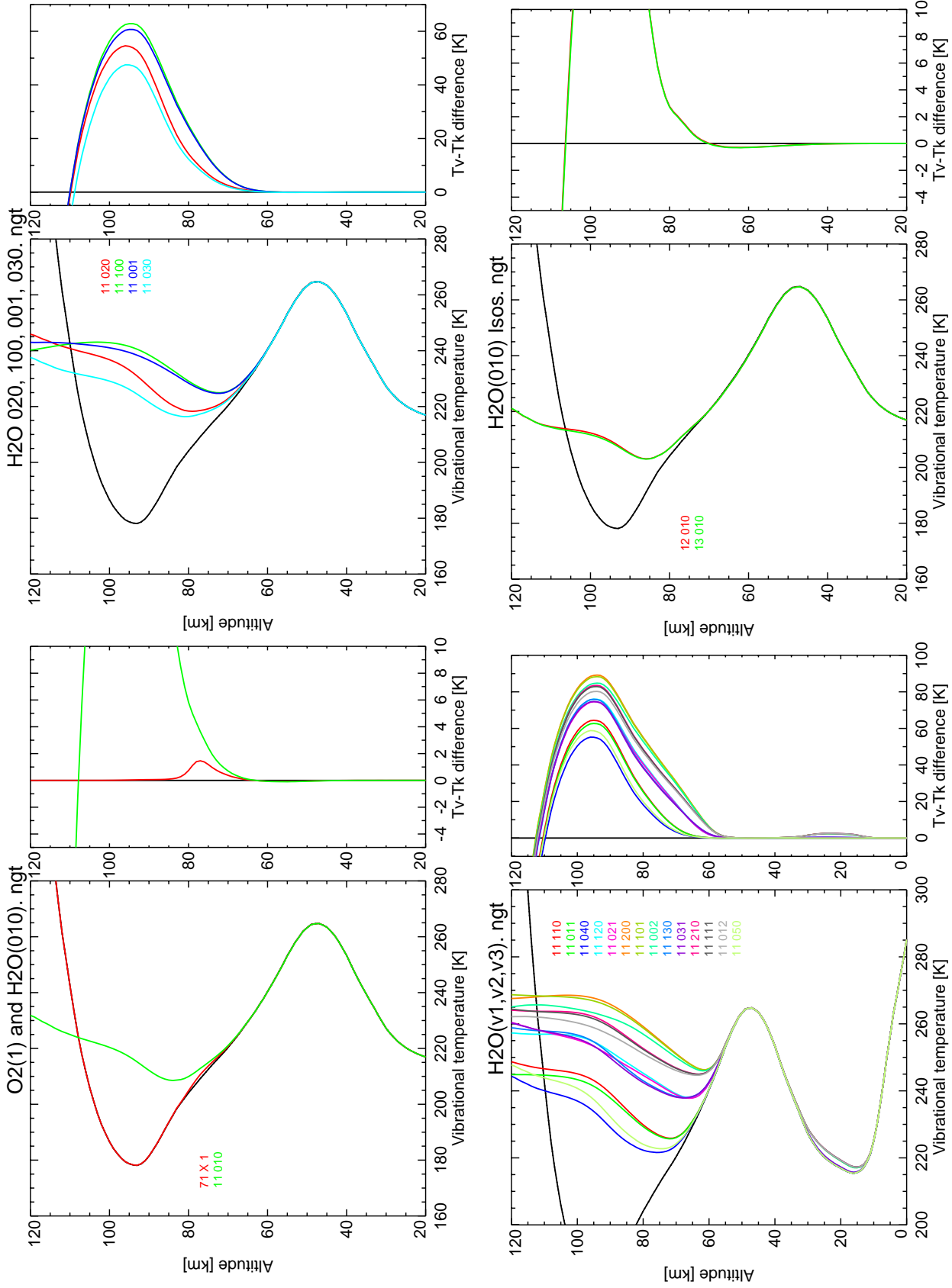


Figure 15: Vibrational temperatures for H_2O and $\text{O}_2(1)$ levels, for reference atmosphere #2, night.

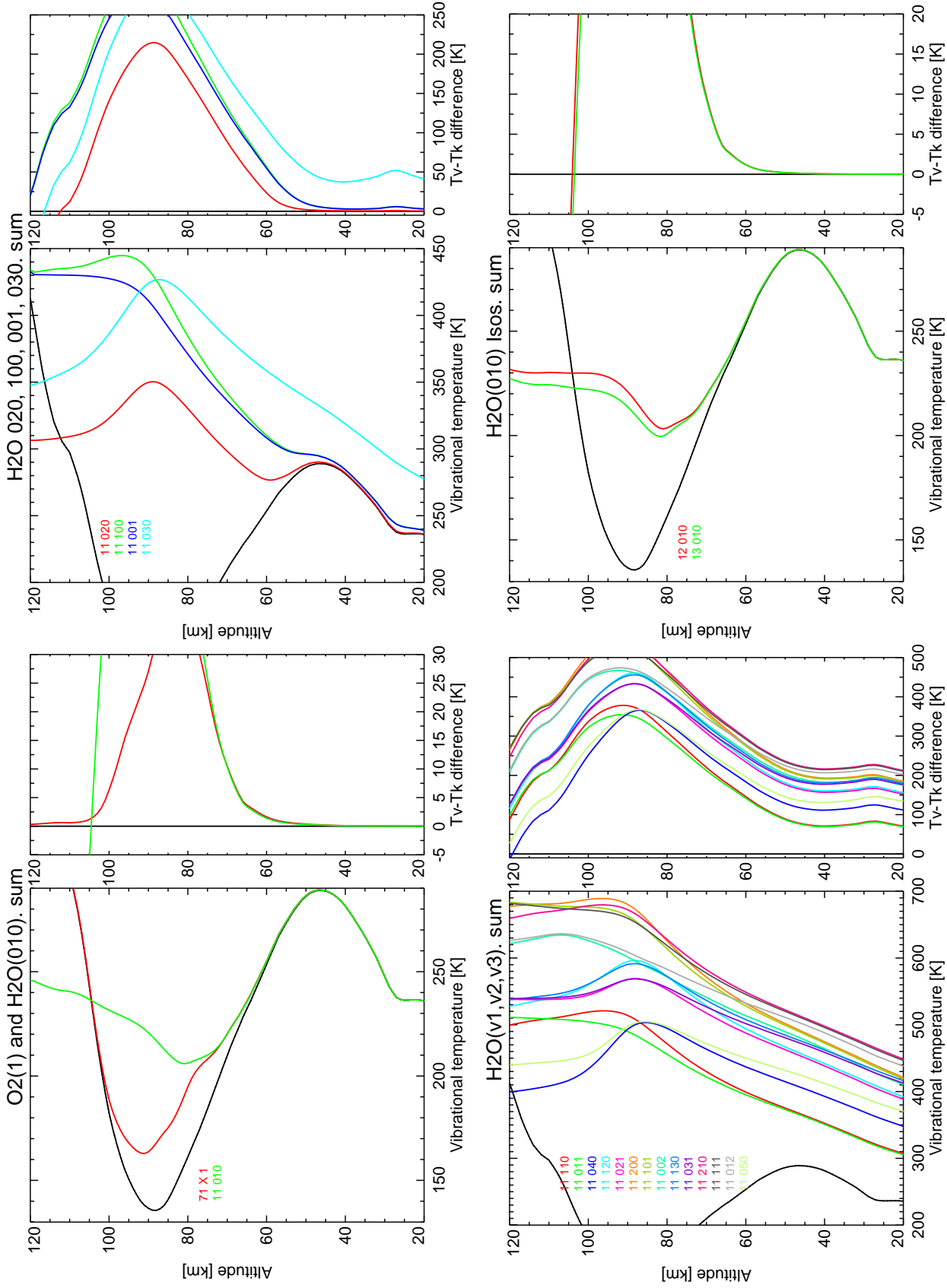


Figure 16: Vibrational temperatures for H_2O and $\text{O}_2(1)$ levels, for reference atmosphere #3, summer.

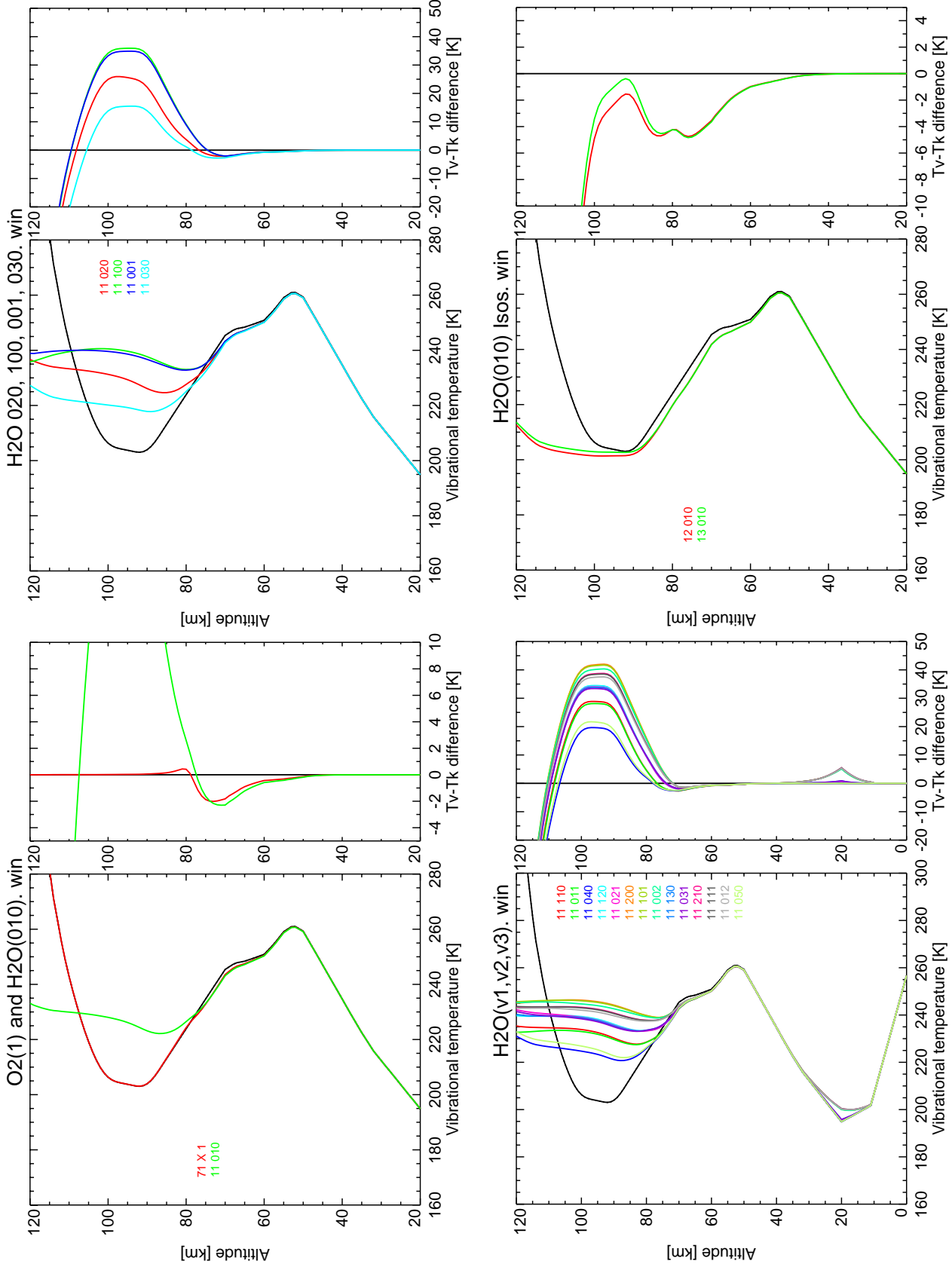


Figure 17: Vibrational temperatures for H₂O and O₂(1) levels, for reference atmosphere #4, winter.

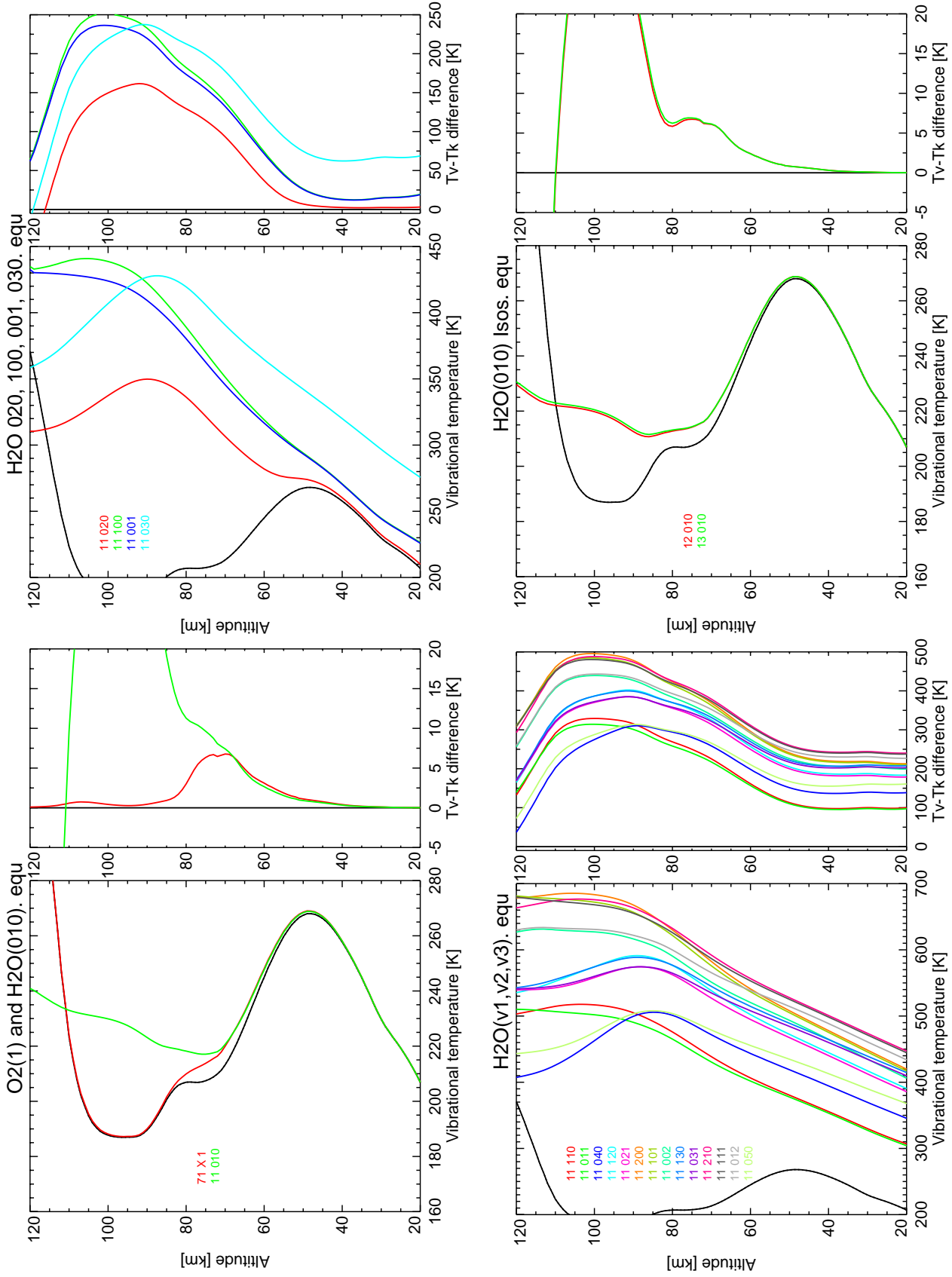


Figure 18: Vibrational temperatures for H_2O and $\text{O}_2(1)$ levels, for reference atmosphere #5, equator.

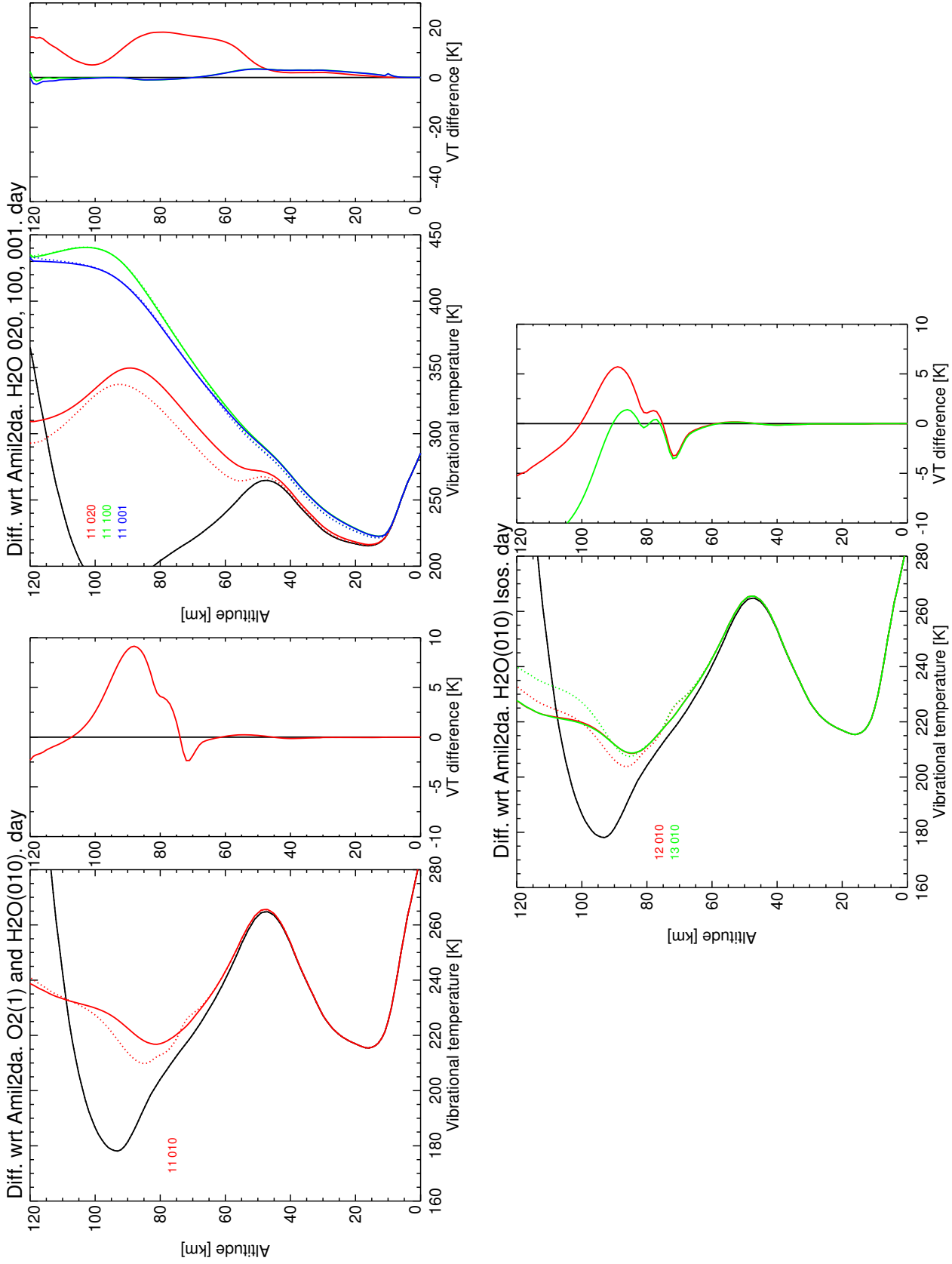


Figure 19: Differences in vibrational temperatures w.r.t. AMIL2DA, H₂O, for reference atmosphere #1, day. Solid: this study; dash: AMIL2DA. Right panels: this study-AMIL2DA.

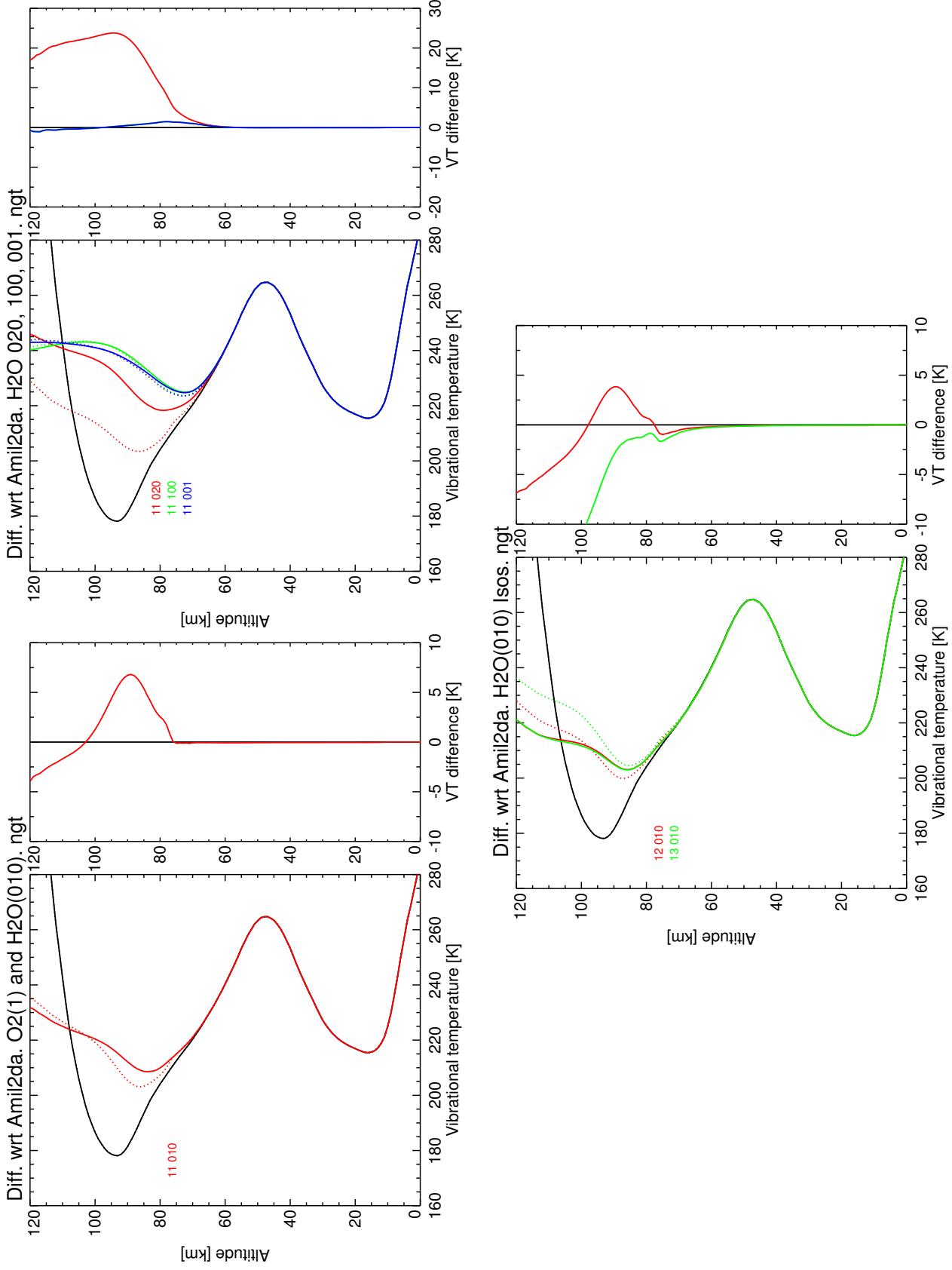


Figure 20: Differences in vibrational temperatures w.r.t. AMIL2DA, H_2O , for reference atmosphere #2, night. Solid: this study; dash: AMIL2DA. Right panels: this study–AMIL2DA.

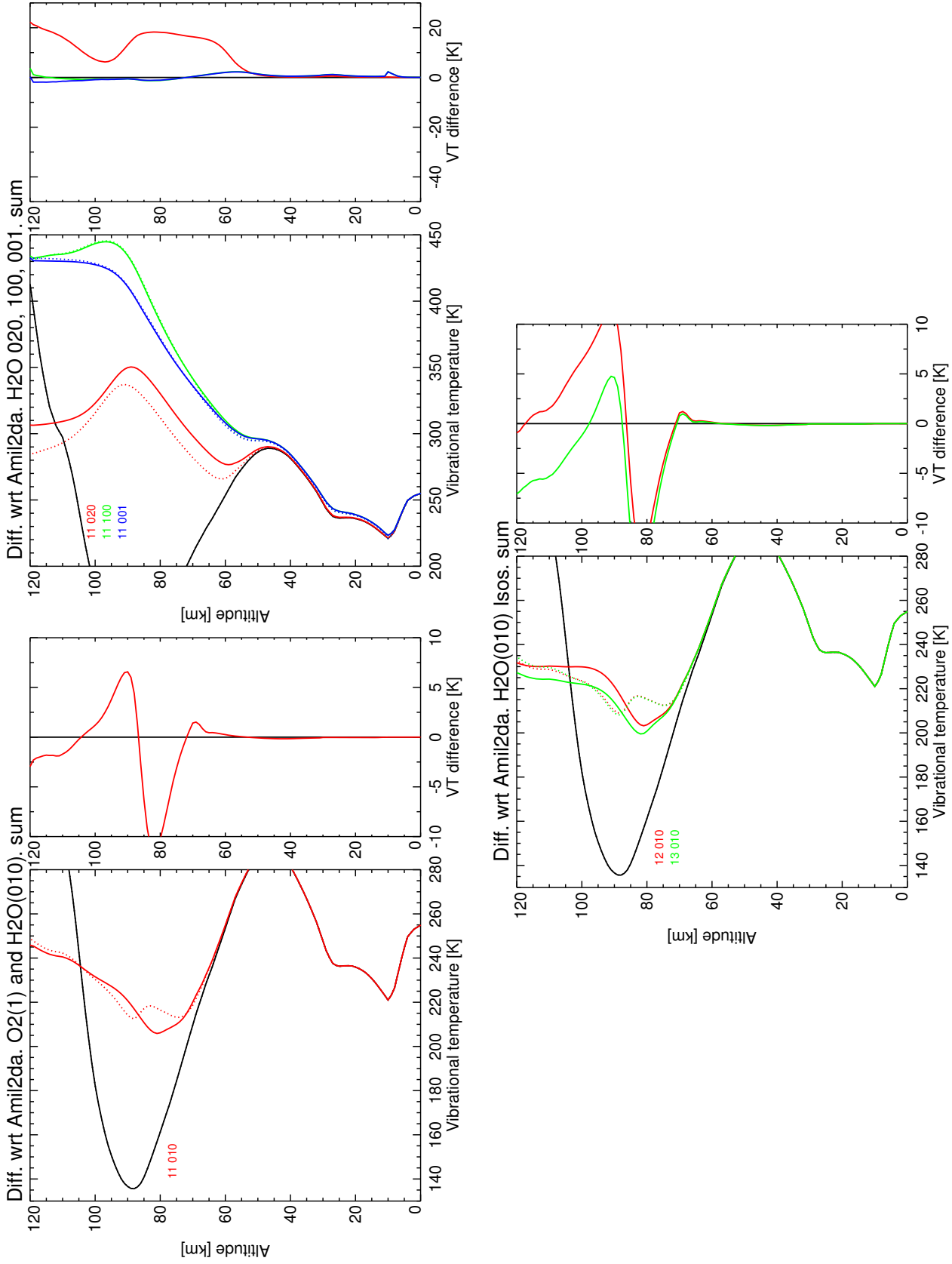


Figure 21: Differences in vibrational temperatures w.r.t. AMIL2DA, H_2O , for reference atmosphere #3, summer. Solid: this study; dash: AMIL2DA. Right panels: this study-AMIL2DA.

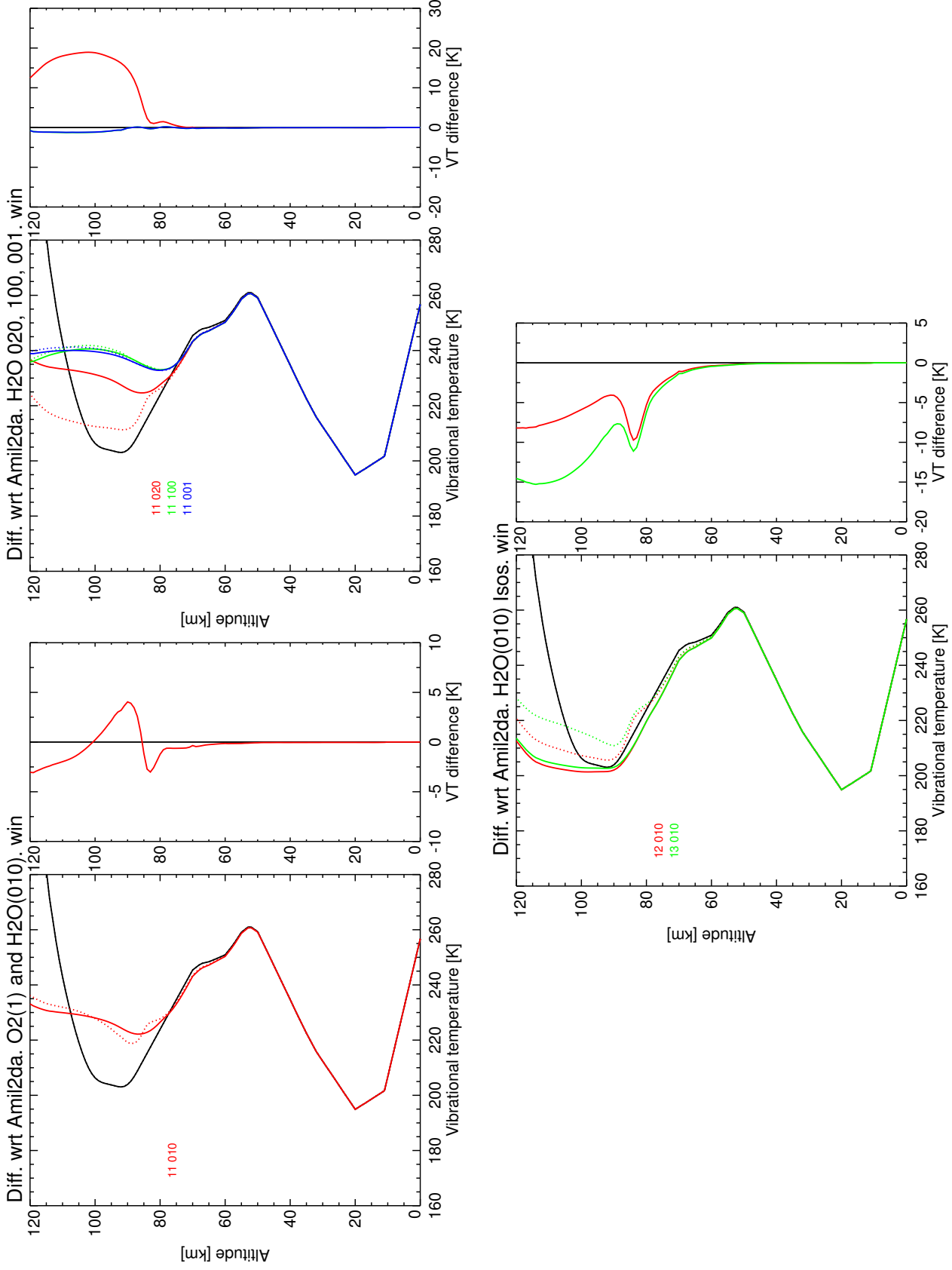


Figure 22: Differences in vibrational temperatures w.r.t. AMIL2DA, H_2O , for reference atmosphere #4, winter. Solid: this study; dash: AMIL2DA. Right panels: this study–AMIL2DA.

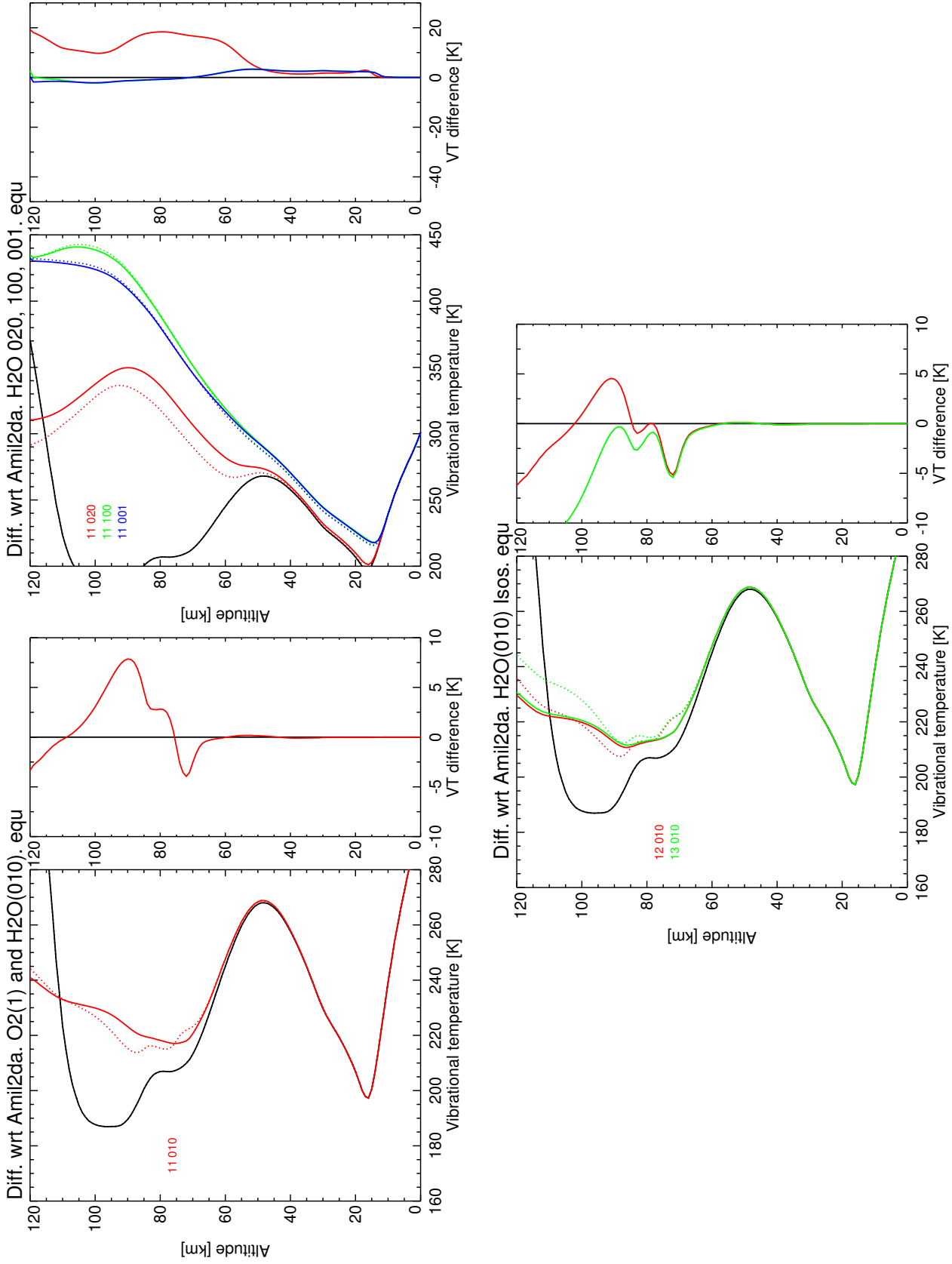


Figure 23: Differences in vibrational temperatures w.r.t. AMIL2DA H_2O , for reference atmosphere #5, equator. Solid: this study; dash: AMIL2DA. Right panels: this study-AMIL2DA.

3.3 CO₂

The vibrational temperatures of CO₂ levels have been significantly updated, benefiting from several studies of SABER and MIPAS data, as well as from other studies performed and available in the literature. In particular, from the MIPAS analysis of the CO₂ 4.3 μm emission (López-Puertas et al., 2005b); from the MIPAS analysis in the CO₂ 10 μm region using equivalent latitudes (López-Puertas, 2006a,b); from the study performed by Kutepov et al. (2006) about the effect of the exchange of v_2 quanta in CO₂-CO₂ collisions in the populations of the CO₂ 15 μm levels and subsequent effects on SABER temperature retrieval in the summer mesopause; from the new rate adopted for the CO₂(010)-O collisional rate, 2 times faster; and from the analysis of SABER CO₂ 4.3 μm nighttime radiance carried out by López-Puertas et al. (2004b). We discuss in some detail these studies below.

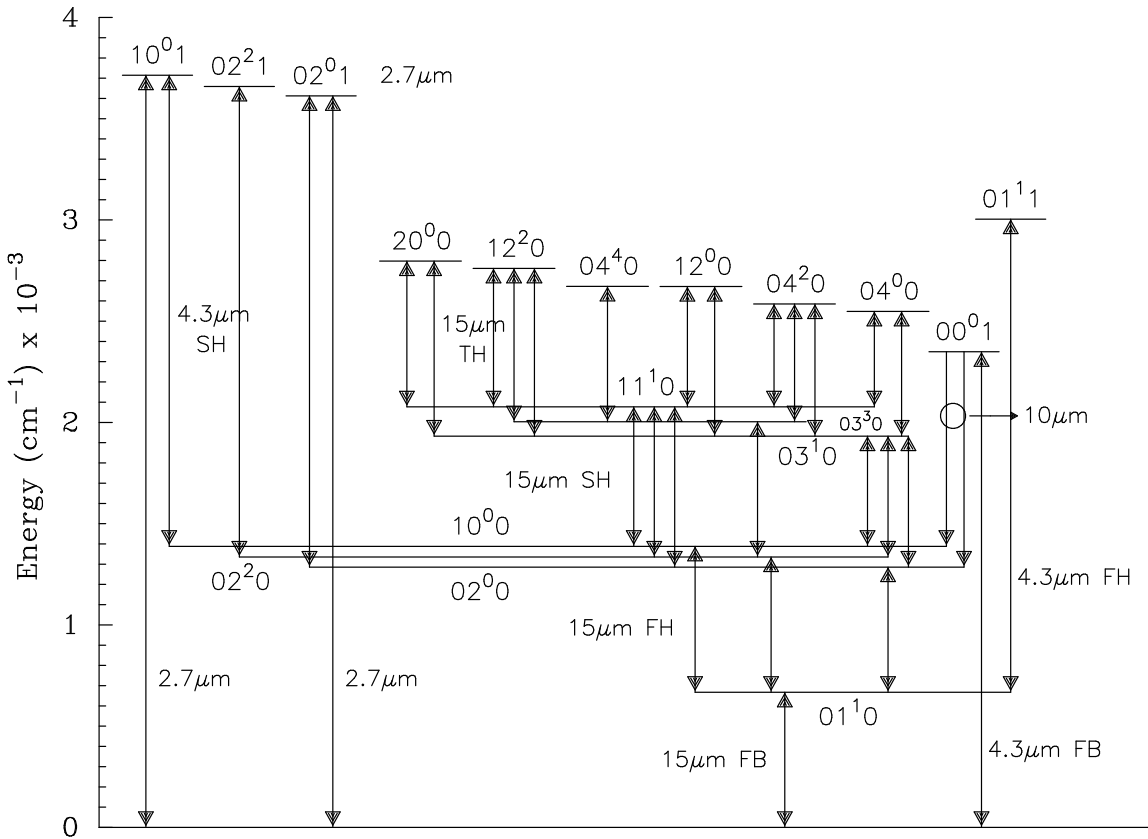
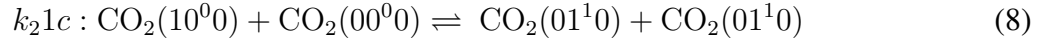
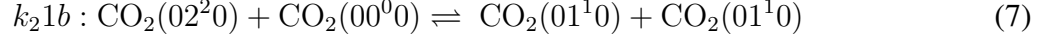
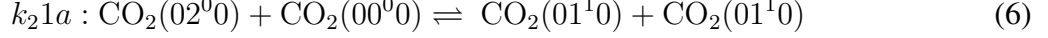


Figure 24: Energy levels diagram for CO₂.

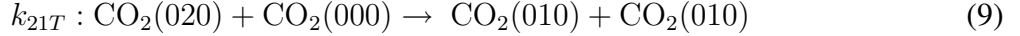
The collisional deactivation of CO₂(010) level by O is still a major uncertainty in the calculation of the populations of CO₂(010) in the upper atmosphere and lower thermosphere. There is a discrepancy of about a factor of 4 between the rates measured in the laboratory and those deduced from the analysis of atmospheric measurements (see, e.g., García-Comas et al., 2008). In this study we have changes the value used before of 3×10^{-12} to 6×10^{-12} at 300 K, maintaining its previous temperature dependency. The reason for the change is to use a value more in accordance to atmospheric measurements and that fact that the larger value is used in SABER temperatures. This would make easier any comparison and validation. We also use the same rate in the IAA/IMK temperatures retrievals from MIPAS MA and UA measurements.

Another aspect which has been deeply revised is the collisional vibrational-vibrational energy transfer (V-V) between in collisions of CO₂(0v20) with CO₂ⁱ(0,v2,0), where *i* stand for the different CO₂ isotopes. Two aspects have been upgraded. First, the exchange rate of *v*₂ quanta in CO₂-CO₂ VV collisions is now 2 times faster. Second, a new V-V *v*₂ collisional scheme has been included.

Regarding the first point, the measurements available for the CO₂ *v*₂ V-V energy transfer rates only refer to levels in the CO₂(020 group). These processes are:



or grouping all three levels (02⁰0, 02²0, and 10⁰0) in the 020 triad:



Seeber (1971) measured the rate for the process involving the whole 020 triad, and obtained $k_{21T} = 1.6 \times 10^{-11} \text{ cm}^3\text{s}^{-1}$. *Huddleston and Weitz*, (1981) also measured the rate for the process involving the whole 020 triad, and obtained $k_{21T} = 1.2 \times 10^{-11} \text{ cm}^3\text{s}^{-1}$. *Dang et al.*, (1983) measured the rates for the three processes involving each level in the triad, and obtained: $k_{21a} = 4.0 \times 10^{-12} \text{ cm}^3\text{s}^{-1}$, $k_{21b} = 4.7 \times 10^{-11} \text{ cm}^3\text{s}^{-1}$ and $k_{21c} = 4.0 \times 10^{-12} \text{ cm}^3\text{s}^{-1}$, i.e., the rate for the 02²0 level is about 20 times faster than for the 02⁰0 or 10⁰0 levels. Assuming LTE within the levels in the triad, that yields $k_{21T} = 2.55 \times 10^{-11} \text{ cm}^3\text{s}^{-1}$. *Orr and Smith* (1987), based on theoretical arguments, agreed with the values provided by *Dang et al.* (1983), corroborating that the values involving the 02²0 were significantly faster than those involving the 02⁰0 or 10⁰0 levels.

Those values have now been included in the model. In the previous version, we assumed the rate of *Dang et al.*, taken at 280 K and we only allowed VV exchange with the 01¹0 level of the 626 isotope.

The rates used for the inter-isotope V-V exchange, i.e., levels of the *i* and *j* isotopes,



are taken from those measurements but scaled using the harmonic oscillator law, i.e., $k_{11} = k_{21b}/v_2 = k_{21b}/2 = 2.35 \times 10^{-11} \text{ cm}^3\text{s}^{-1}$.

For the V-V exchange within a given isotope:



where $v_{2,e}$ represents the effective *v*₂ of the group (i.e. $v_{2,e} = 2v_1 + v_2$), we assume an energy gap law (to fit *Dang et al.*'s k_{21a} , k_{21b} , k_{21c}) together with the harmonic oscillator law:

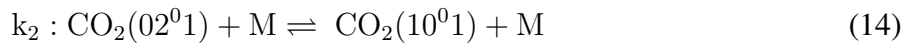
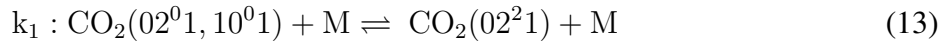
$$k_{VV}(v_{2,e}) = v_{2,e} 2.394 \times 10^{-11} \exp\left(\frac{-9.788 c_1 \Delta E}{T}\right). \quad (12)$$

The results of applying that expression to the different VV processes are listed in Table 5. These values have been calculated taking into account the measurements of *Dang et al.* (1983), consistent with the other rates discussed above.

Table 5: Collisional deactivation rates for CO₂-CO₂ V-V collisions for a given isotope.

Upper level	Lower level	Rate [cm ³ s ⁻¹]	Overall Rate
Group 020			
02 ⁰ 0	01 ¹ 0	4.0e-12	2.5e-11
02 ² 0	01 ¹ 0	4.7e-11	
10 ⁰ 0	01 ¹ 0	3.3e-12	
Group 030			
03 ¹ 0	02 ⁰ 0	2.6e-11	4.5e-11
03 ¹ 0	02 ² 0	2.1e-12	
03 ¹ 0	10 ⁰ 0	1.5e-13	
03 ³ 0	02 ⁰ 0	5.7e-12	
03 ³ 0	02 ² 0	6.9e-11	
03 ³ 0	10 ⁰ 0	5.2e-12	
11 ¹ 0	02 ⁰ 0	1.4e-13	
11 ¹ 0	02 ² 0	1.7e-12	
11 ¹ 0	10 ⁰ 0	2.5e-11	
Group 040			
04 ⁰ 0	03 ¹ 0	7.2e-12	5.4e-11
04 ⁰ 0	03 ³ 0	2.0e-13	
04 ⁰ 0	11 ¹ 0	5.0e-15	
04 ² 0	03 ¹ 0	4.5e-11	
04 ² 0	03 ³ 0	1.3e-12	
04 ² 0	11 ¹ 0	3.2e-14	
12 ⁰ 0	03 ¹ 0	2.7e-12	
12 ⁰ 0	03 ³ 0	9.3e-11	
12 ⁰ 0	11 ¹ 0	2.4e-12	
04 ⁴ 0	03 ¹ 0	2.6e-12	
04 ⁴ 0	03 ³ 0	9.1e-11	
04 ⁴ 0	11 ¹ 0	2.5e-12	
12 ² 0	03 ¹ 0	2.9e-14	
12 ² 0	03 ³ 0	1.0e-12	
12 ² 0	11 ¹ 0	4.2e-11	
20 ⁰ 0	03 ¹ 0	4.7e-15	
20 ⁰ 0	03 ³ 0	1.6e-13	
20 ⁰ 0	11 ¹ 0	6.7e-12	

New rates for the relaxation of CO₂ 2.7μm Fermi levels obtained from the analysis of MIPAS spectra has been included (López-Puertas et al., 2005b). In particular for the processes



we were using rates of 1.5×10⁻¹³ and 3×10⁻¹¹ cm³s⁻¹, respectively. These rates have been up-

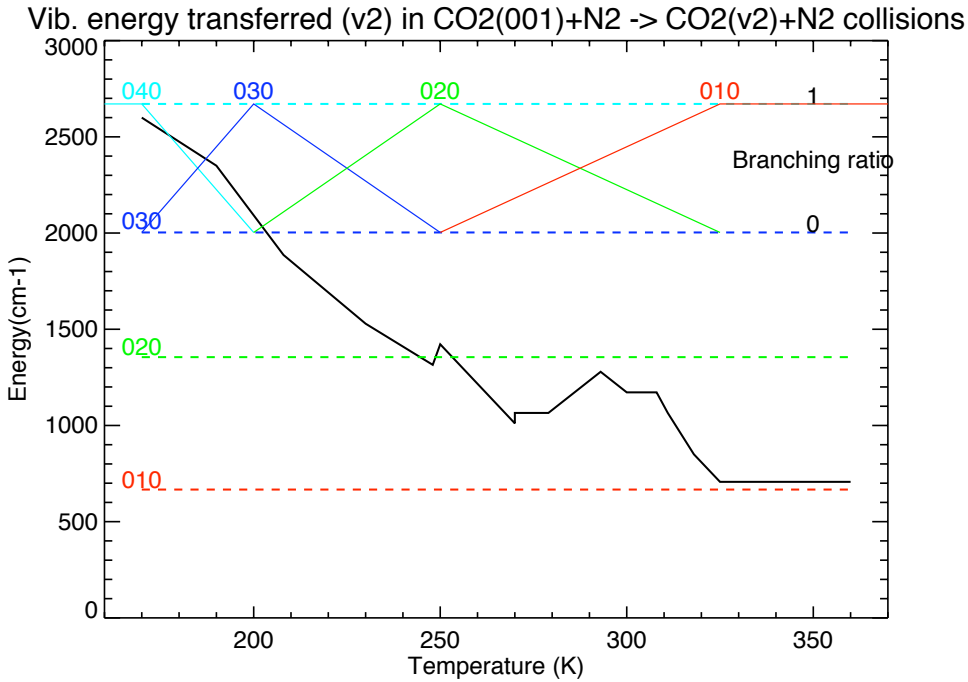
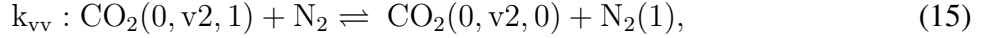


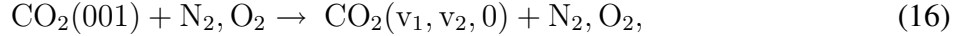
Figure 25: Collisional deactivation of $\text{CO}_2(001)$ into $\text{CO}_2(v_2=1-4)$ levels.

dated to the values found in the MIPAS analysis of 5.5×10^{-13} and $1.9 \times 10^{-13} \text{ cm}^3 \text{s}^{-1}$, respectively. Analogously, in the same study, we found for the V-V coupling of $\text{CO}_2(v_3)$ with N_2 ,



the values of $k_{vv}(v_2=0,1,3) = 5.0 \times 10^{13}$ and $k_{vv}(v_2=2,4) = 6.5 \times 10^{-13} \text{ cm}^3 \text{s}^{-1}$. These values have also been included in this study. Previously we were using a common value of $5.0 \times 10^{-13} \text{ cm}^3 \text{s}^{-1}$ regardless of the v_2 excitation of the $\text{CO}_2(0, v_2, 1)$ level.

A new relaxation scheme for the relaxation of $\text{CO}_2(001)$ in collisions with N_2 and O_2 :



has been included (see Fig. 25). This has very important consequences for the population of $\text{CO}_2(001)$ in the mesosphere.

The temperature dependence for the rates of the collisional relaxation of $\text{CO}_2(0v_20)$ with N_2 and O_2 was included in previous studies as shown in Figs. 26 and 27. However, below 150 K no measurements were reported and the extrapolated values from measurements at higher temperatures (as shown in those figures) resulted in very cold temperatures retrievals around the polar summer mesopause. Hence the rates in those figures were included in this study except at temperatures below 150 K, where a constant value of $1.0 \times 10^{-15} \text{ cm}^3 \text{s}^{-1}$ was assumed.

We have also included the larger excitation (by a factor of 3) of the $\text{CO}_2(001)$ level at night, through V-V energy transfer with $\text{N}_2(1)$, from the OH(v) vibrationally excited (López-Puertas

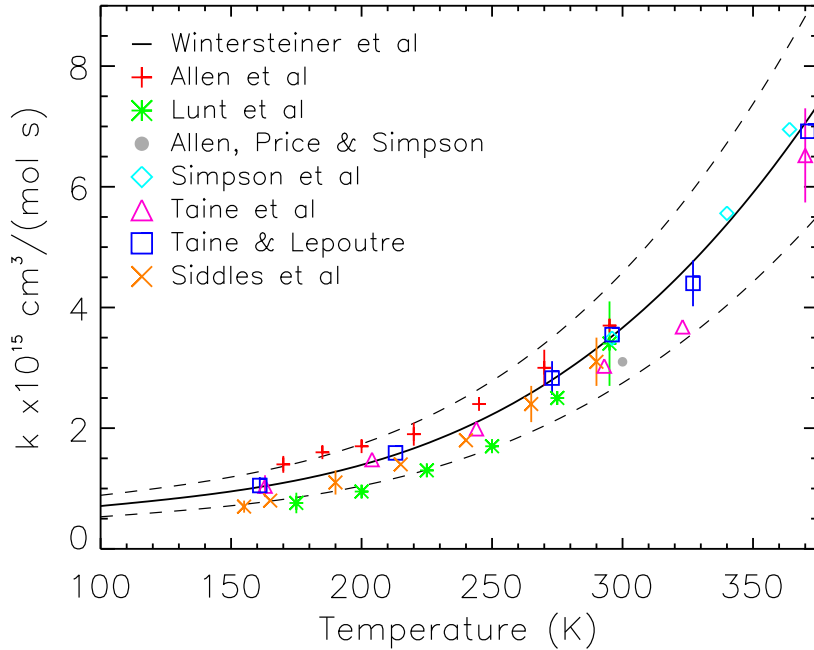


Figure 26: Temperature dependence of the collisional deactivation of CO₂(0v20) by N₂.

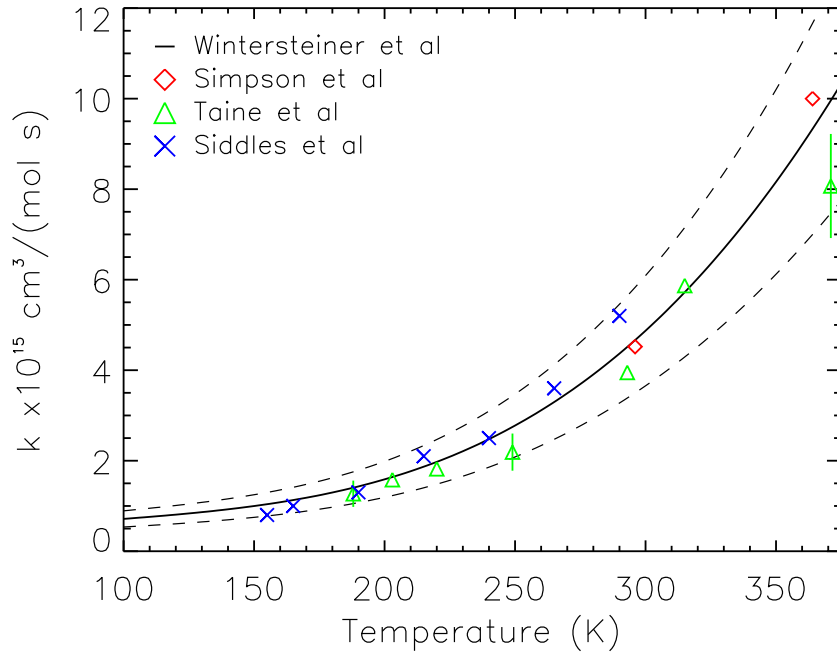


Figure 27: Temperature dependence of the collisional deactivation of CO₂(0v20) by O₂.

et al., 2004). This leads to larger populations of the CO₂(001) level in the mesosphere during nighttime conditions.

The model has also been extended to many vibrational levels in the 15 μm and 2.0 μm regions

(see below).

Figures 28-42 shows the vibrational temperatures for the CO₂ energy levels from the lowest energy (15 μm) to higher (2.0 μm), and also for the isotopes included, for the five reference atmospheres.

Figures 43-57 shows the differences in the vibrational temperatures for the CO₂ energy levels with respect to previous version for all reference atmospheres. The major differences can be summarized in:

- One of the major differences is the extension of the calculations of vibrational temperatures to a much larger number of vibrational states, including:
 - 26 energy levels of (050), (060) and (070) of the CO₂ major isotope (see Fig. 28), top right;
 - 6 levels of (040) for the 636 isotope (see Fig. 28), bottom right;
 - 19 levels of high energy, of the type (031), (042), (051) and (061) (see Fig. 29), bottom left;
 - 10 levels of high energy of type (012), (022), and (032) (see Fig. 29), bottom right; and
 - 11 energy levels of type (021), (031), (041) and (011) of some minor isotopes (see Fig. 30).
- Larger vibrational temperatures for CO₂(v₂) levels at higher altitudes because of the larger k(CO₂(010)-O) collisional deactivation rate.
- CO₂(001) is more populated now in the daytime mesosphere because of weaker collisional reaction of CO₂(001) with M (N₂ and O₂) to relax to lower CO₂ v₂=1, 2, 3, 4 levels.
- Because of the process above, the CO₂(040) levels have also changed significantly their vibrational temperatures in the daytime mesosphere, being now significantly smaller.
- The vibrational temperatures of the 15 μm hot and isotopic levels in the summer mesopause are generally smaller because of the larger $k_{vv}(v_2)$ value used now.

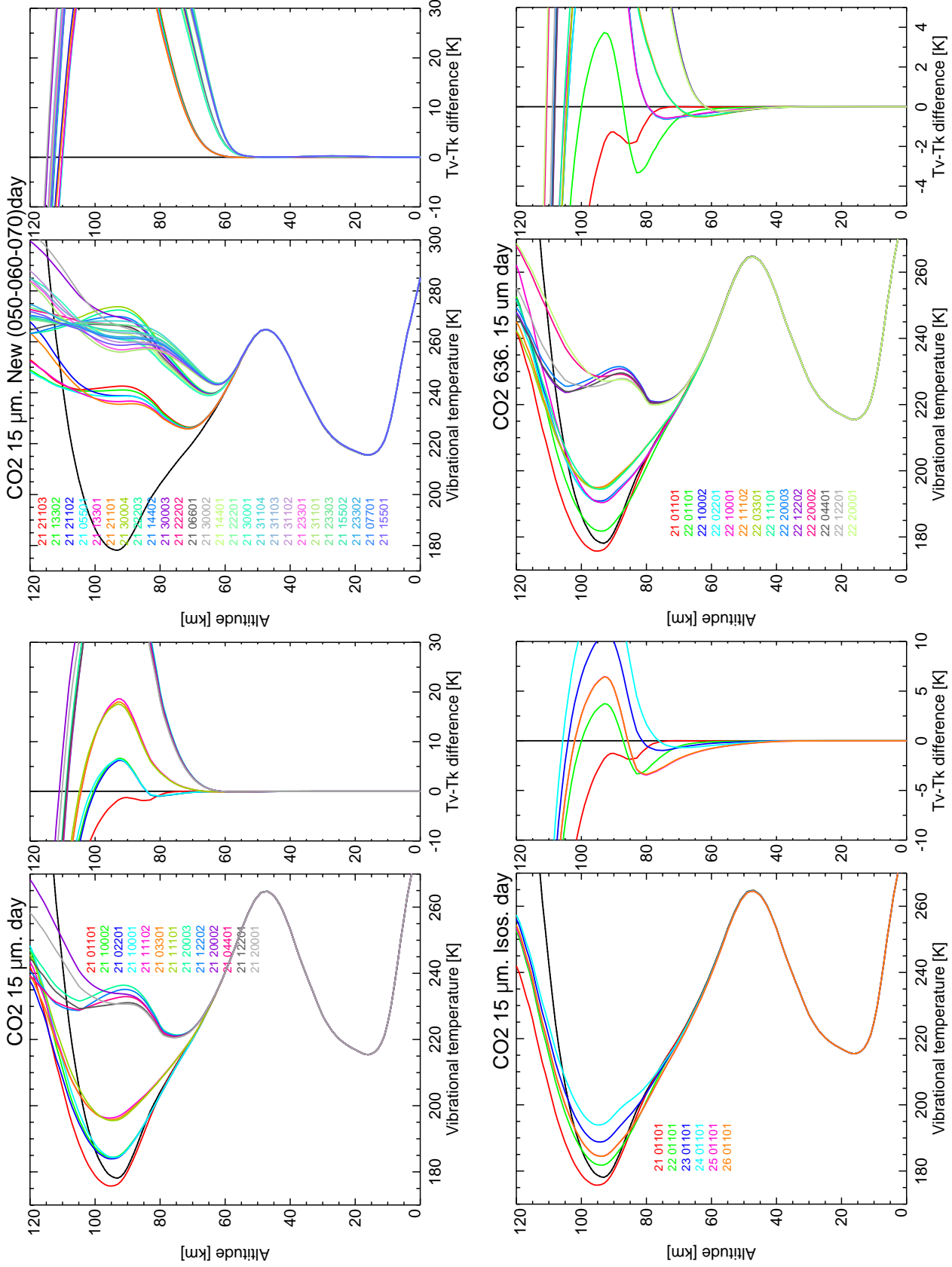


Figure 28: Vibrational temperatures for CO_2 15 μm levels, for reference atmosphere #1, day.

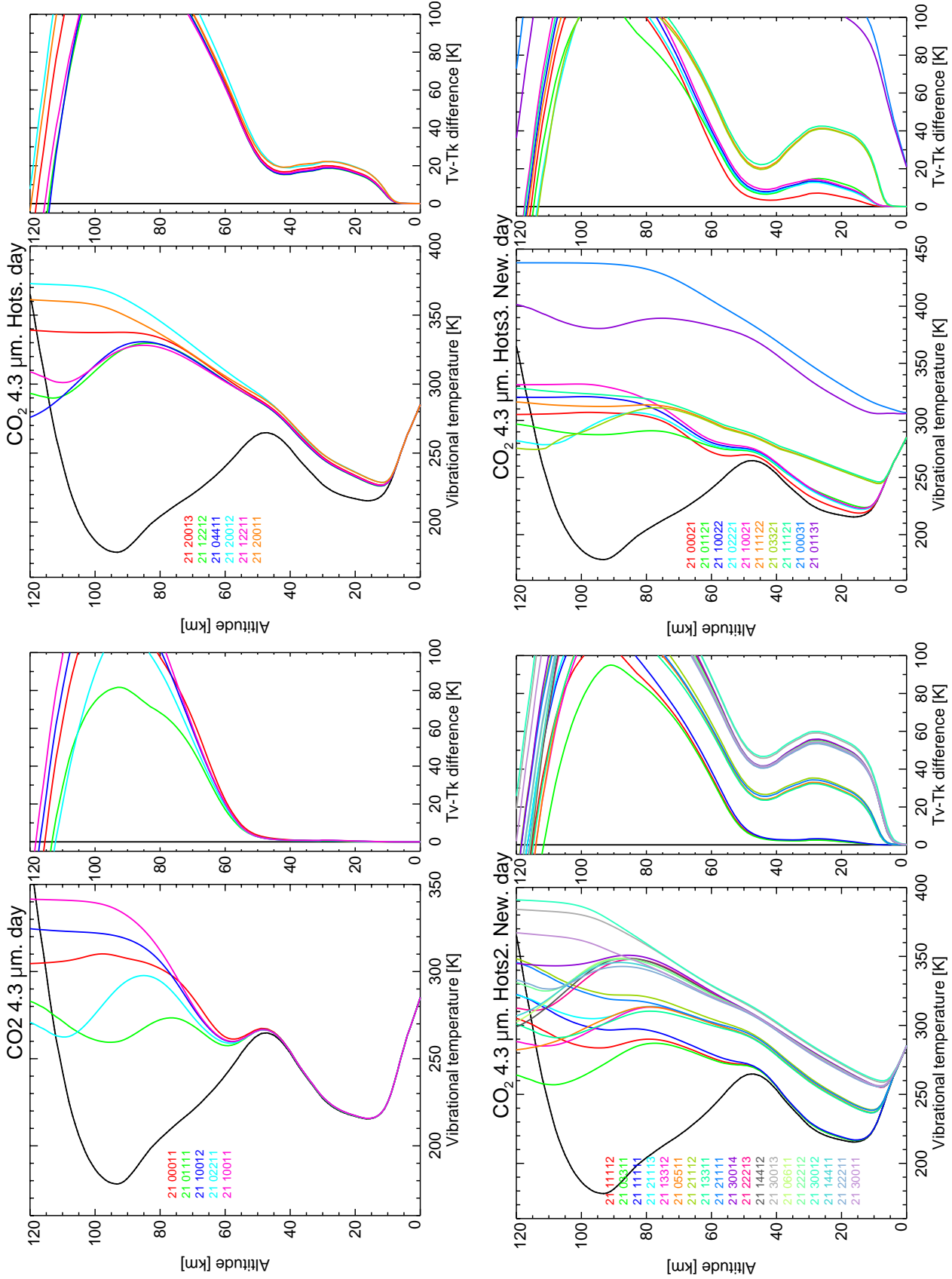


Figure 29: Vibrational temperatures for CO_2 4.3 μm levels, for reference atmosphere #1, day.

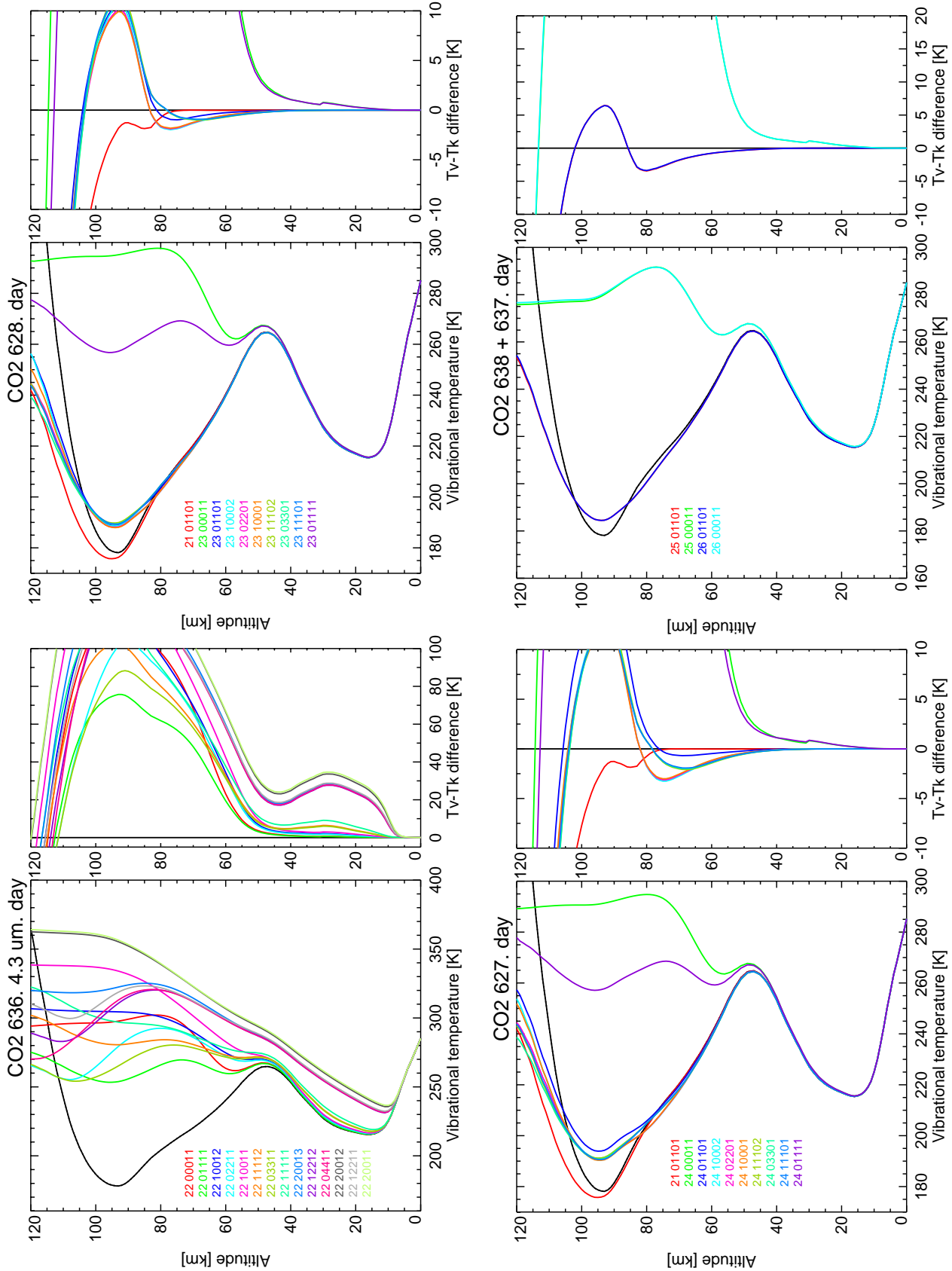


Figure 30: Vibrational temperatures for CO₂ isotopic levels, for reference atmosphere #1, day.

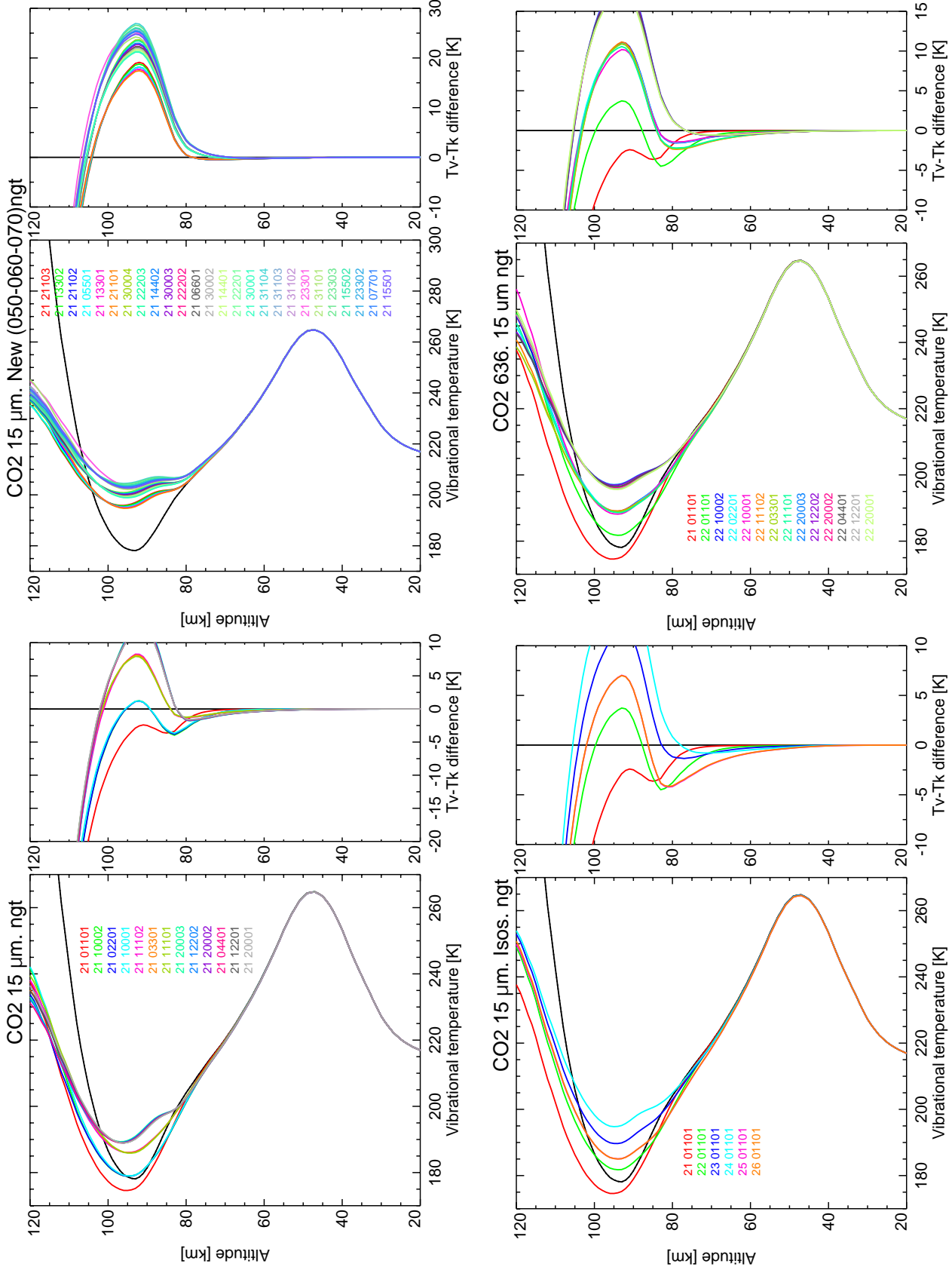


Figure 31: Vibrational temperatures for CO₂ 15 μm levels, for reference atmosphere #2, night.

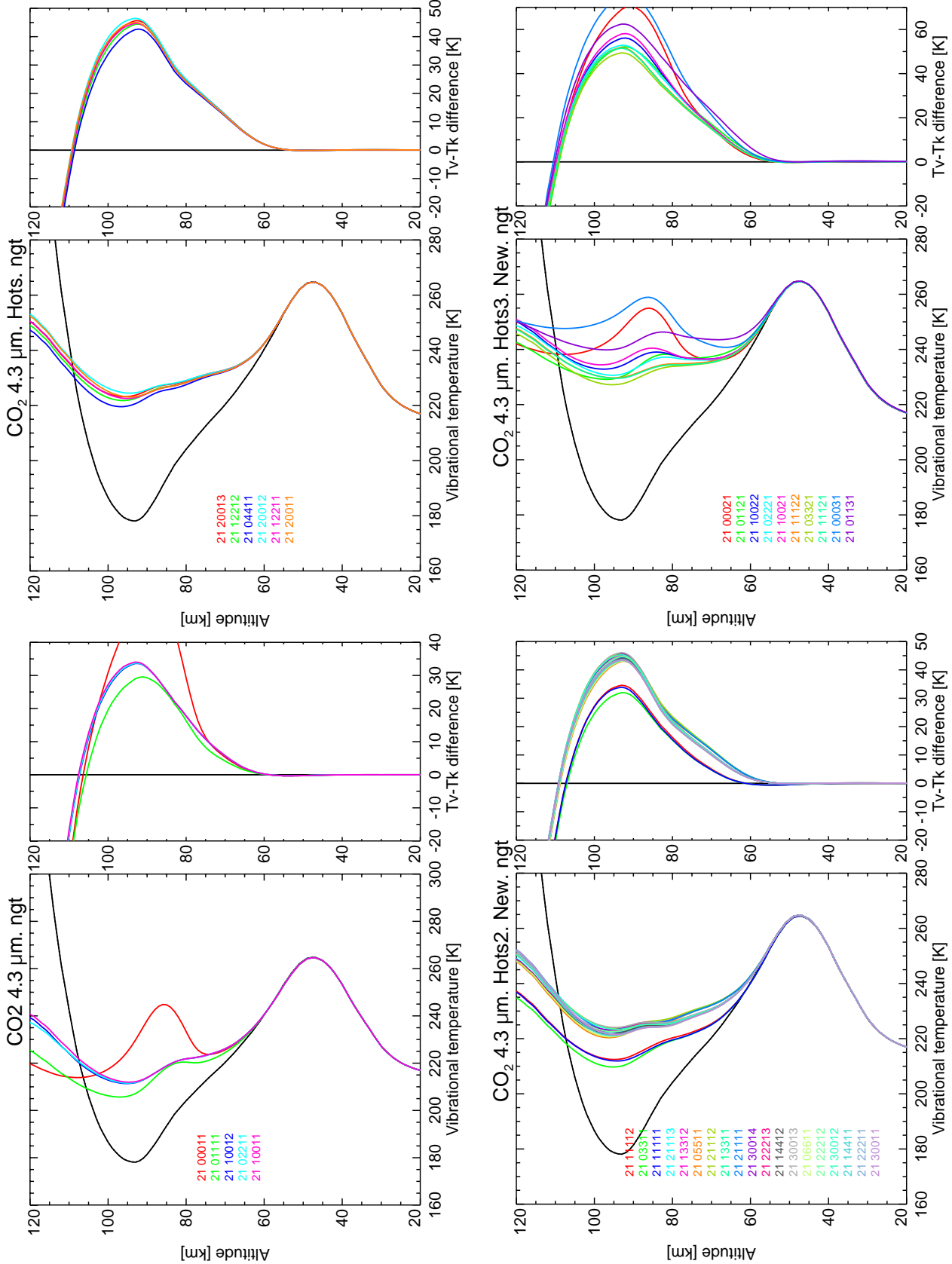


Figure 32: Vibrational temperatures for CO_2 4.3 μm levels, for reference atmosphere #2, night.

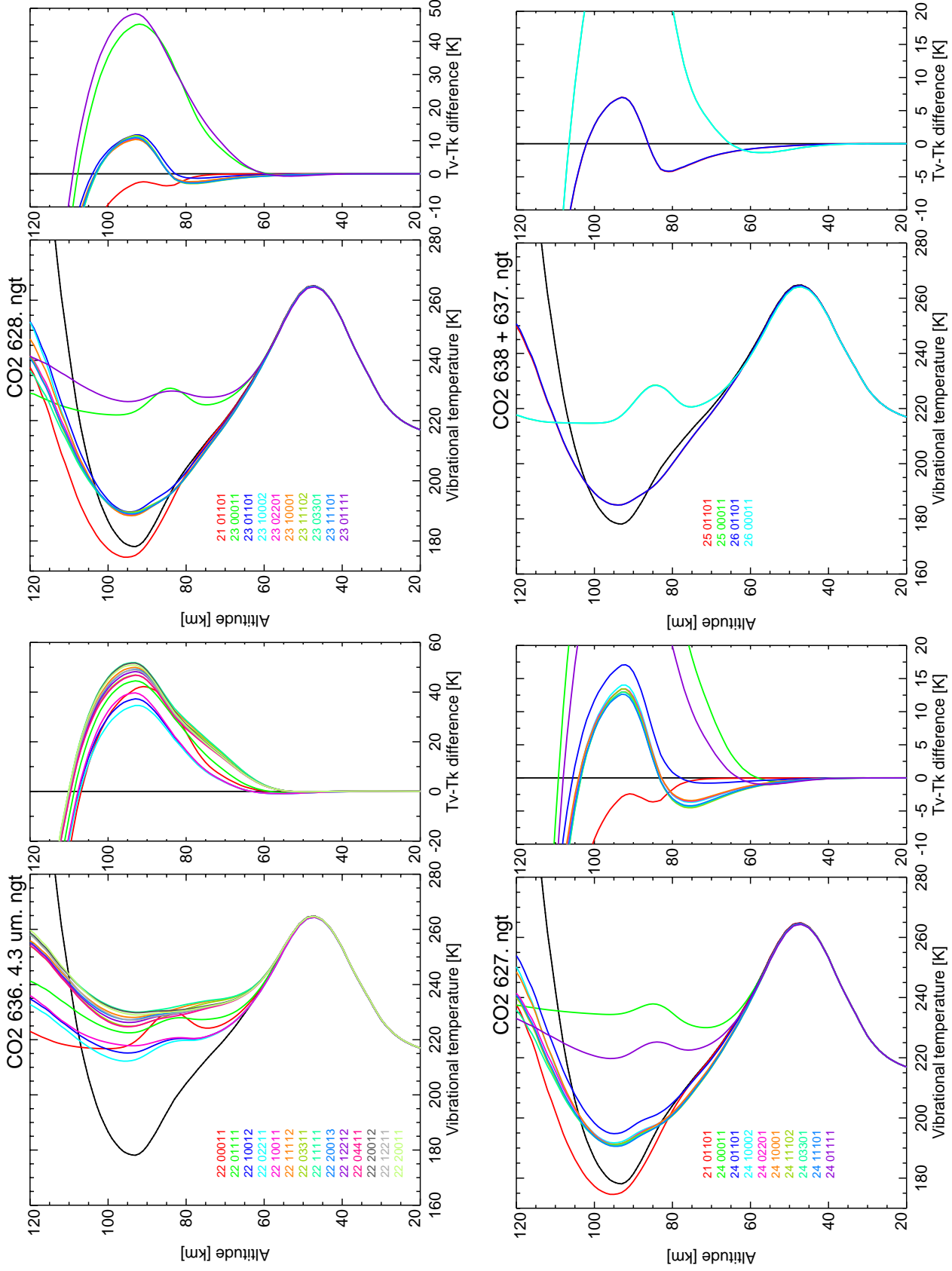


Figure 33: Vibrational temperatures for CO₂ isotopic levels, for reference atmosphere #2, night.

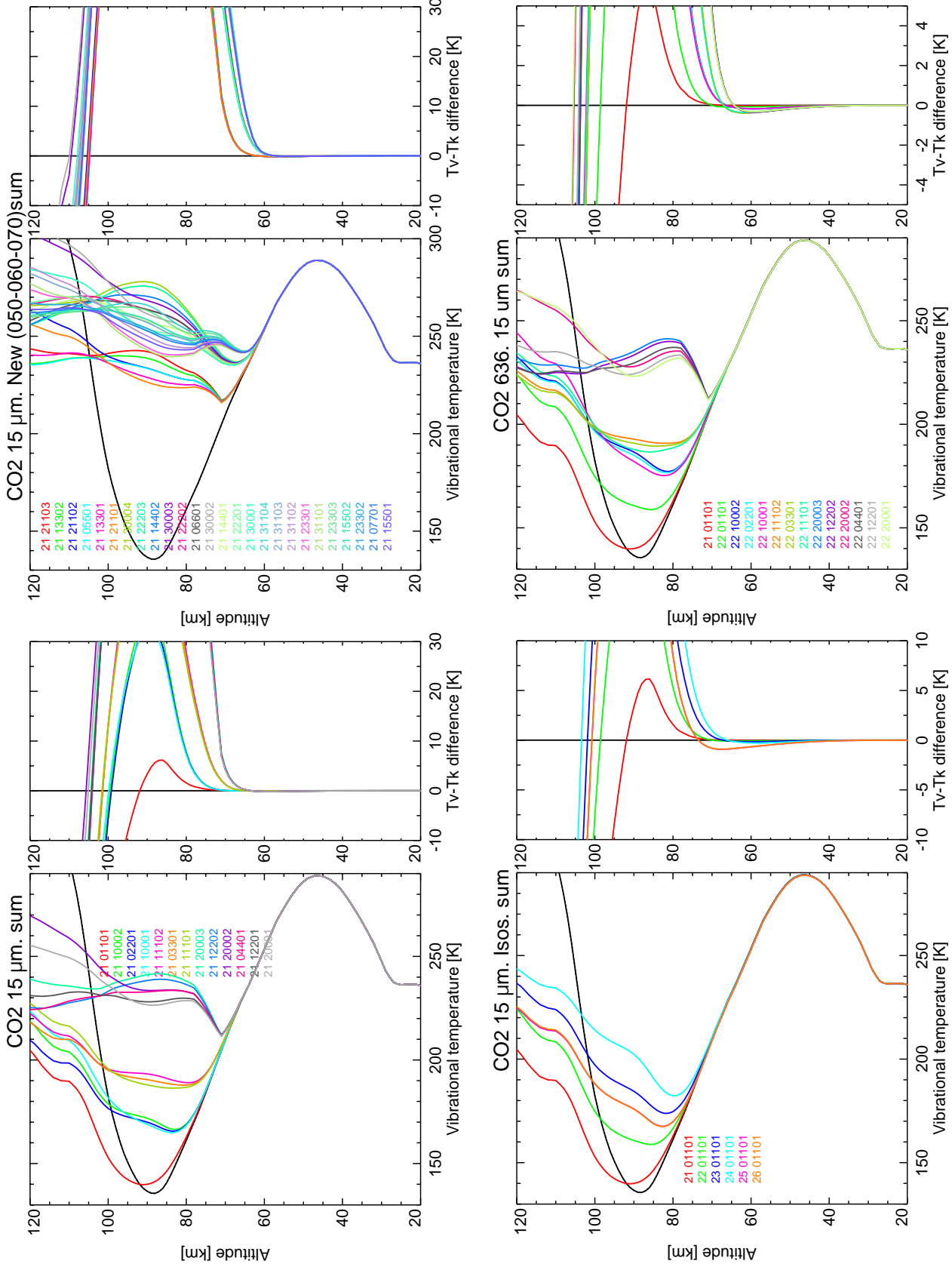


Figure 34: Vibrational temperatures for CO_2 15 μm levels, for reference atmosphere #3, summer.

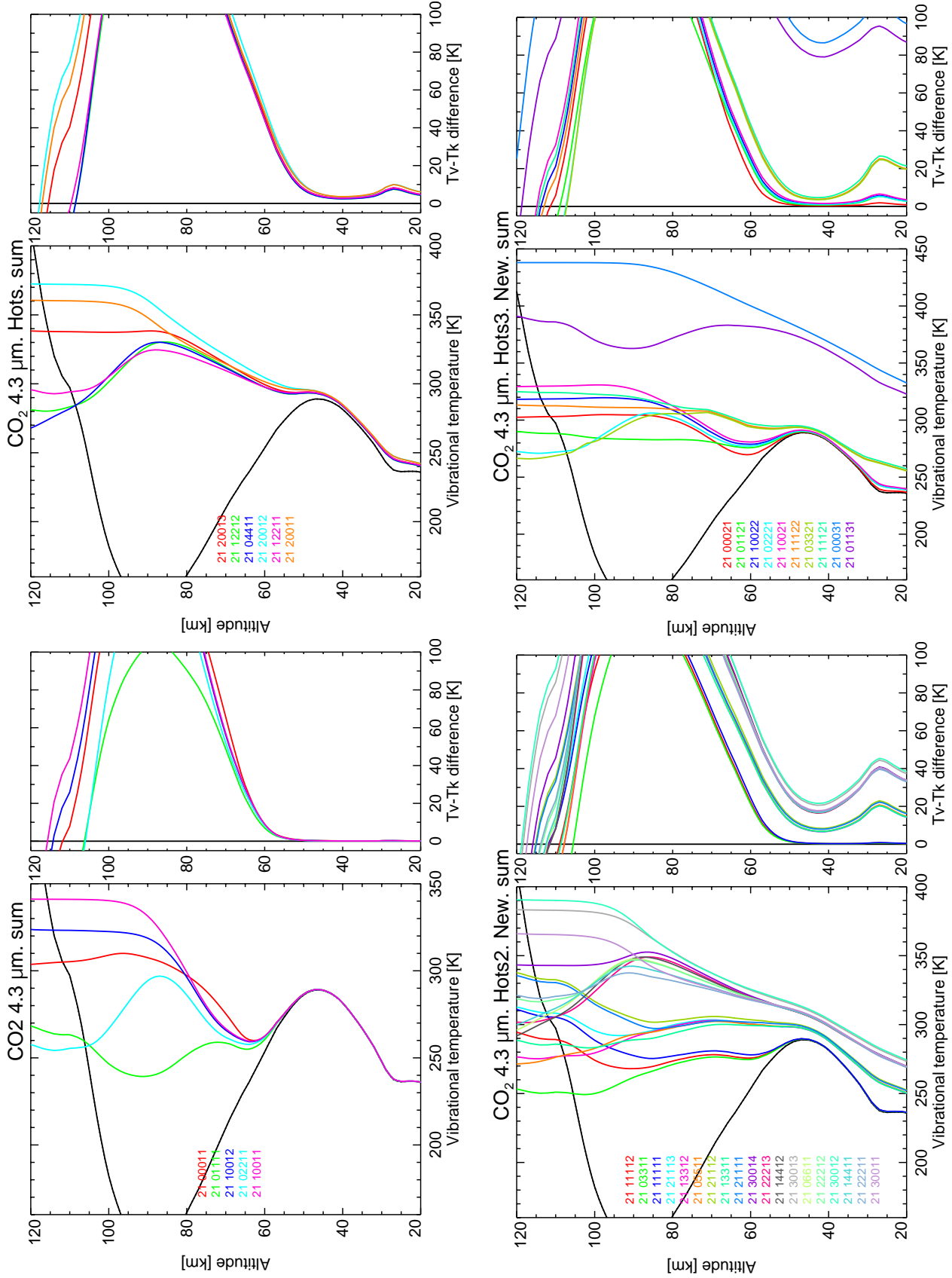


Figure 35: Vibrational temperatures for CO_2 4.3 μm levels, for reference atmosphere #3, summer.

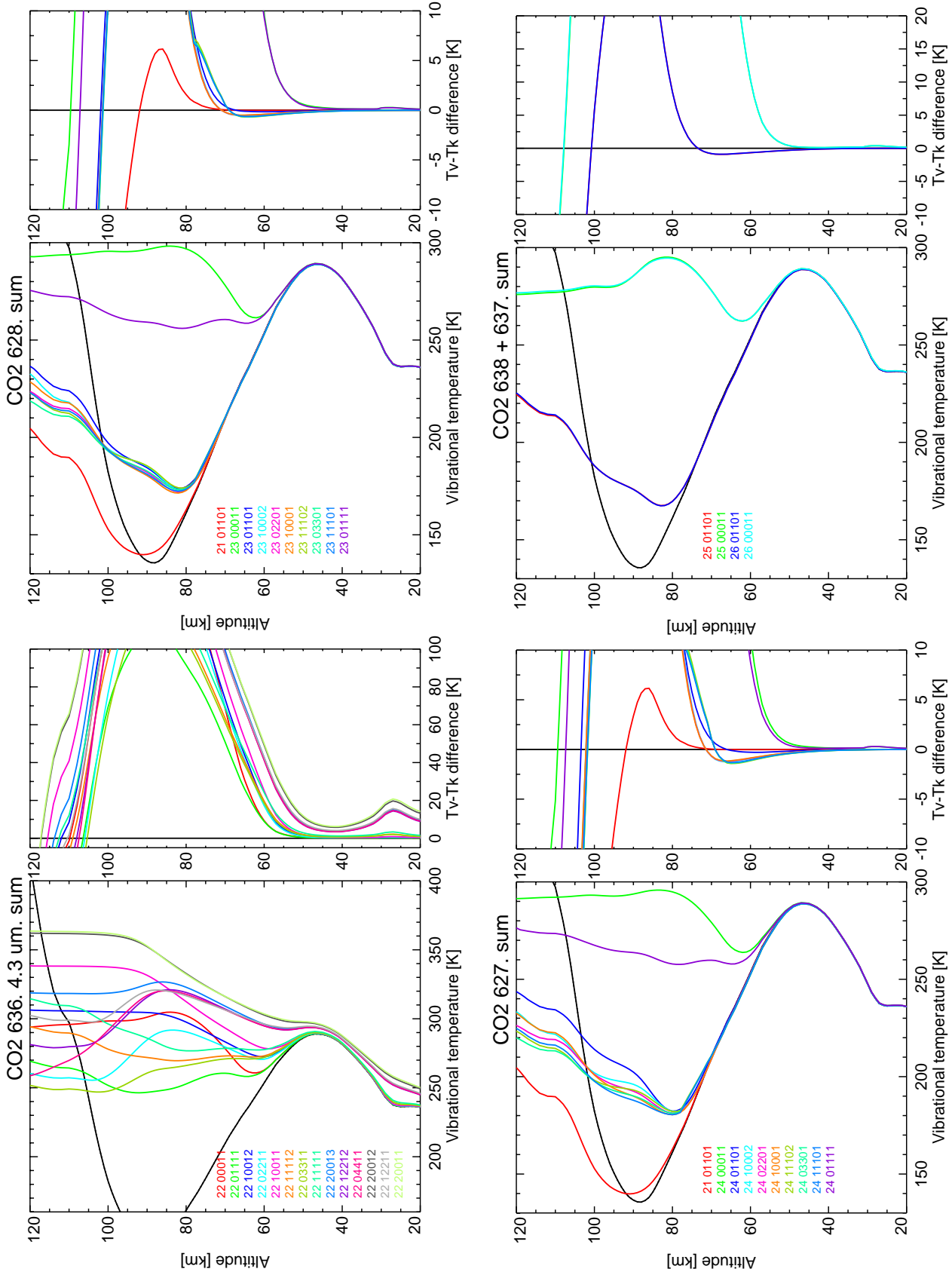


Figure 36: Vibrational temperatures for CO₂ isotopic levels, for reference atmosphere #3, summer.

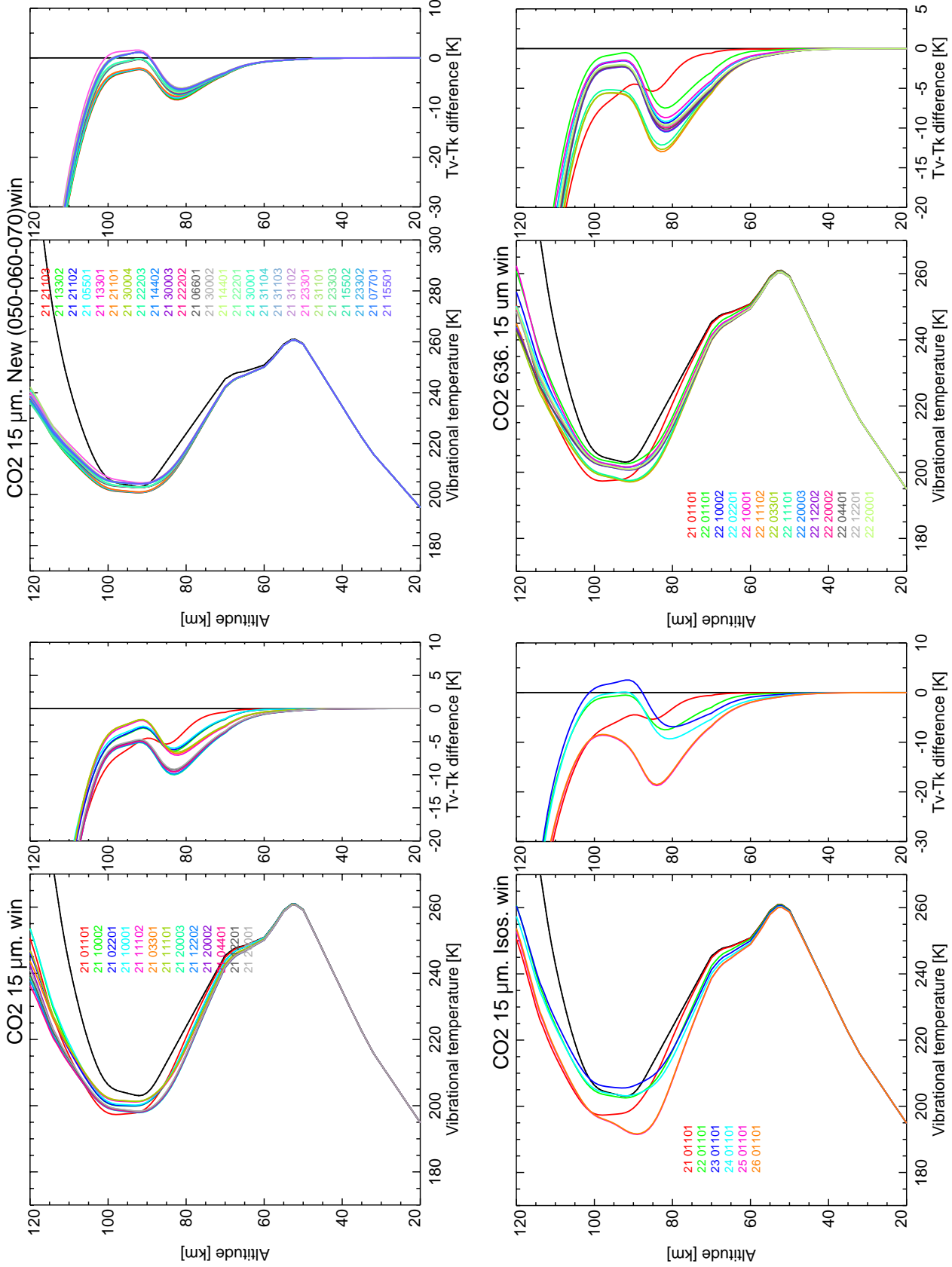


Figure 37: Vibrational temperatures for CO₂ 15 μm levels, for reference atmosphere #4, winter.

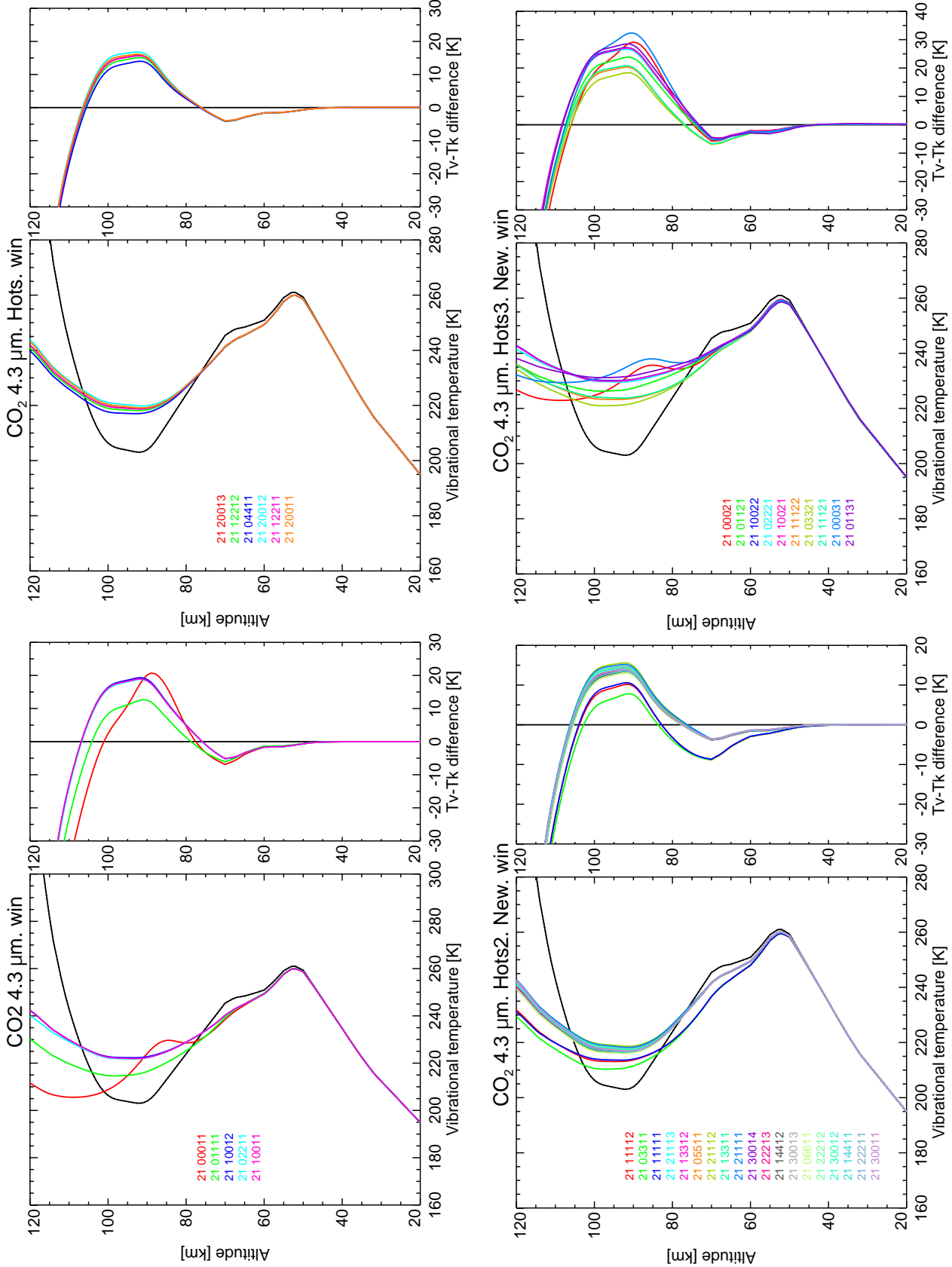


Figure 38: Vibrational temperatures for CO_2 4.3 μm levels, for reference atmosphere #4, winter.

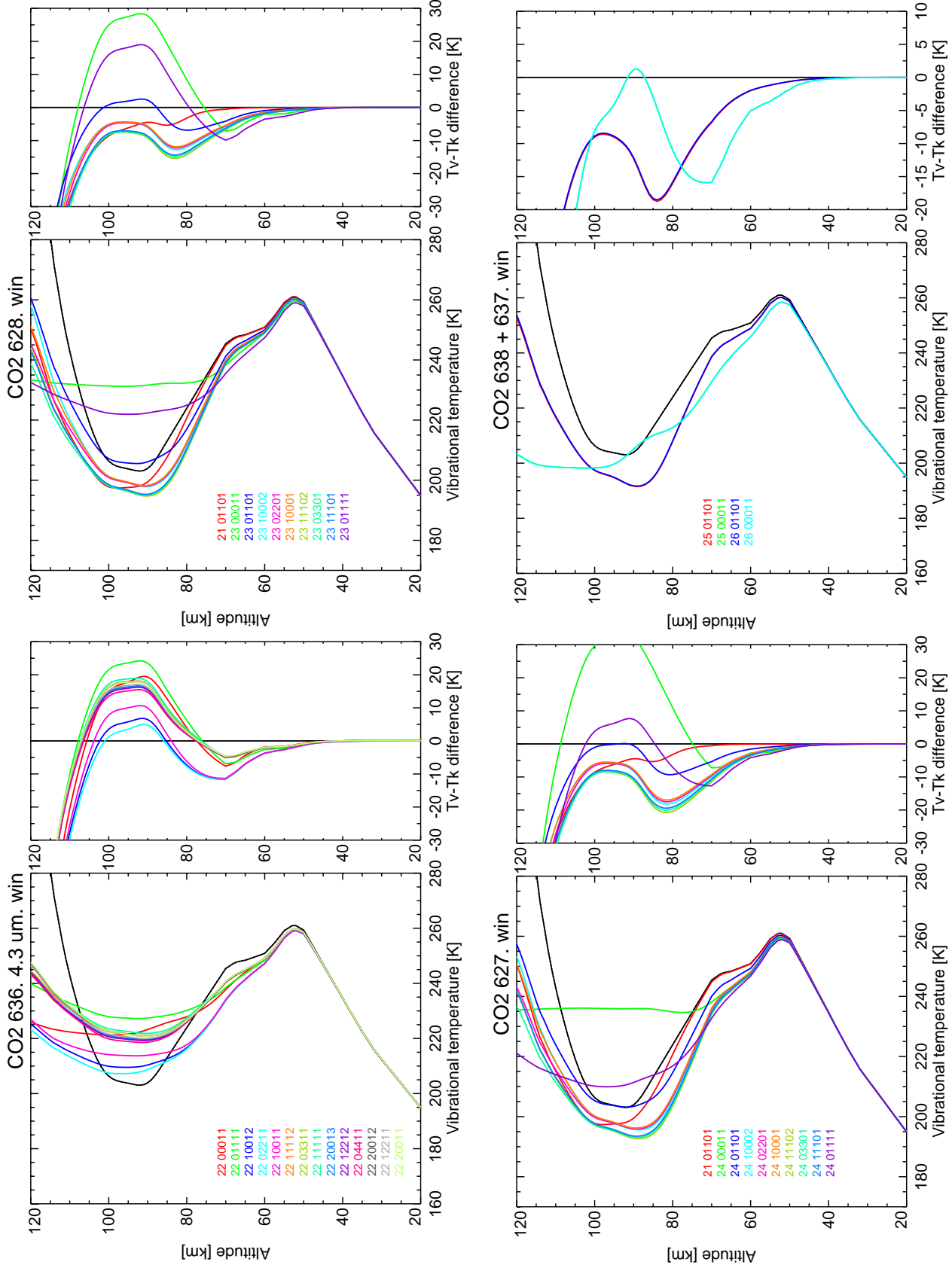


Figure 39: Vibrational temperatures for CO_2 isotopic levels, for reference atmosphere #4, winter.

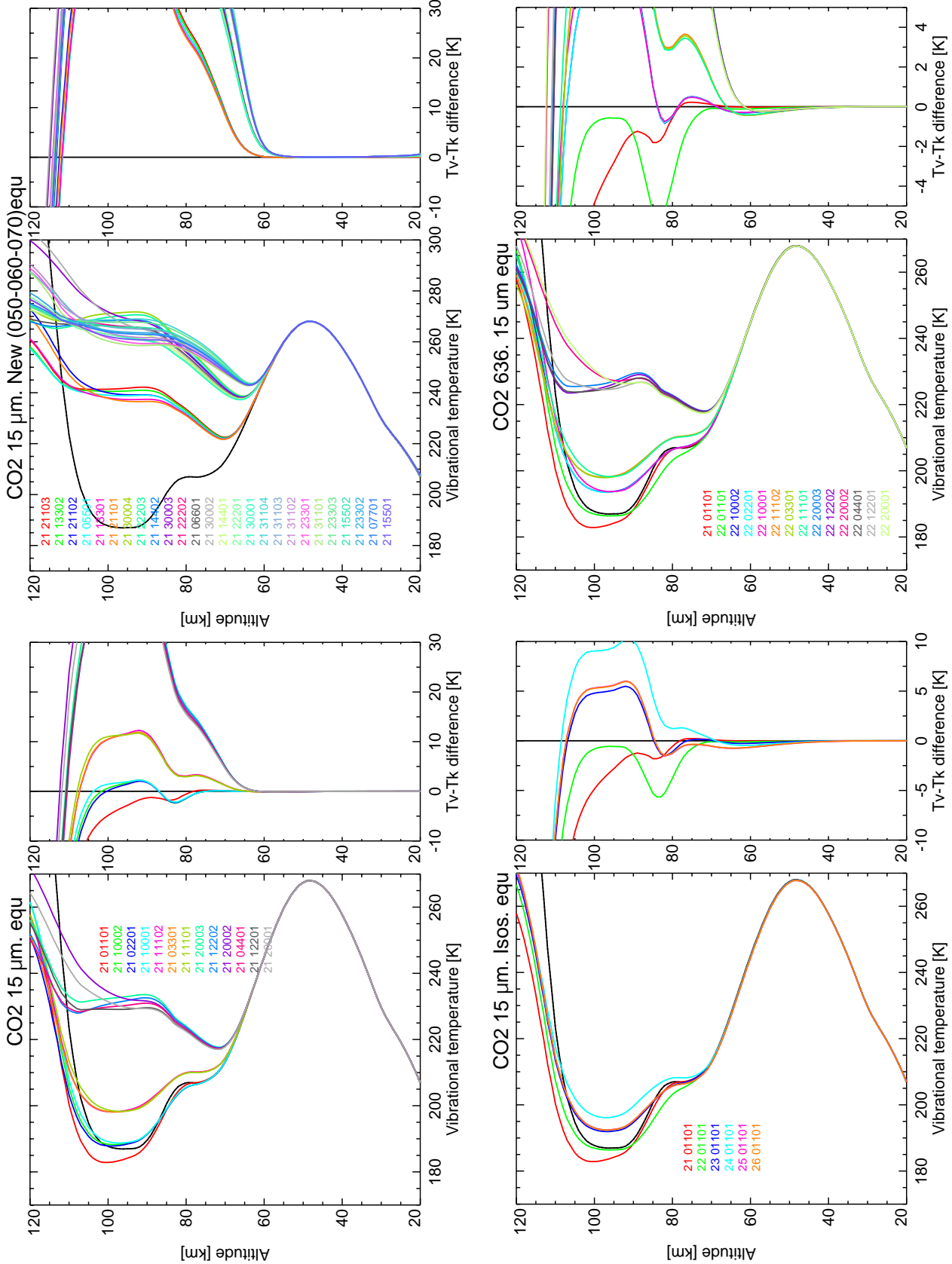


Figure 40: Vibrational temperatures for CO_2 15 μm levels, for reference atmosphere #5, equator.

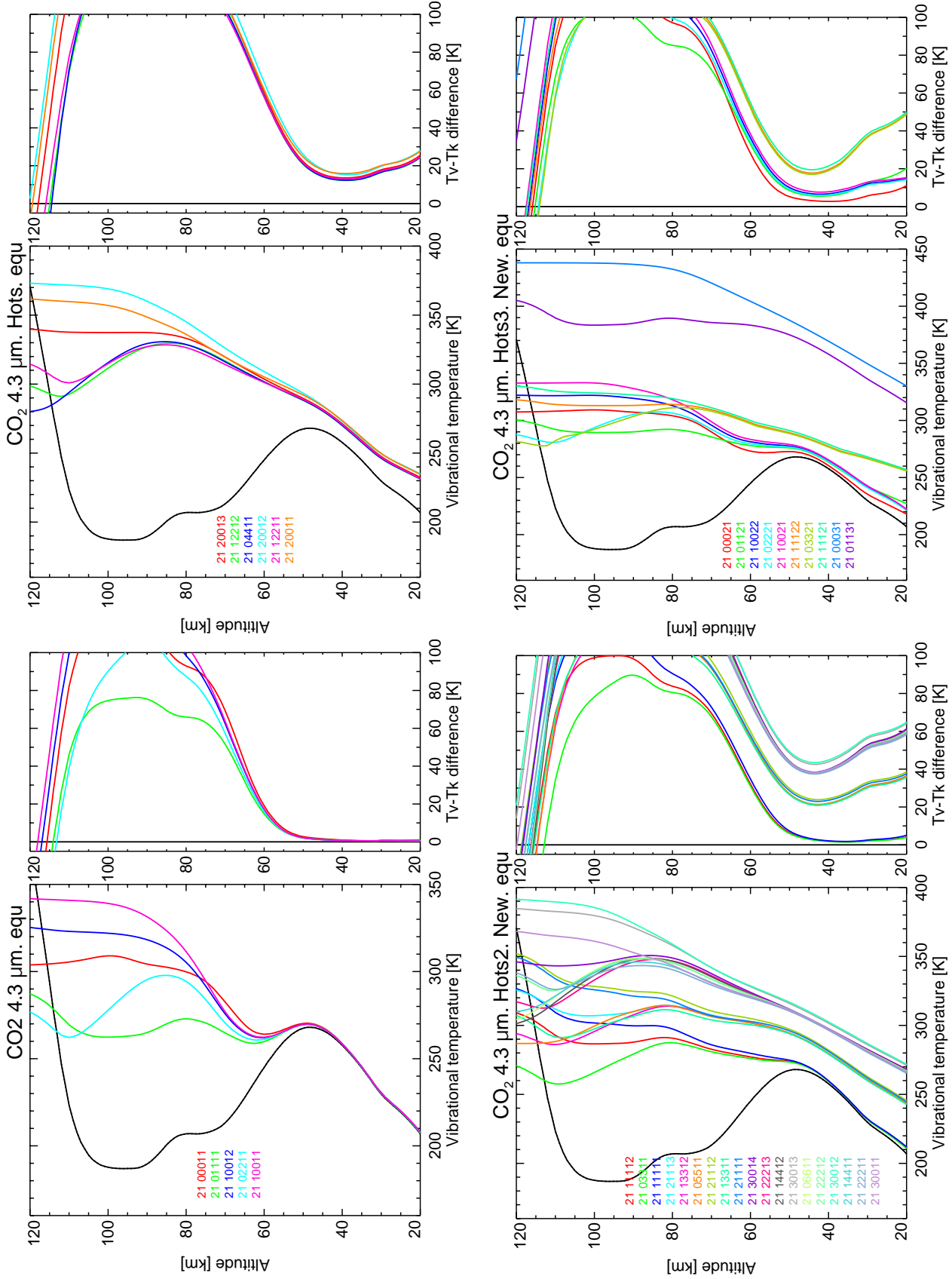


Figure 41: Vibrational temperatures for $\text{CO}_2 4.3 \mu\text{m}$ levels, for reference atmosphere #5, equator.

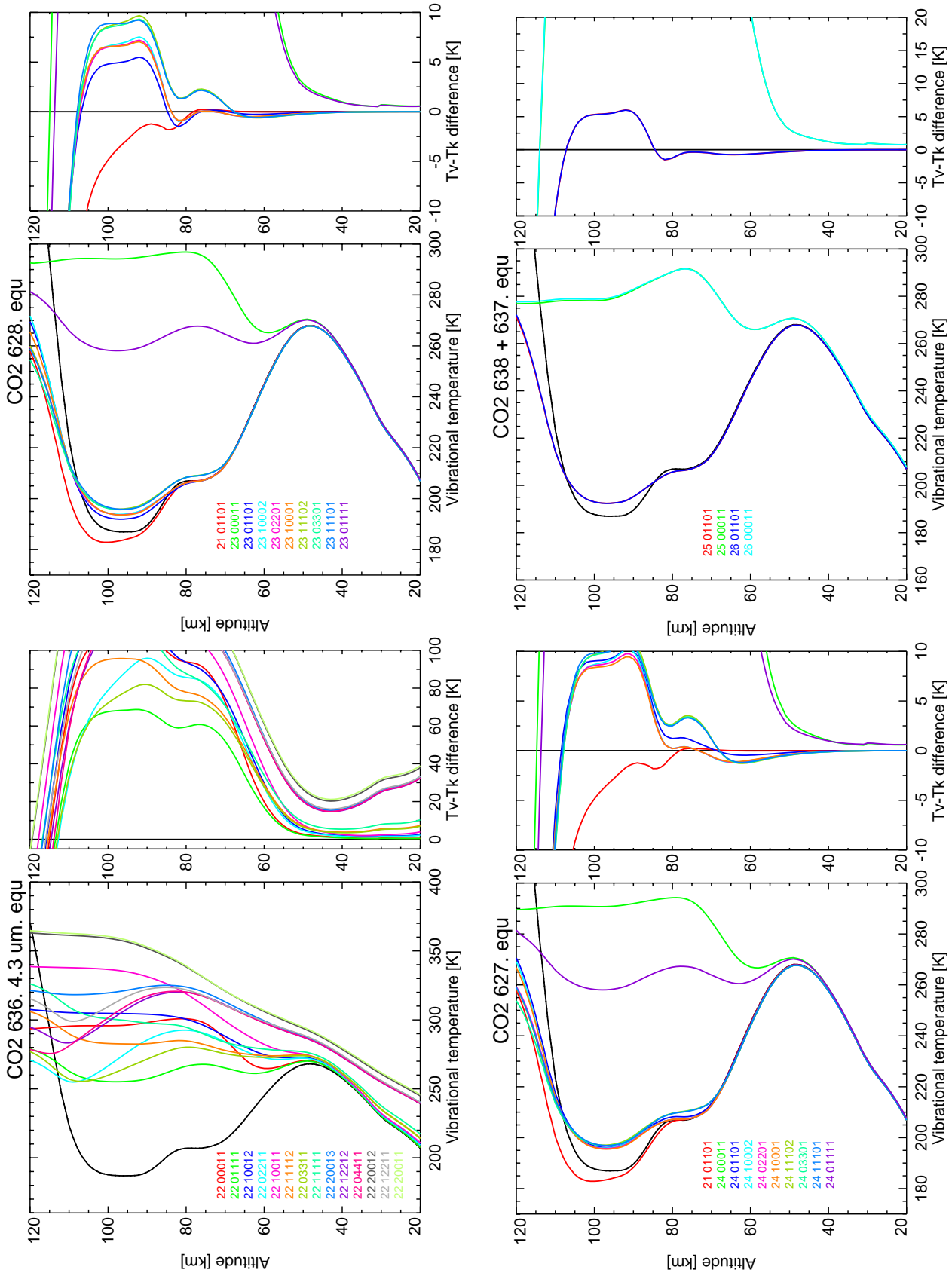


Figure 42: Vibrational temperatures for CO₂ isotopic levels, for reference atmosphere #5, equator.

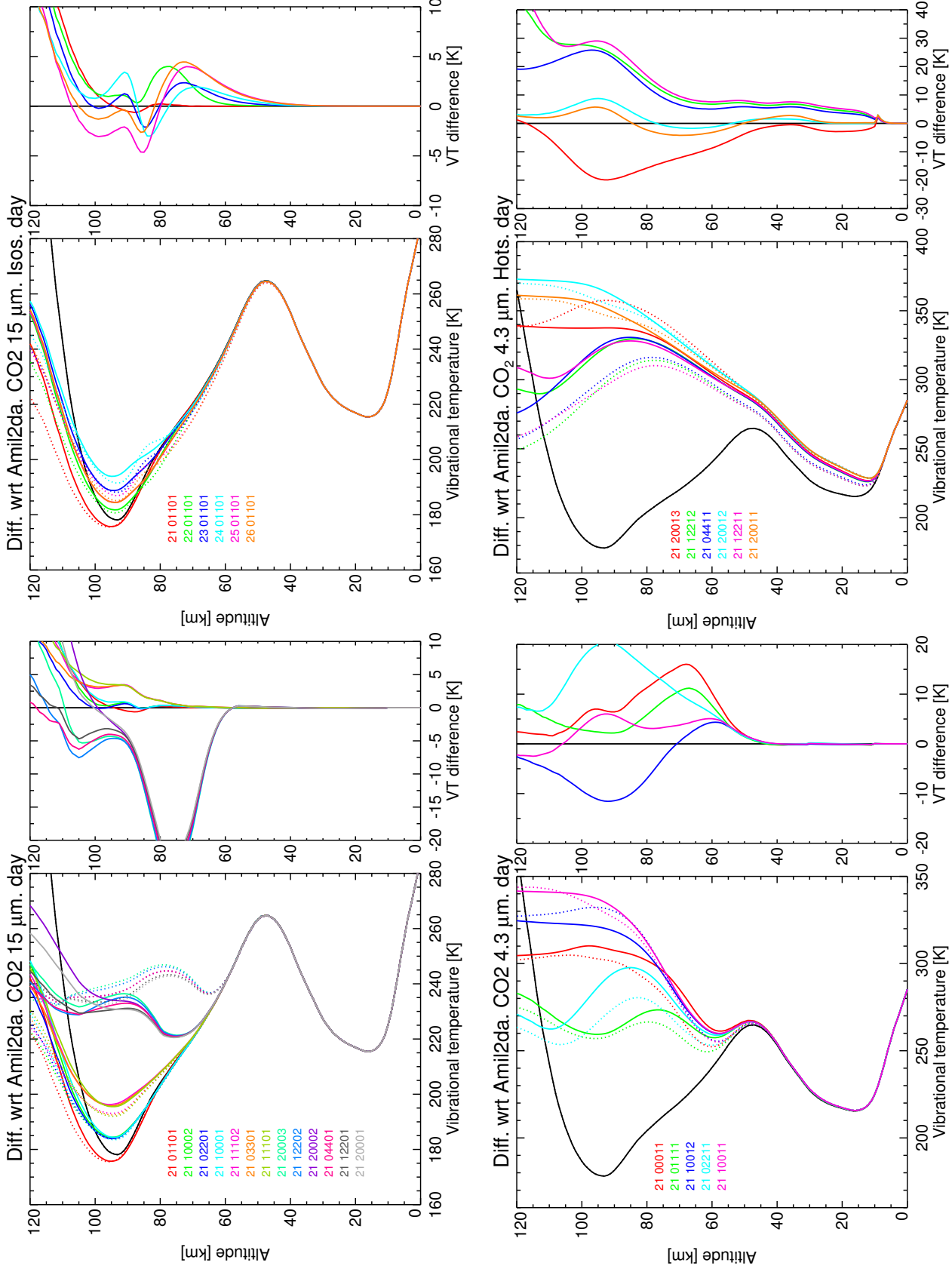


Figure 43: Differences in vibrational temperatures w.r.t. previous version (AMIL2DA) for CO₂ main isotope, for reference atmosphere #1, day. Solid: this study; dash: AMIL2DA. Right panels: this study–AMIL2DA.

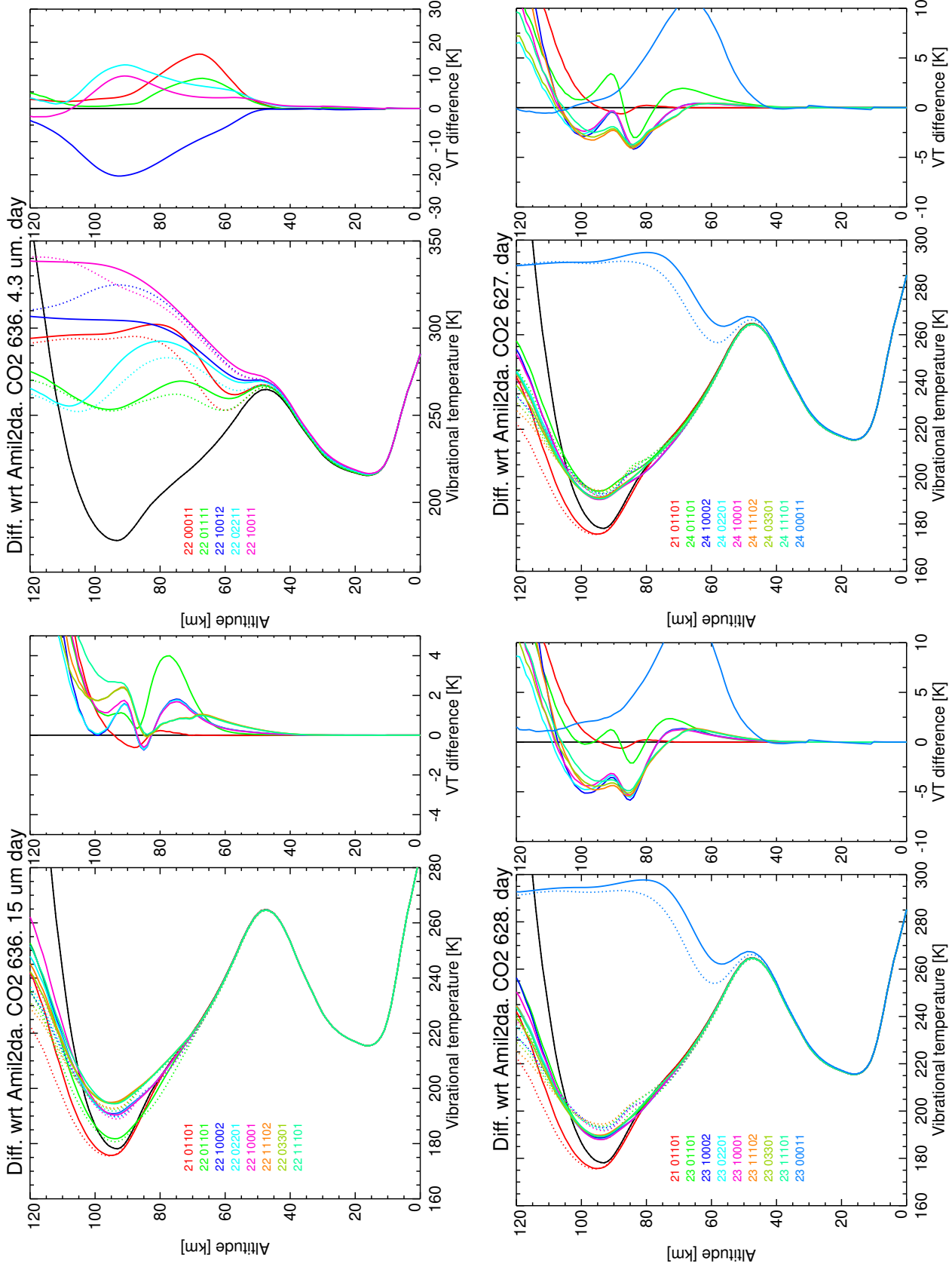


Figure 44: Differences in vibrational temperatures w.r.t. previous version (AMIL2DA) for CO_2 minor isotopes, for reference atmosphere #1, day. Solid: this study; dash: AMIL2DA. Right panels: this study-AMIL2DA.

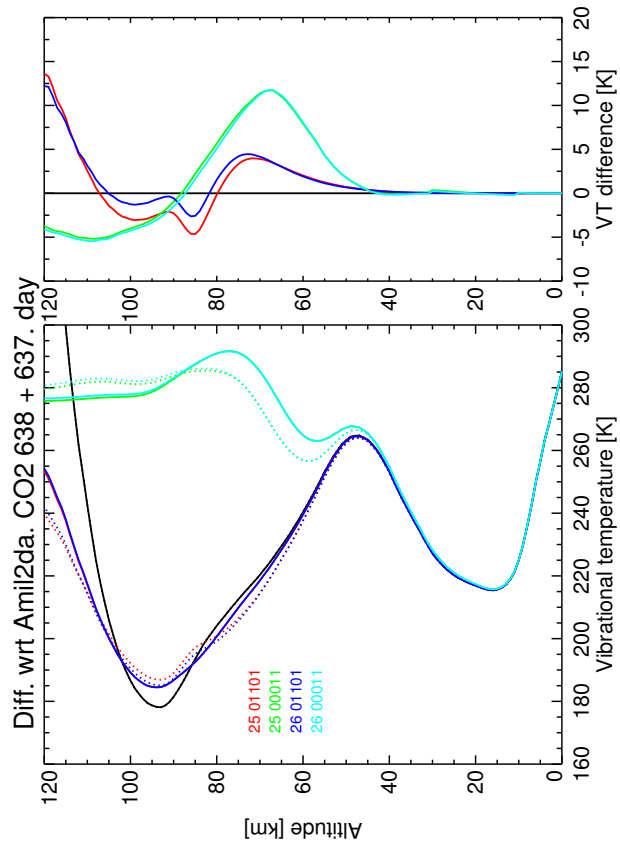


Figure 45: Differences in vibrational temperatures w.r.t. previous version (AMIL2DA) for CO₂ minor isotopes, for reference atmosphere #1, day. Solid: this study; dash: AMIL2DA. Right panels: this study–AMIL2DA.

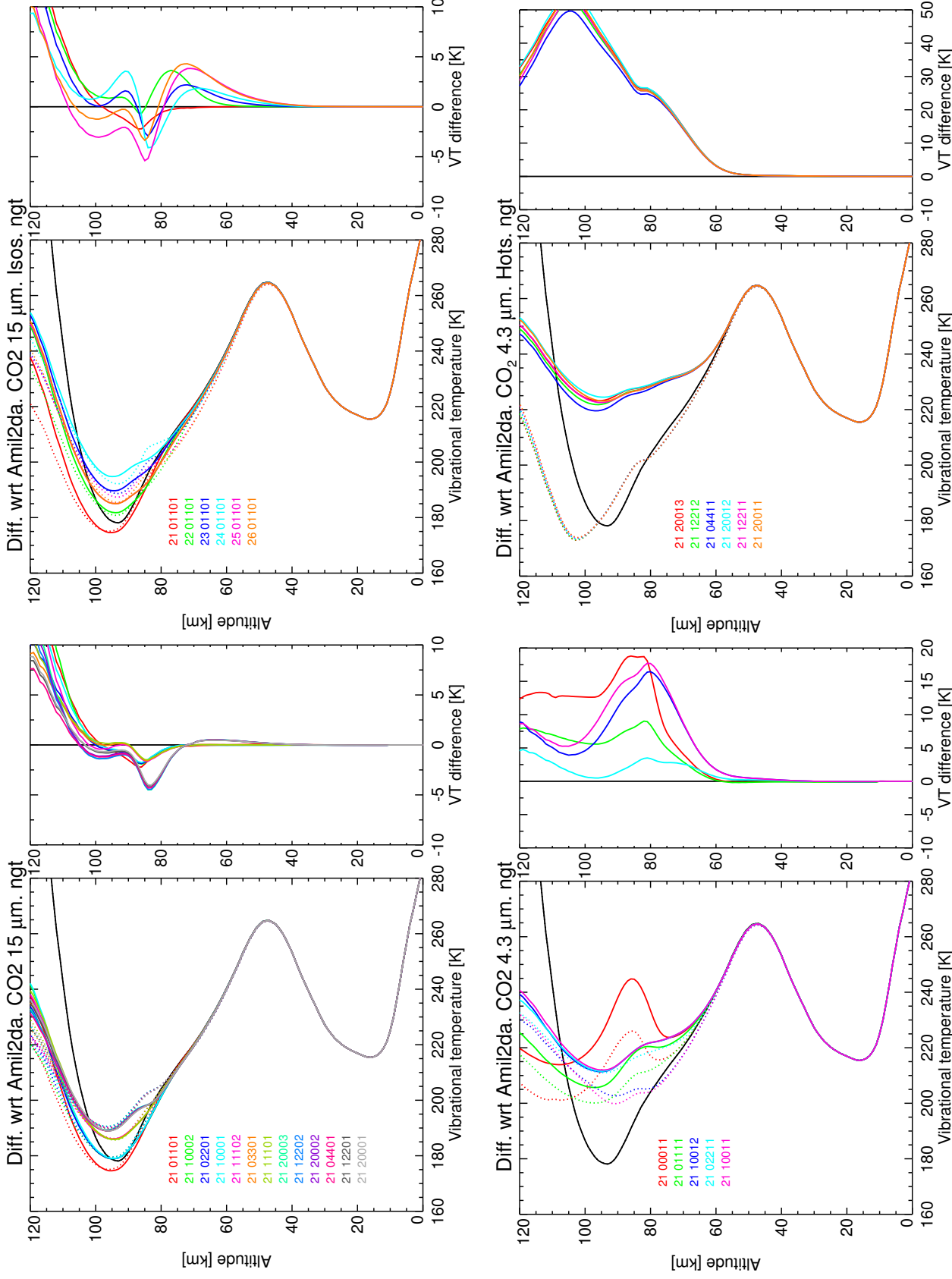


Figure 46: Differences in vibrational temperatures w.r.t. previous version (AMIL2DA) for CO_2 main isotope, for reference atmosphere #2, night. Solid: this study; dash: AMIL2DA. Right panels: this study–AMIL2DA.

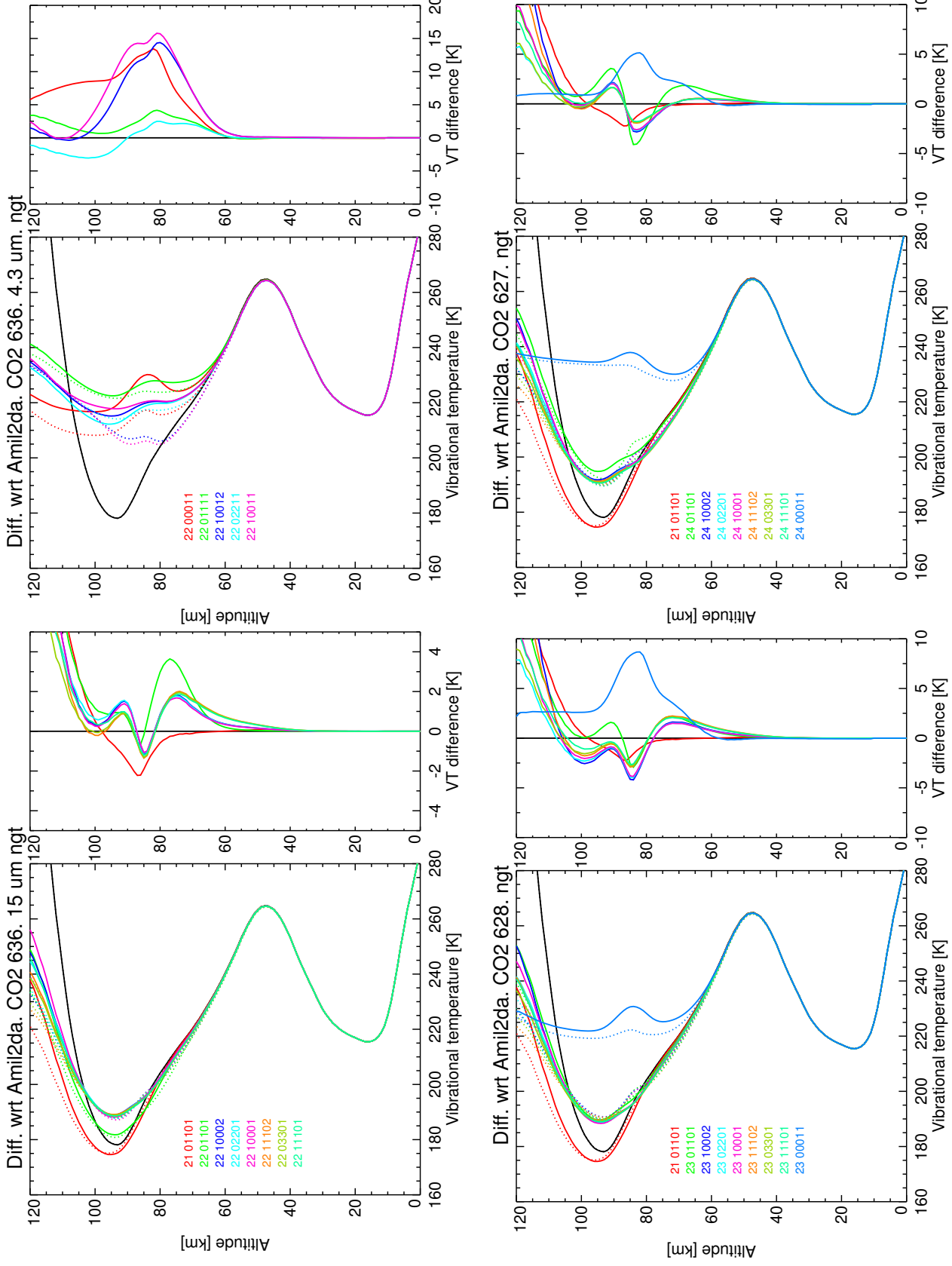


Figure 47: Differences in vibrational temperatures w.r.t. previous version (AMIL2DA) for CO₂ minor isotopes, for reference atmosphere #2, night. Solid: this study; dash: AMIL2DA. Right panels: this study–AMIL2DA.

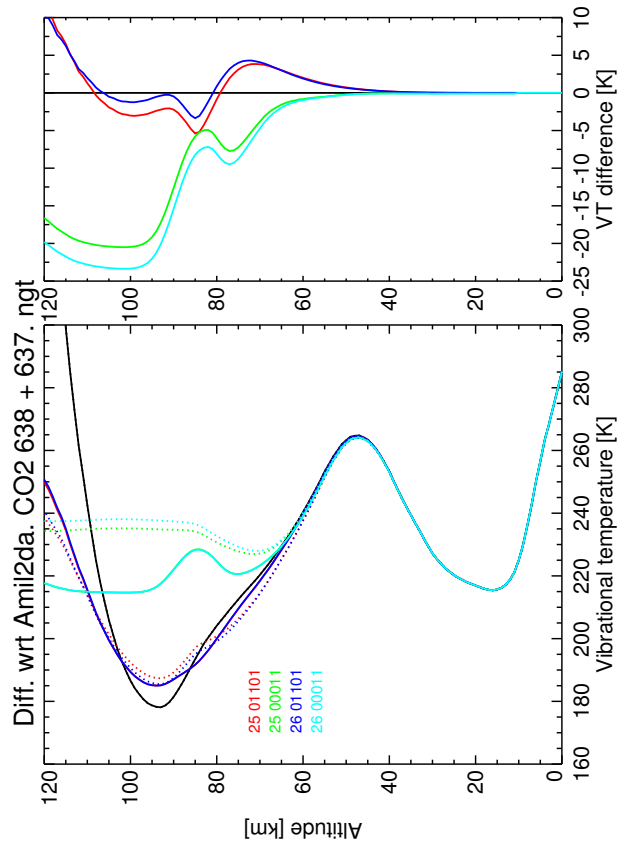


Figure 48: Differences in vibrational temperatures w.r.t. previous version (AMIL2DA) for CO_2 minor isotopes, for reference atmosphere #2, night. Solid: this study; dash: AMIL2DA. Right panels: this study–AMIL2DA.

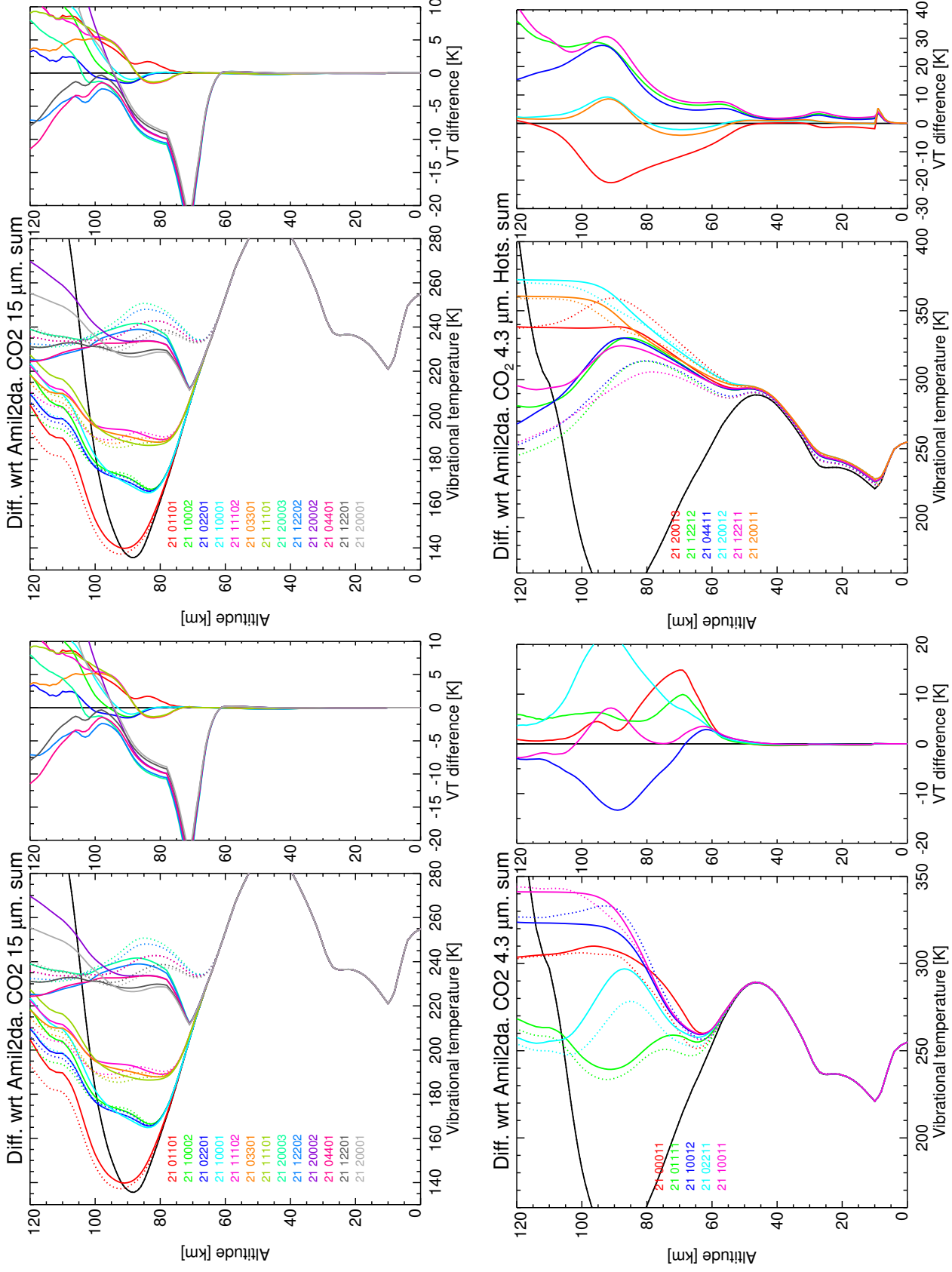


Figure 49: Differences in vibrational temperatures w.r.t. previous version (AMIL2DA) for CO_2 main isotope, for reference atmosphere #3, summer. Solid: this study; dash: AMIL2DA. Right panels: this study–AMIL2DA.

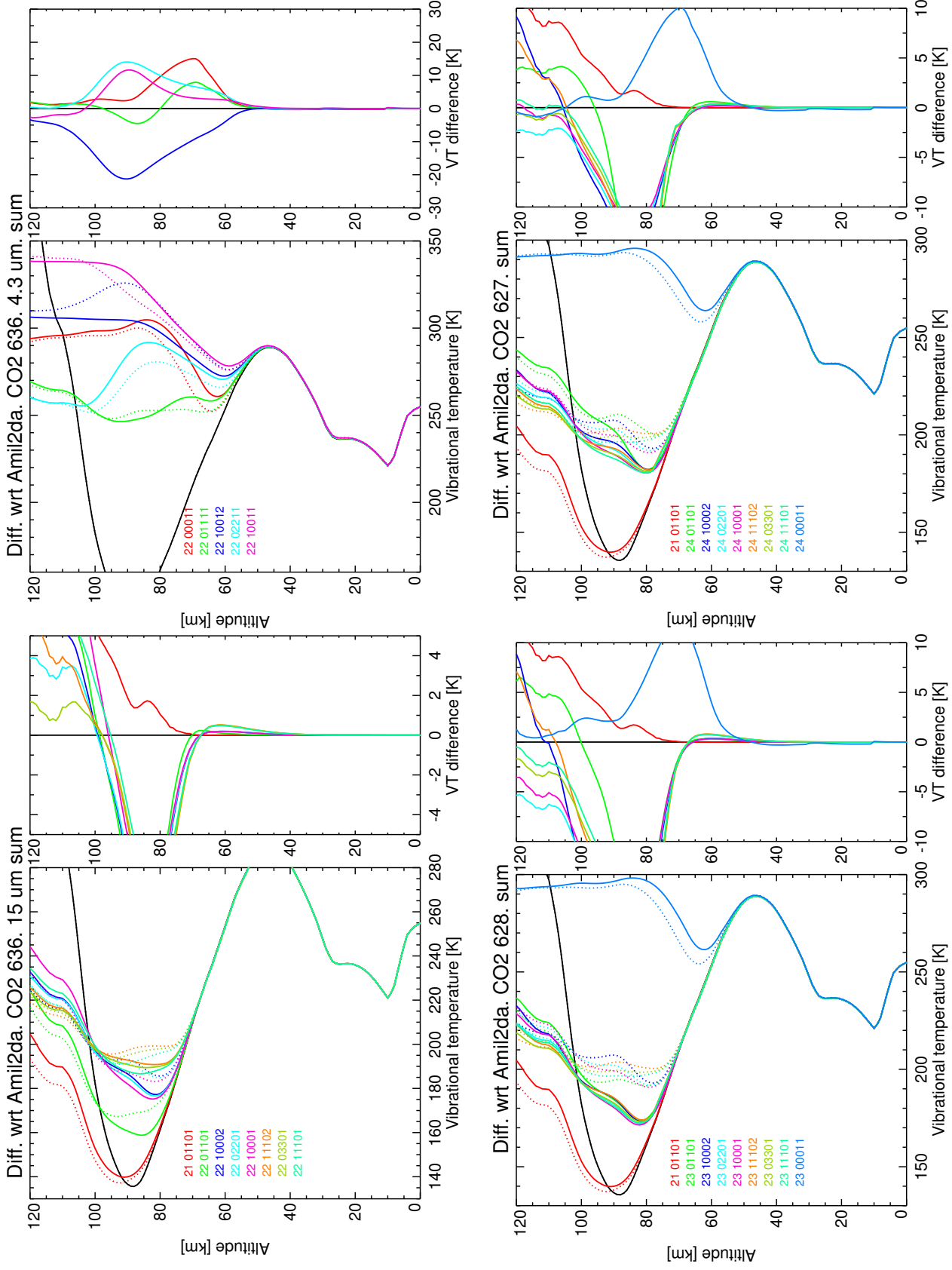


Figure 50: Differences in vibrational temperatures w.r.t. previous version (AMIL2DA) for CO₂ minor isotopes, for reference atmosphere #3, summer. Solid: this study; dash: AMIL2DA. Right panels: this study–AMIL2DA.

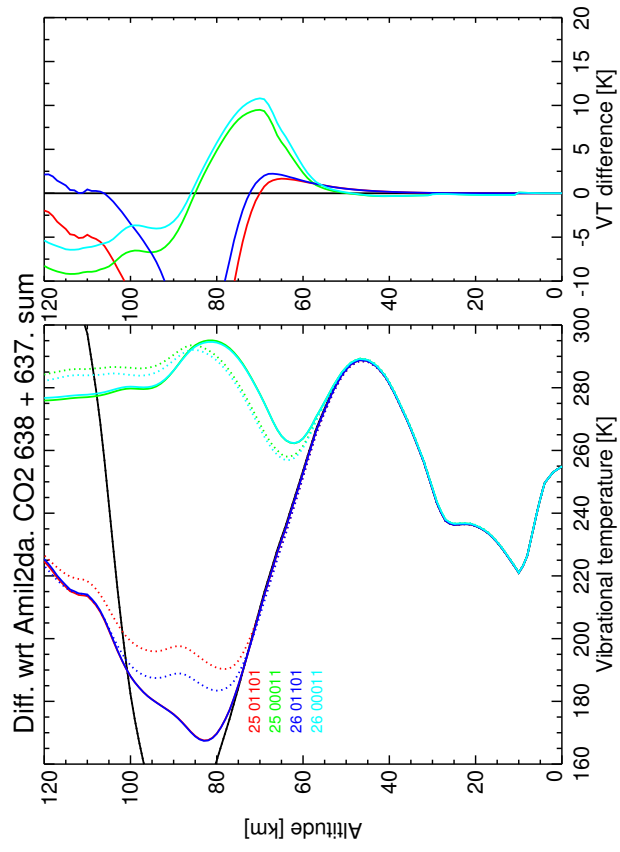


Figure 51: Differences in vibrational temperatures w.r.t. previous version (AMIL2DA) for CO_2 minor isotopes, for reference atmosphere #3, summer. Solid: this study; dash: AMIL2DA. Right panels: this study–AMIL2DA.

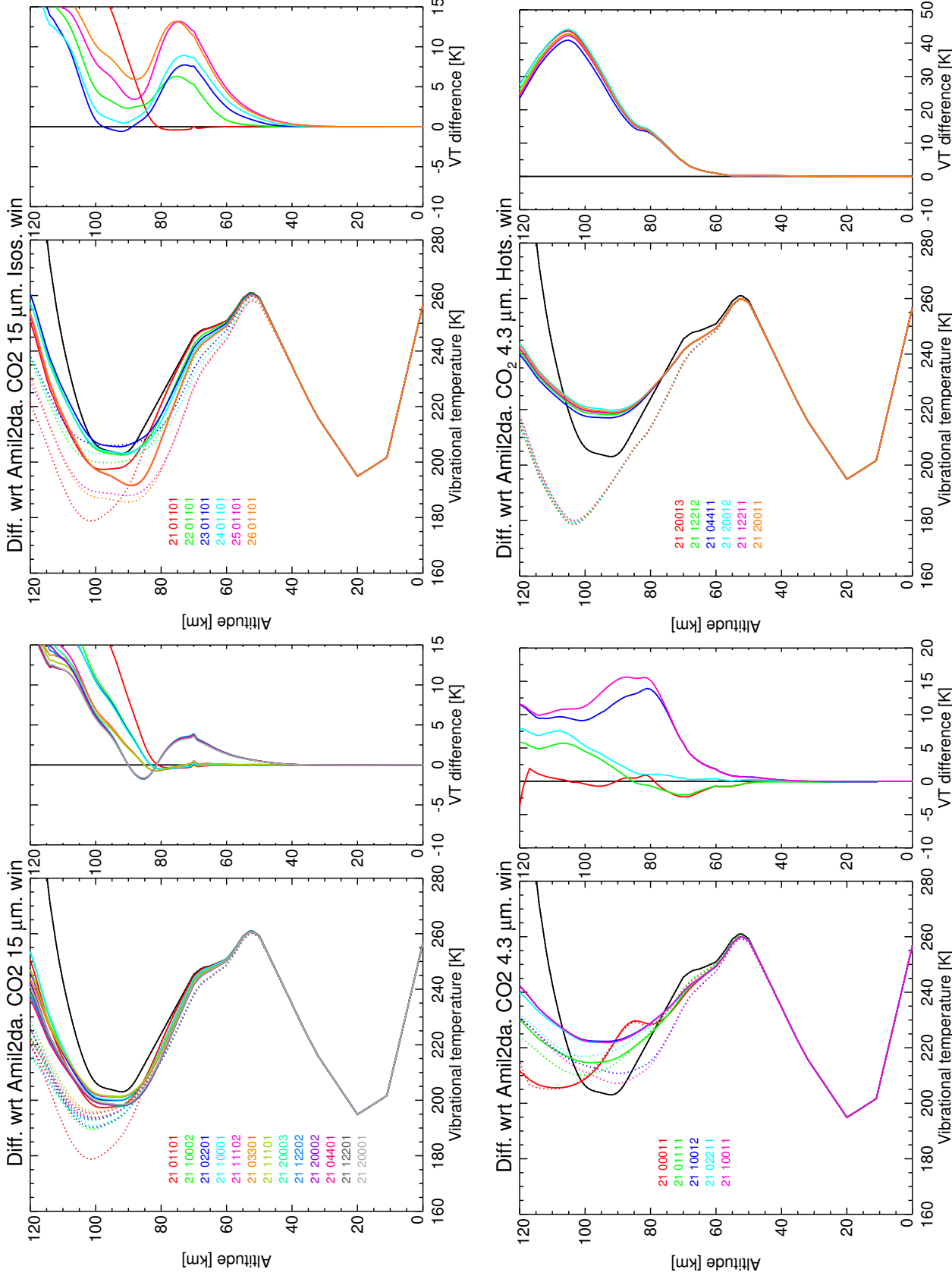


Figure 52: Differences in vibrational temperatures w.r.t. previous version (AMIL2DA) for CO₂ main isotope, for reference atmosphere #4, winter. Solid: this study; dash: AMIL2DA. Right panels: this study–AMIL2DA.

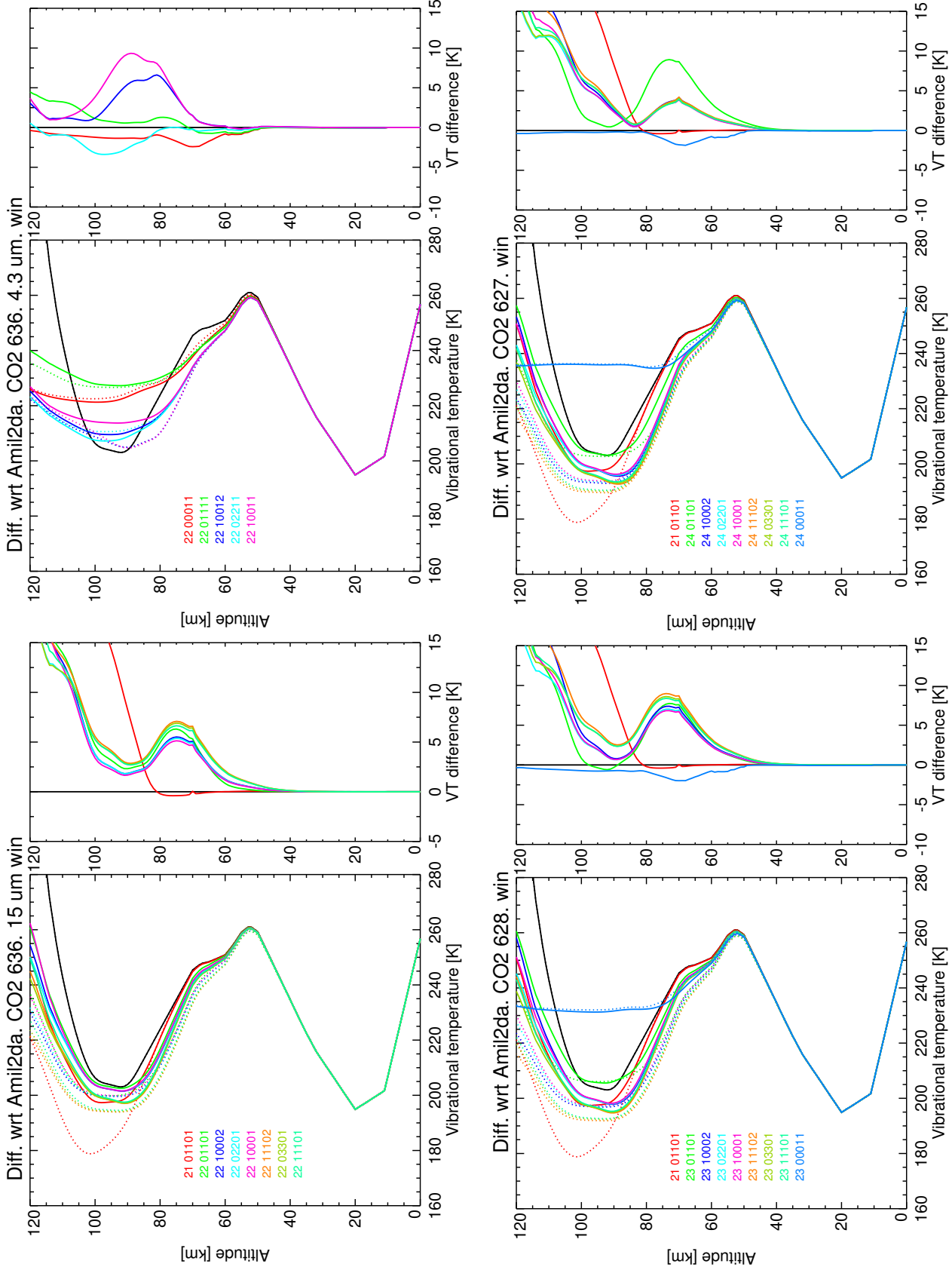


Figure 53: Differences in vibrational temperatures w.r.t. previous version (AMIL2DA) for CO₂ minor isotopes, for reference atmosphere #4, winter. Solid: this study; dash: AMIL2DA. Right panels: this study–AMIL2DA.

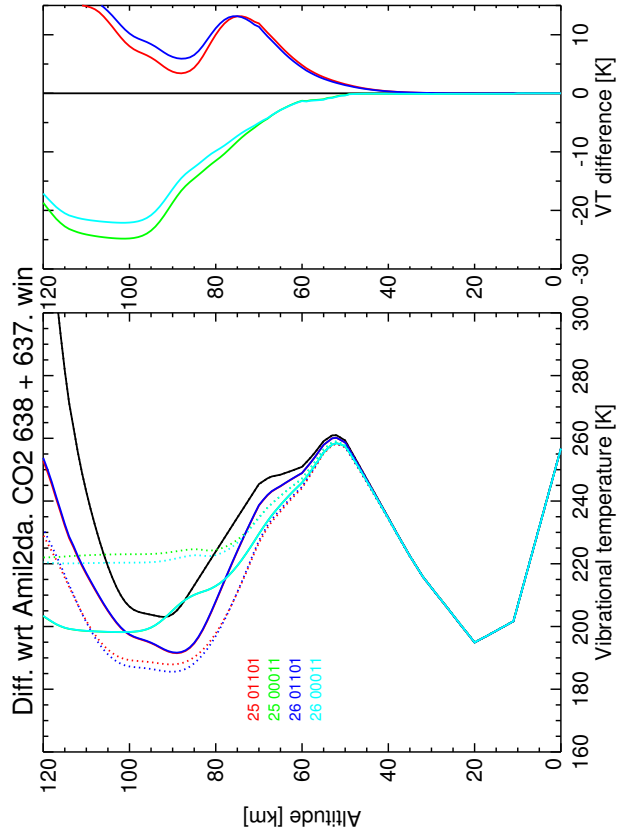


Figure 54: Differences in vibrational temperatures w.r.t. previous version (AMIL2DA) for CO_2 minor isotopes, for reference atmosphere #4, winter. Solid: this study; dash: AMIL2DA. Right panels: this study–AMIL2DA.

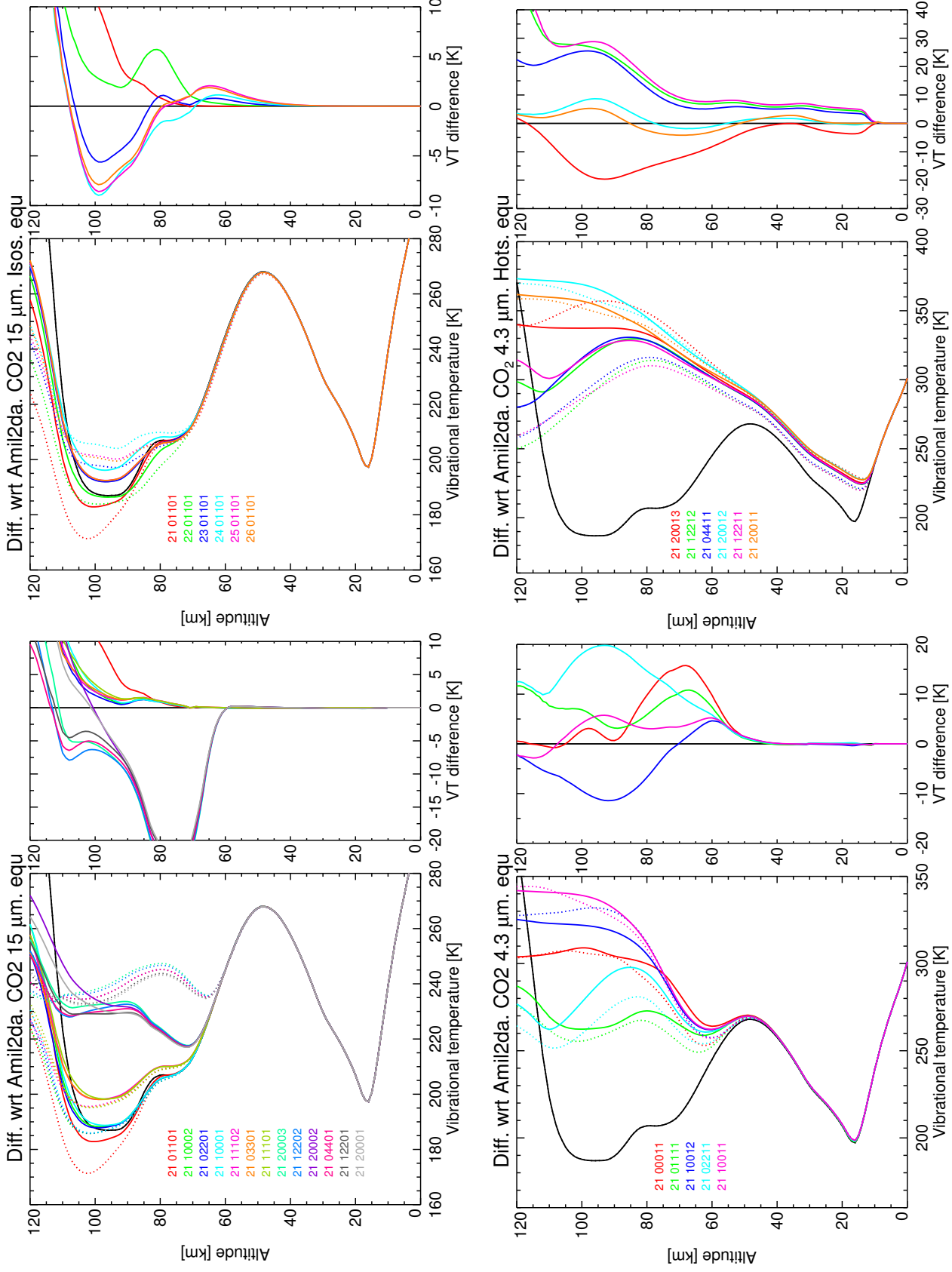


Figure 55: Differences in vibrational temperatures w.r.t. previous version (AMIL2DA) for CO₂ main isotope, for reference atmosphere #5, equator. Solid: this study; dash: AMIL2DA. Right panels: this study–AMIL2DA.

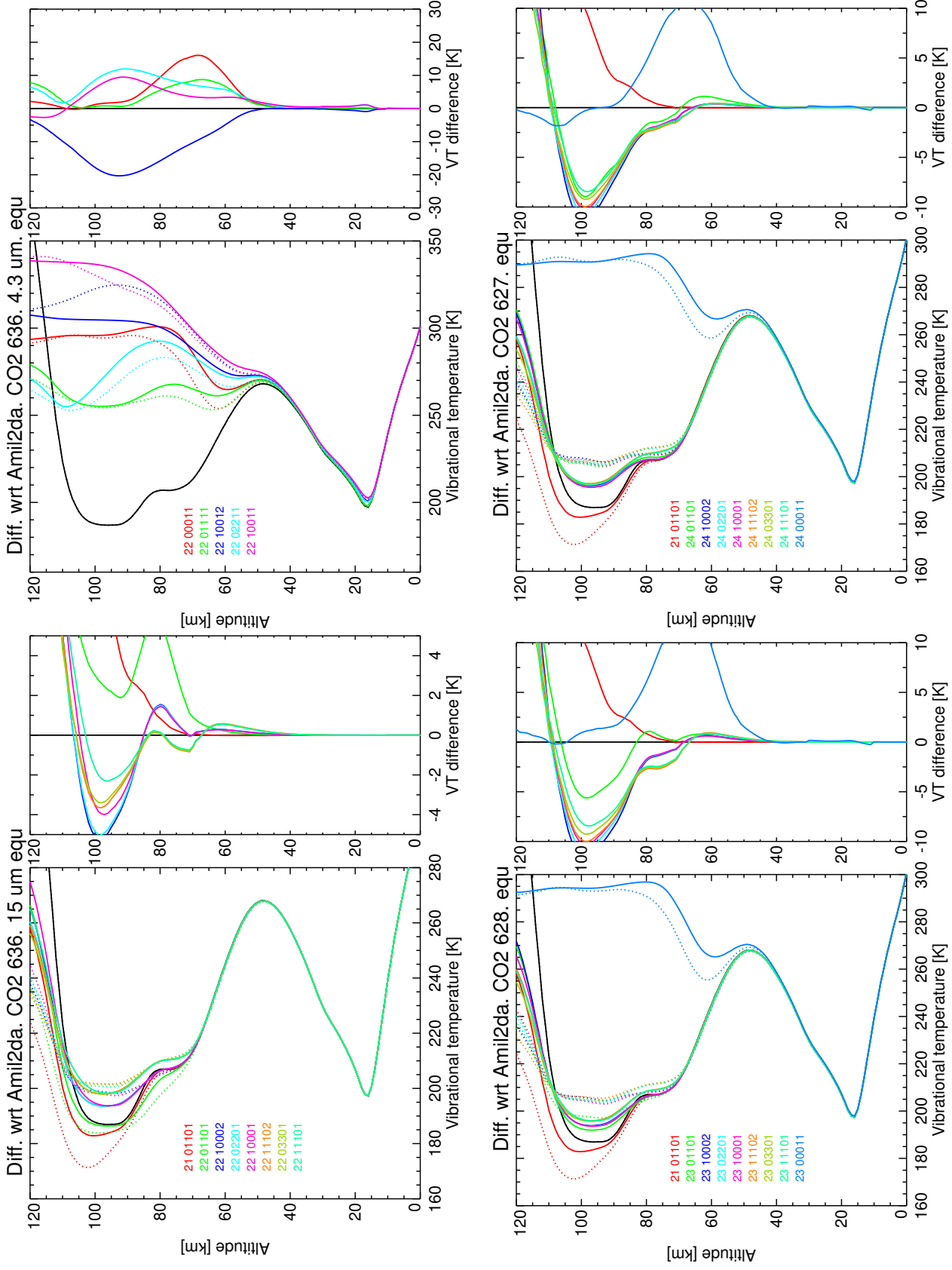


Figure 56: Differences in vibrational temperatures w.r.t. previous version (AMIL2DA) for CO₂ minor isotopes, for reference atmosphere #5, equator. Solid: this study; dash: AMIL2DA. Right panels: this study–AMIL2DA.

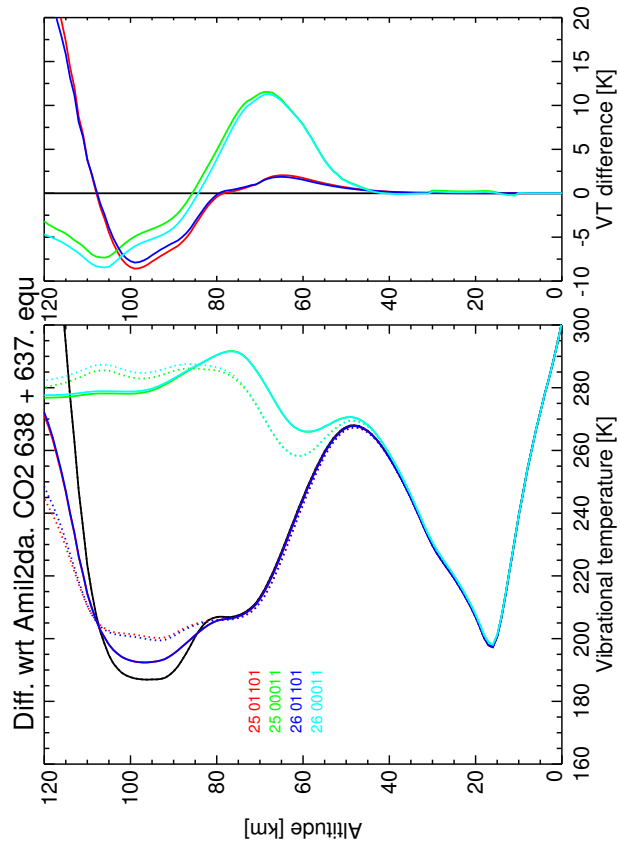


Figure 57: Differences in vibrational temperatures w.r.t. previous version (AMIL2DA) for CO_2 minor isotopes, for reference atmosphere #5, equator. Solid: this study; dash: AMIL2DA. Right panels: this study–AMIL2DA.

3.4 O₃

The O₃ model has not been updated since long time ago. Hence, the new vibrational temperatures incorporates two major sources of improvements. The first comes from the update of the radiative transfer calcualtion which affect mainly to the lower energy levels, the fundamental v_1 , v_2 and v_3 bands. The second set of major improvements comes from the analysis of MIPAS non-LTE spectra in the 4.8 μm region (Gil-López et al. 2006; Kaufmann et al., 2006), which are summarized as follows:

- (i) The models prior to MIPAS measurements underestimated the O₃ daytime emission in the mesosphere. To explain MIPAS radiance the model has to assume an O₃ nascent distribution at 3000 cm^{-1} or a nascent distribution at 4000 cm^{-1} but with the relaxation rates k_{d2} of the O₃ v_1 and v_3 levels to the v_2 levels reduced by a factor of 3 (Gil-López, 2006; Kaufmann et al., 2006).
- (ii) A new collisional relaxation scheme including "accidental resonances" gives also a good agreement with MIPAS spectra at 60-70 km in the 2070-2130 cm^{-1} region without the need to change typical k_{d2} quenching rates, and, in addition, provides a better agreement with MIPAS spectra in the 2000-2080 cm^{-1} region. Also, with this scheme the vibrational temperatures are weakly dependent on the nascent distribution.
- (iii) It was found that the classical Landau-Teller relaxation provides a better agreement than the SSH theory. Hence this was also included.

Figures 58-72 show the vibrational temperatures for the O₃ energy levels from the lowest to the highest energy for the 5 reference atmospheres. The small jump in the daytime O₃ T_v's at about 90 km is caused by the transition from photochemical-equilibrium atomic oxygen to the prescribed atomic oxygen. The figures have been grouped in different "sets" of T_v's. Set 1 includes four figures of T_v's for a) the levels of the fundamental transitions (v_1 , v_2 and v_3); b) for the $v_1=1-5$ levels; c) for the $v_2=2-9$ levels; and d) for the $v_3=1-6$ levels. The set 2 includes another four figures of T_v's for higher energy levels, grouped from G1 to G4 with increasing energy. The set 3 includes the figure of T_v's for the highest energy levels of O₃.

Figures 73-87 show the differences in the vibrational temperatures for the O₃ energy levels with respect to previous (AMIL2DA) version. The major differences are:

- The lowest energy levels (010), (100) and (001) have larger VTs from 65 km to 90 km and lower above this altitude. This is due essentially to the more accurate calculation of radiative transfer (see above).
- The low- to mid-energy levels have, in general, larger VTs in the mesosphere.
- The mid- to high energy levels have, in general, smaller VTs in the mesosphere.

We should note that for the two cases above (low- to high-energy levels) the major differences w.r.t previous calculations are related to the new collisional scheme.

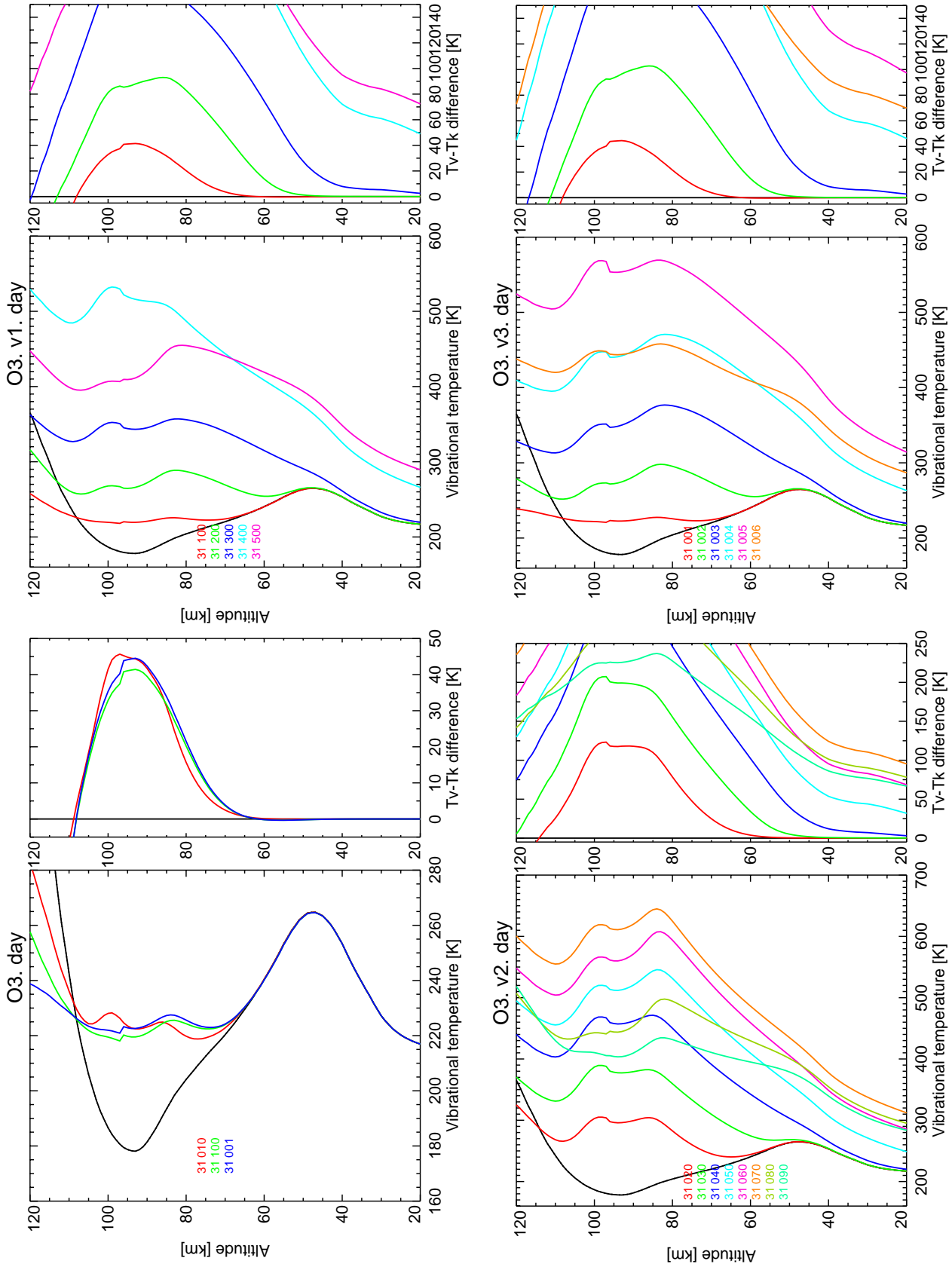


Figure 58: Vibrational temperatures for O₃ levels, set 1, for reference atmosphere #1, day.

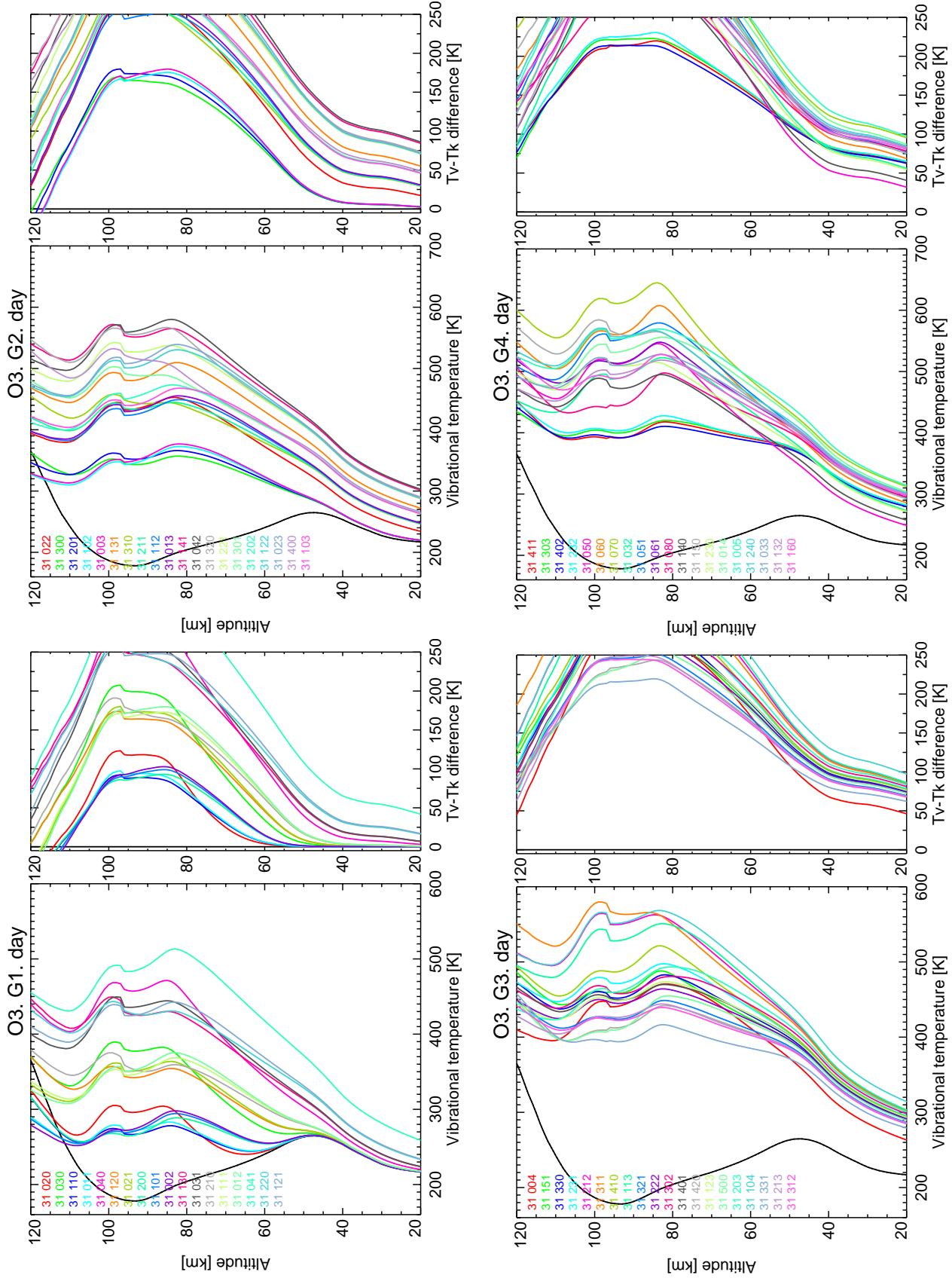


Figure 59: Vibrational temperatures for O₃ levels, set 2, for reference atmosphere #1, day.

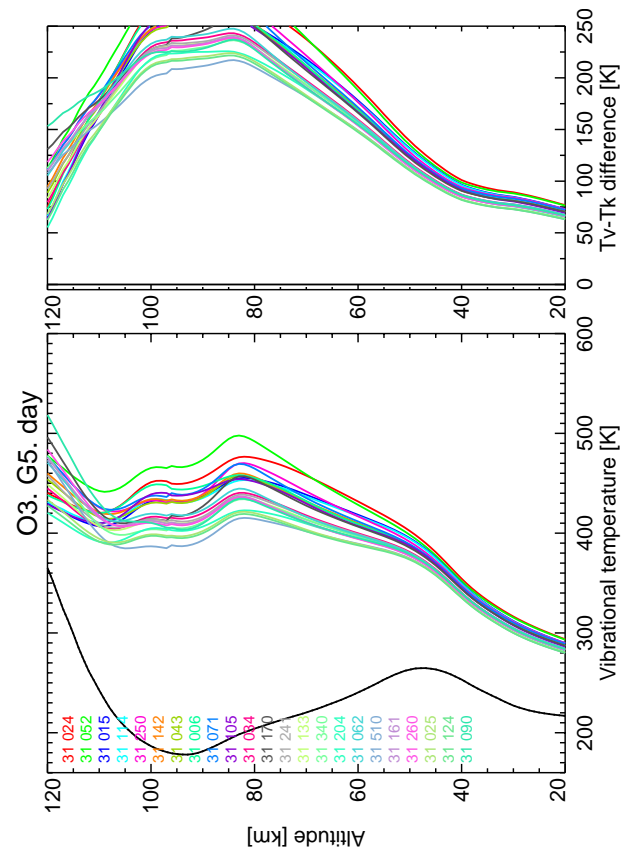


Figure 60: Vibrational temperatures for O₃ levels, set 3, for reference atmosphere #1, day.

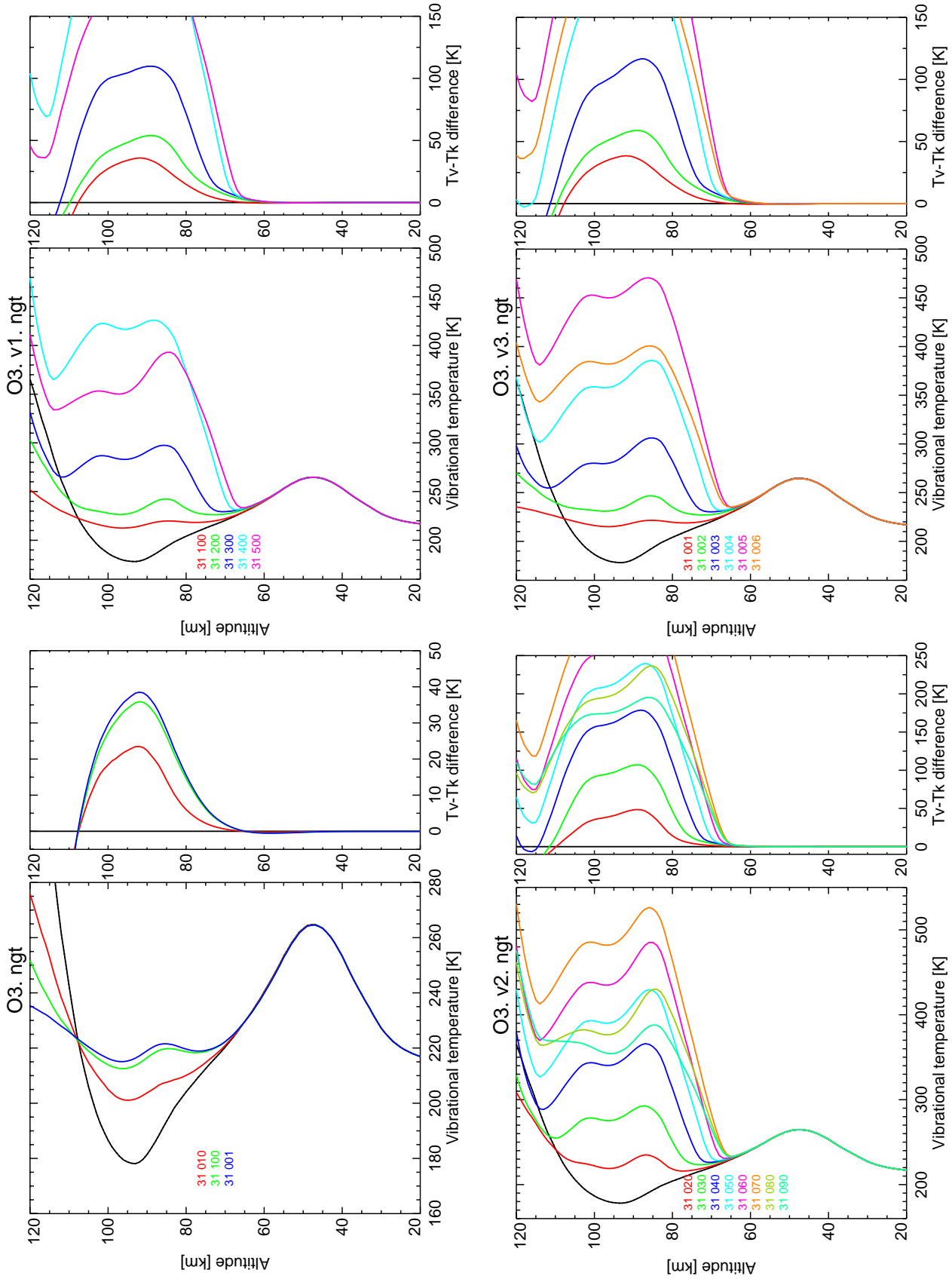


Figure 61: Vibrational temperatures for O_3 levels, set 1, for reference atmosphere #2, night.

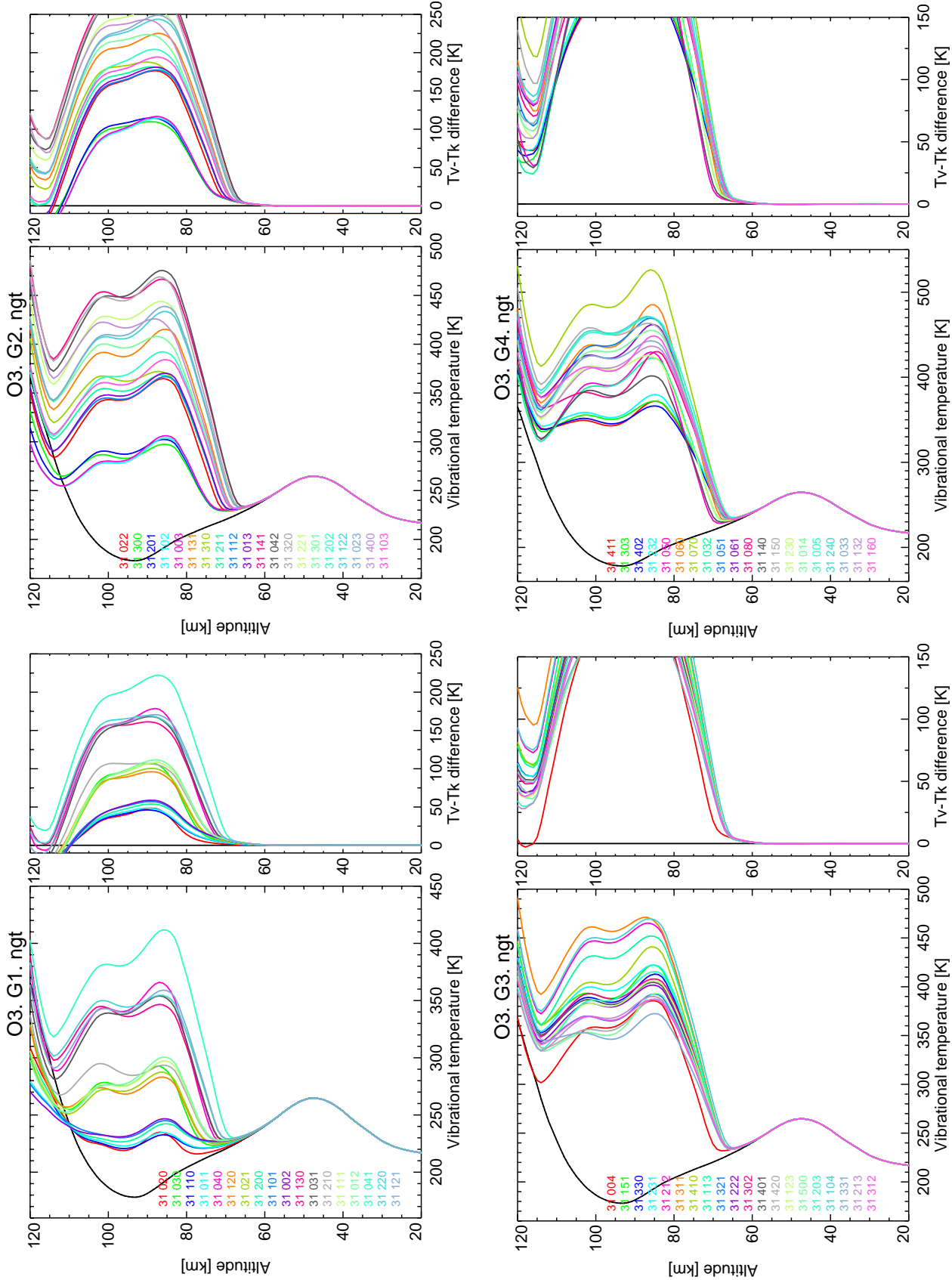


Figure 62: Vibrational temperatures for O₃ levels, set 2, for reference atmosphere #2, night.

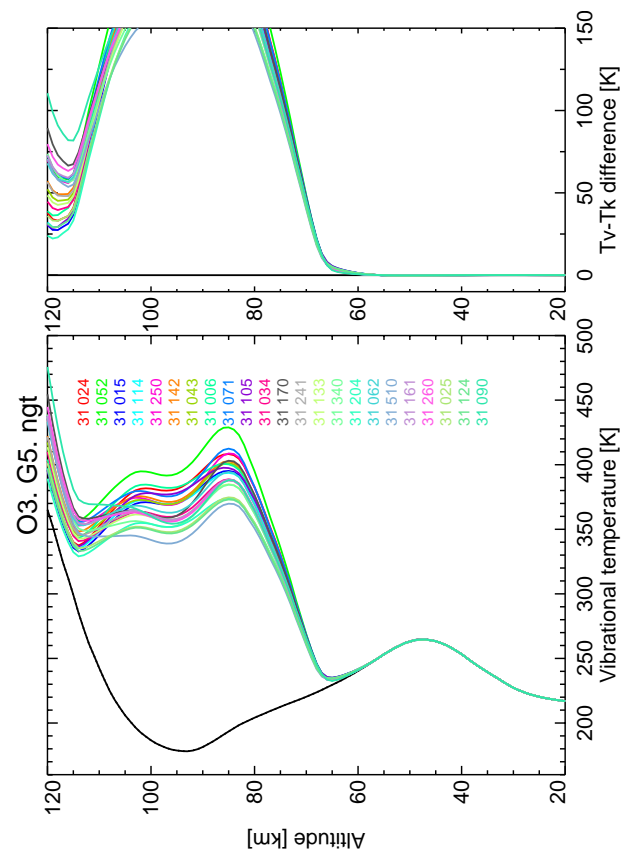


Figure 63: Vibrational temperatures for O_3 levels, set 3, for reference atmosphere #2, night.

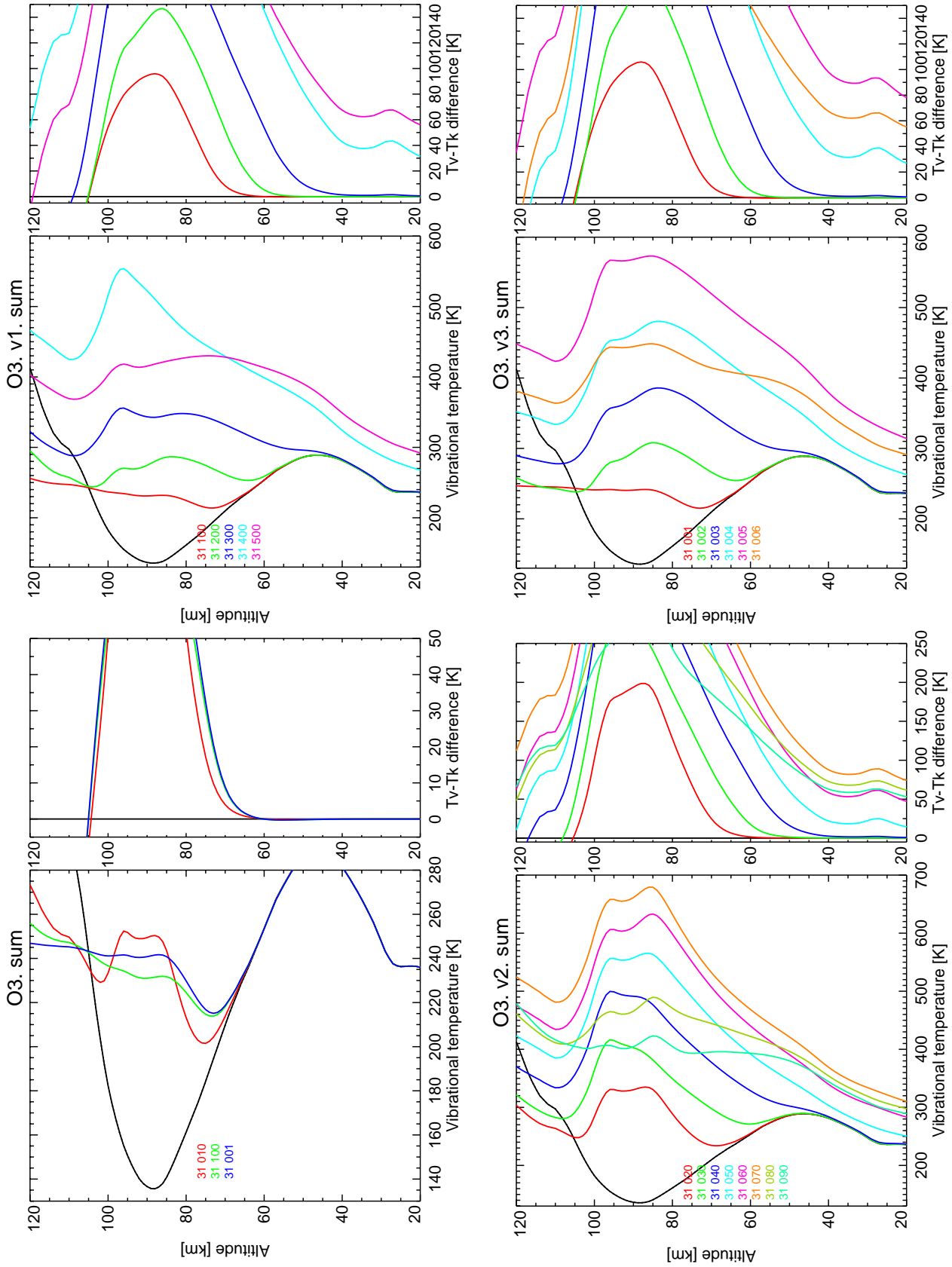


Figure 64: Vibrational temperatures for O_3 levels, set 1, for reference atmosphere #3, summer.

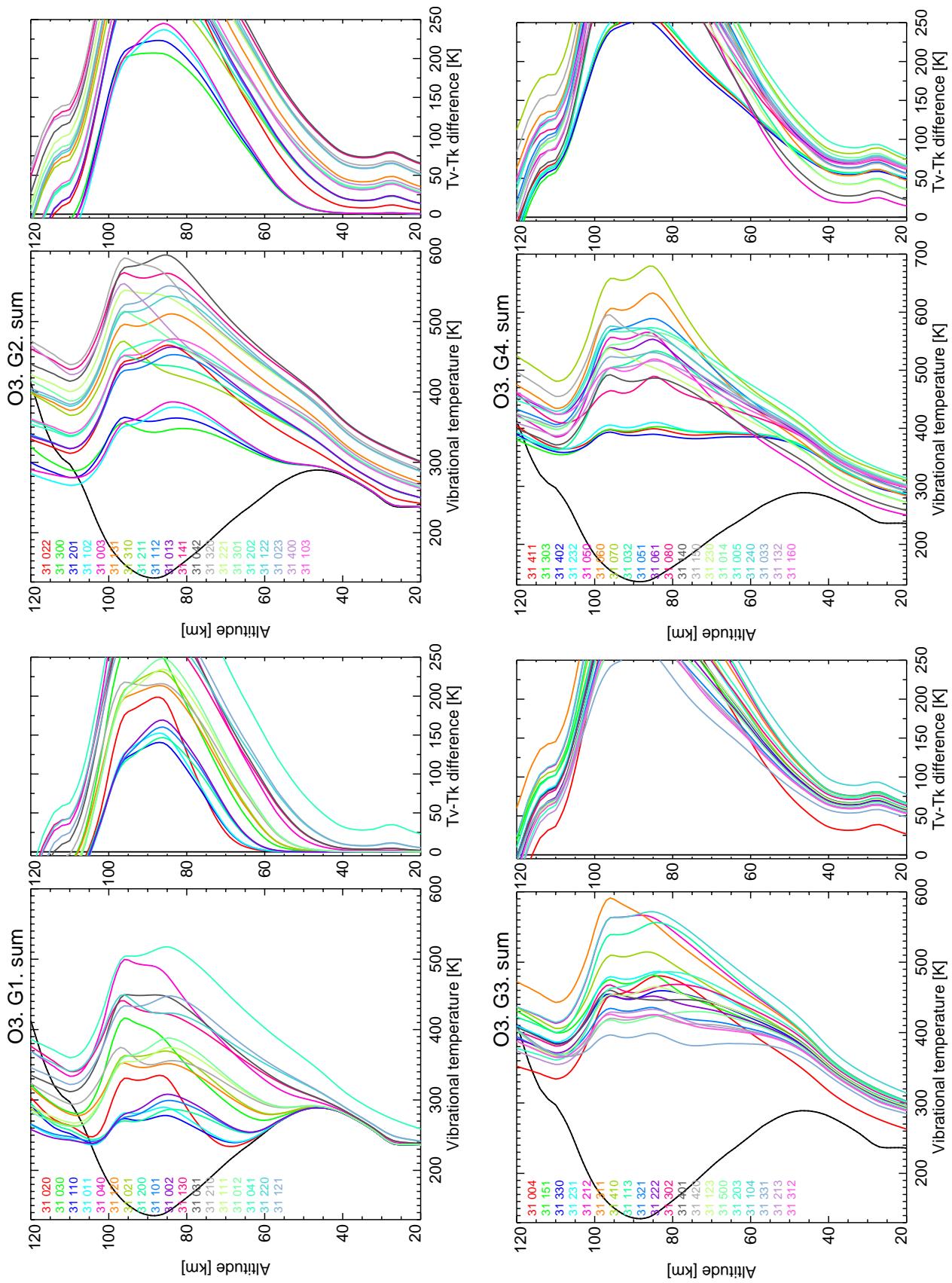


Figure 65: Vibrational temperatures for O_3 levels, set 2, for reference atmosphere #3, summer.

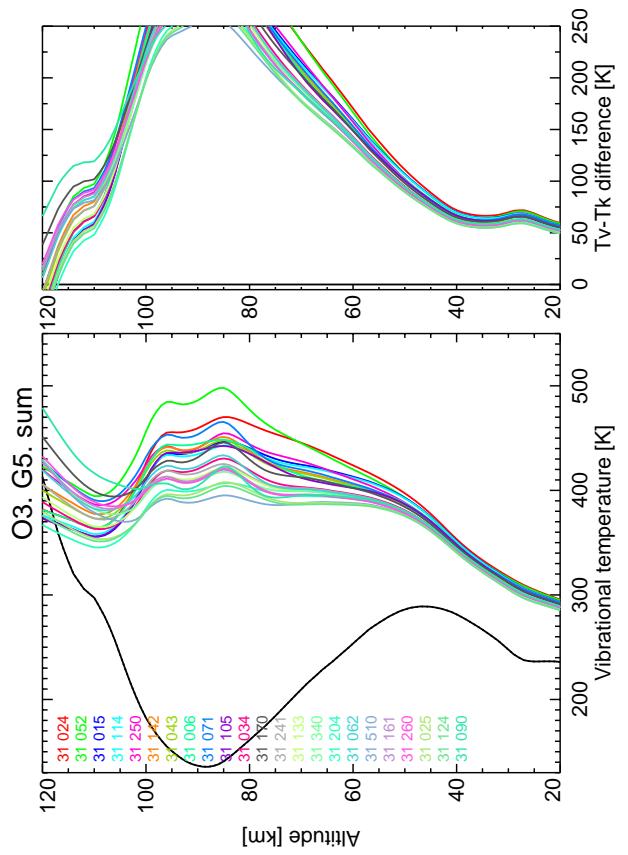


Figure 66: Vibrational temperatures for O₃ levels, set 3, for reference atmosphere #3, summer.

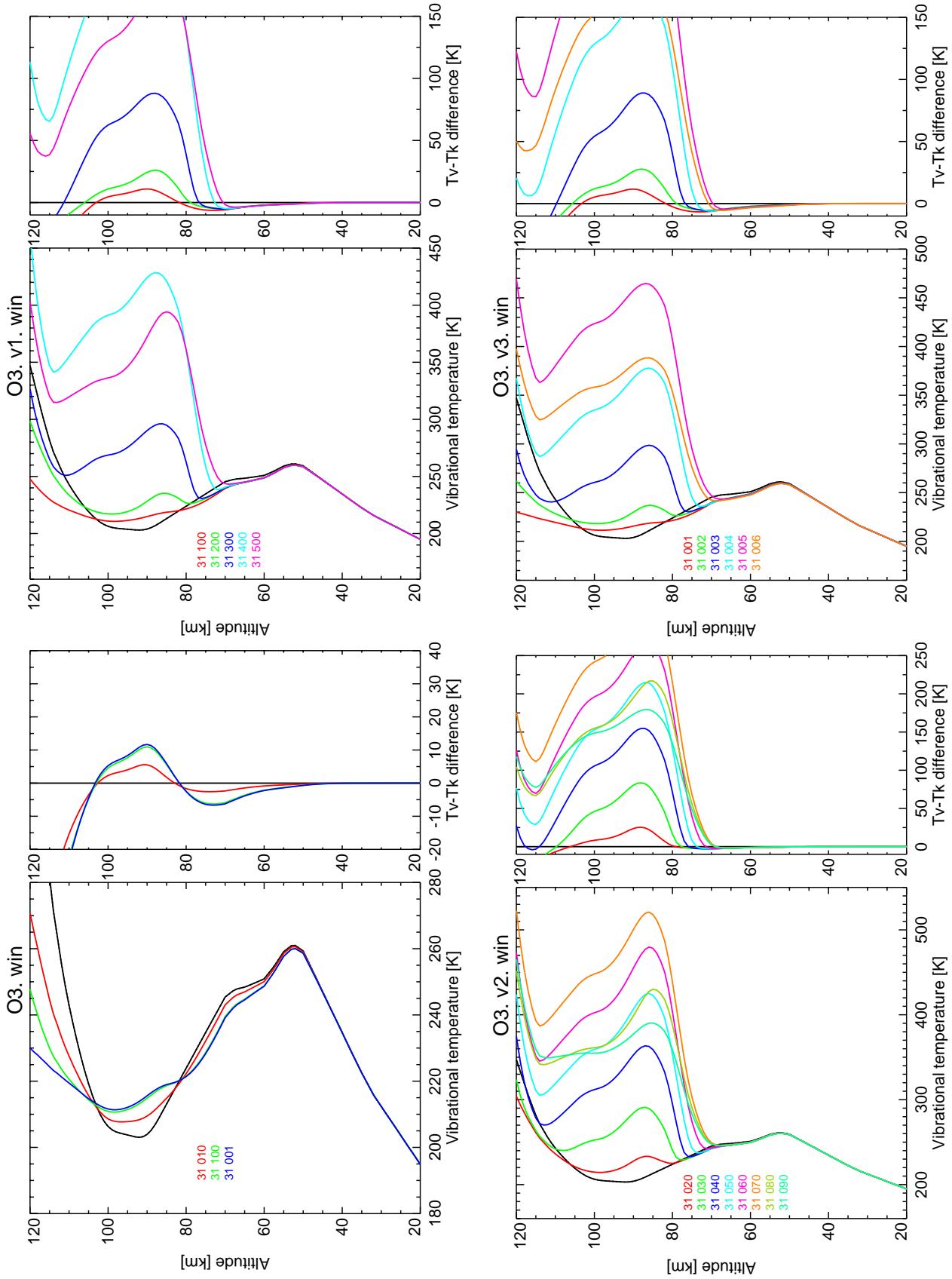


Figure 67: Vibrational temperatures for O_3 levels, set 1, for reference atmosphere #4, winter.

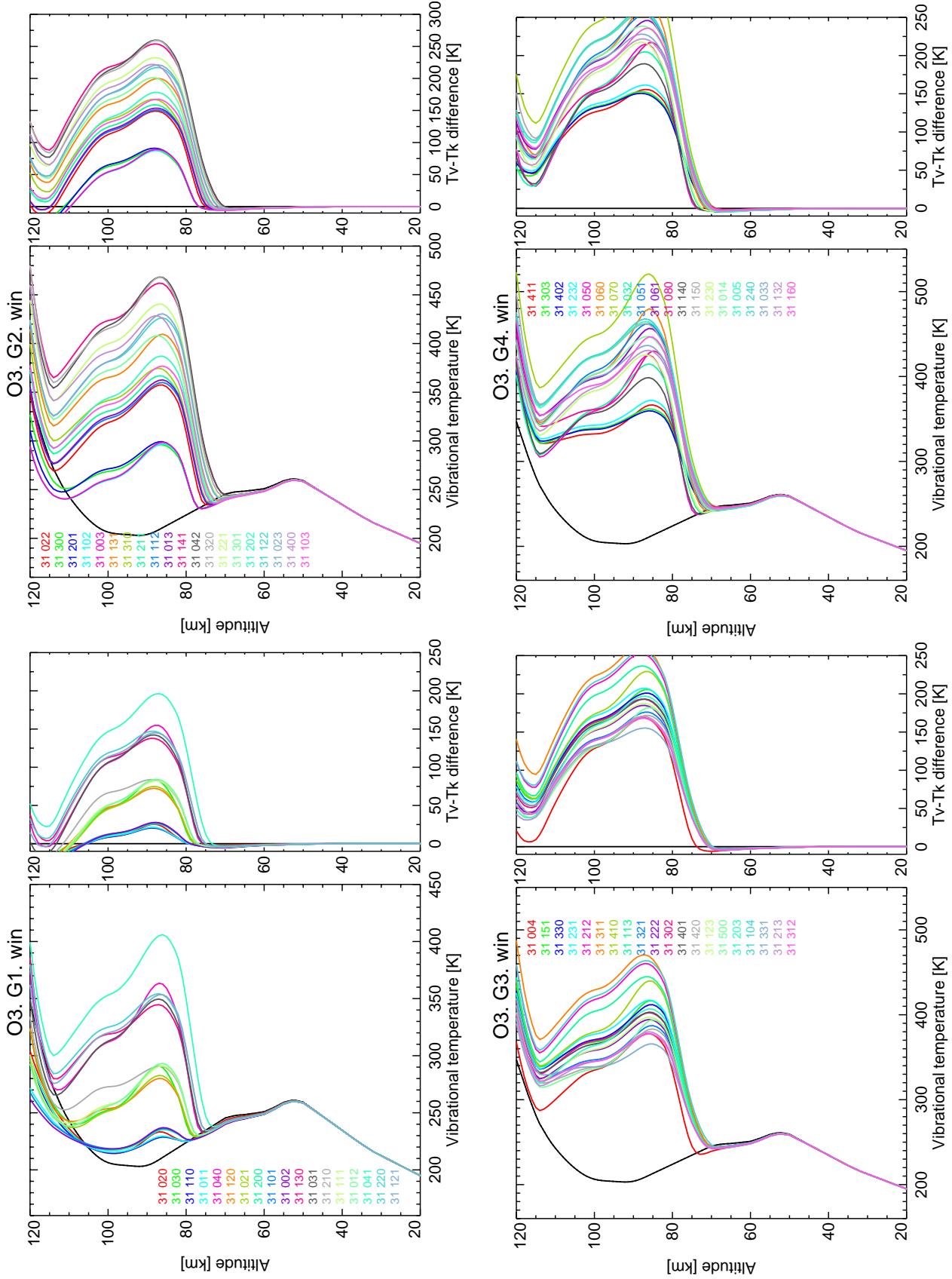


Figure 68: Vibrational temperatures for O_3 levels, set 2, for reference atmosphere #4, winter.

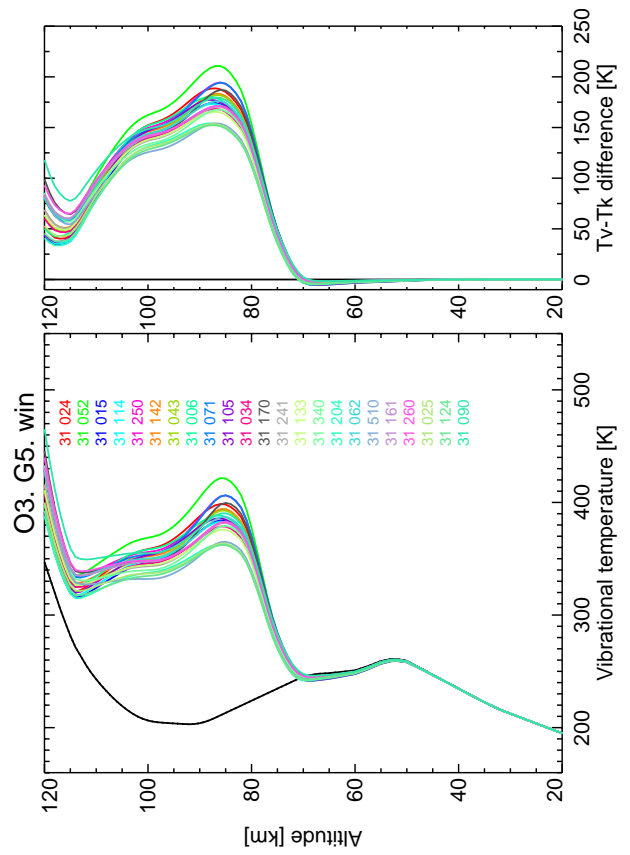


Figure 69: Vibrational temperatures for O_3 levels, set 3, for reference atmosphere #4, winter.

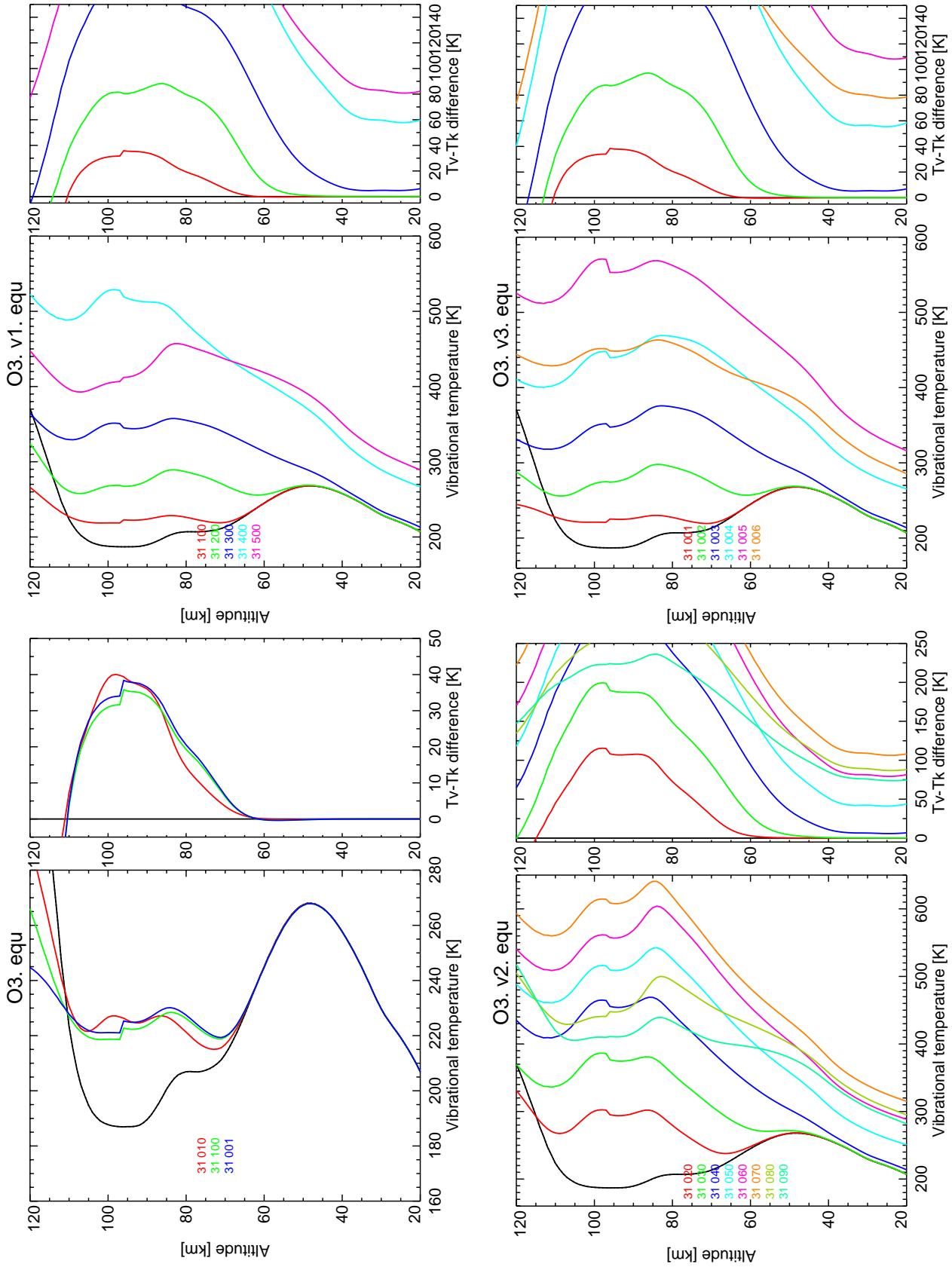


Figure 70: Vibrational temperatures for O_3 levels, set 1, for reference atmosphere #5, equator.

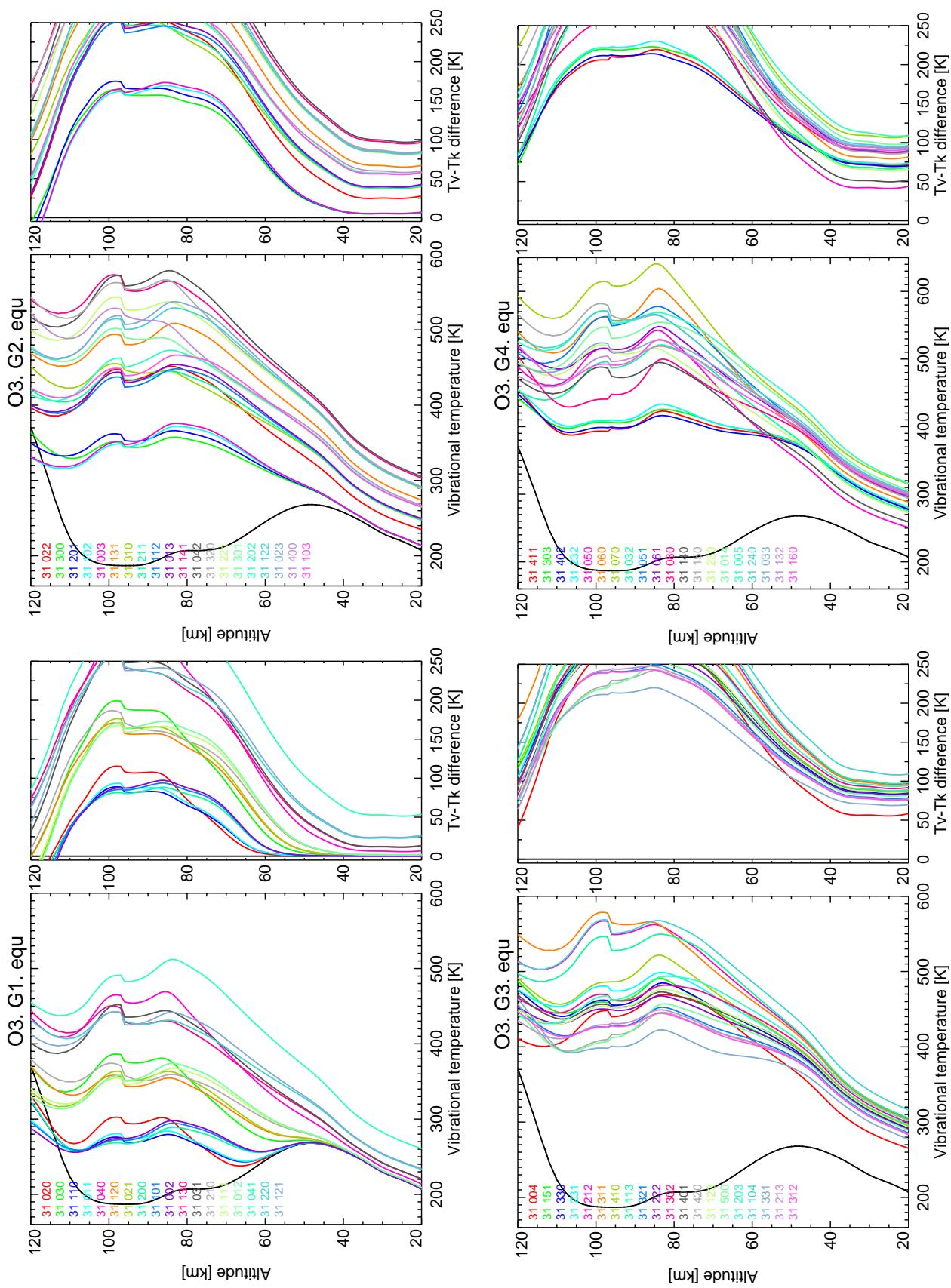


Figure 71: Vibrational temperatures for O₃ levels, set 2, for reference atmosphere #5, equator.

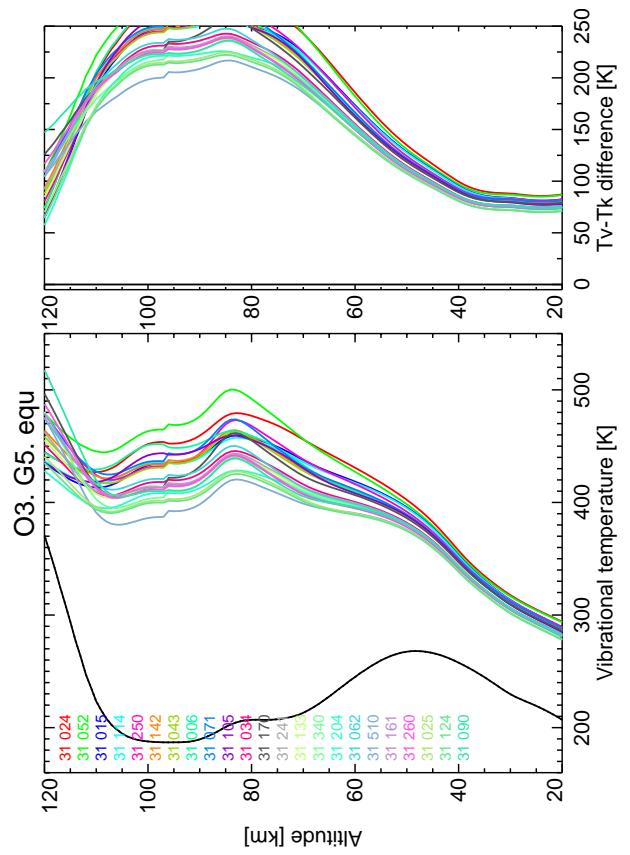


Figure 72: Vibrational temperatures for O₃ levels, set 3, for reference atmosphere #5, equator.

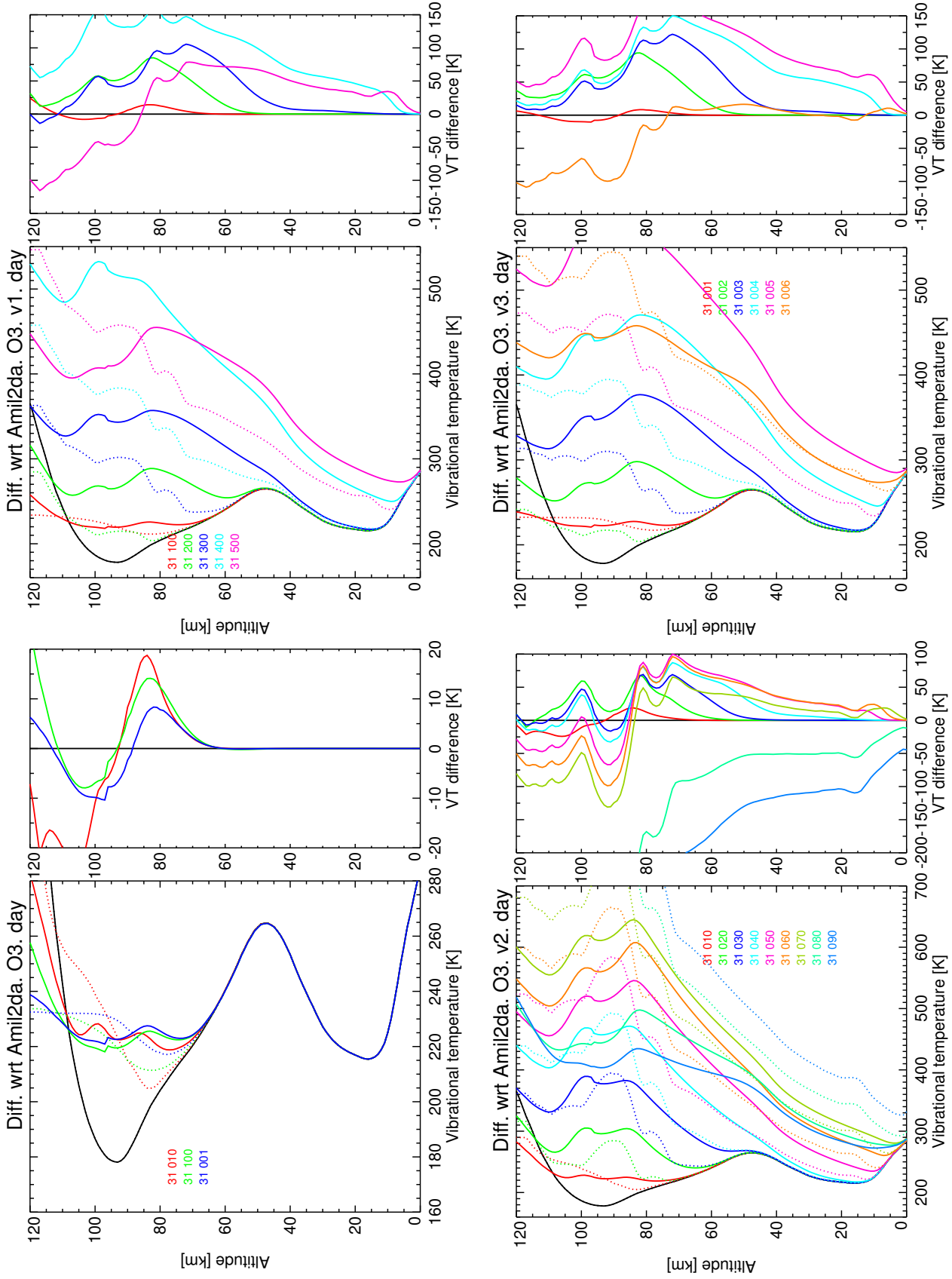


Figure 73: Differences in vibrational temperatures w.r.t. previous version (AMIL2DA) for O₃ levels, set 1, for reference atmosphere #1, day. Solid: this study; dash: AMIL2DA. Right panels: this study–AMIL2DA.

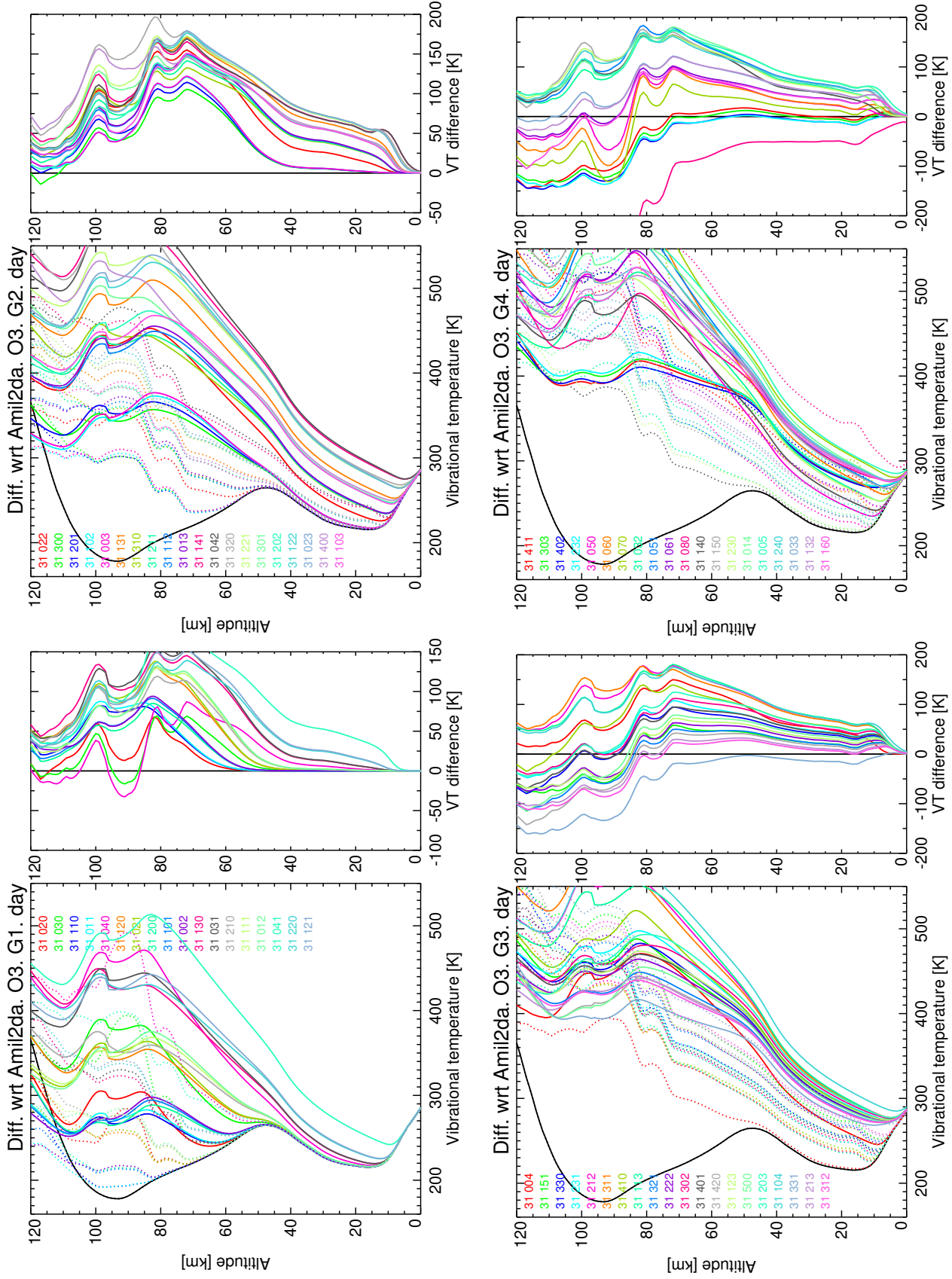


Figure 74: Differences in vibrational temperatures w.r.t. previous version (AMIL2DA) for O₃ levels, set 2, for reference atmosphere #1, day. Solid: this study; dash: AMIL2DA. Right panels: this study–AMIL2DA.

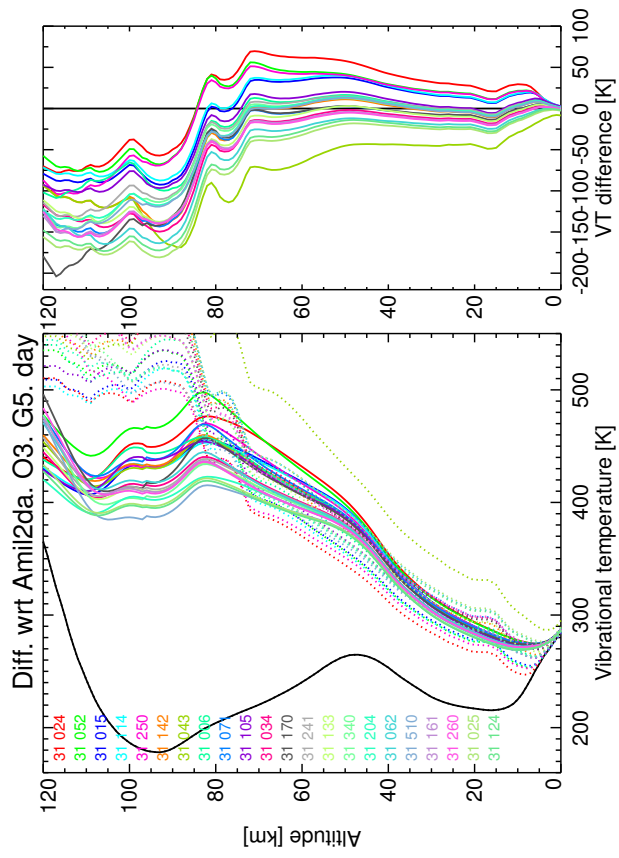


Figure 75: Differences in vibrational temperatures w.r.t. previous version (AMIL2DA) for O_3 levels, set 3, for reference atmosphere #1, day. Solid: this study; dash: AMIL2DA. Right panels: this study–AMIL2DA.

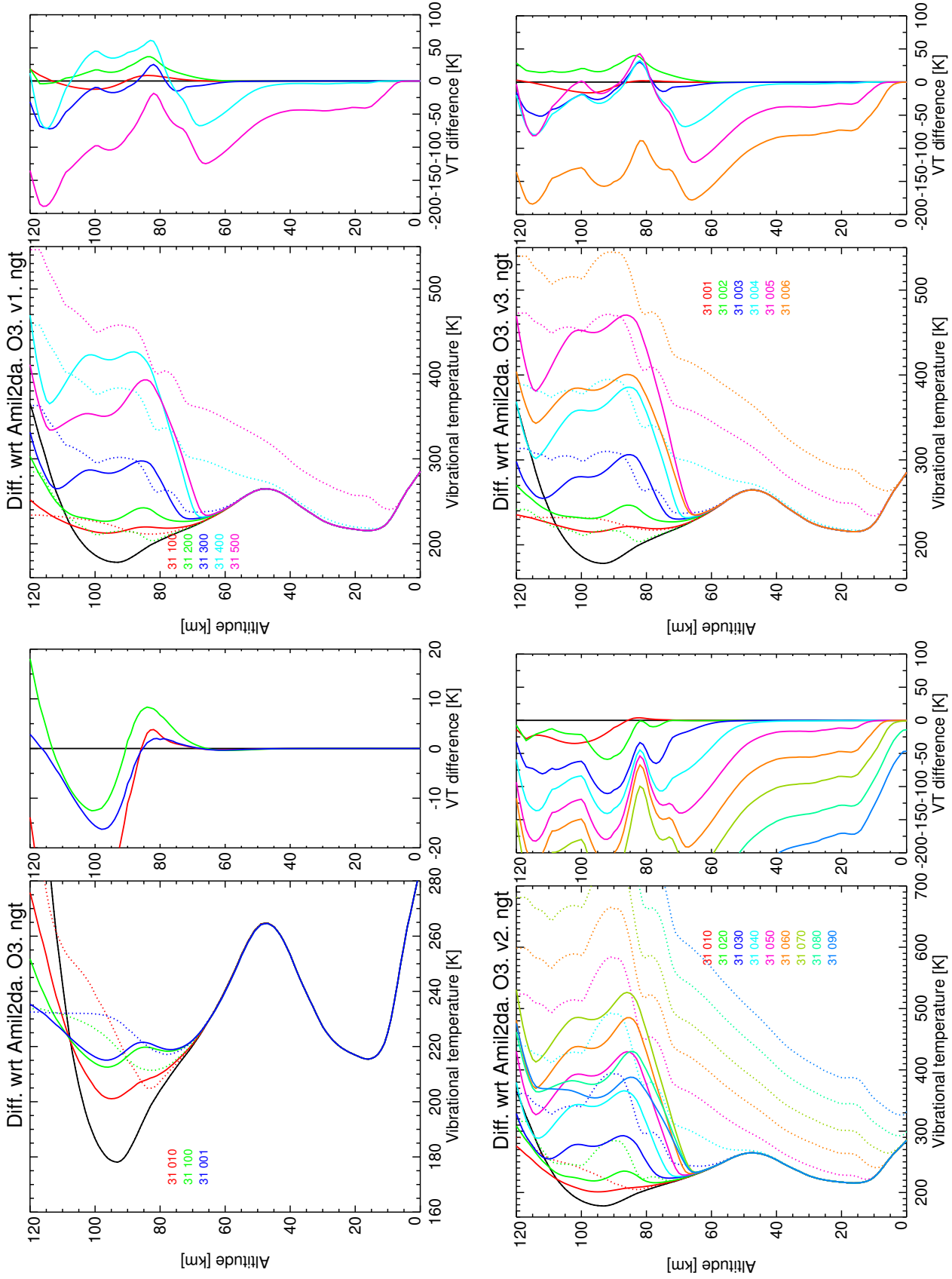


Figure 76: Differences in vibrational temperatures w.r.t. previous version (AMIL2DA) for O₃ levels, set 1, for reference atmosphere #2, night. Solid: this study; dash: AMIL2DA. Right panels: this study-AMIL2DA.

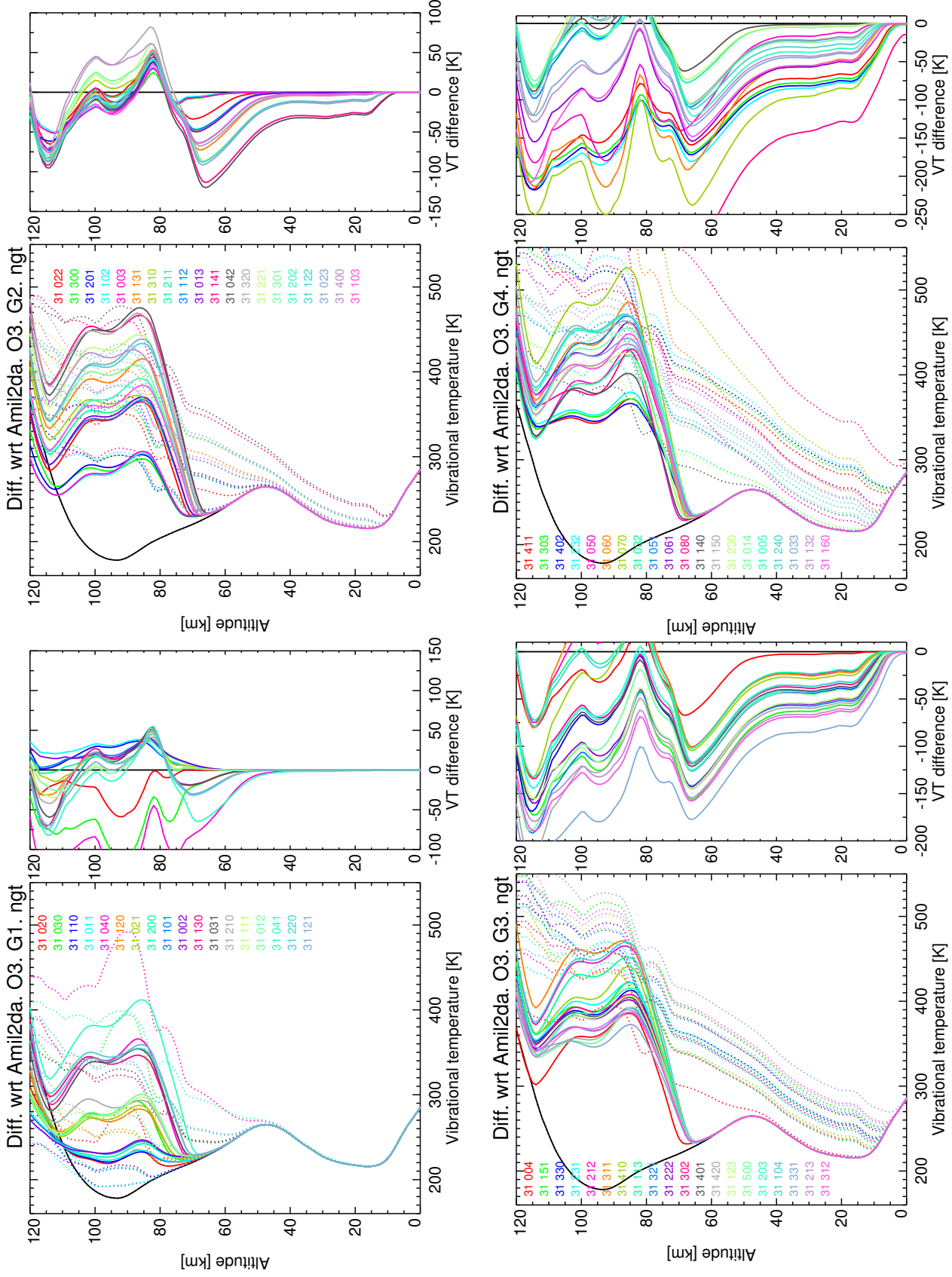


Figure 77: Differences in vibrational temperatures w.r.t. previous version (AMIL2DA) for O₃ levels, set 2, for reference atmosphere #2, night. Solid: this study; dash: AMIL2DA. Right panels: this study-AMIL2DA.

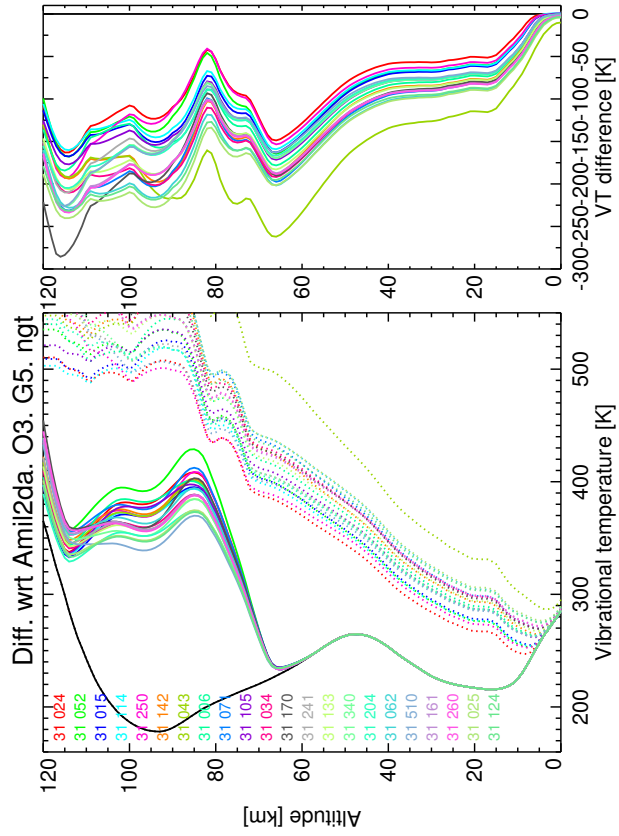


Figure 78: Differences in vibrational temperatures w.r.t. previous version (AMIL2DA) for O₃ levels, set 3, for reference atmosphere #2, nigh. Solid: this study; dash: AMIL2DA. Right panels: this study–AMIL2DA.

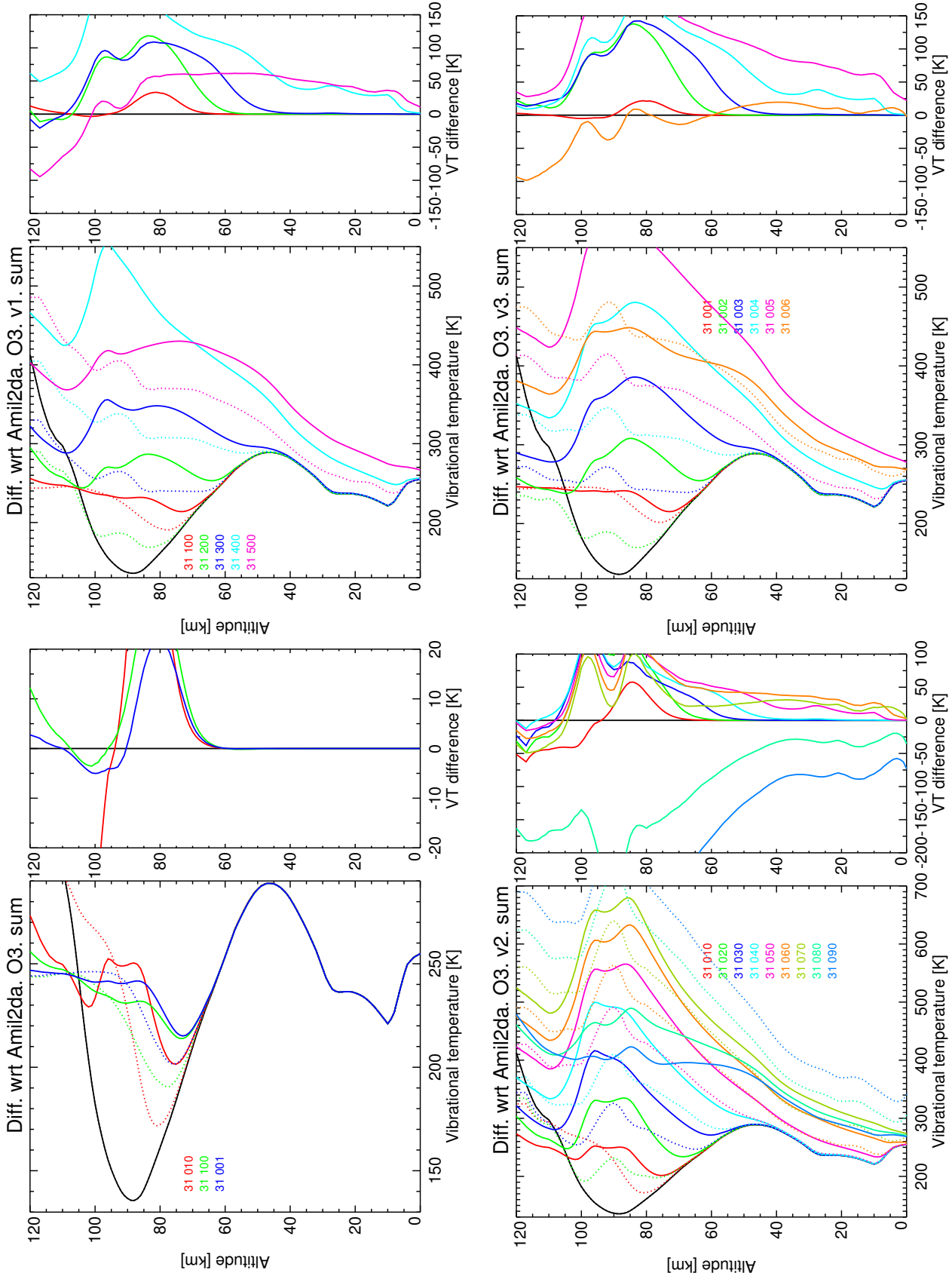


Figure 79: Differences in vibrational temperatures w.r.t. previous version (AMIL2DA) for O₃ levels, set 1, for reference atmosphere #3, summer. Solid: this study; dash: AMIL2DA. Right panels: this study–AMIL2DA.

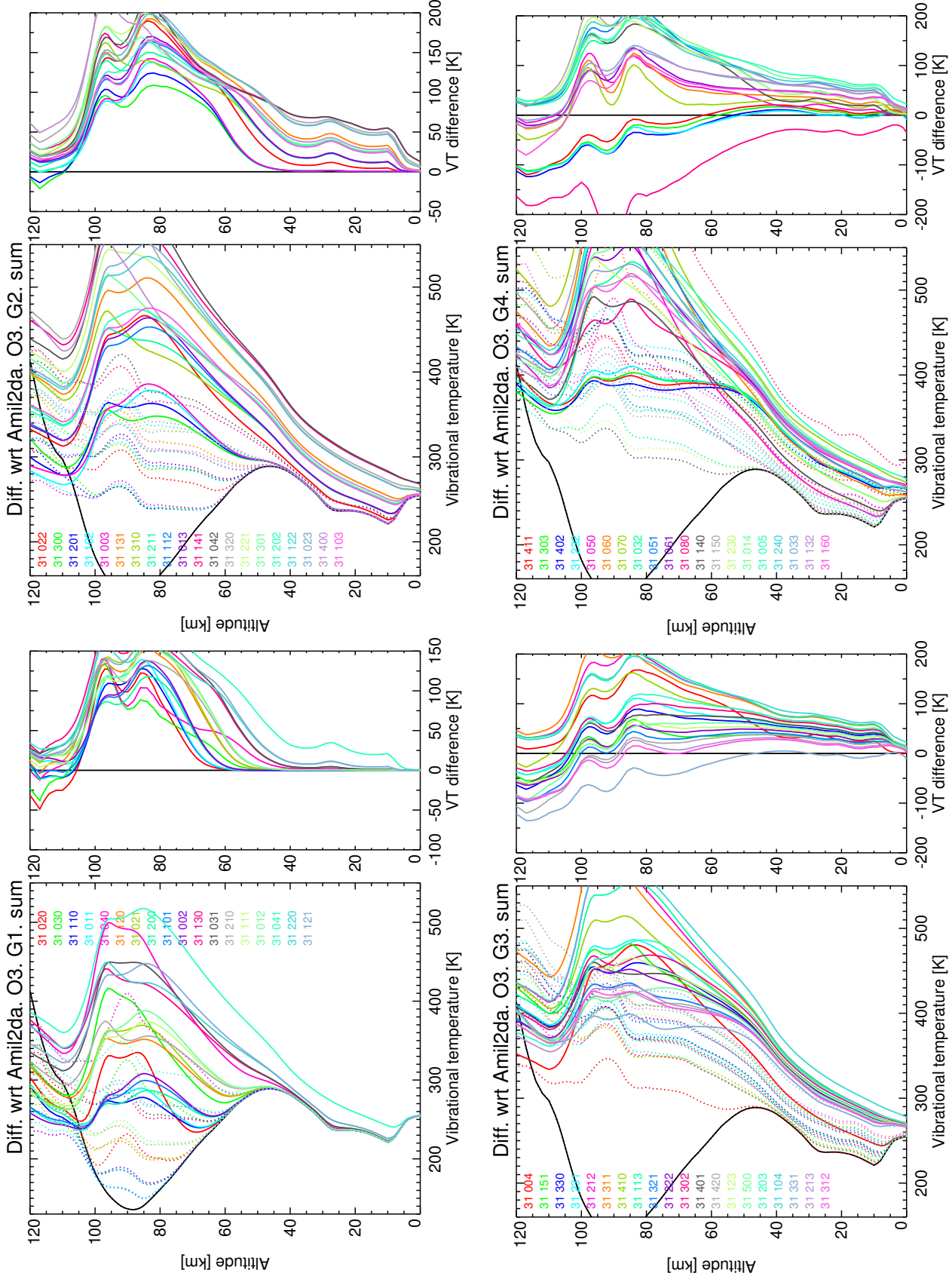


Figure 8: Differences in vibrational temperatures w.r.t. previous version (AMIL2DA) for O₃ levels, set 2, for reference atmosphere #3, summer. Solid: this study; dash: AMIL2DA. Right panels: this study–AMIL2DA.

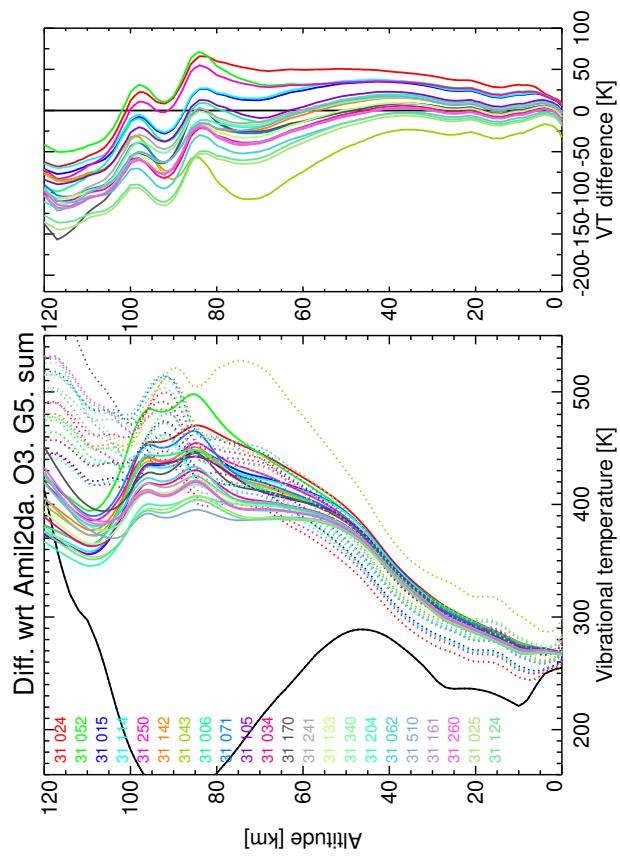


Figure 81: Differences in vibrational temperatures w.r.t. previous version (AMIL2DA) for O_3 levels, set 3, for reference atmosphere #3, summer. Solid: this study; dash: AMIL2DA. Right panels: this study–AMIL2DA.

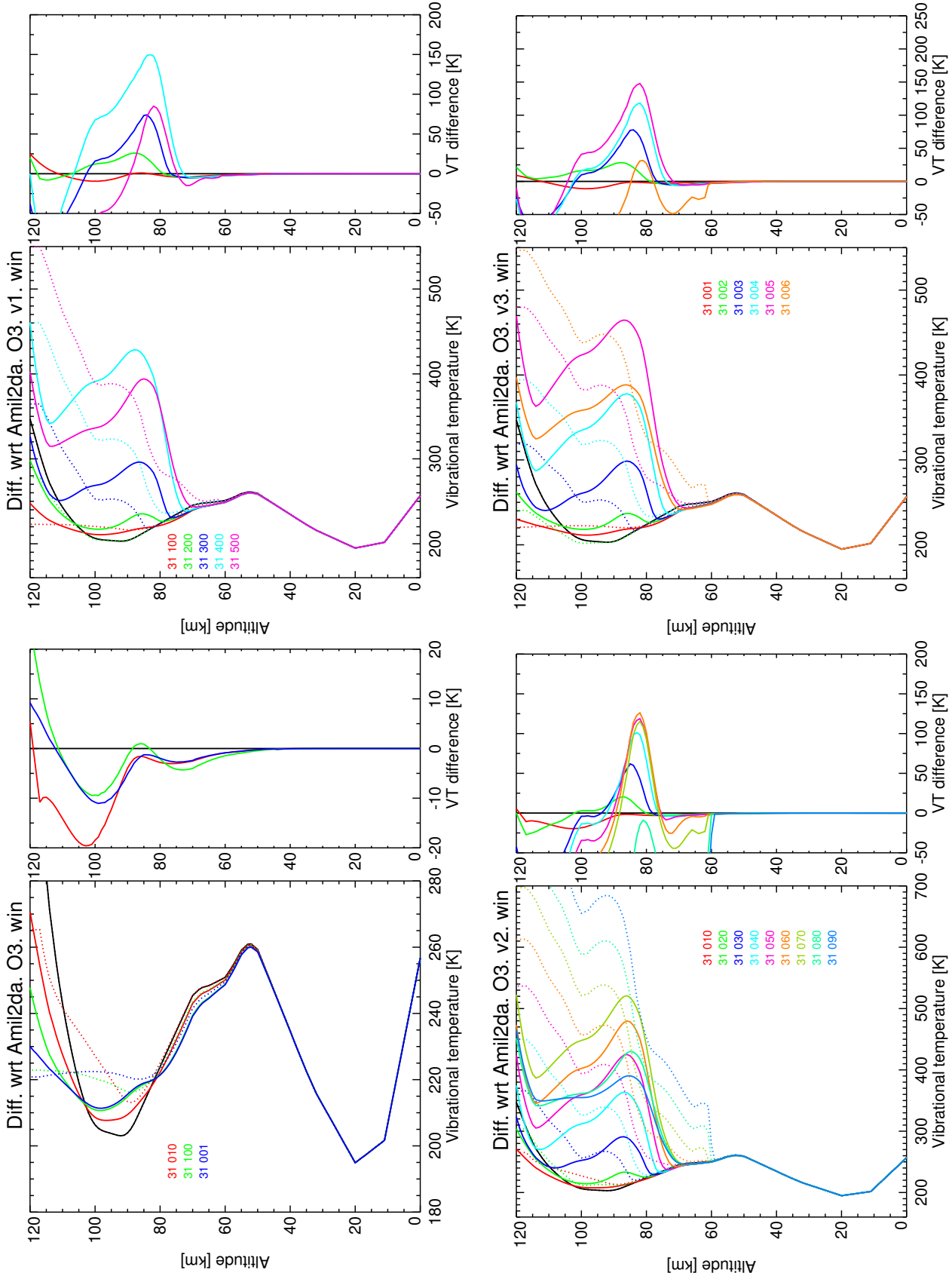


Figure 82: Differences in vibrational temperatures w.r.t. previous version (AMIL2DA) for O₃ levels, set 1, for reference atmosphere #4, winter. Solid: this study; dash: AMIL2DA. Right panels: this study–AMIL2DA.

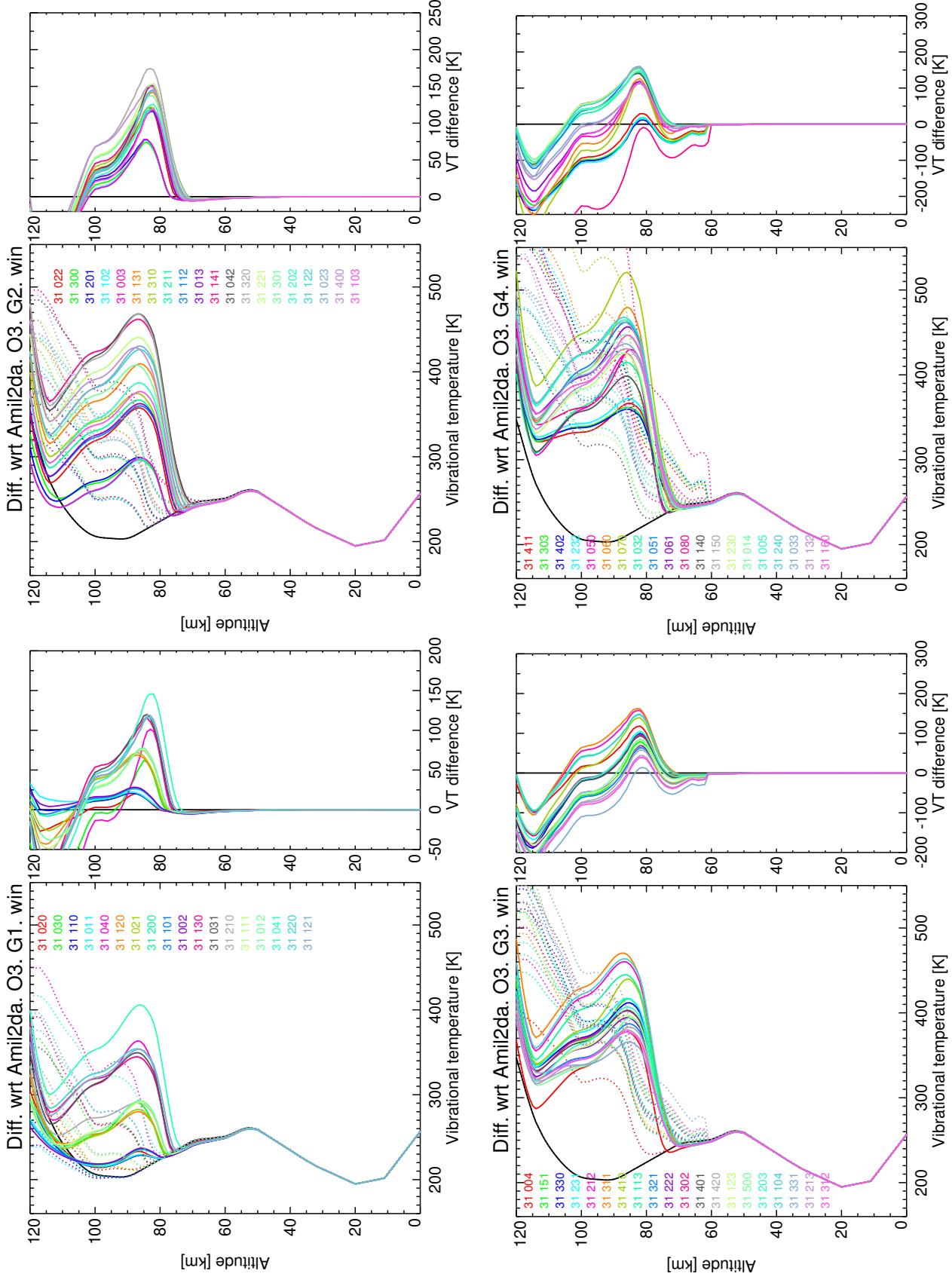


Figure 83: Differences in vibrational temperatures w.r.t. previous version (AMIL2DA) for O₃ levels, set 2, for reference atmosphere #4, winter. Solid: this study; dash: AMIL2DA. Right panels: this study–AMIL2DA.

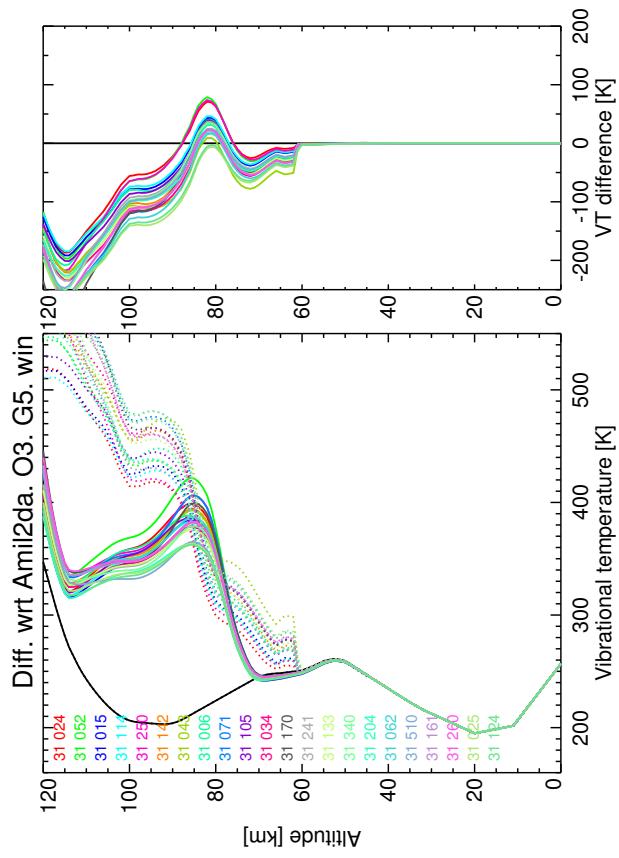


Figure 84: Differences in vibrational temperatures w.r.t. previous version (AMIL2DA) for O₃ levels, set 3, for reference atmosphere #4, winter. Solid: this study; dash: AMIL2DA. Right panels: this study–AMIL2DA.

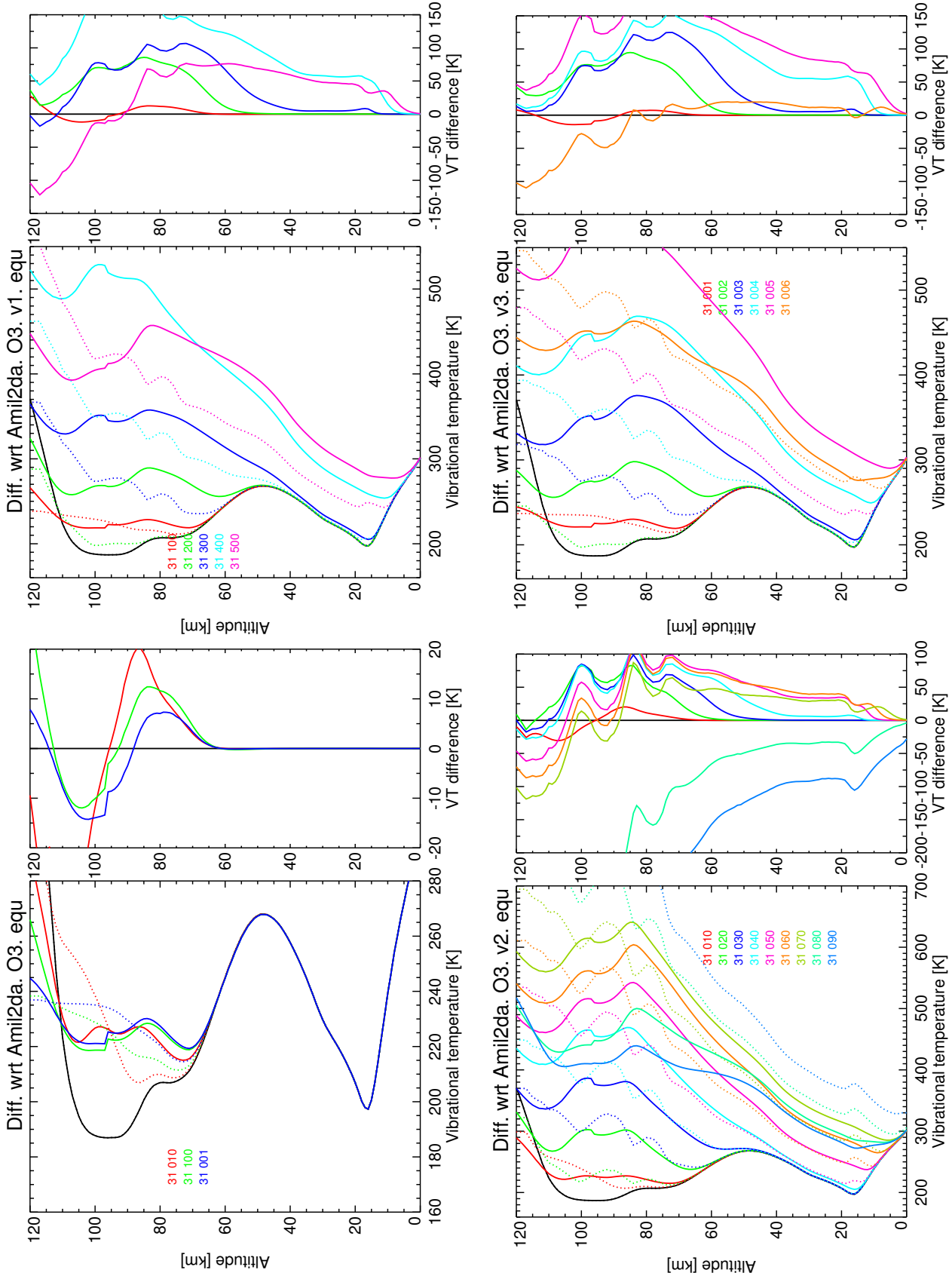


Figure 85: Differences in vibrational temperatures w.r.t. previous version (AMIL2DA) for O_3 levels, set 1, for reference atmosphere #5, equator. Solid: this study; dash: AMIL2DA. Right panels: this study–AMIL2DA.

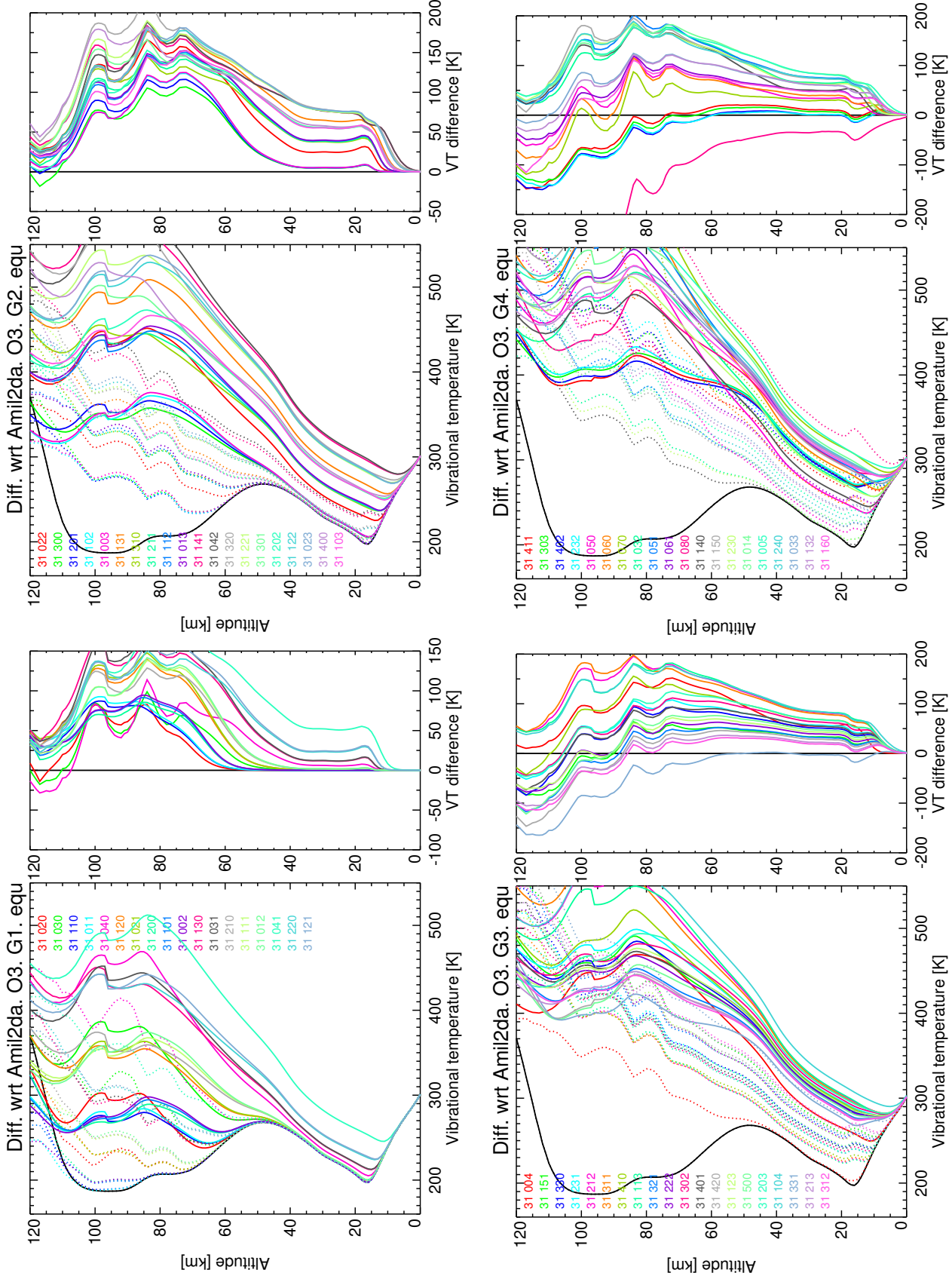


Figure 8: Differences in vibrational temperatures w.r.t. previous version (AMIL2DA) for O_3 levels, set 2, for reference atmosphere #5, equator. Solid: this study; dash: AMIL2DA. Right panels: this study–AMIL2DA.

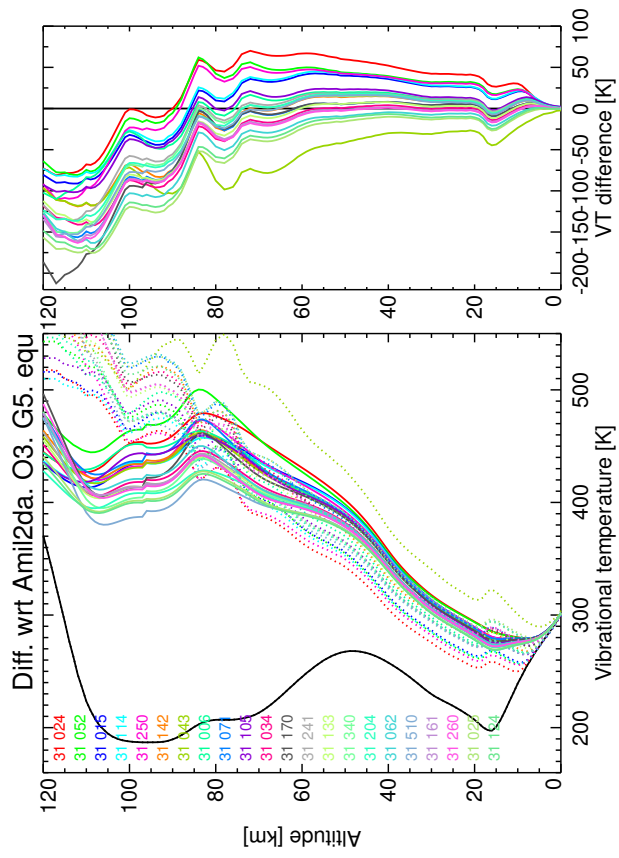


Figure 87: Differences in vibrational temperatures w.r.t. previous version (AMIL2DA) for O₃ levels, set 3, for reference atmosphere #5, equat or. Solid: this study; dash: AMIL2DA. Right panels: this study–AMIL2DA.

3.5 N₂O

The major upgrade in the N₂O non-LTE model is a more accurate calculation of the radiative transfer. We should also mention, that the non-LTE model prediction of the N₂O v_3 emission at 4.5 μm previously calculated has been confirmed with the analysis of the MIPAS spectra (López-Puertas et al., 2007).

Figures 88-92 show the vibrational temperatures for the N₂O energy levels from the lowest to the highest energy.

Figures 93-97 show the differences in the vibrational temperatures for the N₂O energy levels with respect to previous (AMIL2DA) version. In general, the new vibrational temperatures are larger than previous ones in the non-LTE region, due to the more accurate radiative transfer.

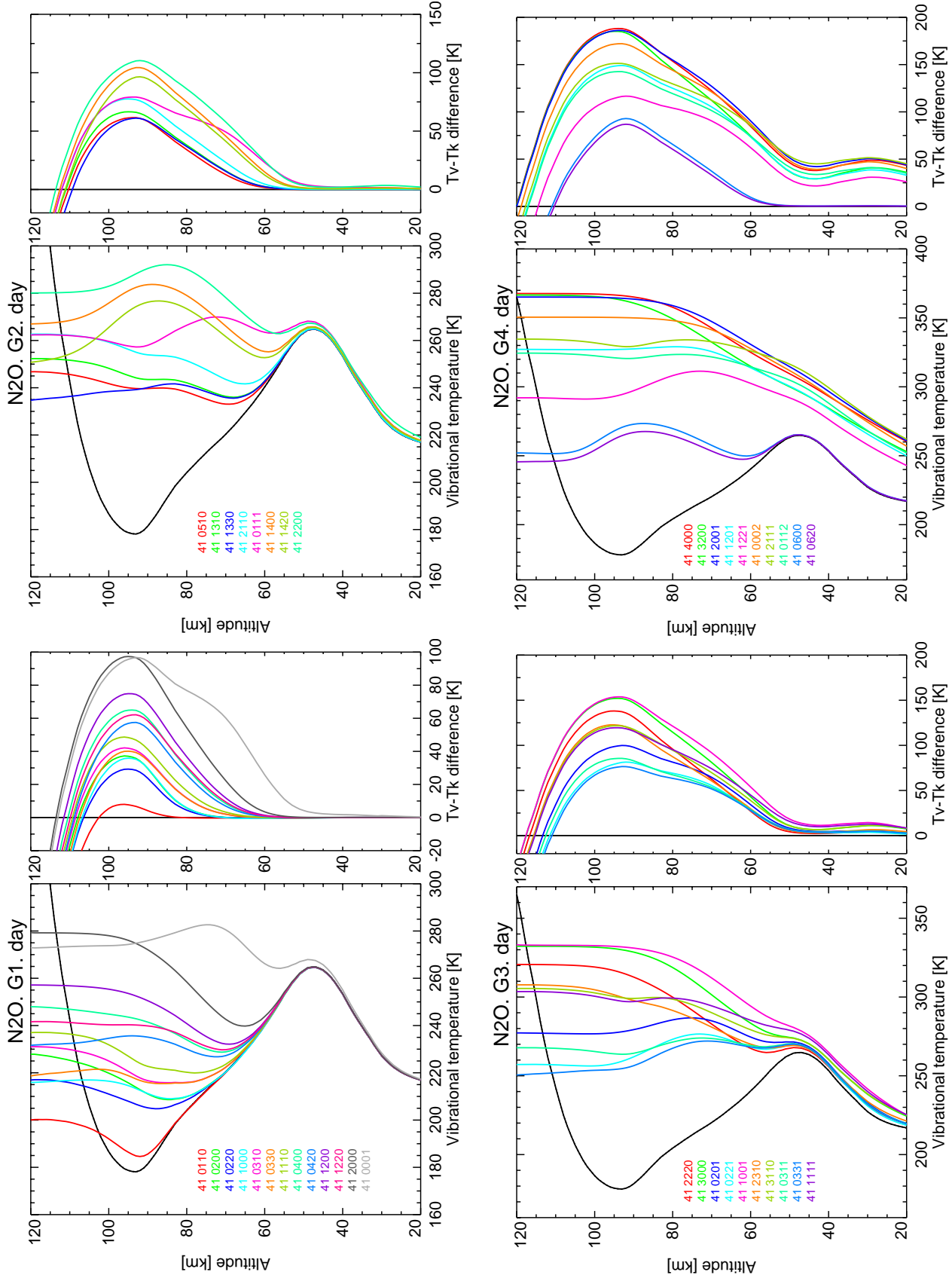


Figure 88: Vibrational temperatures for N_2O levels, for reference atmosphere #1, day.

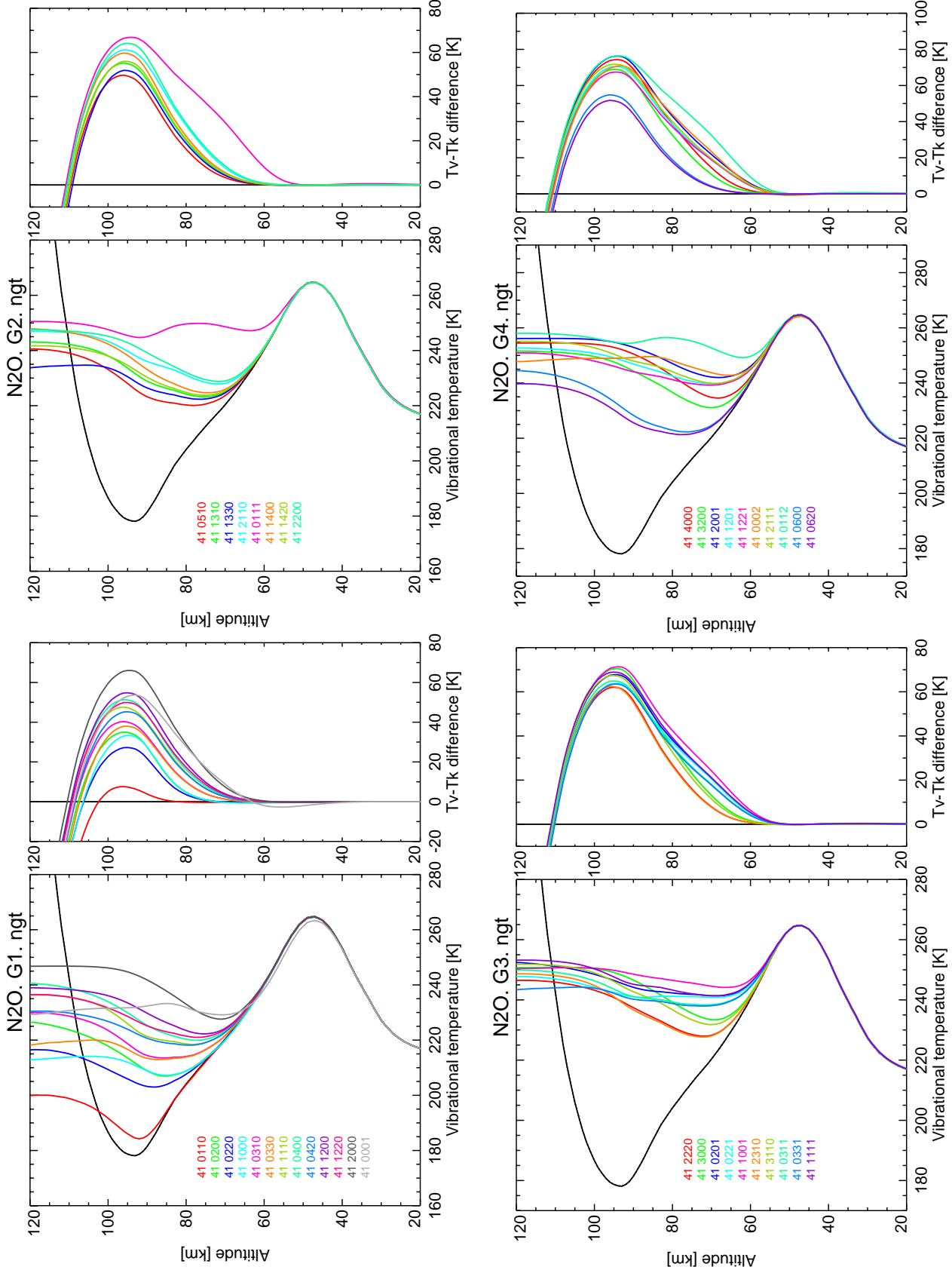


Figure 89: Vibrational temperatures for N₂O levels, for reference atmosphere #2, night.

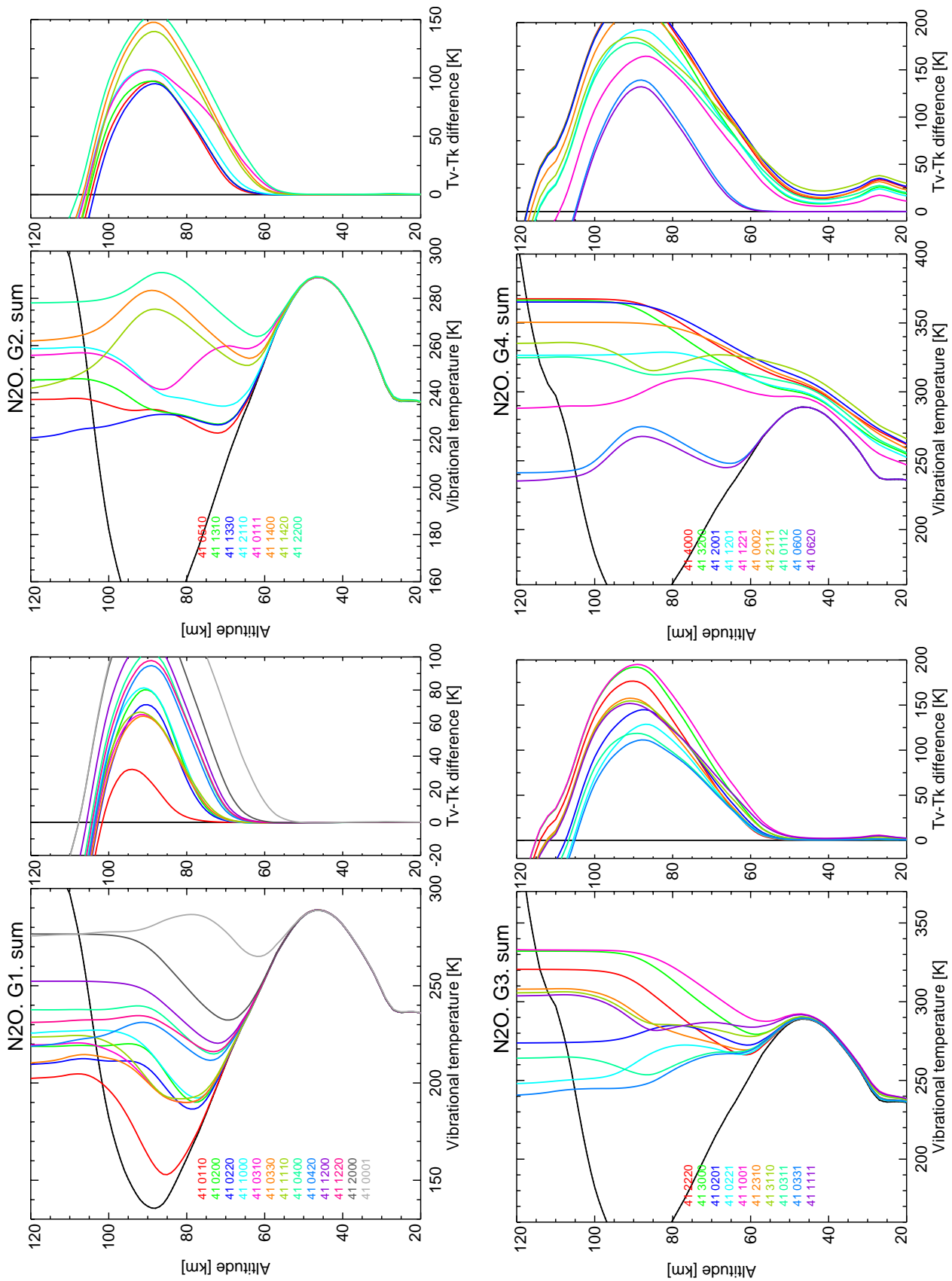


Figure 90: Vibrational temperatures for N_2O levels, for reference atmosphere #3, summer.

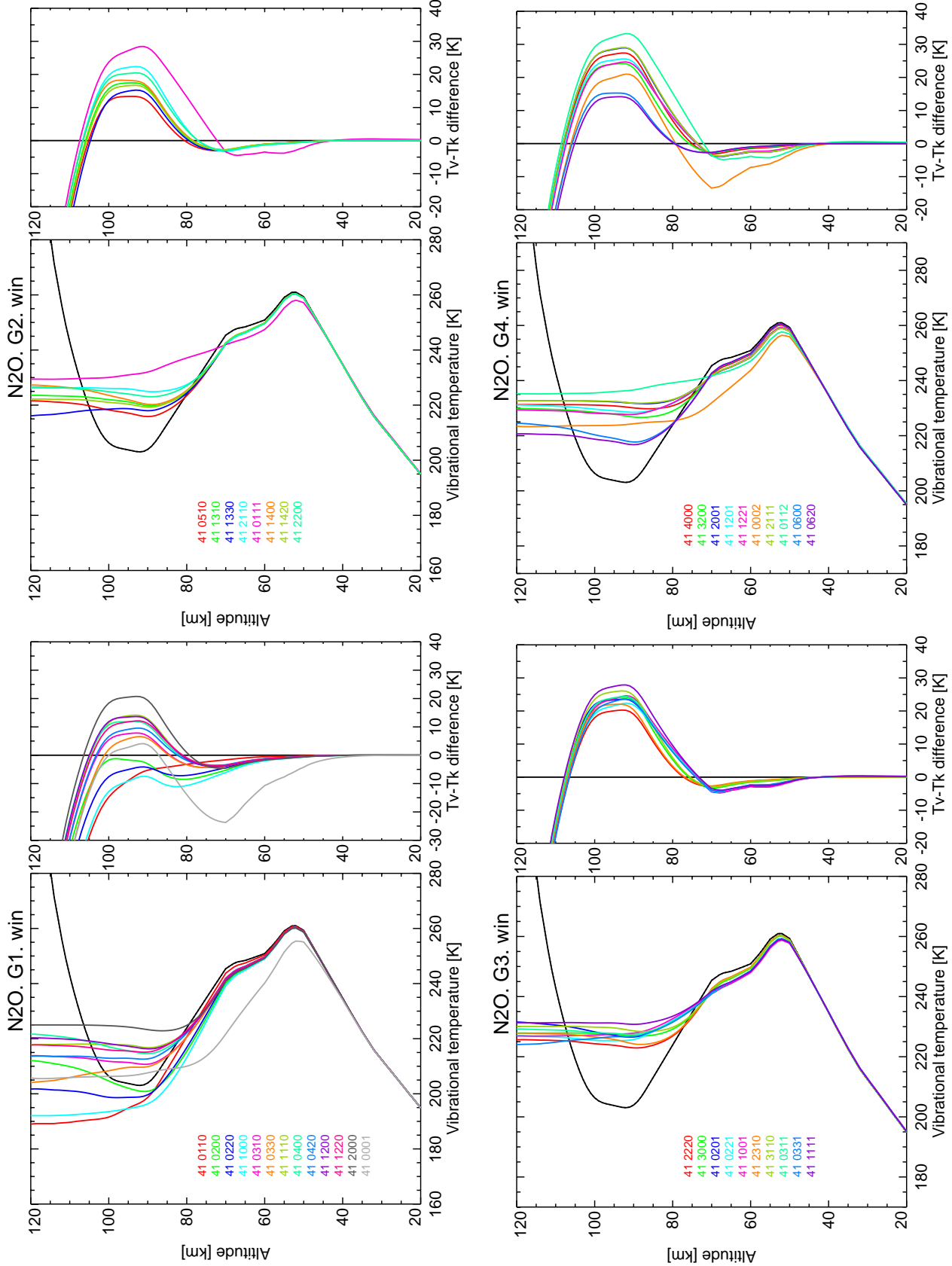


Figure 91: Vibrational temperatures for N_2O levels, for reference atmosphere #4, winter.

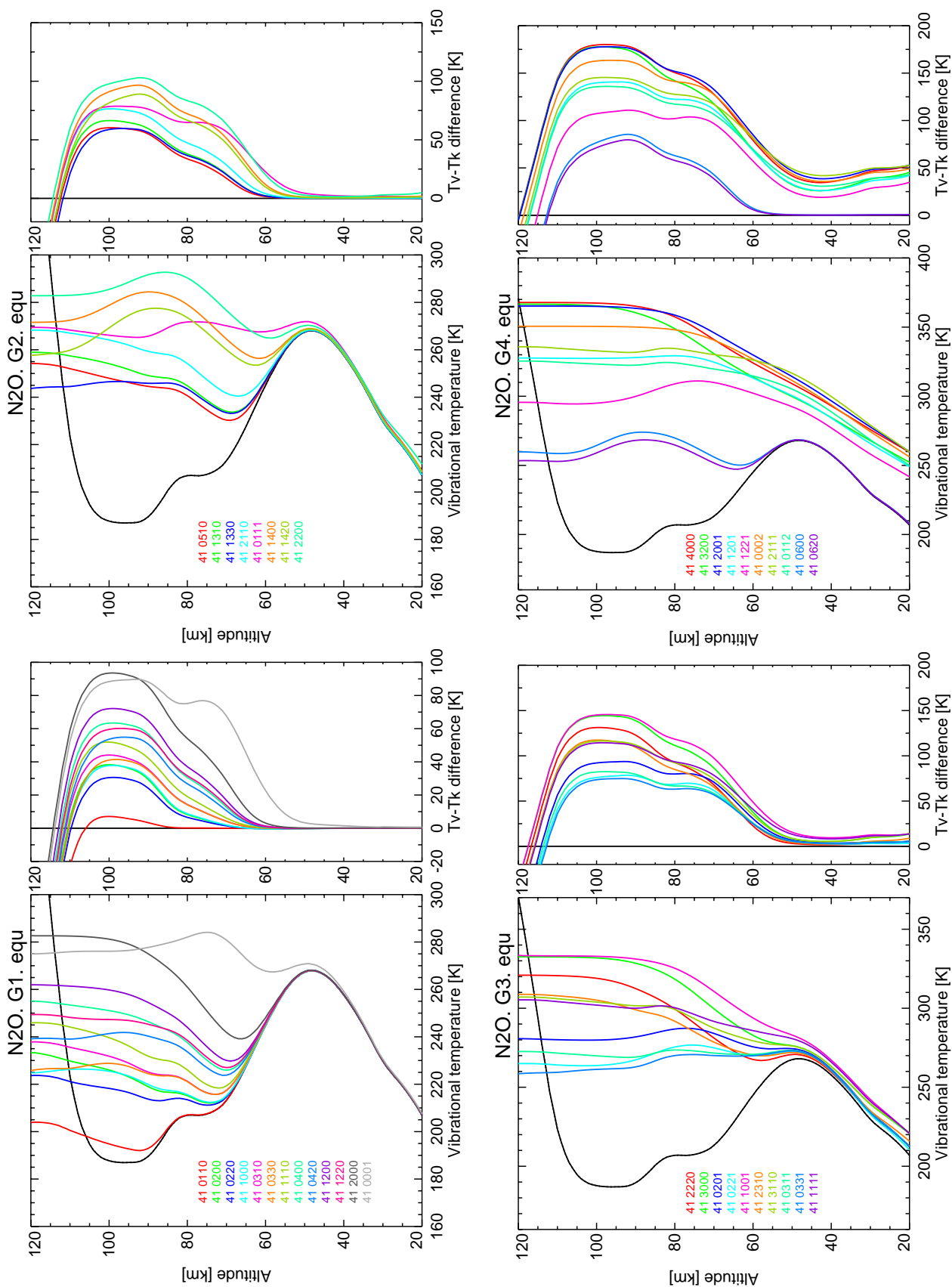


Figure 92: Vibrational temperatures for N₂O levels, for reference atmosphere #5, equator.

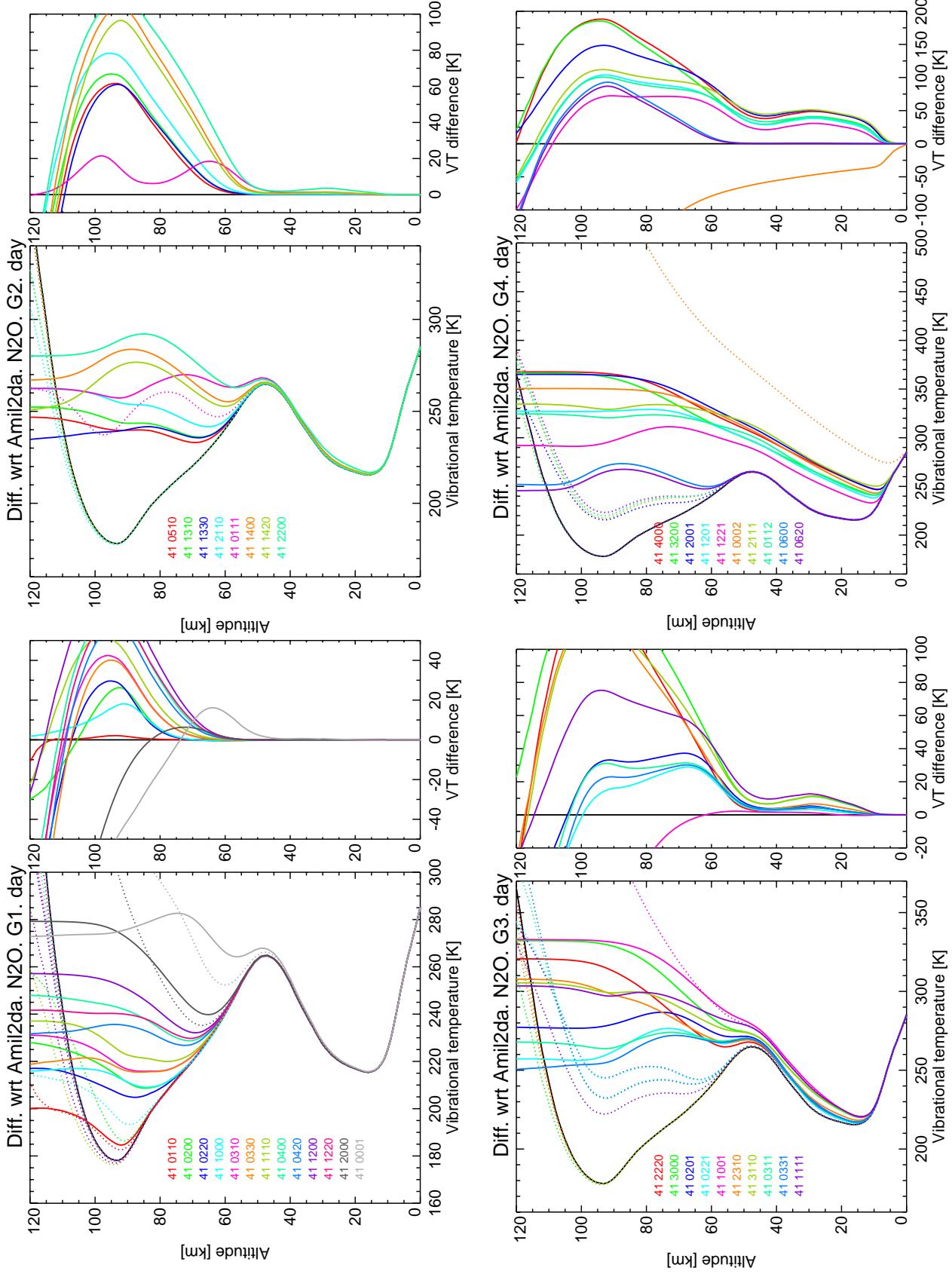


Figure 93: Differences in vibrational temperatures w.r.t. previous version (AMIL2DA) for N_2O levels, for reference atmosphere #1, day.
 Solid: this study; dash: AMIL2DA. Right panels: this study–AMIL2DA.

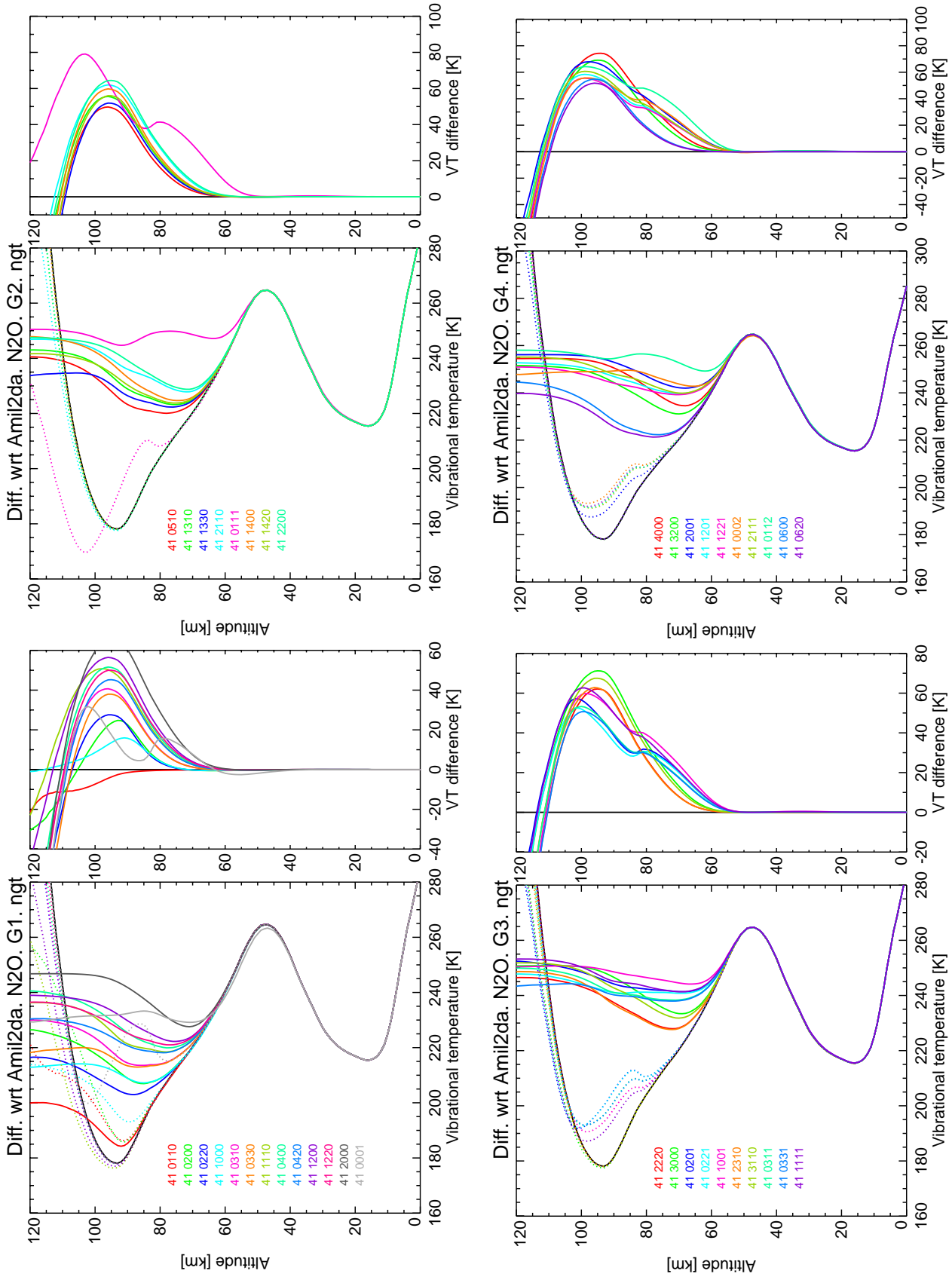


Figure 94: Differences in vibrational temperatures w.r.t. previous version (AMIL2DA) for N₂O levels, for reference atmosphere #2, night. Solid: this study; dash: AMIL2DA. Right panels: this study–AMIL2DA.

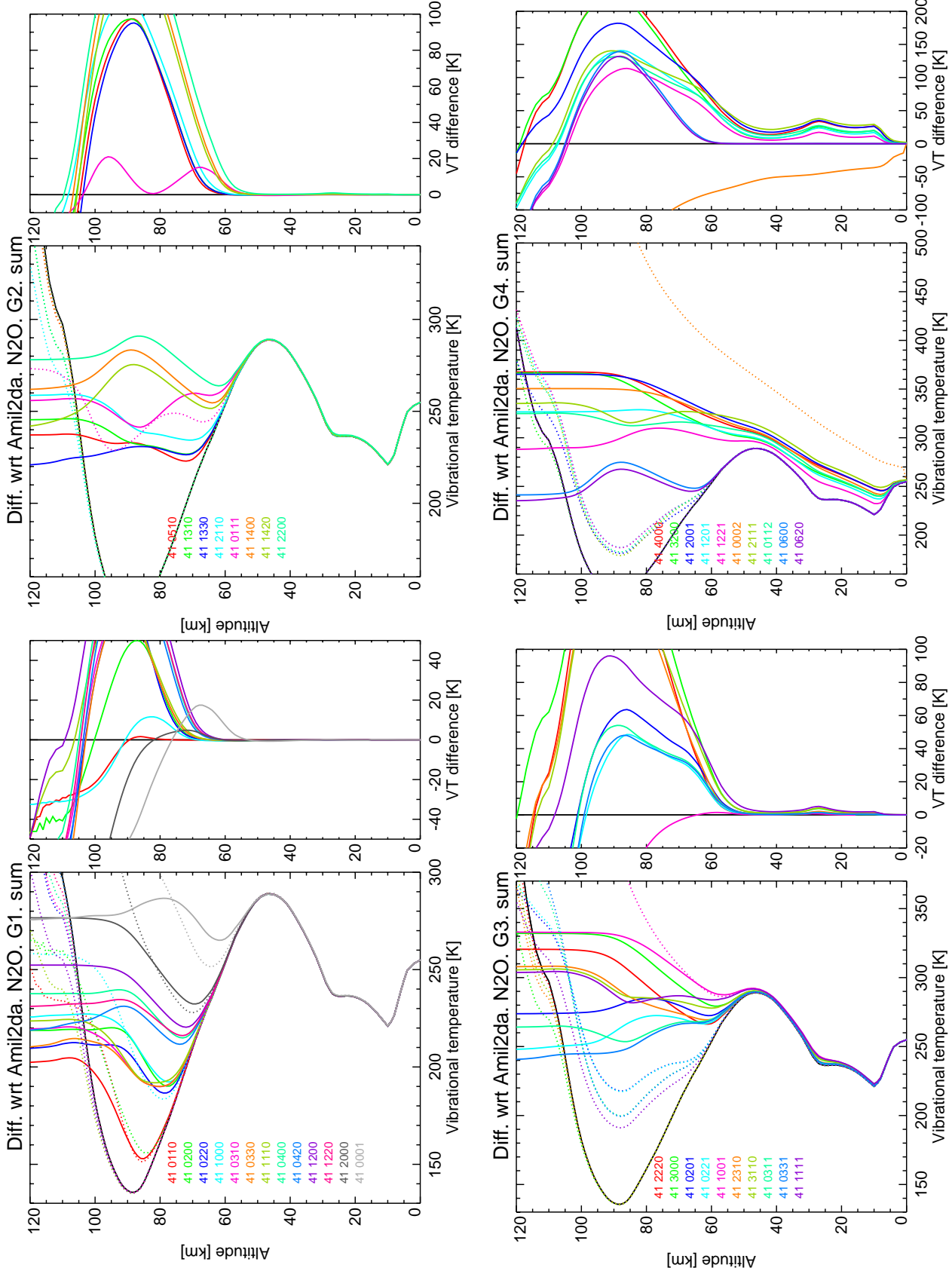


Figure 95: Differences in vibrational temperatures w.r.t. previous version (AMIL2DA) for N_2O levels, for reference atmosphere #3, sum.
 Solid: this study; dash: AMIL2DA. Right panels: this study–AMIL2DA.

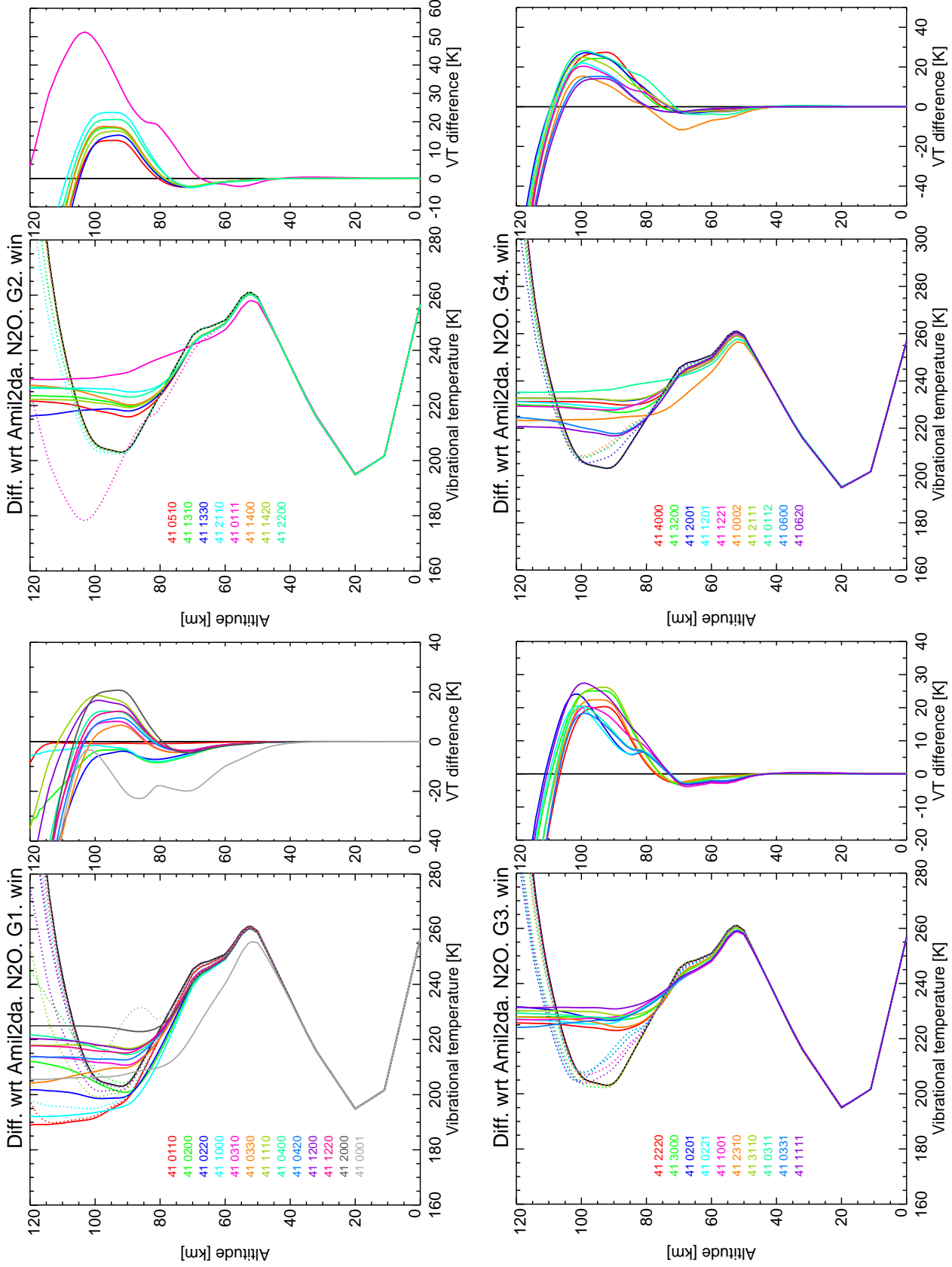


Figure 96: Differences in vibrational temperatures w.r.t. previous version (AMIL2DA) for N₂O levels, for reference atmosphere #4, winter. Solid: this study; dash: AMIL2DA. Right panels: this study–AMIL2DA.

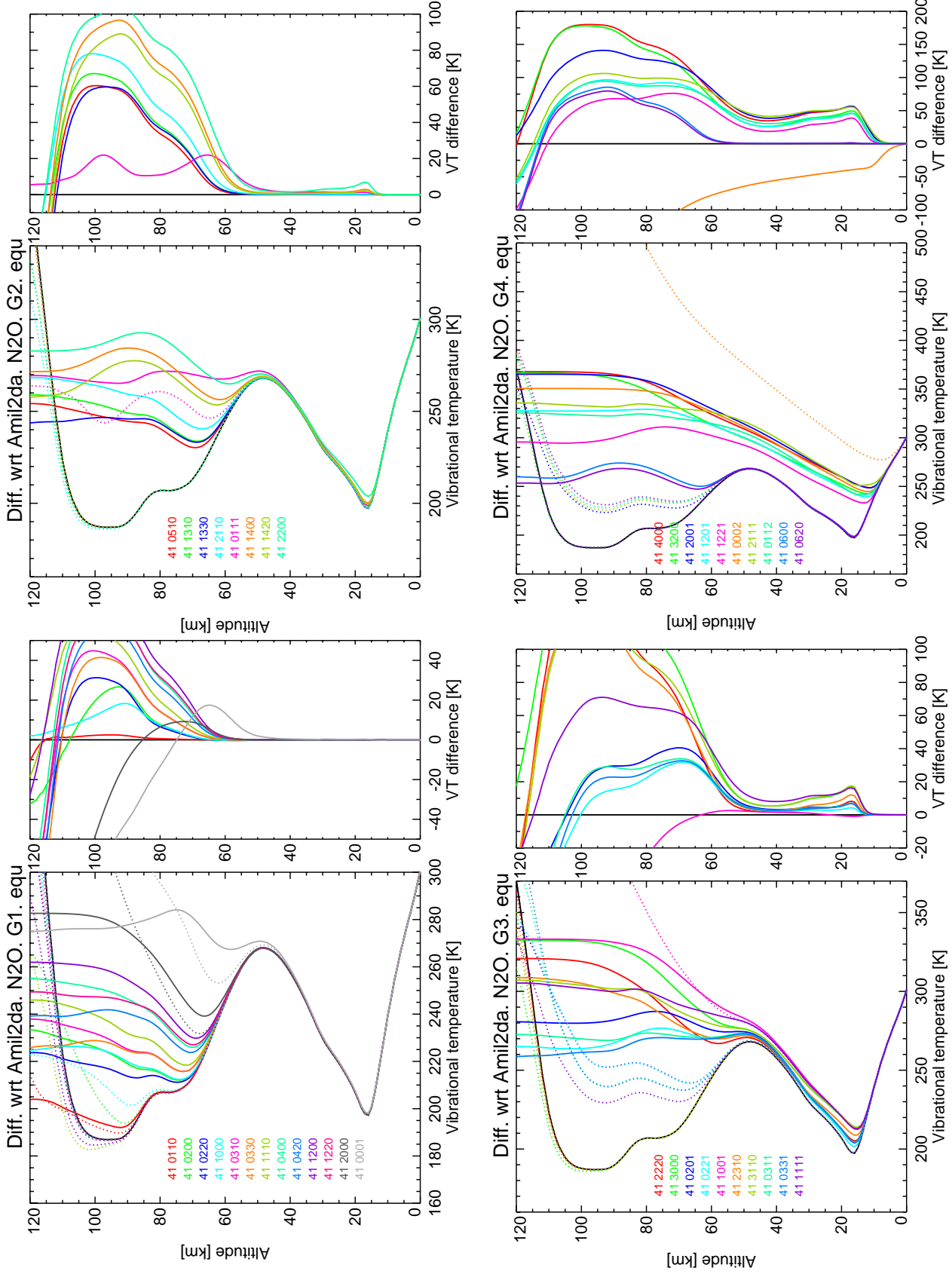


Figure 97: Differences in vibrational temperatures w.r.t. previous version (AMIL2DA) for N_2O levels, for reference atmosphere #5, equator. Solid: this study; dash: AMIL2DA. Right panels: this study–AMIL2DA.

3.6 CO

The major upgrades in the CO non-LTE model are the improvements resulting from a more accurate CO₂(001) population (since it affect CO(1) through VV transfer from CO₂(001) to N₂(1) and to CO(1)), and from the update of the solar flux at 4.6 μm . A very detailed study of the MIPAS spectra has been carried out, whereby the CO(1) fundamental, first hot, and isotopic bands were all simultaneously fitted to MIPAS spectra within a 5% difference (Funke et al., 2007).

Figures 98-102 show the vibrational temperatures for the CO energy levels.

Figures 103-107 show the differences in the vibrational temperatures for the CO energy levels with respect to previous (AMIL2DA) version. The main result is a larger daytime VT in the 40-80 km region (due to a larger CO₂(001) population), and smaller above 80 km because of the smaller solar flux at 4.7 μm .

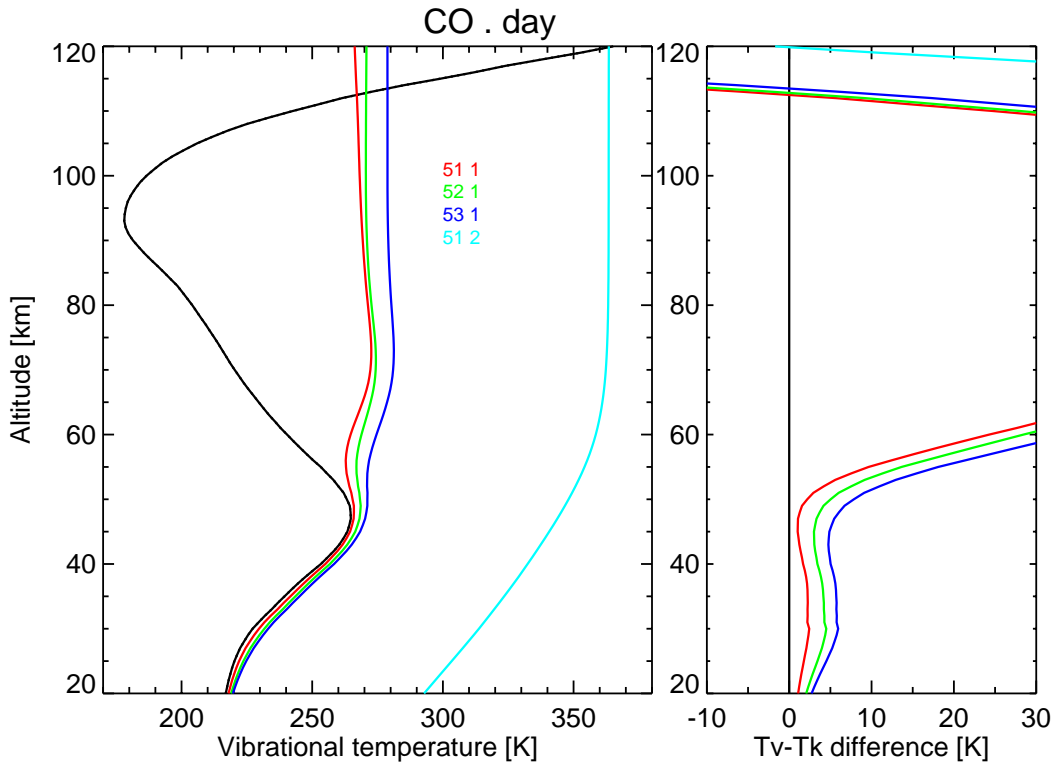


Figure 98: Vibrational temperatures for CO levels, for reference atmosphere #1, day.

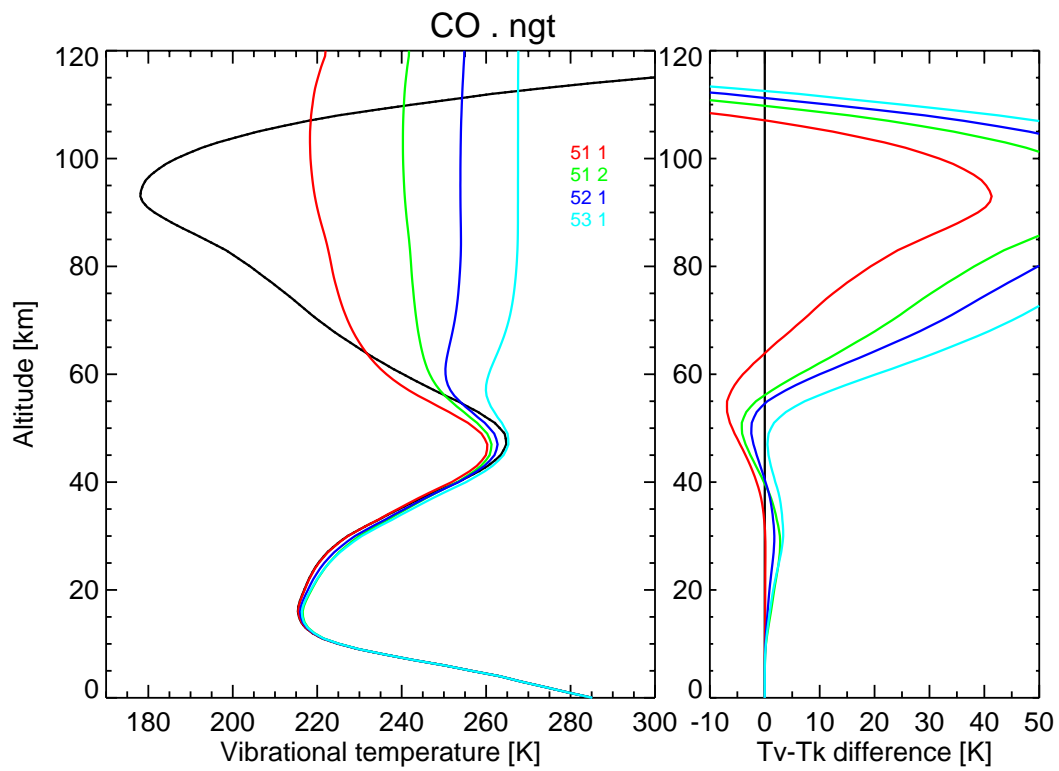


Figure 99: Vibrational temperatures for CO levels, for reference atmosphere #2, night.

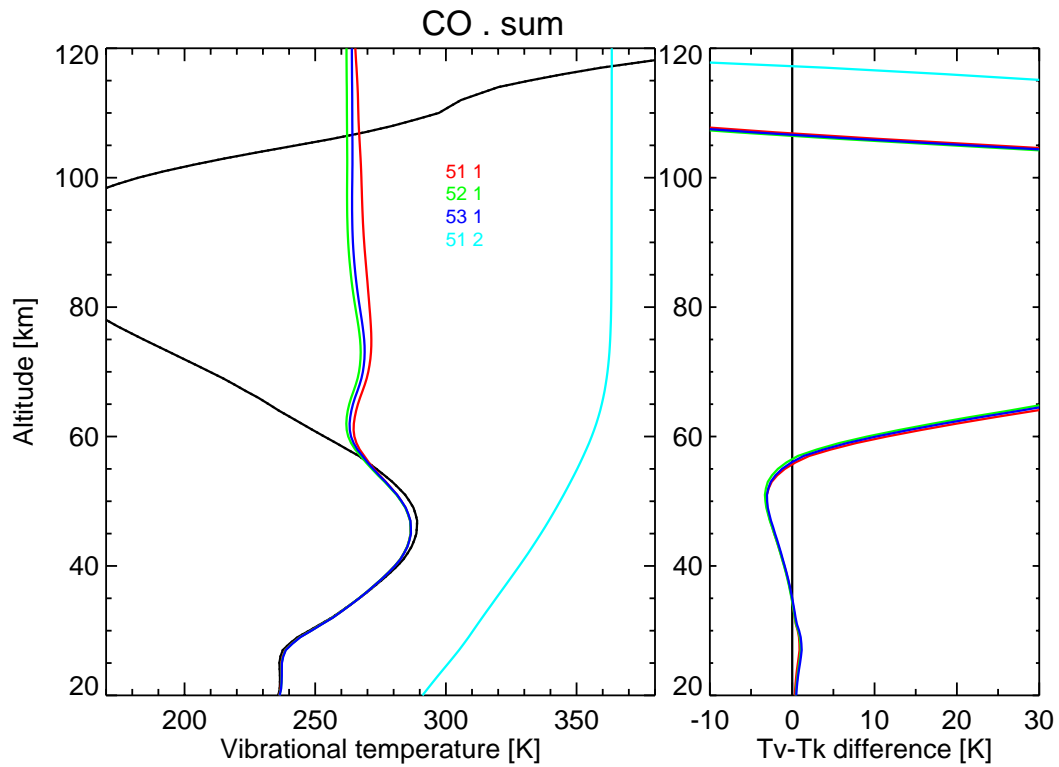


Figure 100: Vibrational temperatures for CO levels, for reference atmosphere #3, summer.

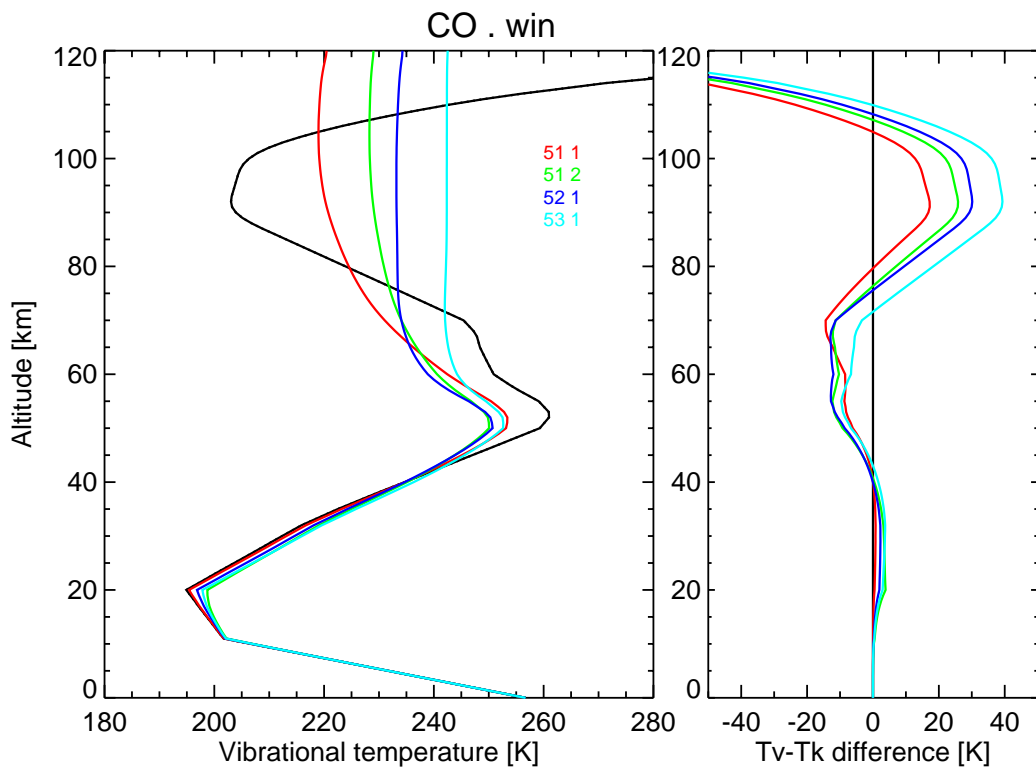


Figure 101: Vibrational temperatures for CO levels, for reference atmosphere #4, winter.

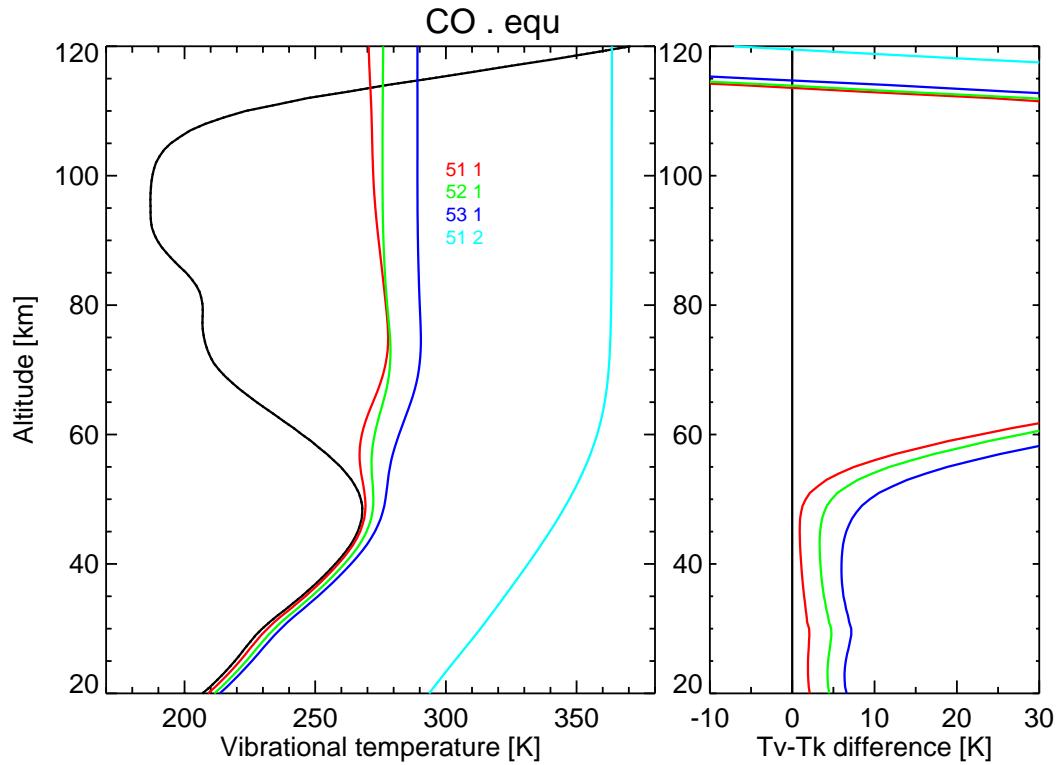


Figure 102: Vibrational temperatures for CO levels, for reference atmosphere #5, equator.

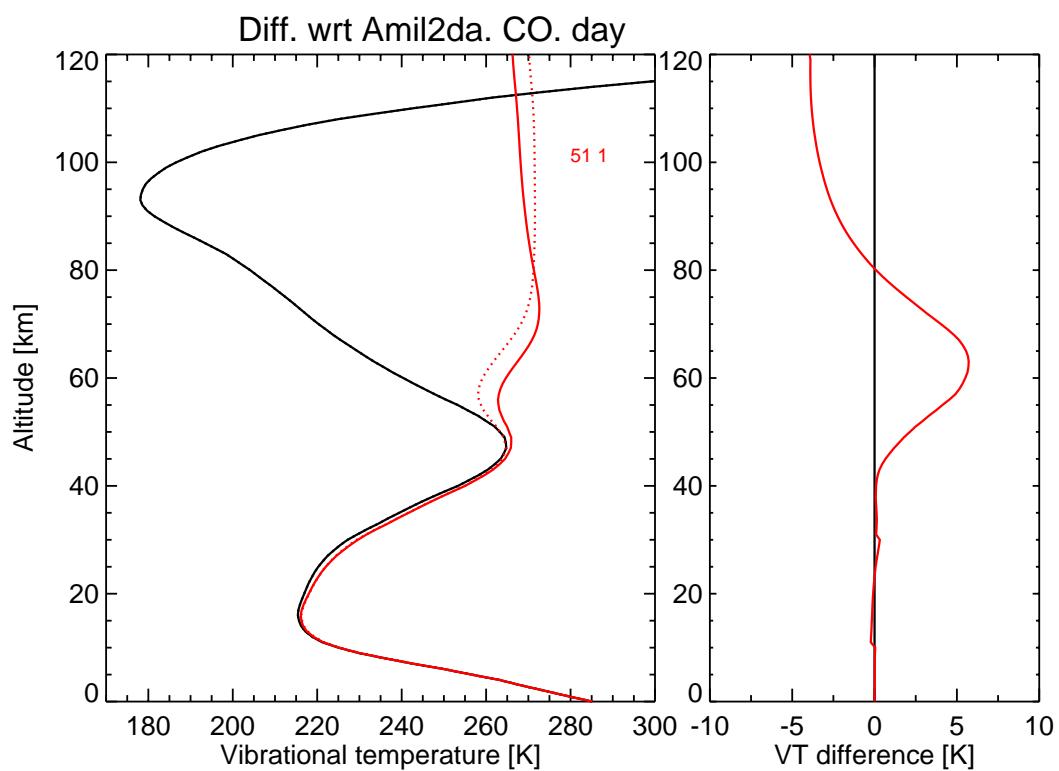


Figure 103: Differences in vibrational temperatures w.r.t. previous version (AMIL2DA) for the CO levels, for reference atmosphere #1, day. Solid: this study; dash: AMIL2DA. Right panels: this study–AMIL2DA.

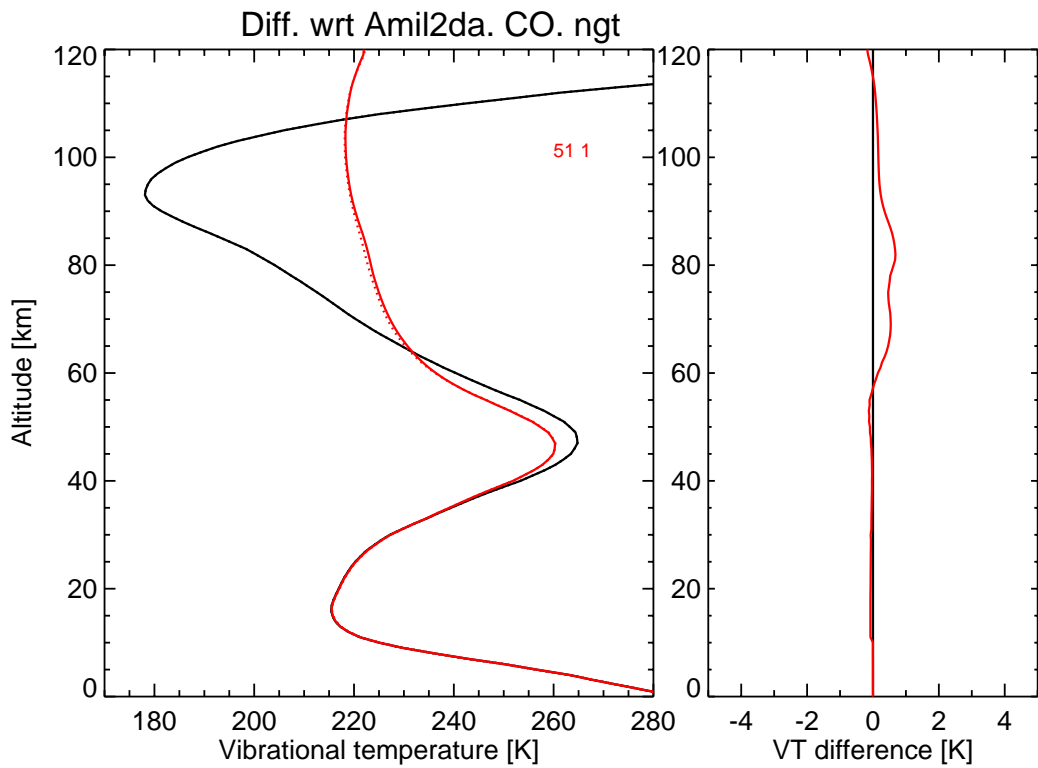


Figure 104: Differences in vibrational temperatures w.r.t. previous version (AMIL2DA) for the CO levels, for reference atmosphere #2, ngt. Solid: this study; dash: AMIL2DA. Right panels: this study–AMIL2DA.

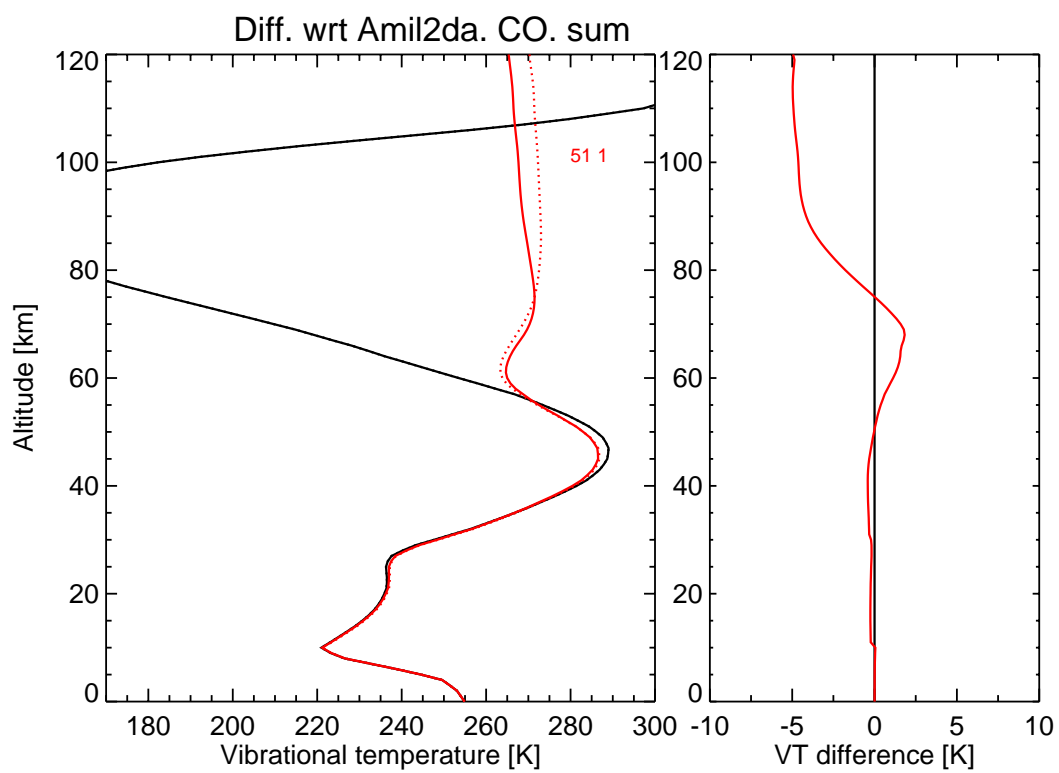


Figure 105: Differences in vibrational temperatures w.r.t. previous version (AMIL2DA) for the CO levels, for reference atmosphere #3, summer. Solid: this study; dash: AMIL2DA. Right panels: this study–AMIL2DA.

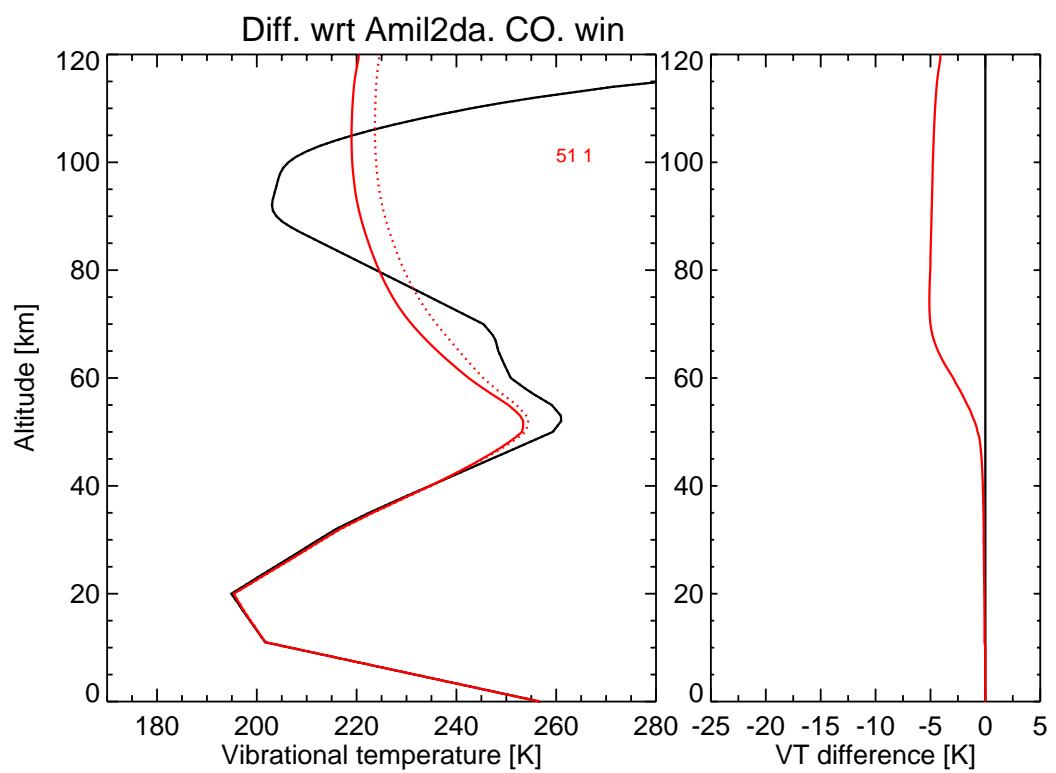


Figure 106: Differences in vibrational temperatures w.r.t. previous version (AMIL2DA) for the CO levels, for reference atmosphere #4, winter. Solid: this study; dash: AMIL2DA. Right panels: this study–AMIL2DA.

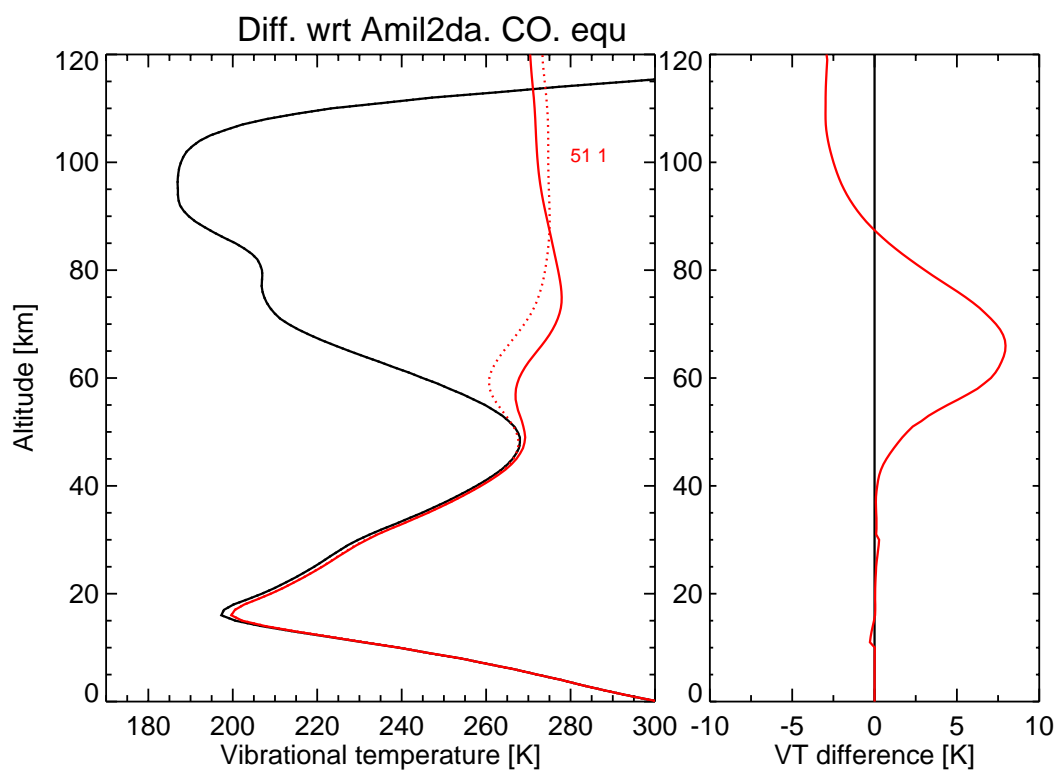


Figure 107: Differences in vibrational temperatures w.r.t. previous version (AMIL2DA) for the CO levels, for reference atmosphere #5, equator. Solid: this study; dash: AMIL2DA. Right panels: this study–AMIL2DA.

3.7 CH₄

The CH₄(v_2, v_4) levels are strongly coupled to those of O₂(1) and H₂O(010) (see Fig. 108). Thus, the major upgrades in the CH₄ non-LTE model come mainly from the updates in the O₂ and H₂O non-LTE models described in Sec 3.2. In addition to those, we have also included the recent measurement of the rate of the V-V collisional exchange between CH₄(v4) and O₂(1) carried out by Boursier et al. (2007). This rate affects to the population of CH₄(v_4) in the mesosphere. However, it does not exert a significant impact on the the population of O₂(1) and H₂O(010) since they act as a much larger reservoir than the CH₄ levels.

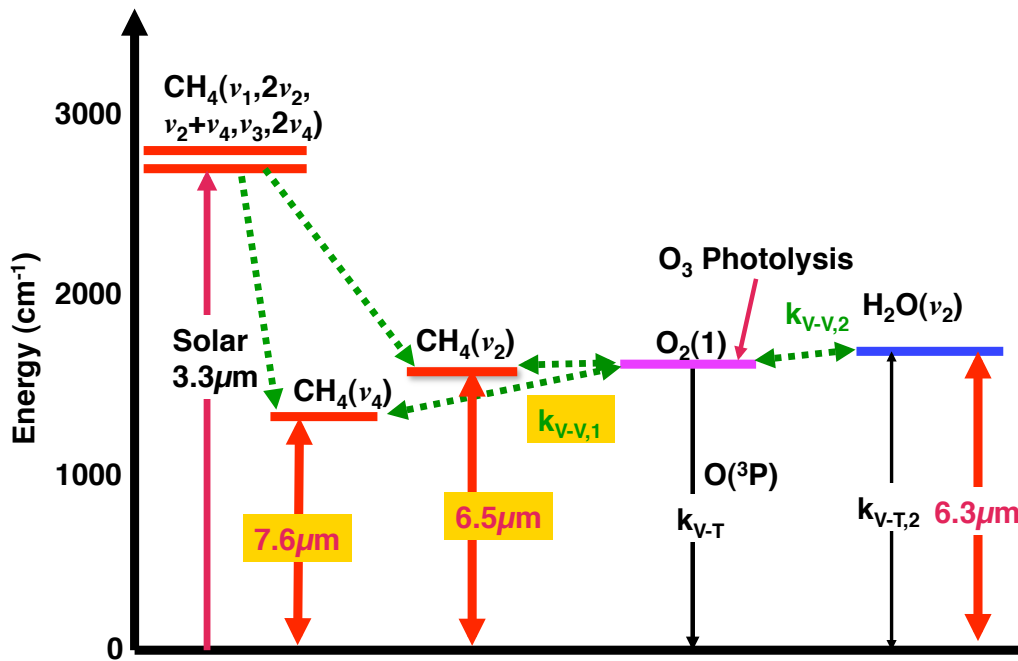


Figure 108: Energy levels of CH₄, H₂O and O₂(1) showing the coupling between them.

Figures 109-113 show the vibrational temperatures for the CH₄ energy levels.

Figures 114-118 show the differences in the vibrational temperatures for the CH₄ energy levels with respect to previous (AMIL2DA) version.

The v_4 level population, whose emission is used for the retrieval of CH₄, has not changed significantly (even the rates for the processes where CH₄ levels are involved have changed substantially). The reason is that the larger relaxation of O₂(1) by O is compensated by a larger excitation of O₂(1) from O₃ photolysis. Similarly, the v_2 level population has only changed very marginally. The higher energy levels are more affected. Some of them have larger populations, because of a better radiative transfer calculation. Other levels have smaller populations because of the larger VV collisional exchange of CH₄ levels with O₂ (Boursier et al., 2007).

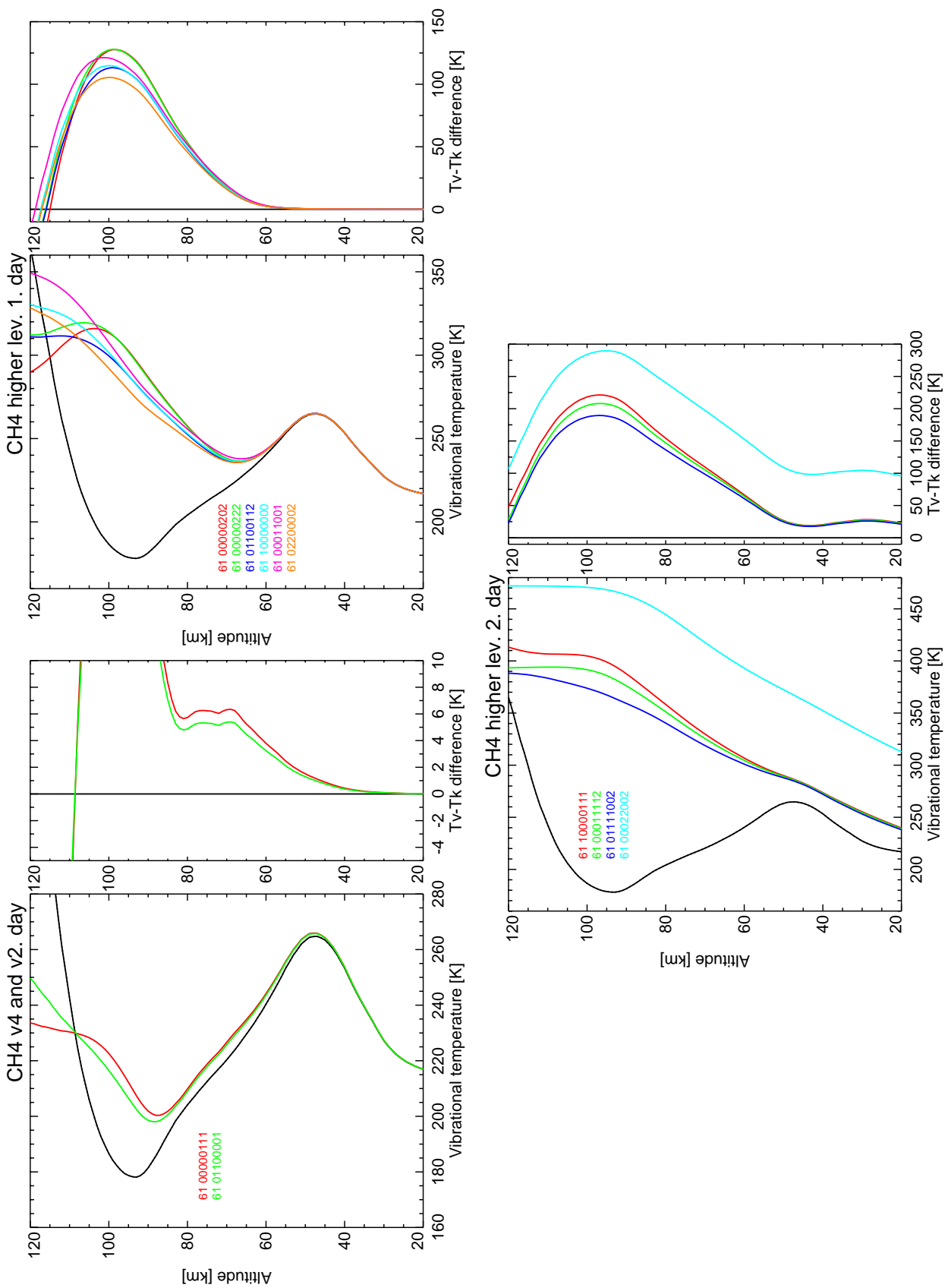


Figure 109: Vibrational temperatures for CH_4 levels, for reference atmosphere #1, day.

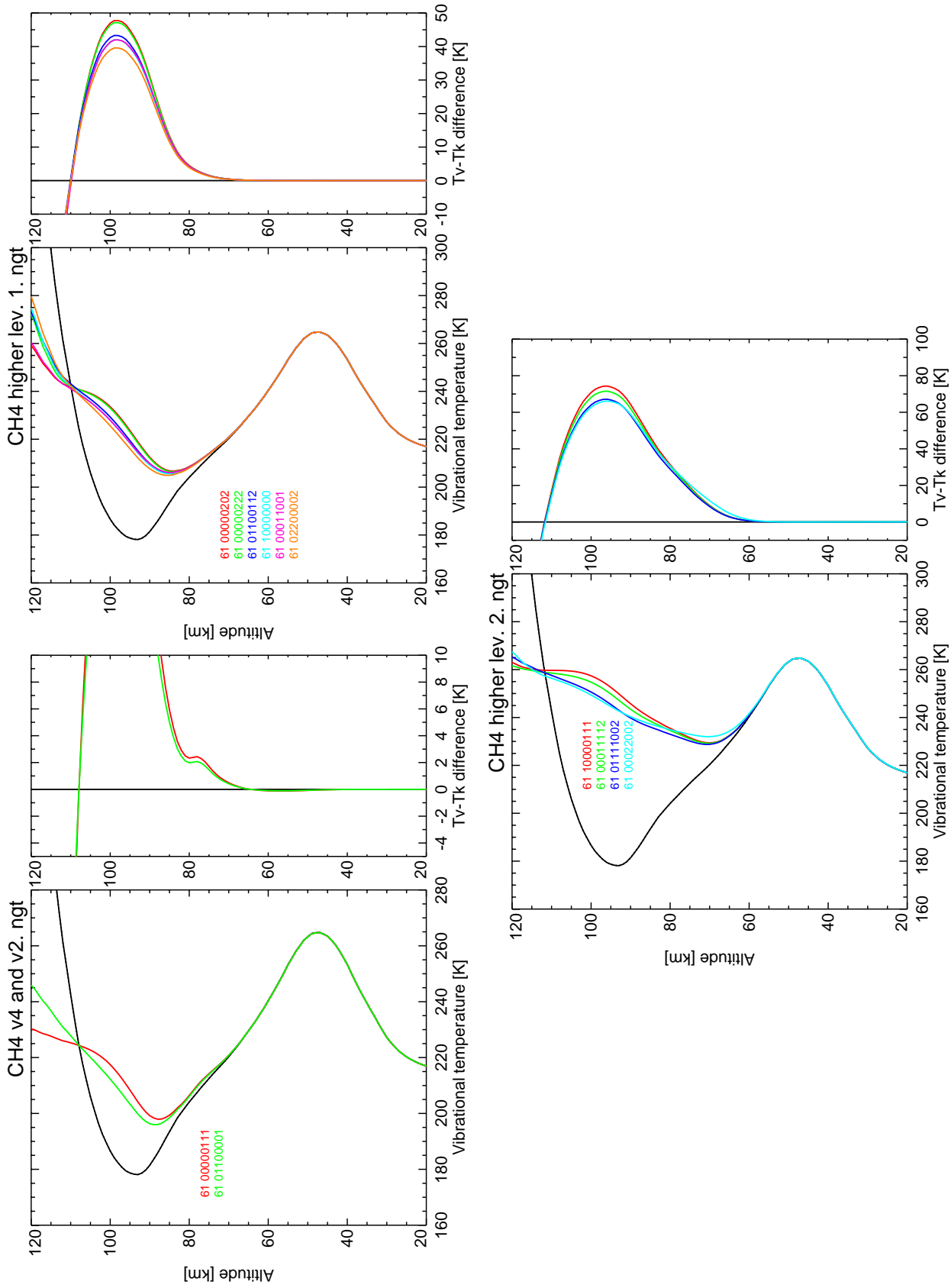


Figure 110: Vibrational temperatures for CH_4 levels, for reference atmosphere #2, night.

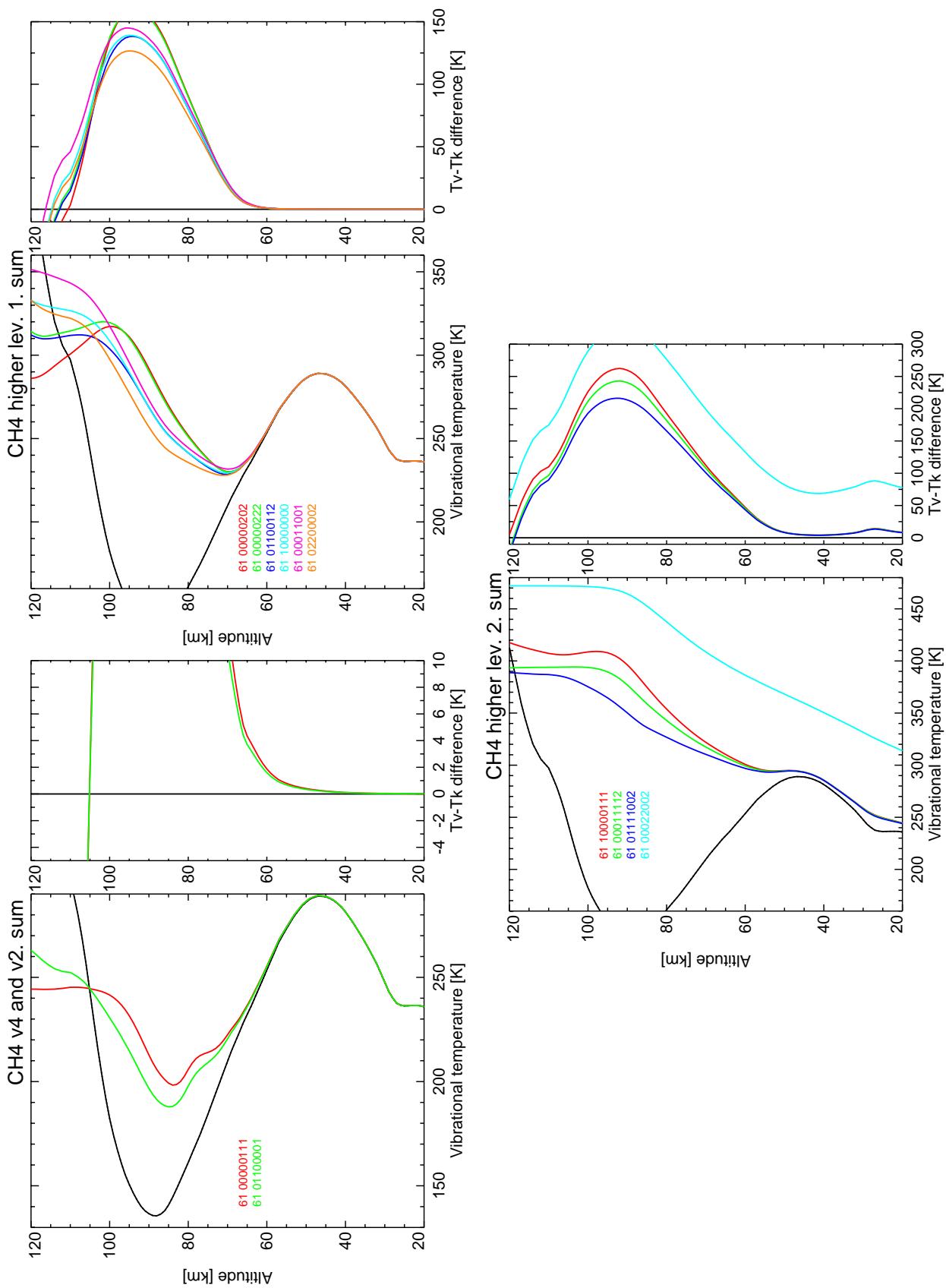


Figure 111: Vibrational temperatures for CH_4 levels, for reference atmosphere #3, summer.

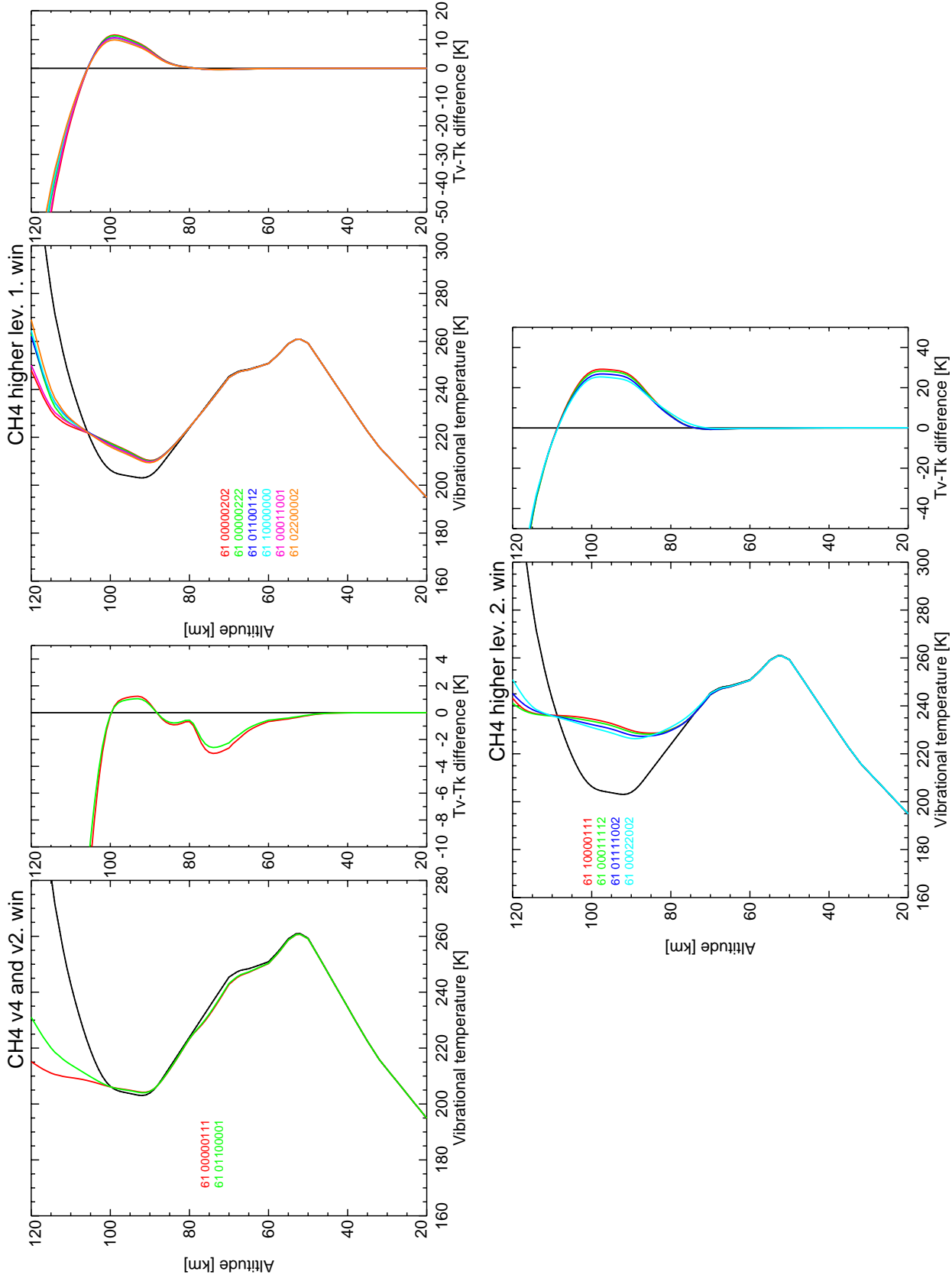


Figure 112: Vibrational temperatures for CH₄ levels, for reference atmosphere #4, winter.

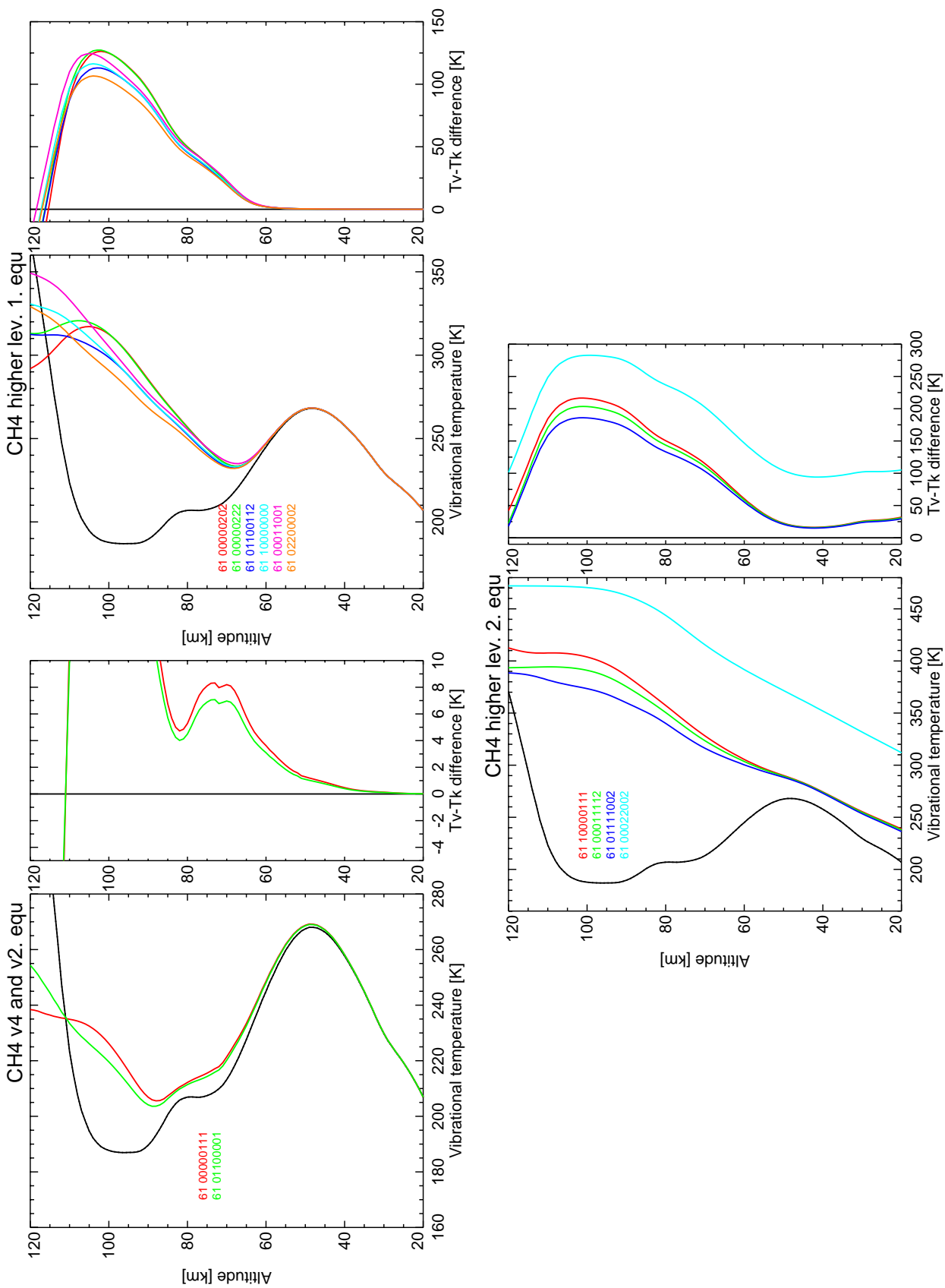


Figure 113: Vibrational temperatures for CH₄ levels, for reference atmosphere #5, equator.

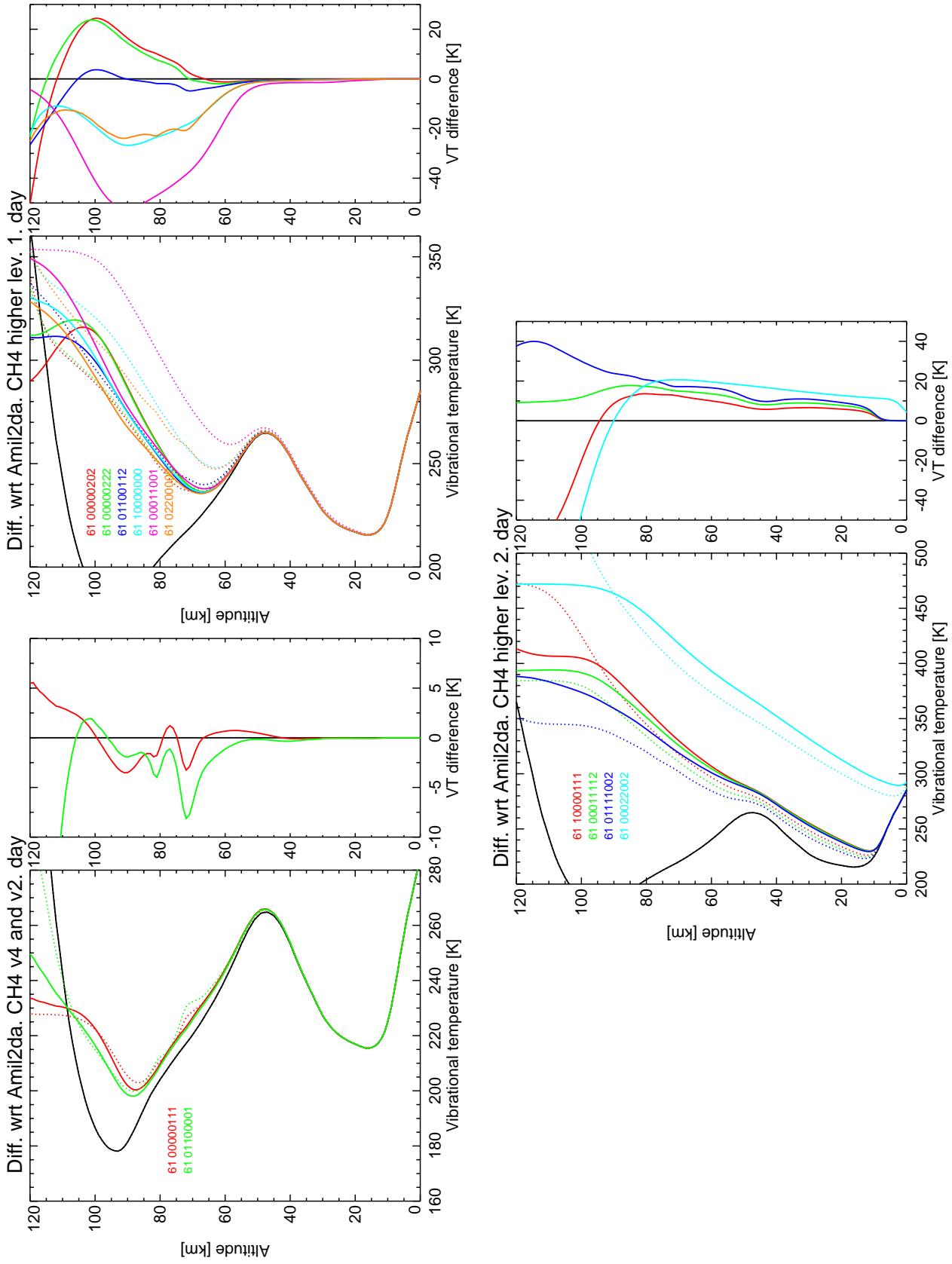


Figure 14: Differences in vibrational temperatures w.r.t. AMIL2DA, CH_4 , for reference atmosphere #1, day. Solid: this study; dash: AMIL2DA. Right panels: this study-AMIL2DA.

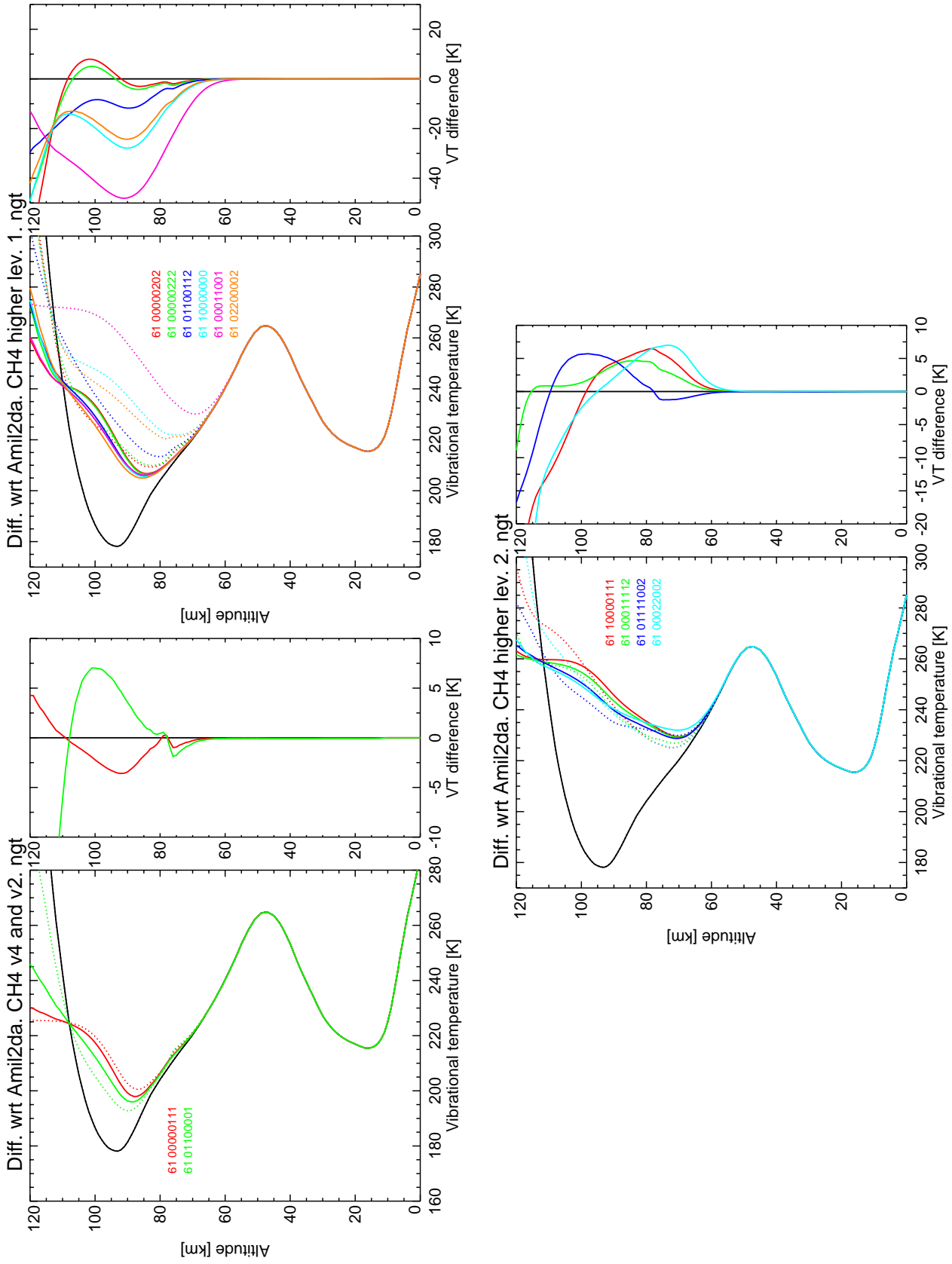


Figure 115: Differences in vibrational temperatures w.r.t. AMIL2DA, CH_4 , for reference atmosphere #2, night. Solid: this study; dash: AMIL2DA. Right panels: this study–AMIL2DA.

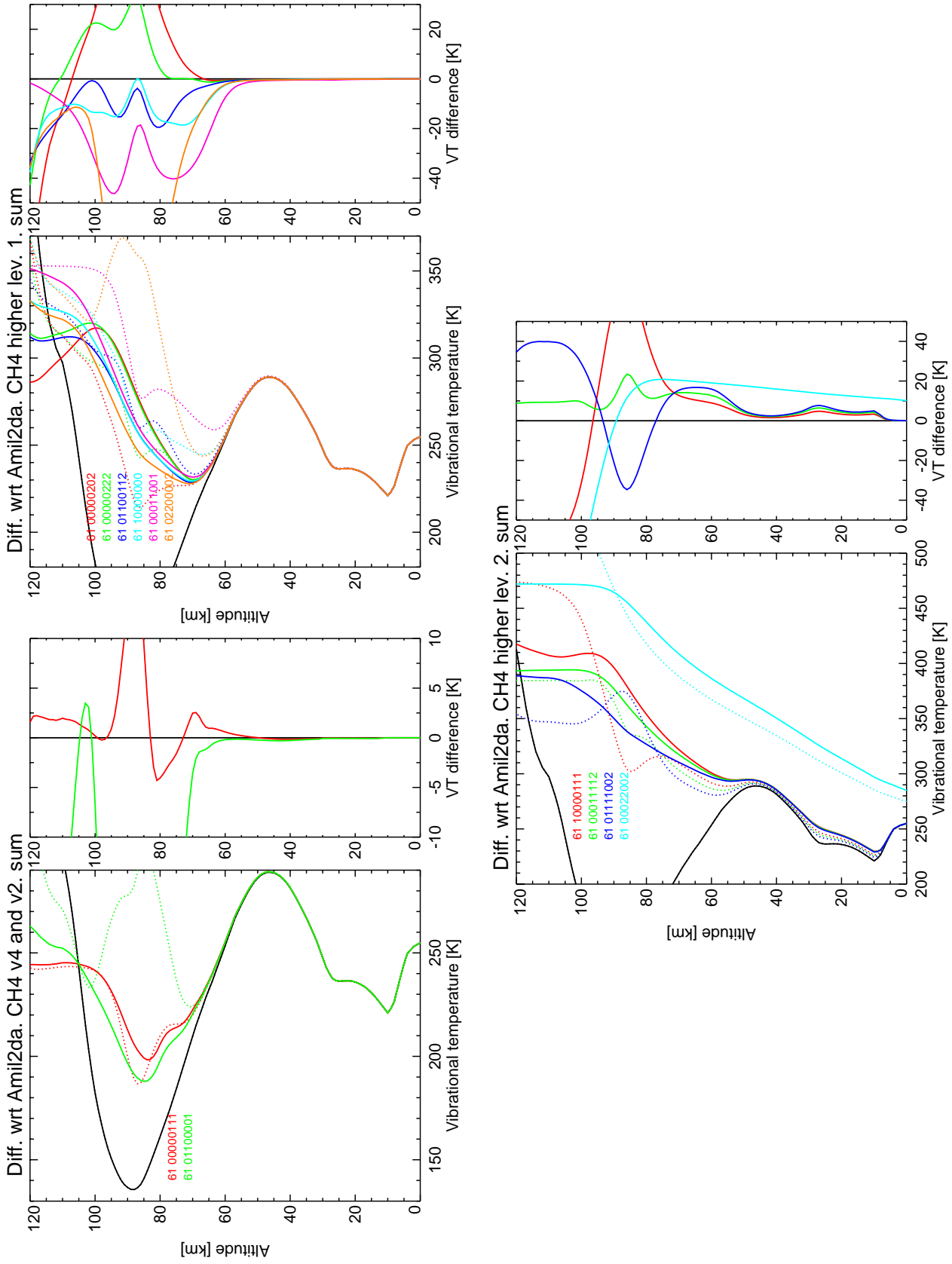


Figure 116: Differences in vibrational temperatures w.r.t. AMIL2DA, CH_4 , for reference atmosphere #3, summer. Solid: this study; dash: AMIL2DA. Right panels: this study–AMIL2DA.

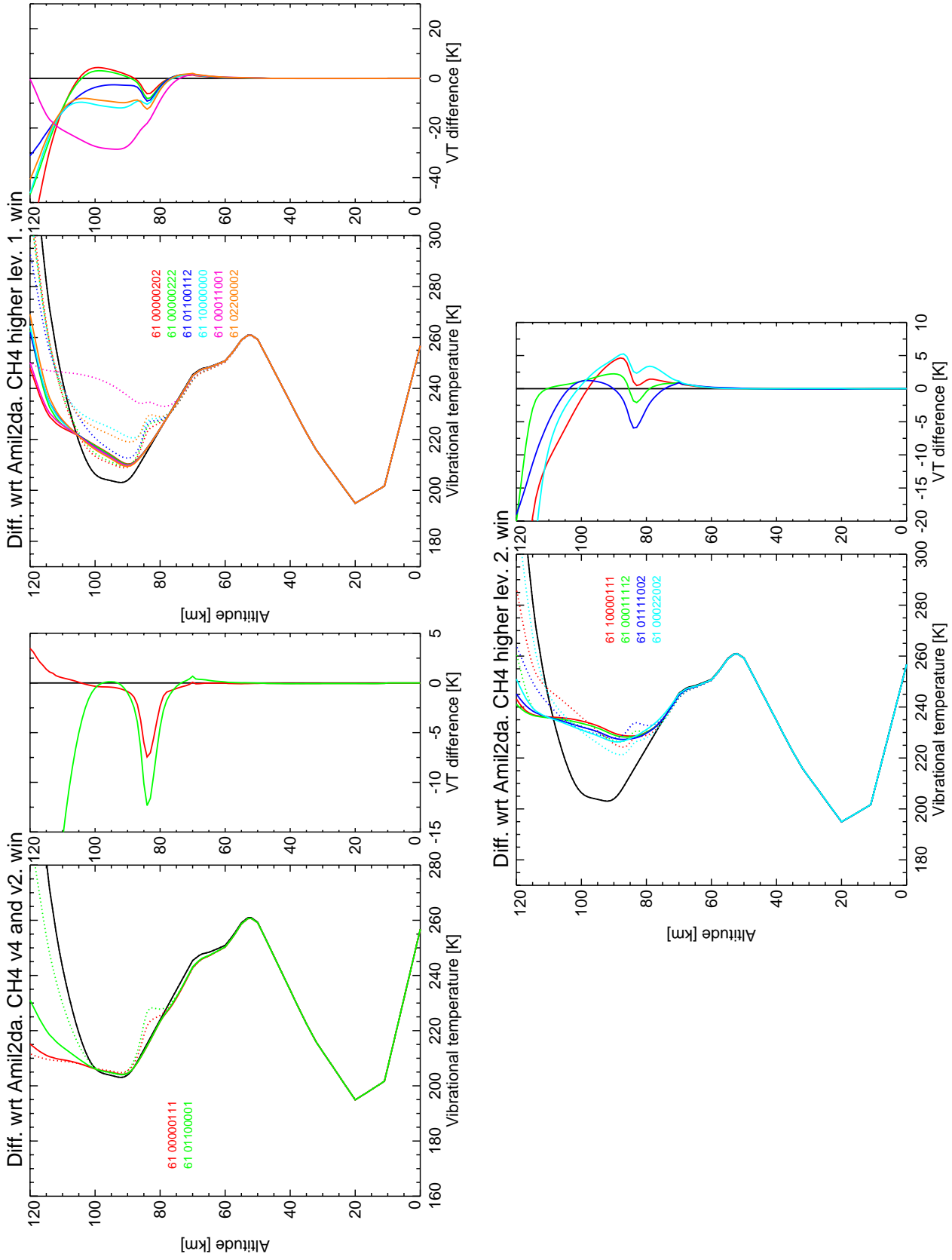


Figure 117: Differences in vibrational temperatures w.r.t. AMIL2DA, CH_4 , for reference atmosphere #4, winter. Solid: this study; dash: AMIL2DA. Right panels: this study–AMIL2DA.

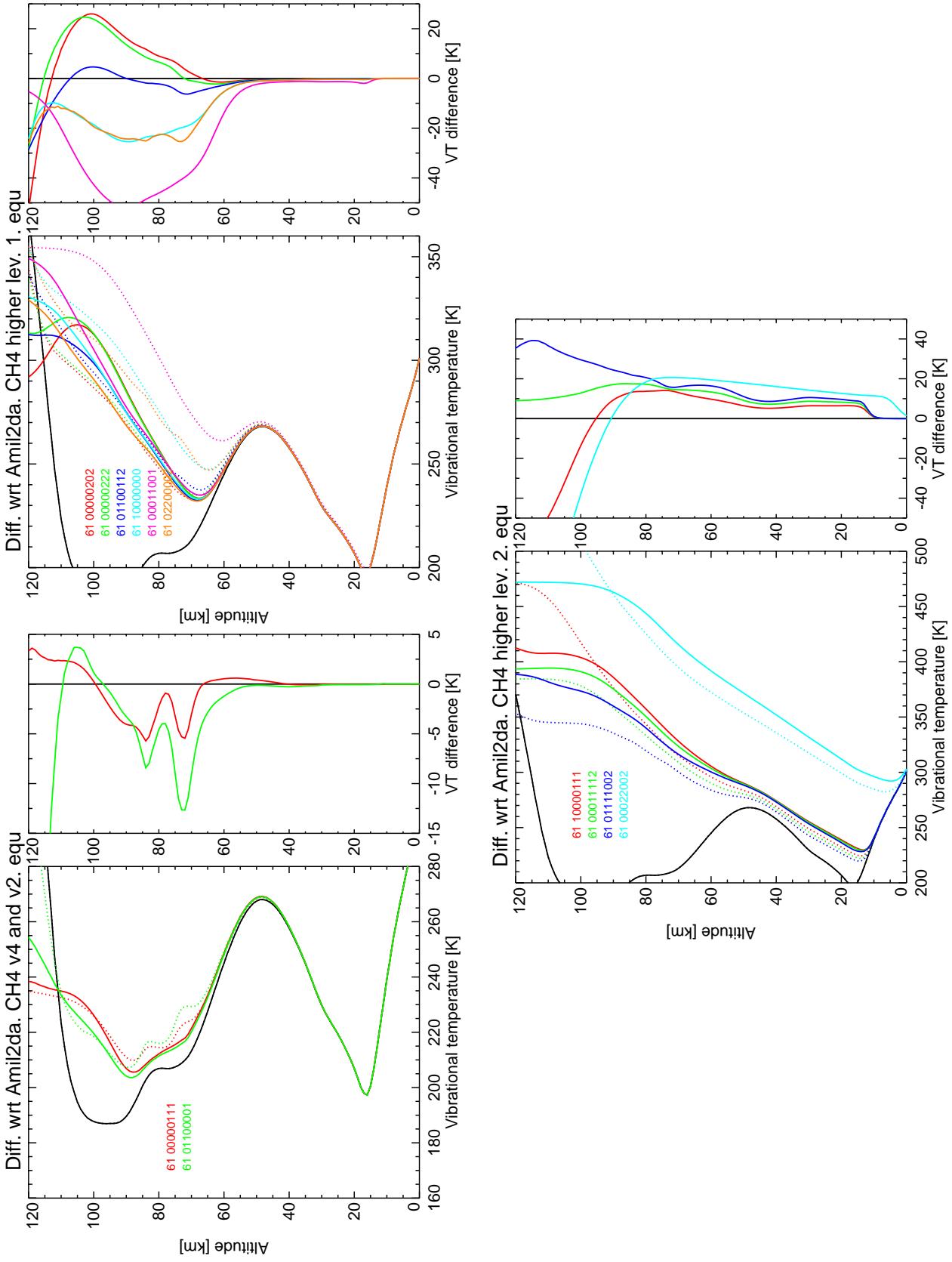


Figure 18: Differences in vibrational temperatures w.r.t. AMIL2DA, CH₄, for reference atmosphere #5, equator. Solid: this study; dash: AMIL2DA. Right panels: this study-AMIL2DA.

3.8 NO

The model for the spin, rotational and vibrational non-LTE populations of NO has suffered only minor changes. We should mention however, that those non-LTE model results have been confirmed by a series of non-LTE studies of MIPAS spectra. First, the non-LTE excitation of NO(1) in the stratosphere previously postulated by Kaye and Kumer (1987) have been confirmed by Funke et al. (2005). In addition, the spin, rotational and vibrational non-LTE predicted in the thermosphere have also been confirmed by the MIPAS analysis carried out by Gardner et al. (2005, 2007).

Figures 119-123 show the vibrational temperatures for the NO vibrational energy levels. The population of a given NO vibrational level is the same regardless of its spin value, 1/2 or 3/2. However, in the data files we provide T_v 's for the two spin populations because in HITRAN the two spin populations are listed and have different energies. The fact of using different energies for levels with the same population produces T_v 's which are slightly different, and so are those listed in the supplied files for the two spin populations. The T_v 's shown in Figures 119-123 correspond to the NO vibrational energy levels with spin=1/2.

Figures 124-128 show the differences in the vibrational temperatures for the NO energy levels with respect to previous (AMIL2DA) version. The differences are very small. Some of them caused by the different abundances of NO_2 and O_3 and other due to minor changes in the thermal relaxation in the thermosphere.

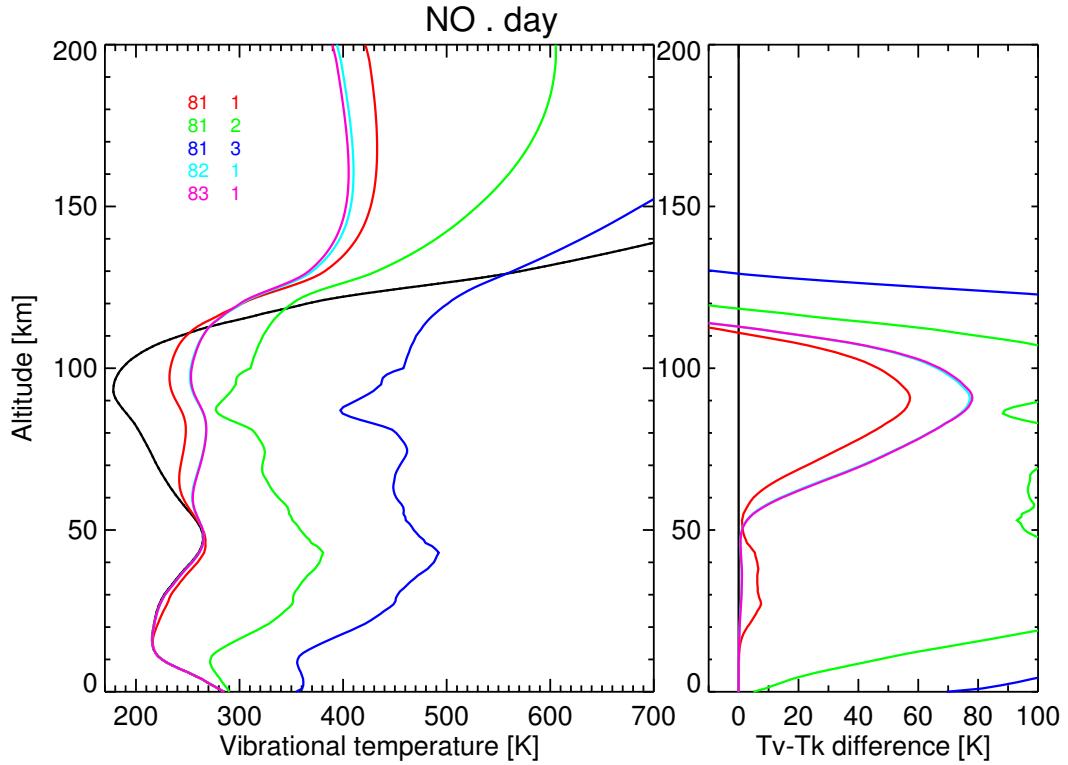


Figure 119: Vibrational temperatures for NO levels, for reference atmosphere #1, day.

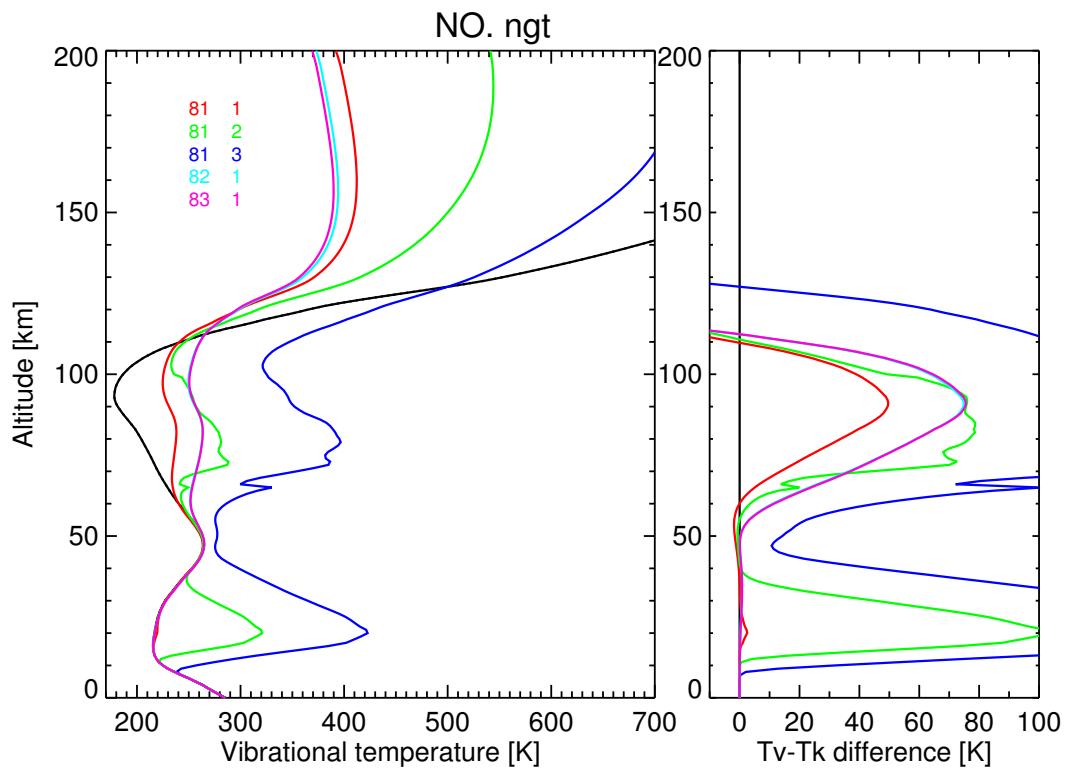


Figure 120: Vibrational temperatures for NO levels, for reference atmosphere #2, night.

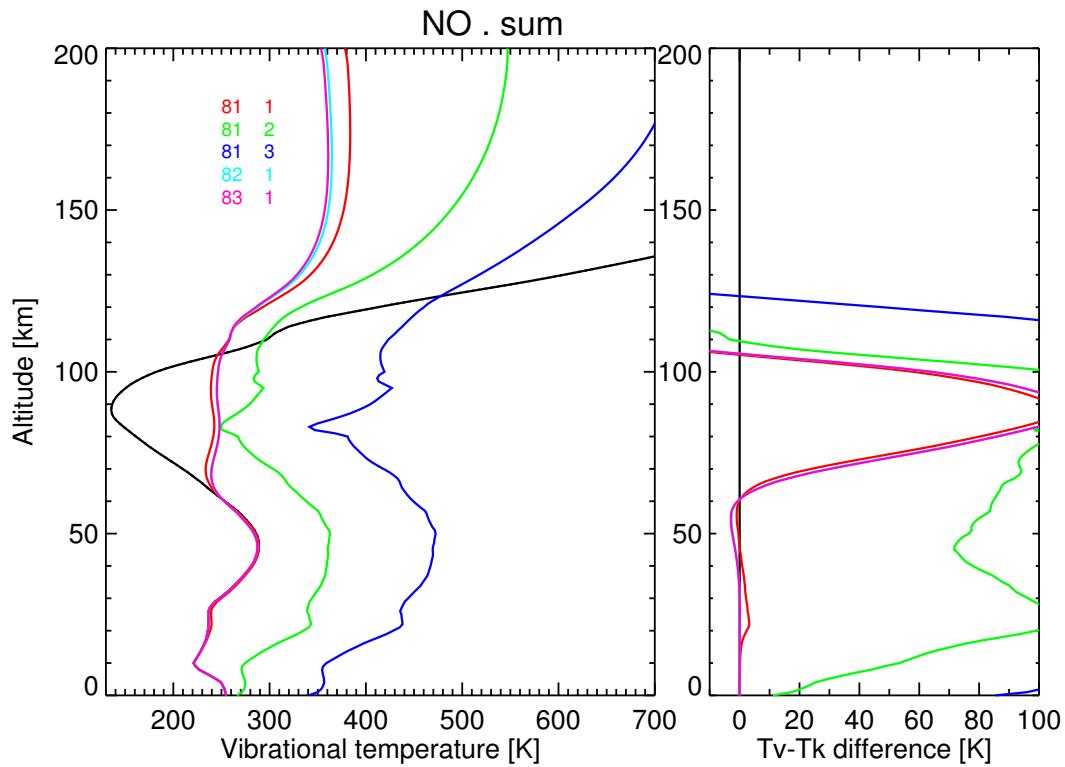


Figure 121: Vibrational temperatures for NO levels, for reference atmosphere #3, summer.

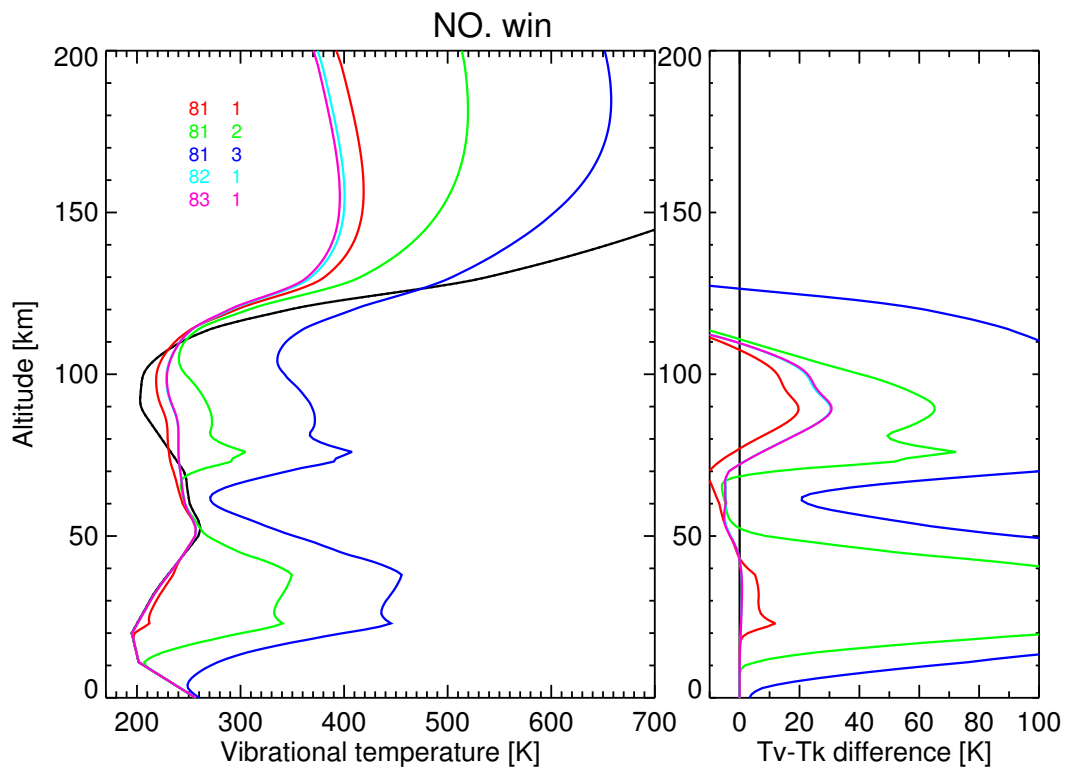


Figure 122: Vibrational temperatures for NO levels, for reference atmosphere #4, winter.

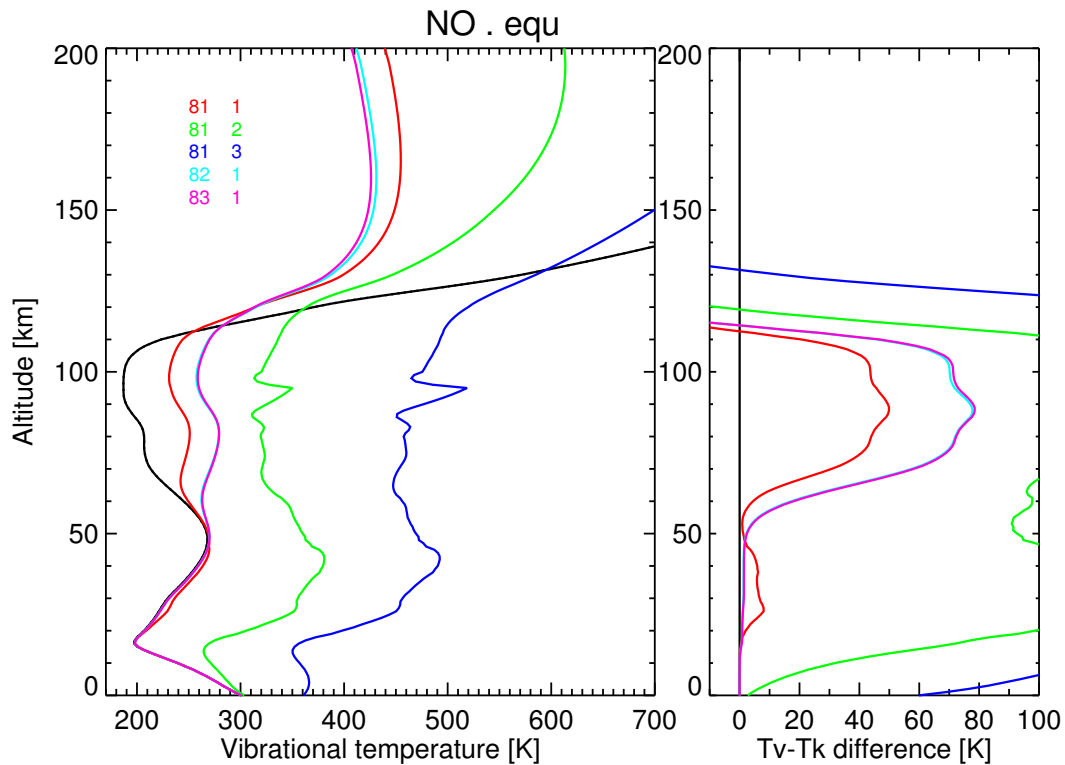


Figure 123: Vibrational temperatures for NO levels, for reference atmosphere #5, equator.

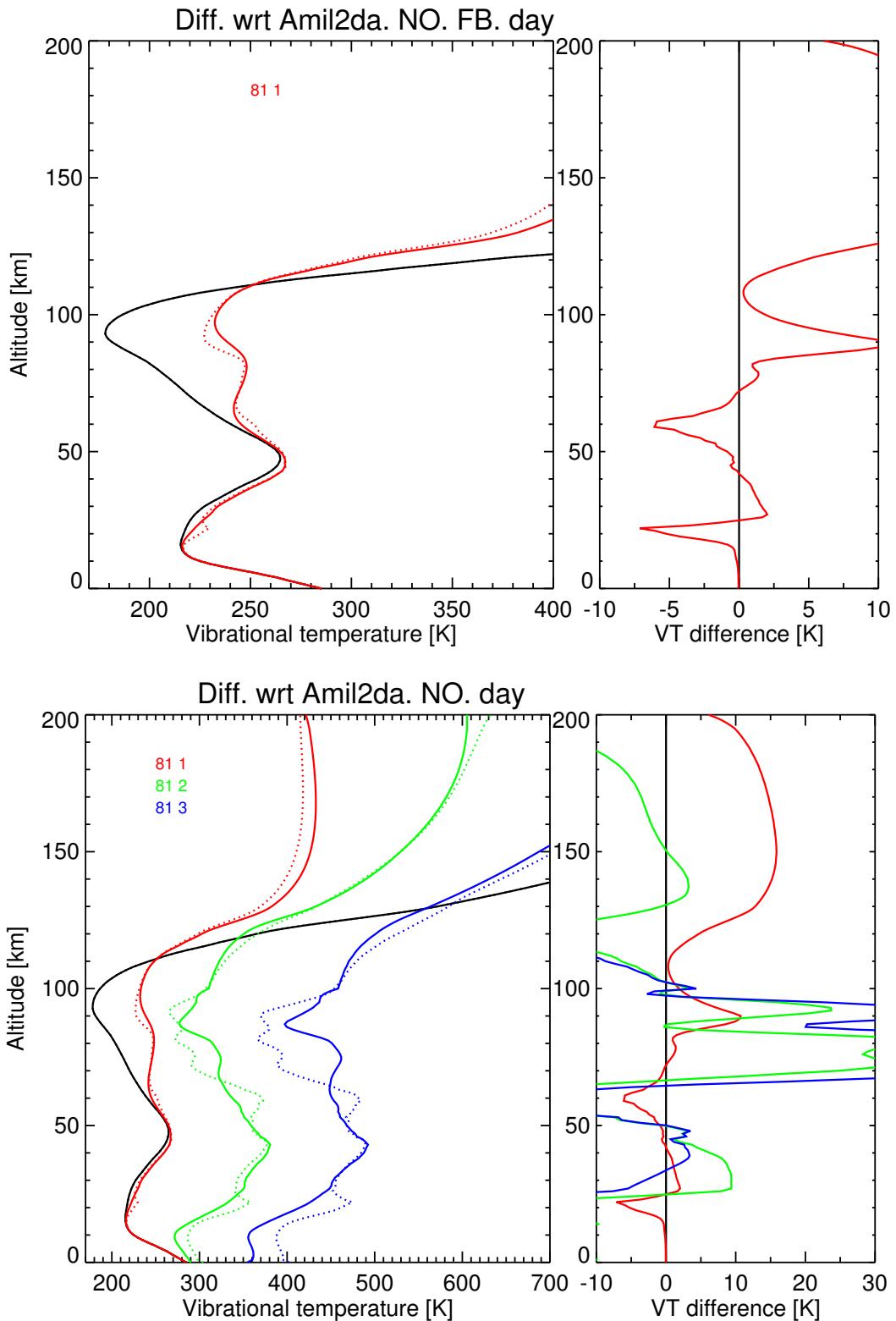


Figure 124: Differences in vibrational temperatures w.r.t. previous version (AMIL2DA) for the NO levels, for reference atmosphere #1, day. Solid: this study; dash: AMIL2DA. Right panels: this study–AMIL2DA.

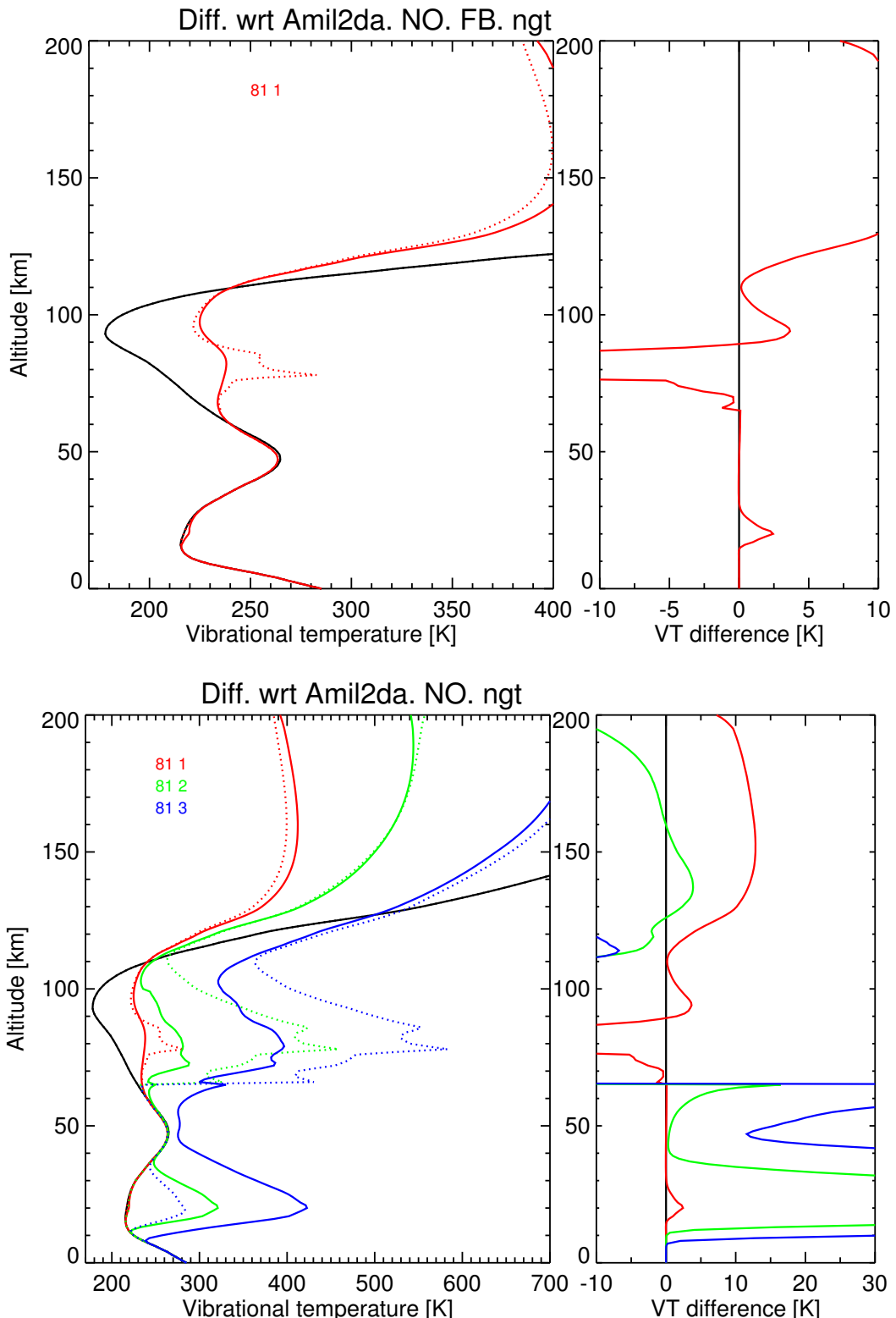


Figure 125: Differences in vibrational temperatures w.r.t. previous version (AMIL2DA) for the NO levels, for reference atmosphere #2, night. Solid: this study; dash: AMIL2DA. Right panels: this study–AMIL2DA.

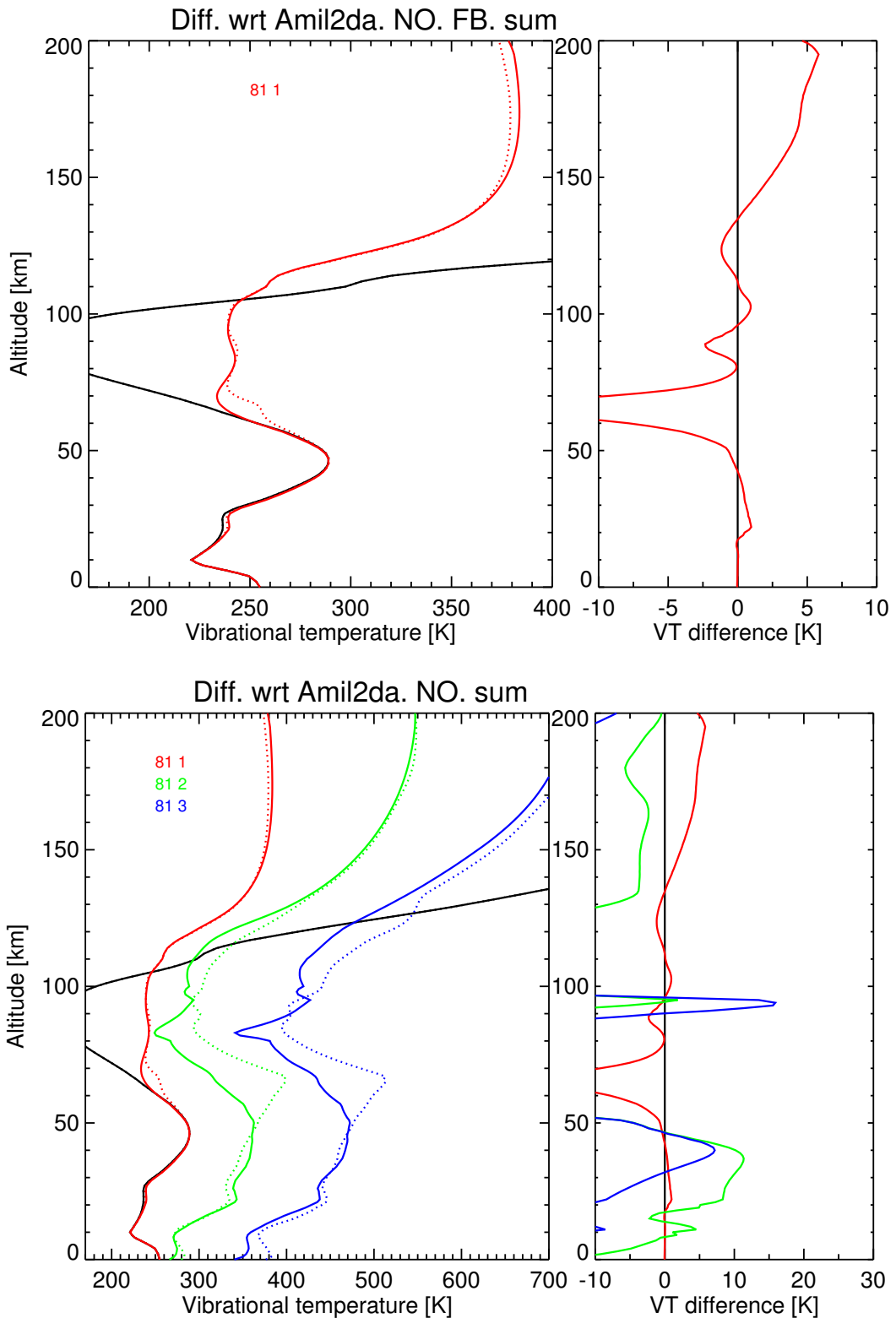


Figure 126: Differences in vibrational temperatures w.r.t. previous version (AMIL2DA) for the NO levels, for reference atmosphere #3, summer. Solid: this study; dash: AMIL2DA. Right panels: this study–AMIL2DA.

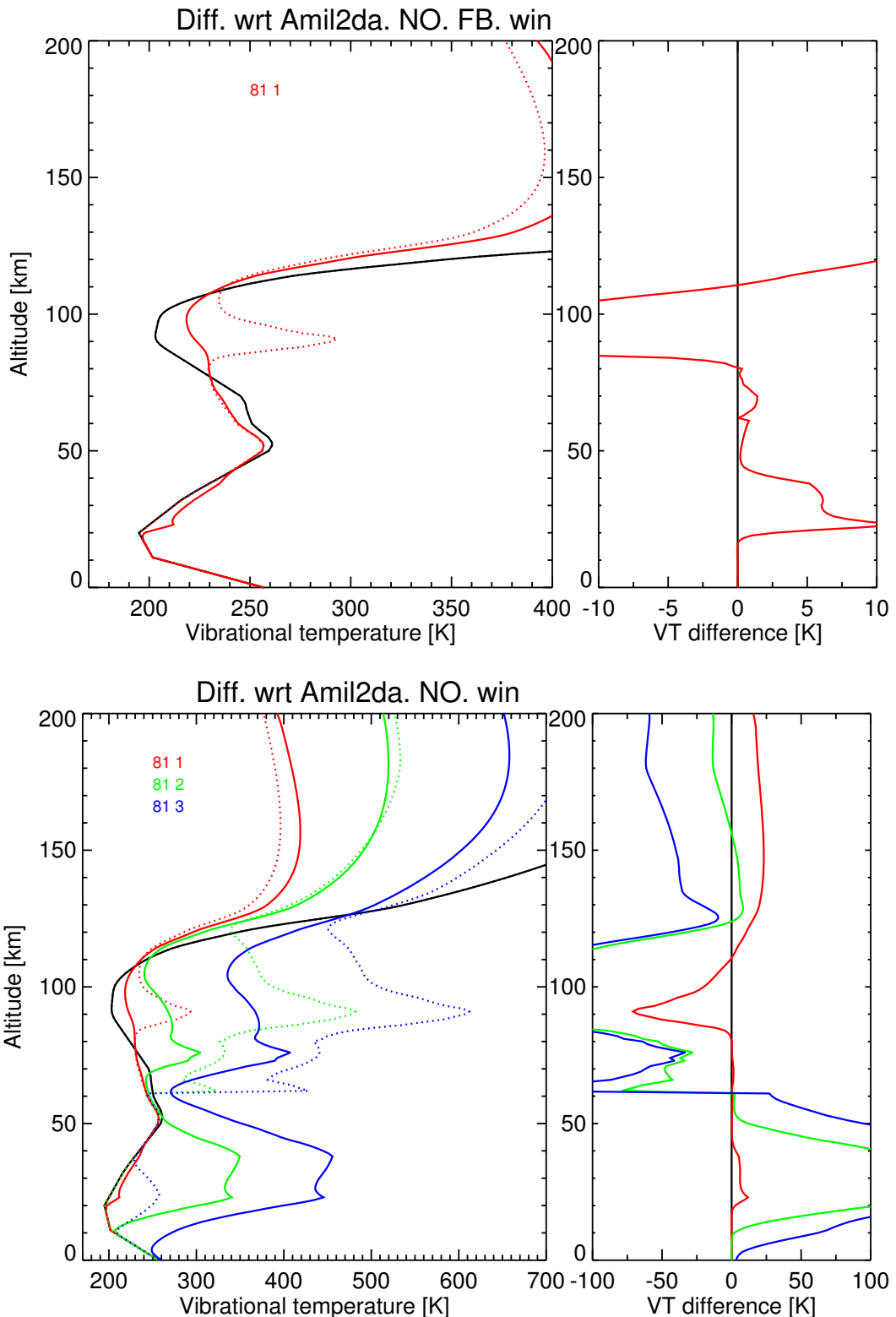


Figure 127: Differences in vibrational temperatures w.r.t. previous version (AMIL2DA) for the NO levels, for reference atmosphere #4, winter. Solid: this study; dash: AMIL2DA. Right panels: this study–AMIL2DA.

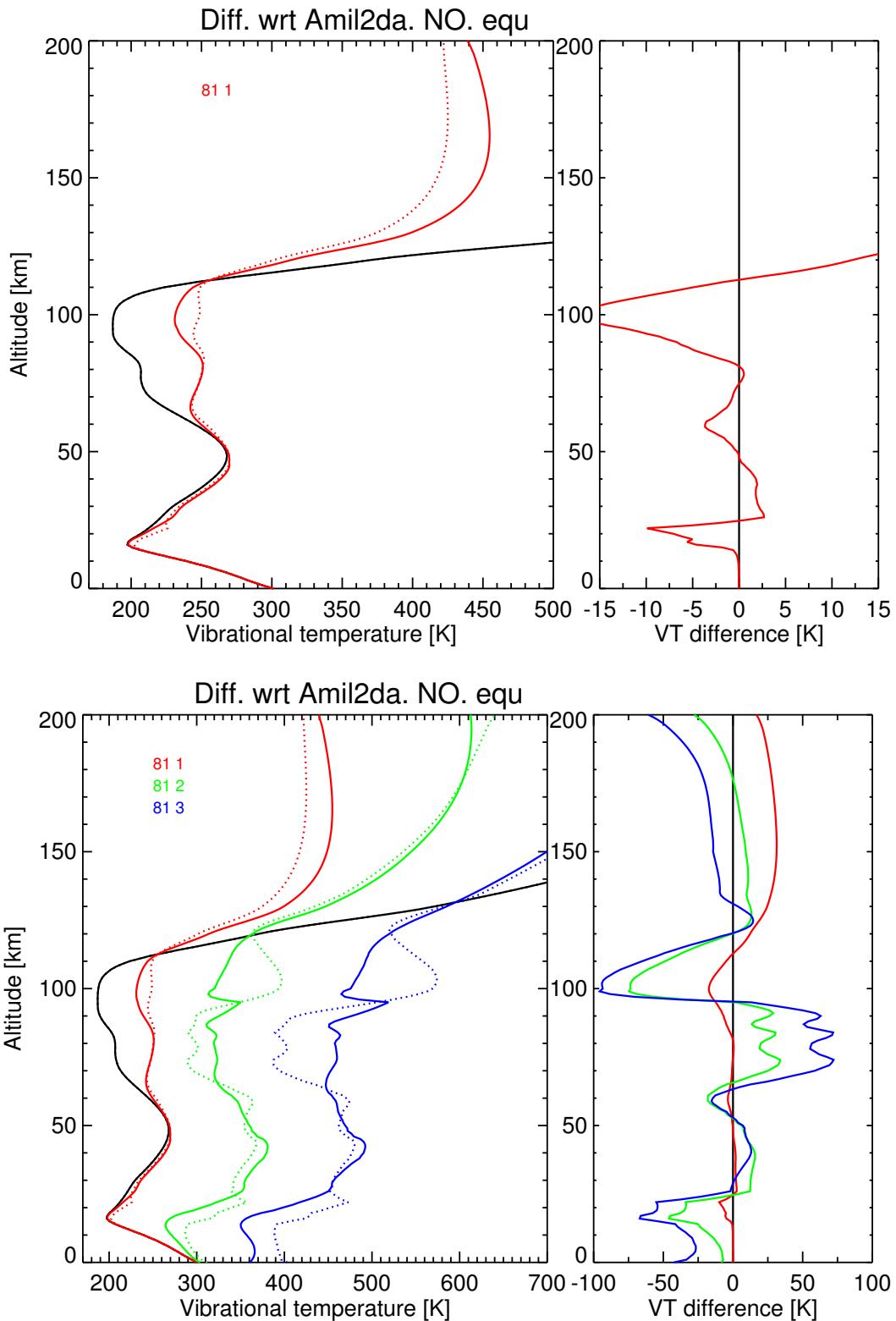


Figure 128: Differences in vibrational temperatures w.r.t. previous version (AMIL2DA) for the NO levels, for reference atmosphere #5, equator. Solid: this study; dash: AMIL2DA. Right panels: this study–AMIL2DA.

3.9 NO₂

The non-LTE model for the populations of NO₂ was already upgraded after the AMIL2DA study to incorporate the much smaller (by a factor of 50) chemical excitation of NO₂(00v₃) found by Funke et al. (2005). In addition to that change, we have also included a rate for the collisional deactivation of NO₂(001) by M,



of $5 \times 10^{-13} \text{ cm}^3 \text{s}^{-1}$, which is about a factor of 8 larger than previous values reported by Toselli et al. (1990) and Bohn et al. (1999). This leads to a smaller non-LTE effect in the population of NO₂(001).

Figures 129-133 show the vibrational temperatures for the NO₂ energy levels from the lowest to the highest energy.

Figures 134-138 show the differences in the vibrational temperatures for the NO₂ energy levels with respect to previous (AMIL2DA) version. The new vibrational temperatures are now much smaller than before and its non-LTE effects is therefore much smaller.

Note that the higher T_v's in the mesosphere/lower thermosphere (particularly during night) are related to much smaller NO₂ vmrs, caused by a larger NO₂+O loss.

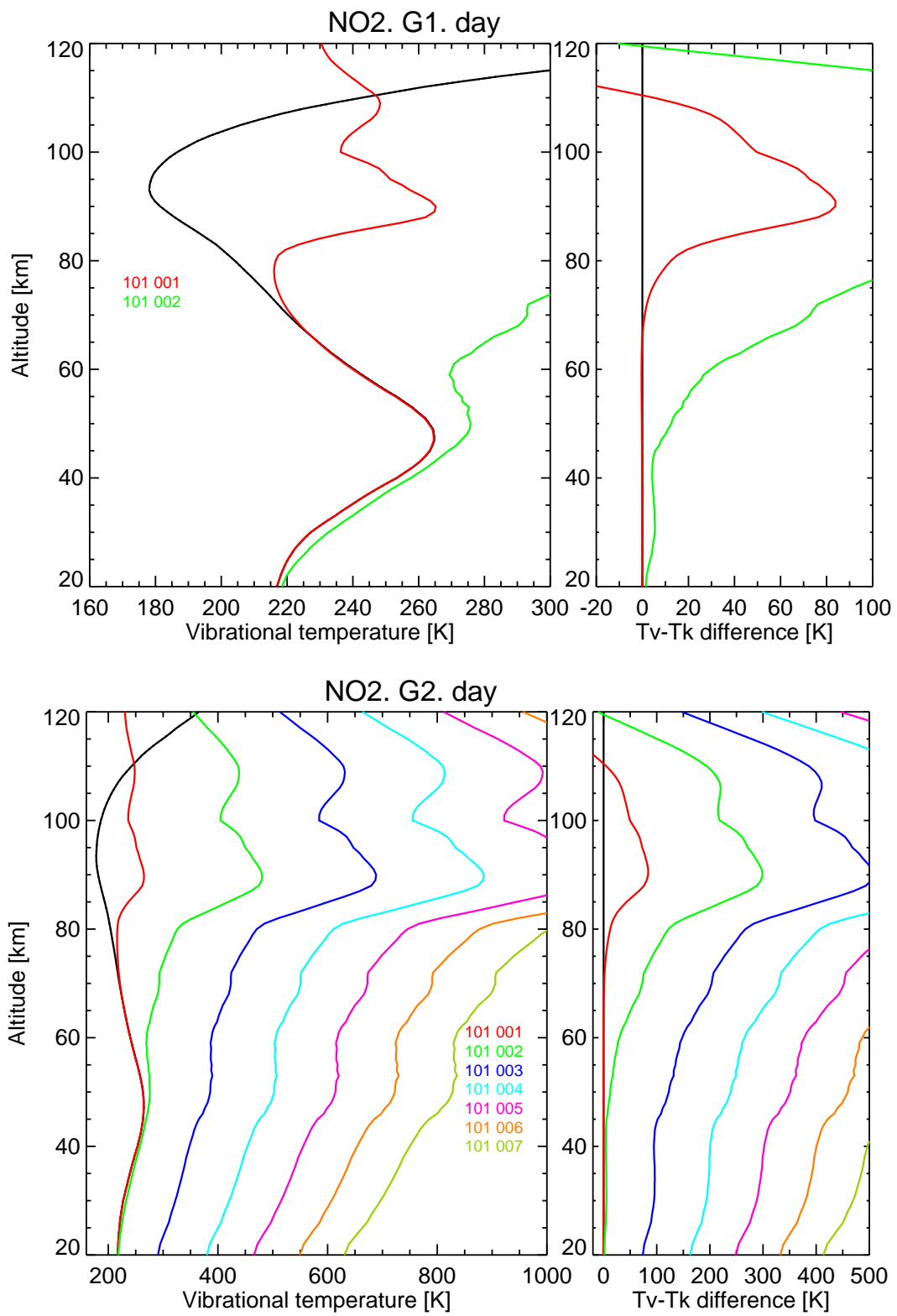


Figure 129: Vibrational temperatures for NO₂ levels, for reference atmosphere #1, day.

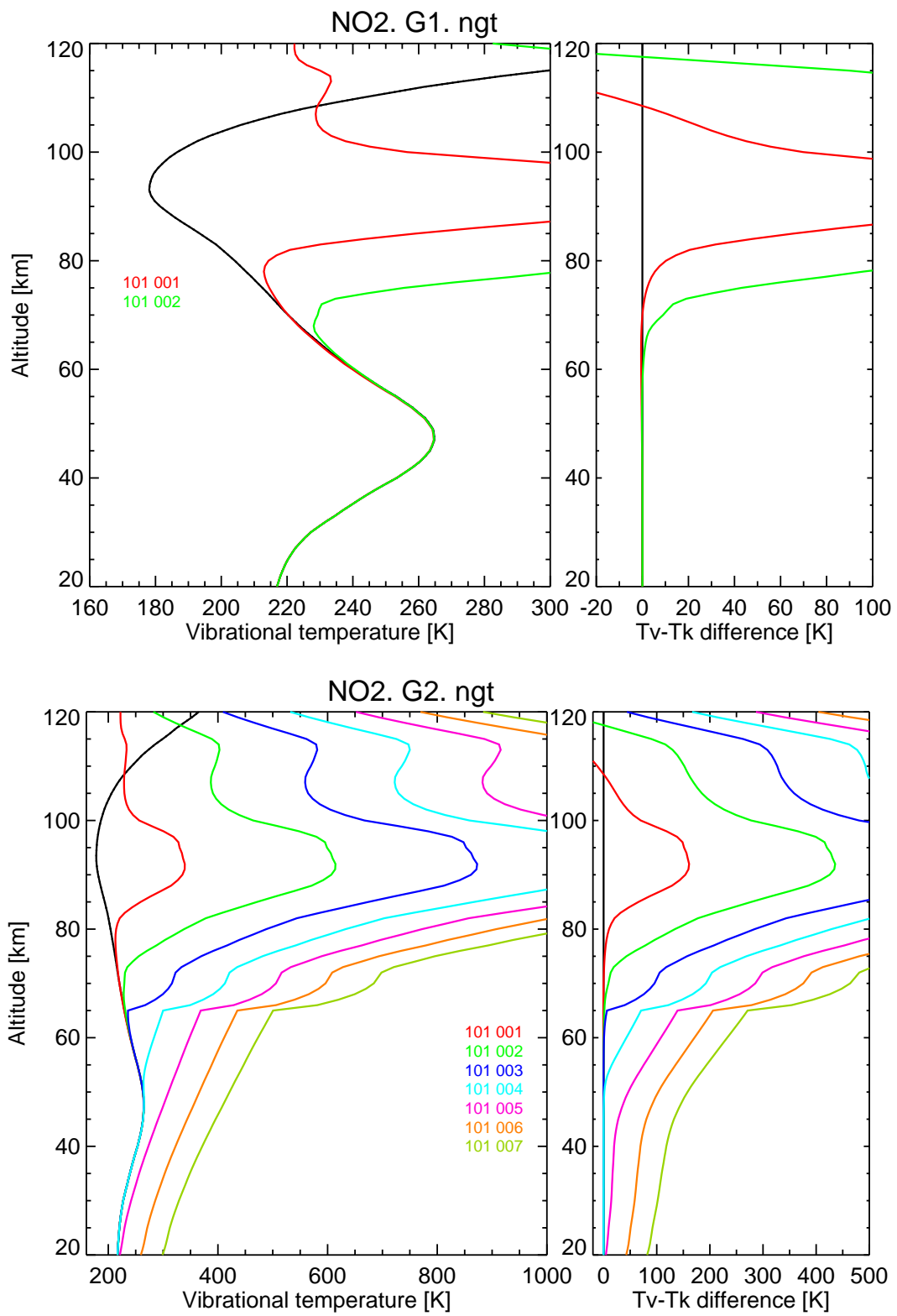


Figure 130: Vibrational temperatures for NO_2 levels, for reference atmosphere #2, night.

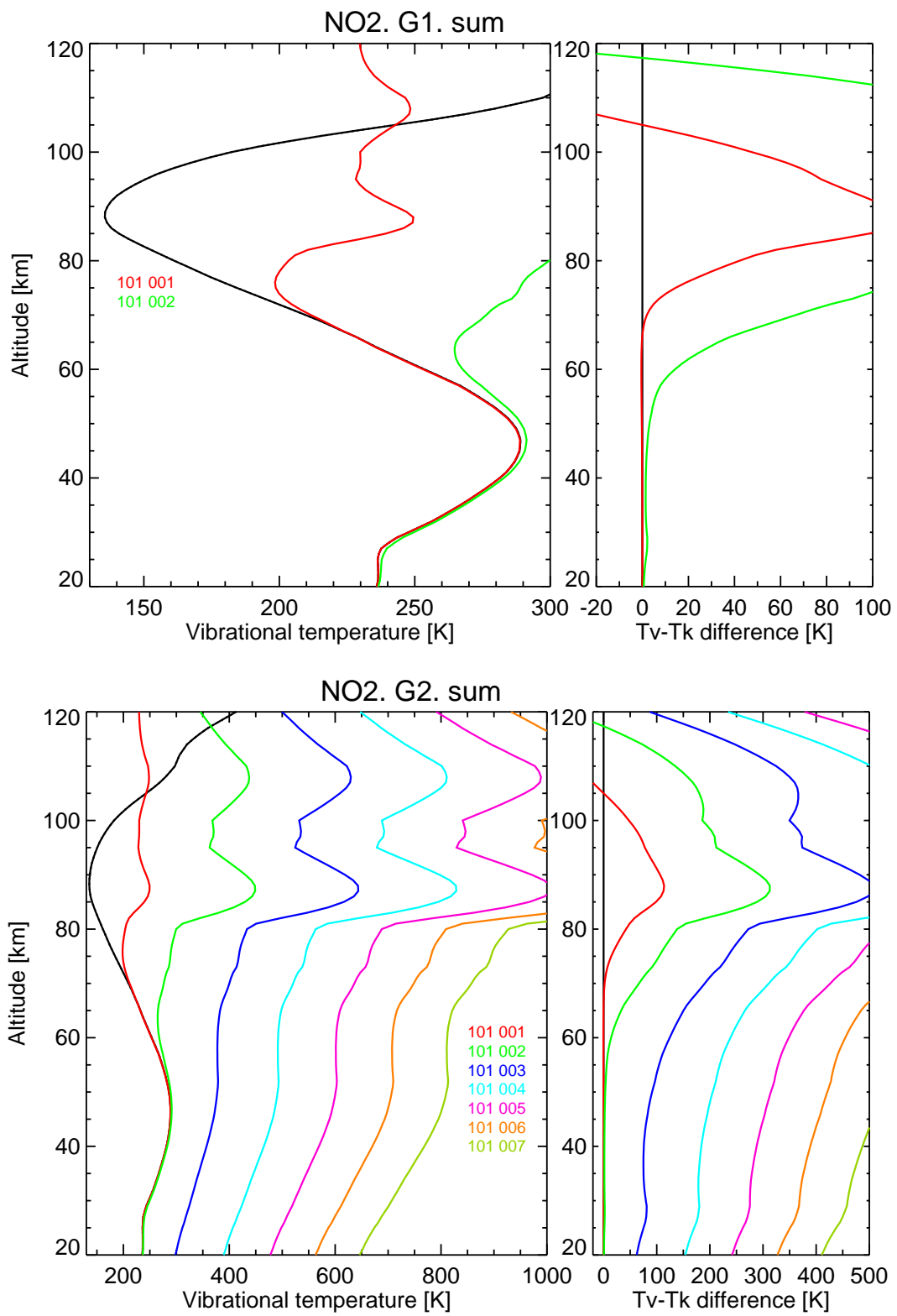


Figure 131: Vibrational temperatures for NO₂ levels, for reference atmosphere #3, summer.

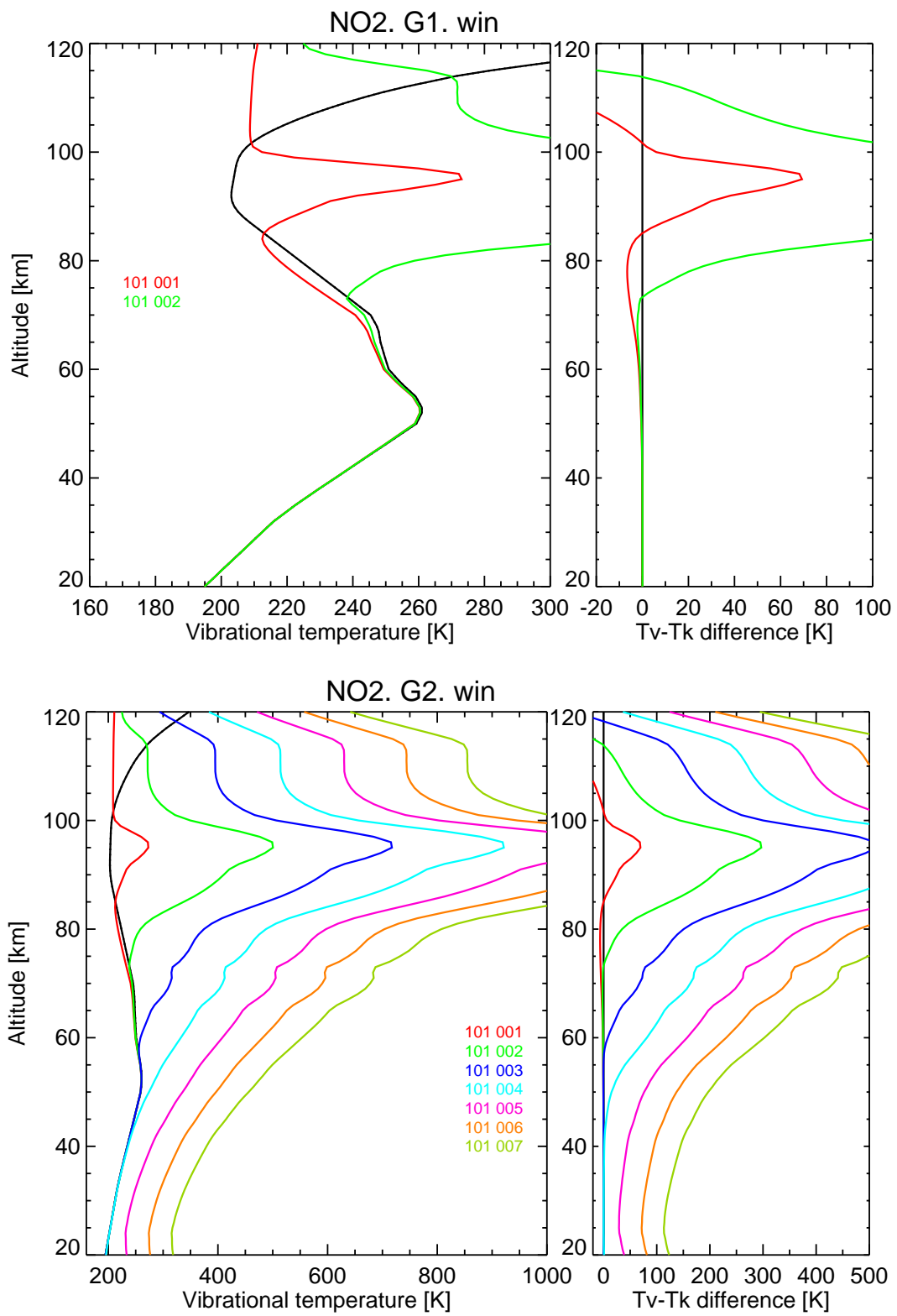


Figure 132: Vibrational temperatures for NO₂ levels, for reference atmosphere #4, winter.

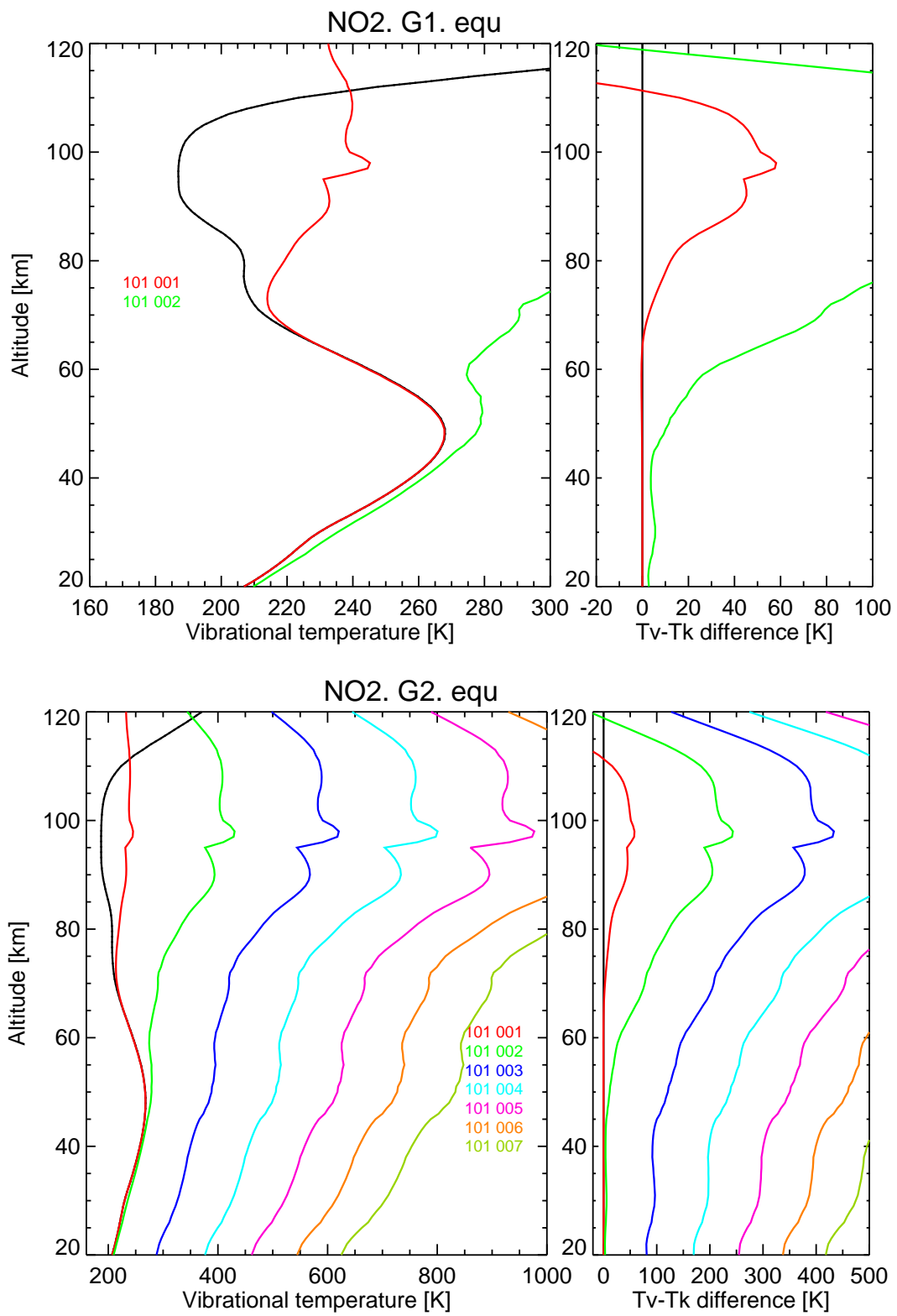


Figure 133: Vibrational temperatures for NO₂ levels, for reference atmosphere #5, equator.

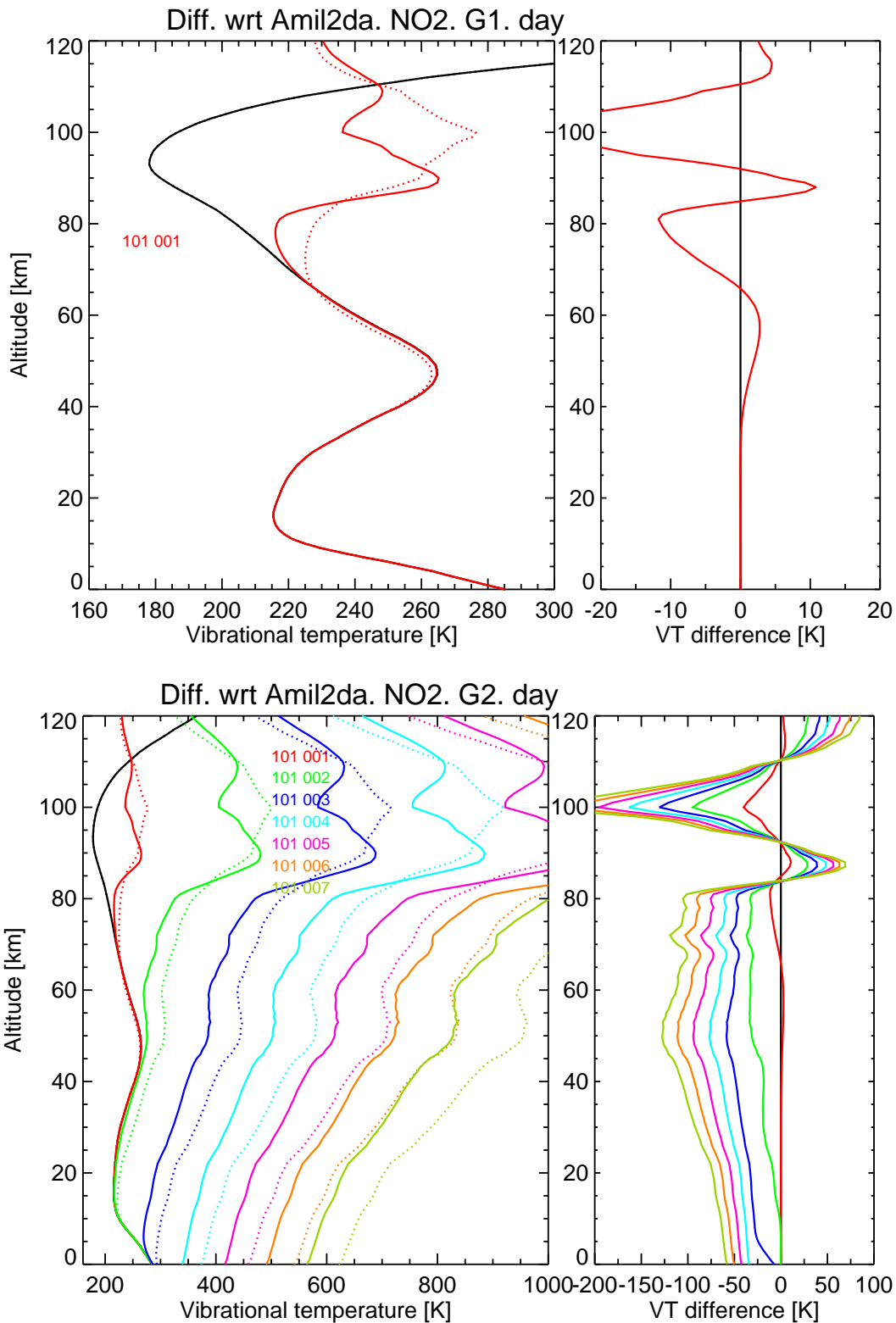


Figure 134: Differences in vibrational temperatures w.r.t. previous version (AMIL2DA) for the NO₂ levels, for reference atmosphere #1, day. Solid: this study; dash: AMIL2DA. Right panels: this study–AMIL2DA.

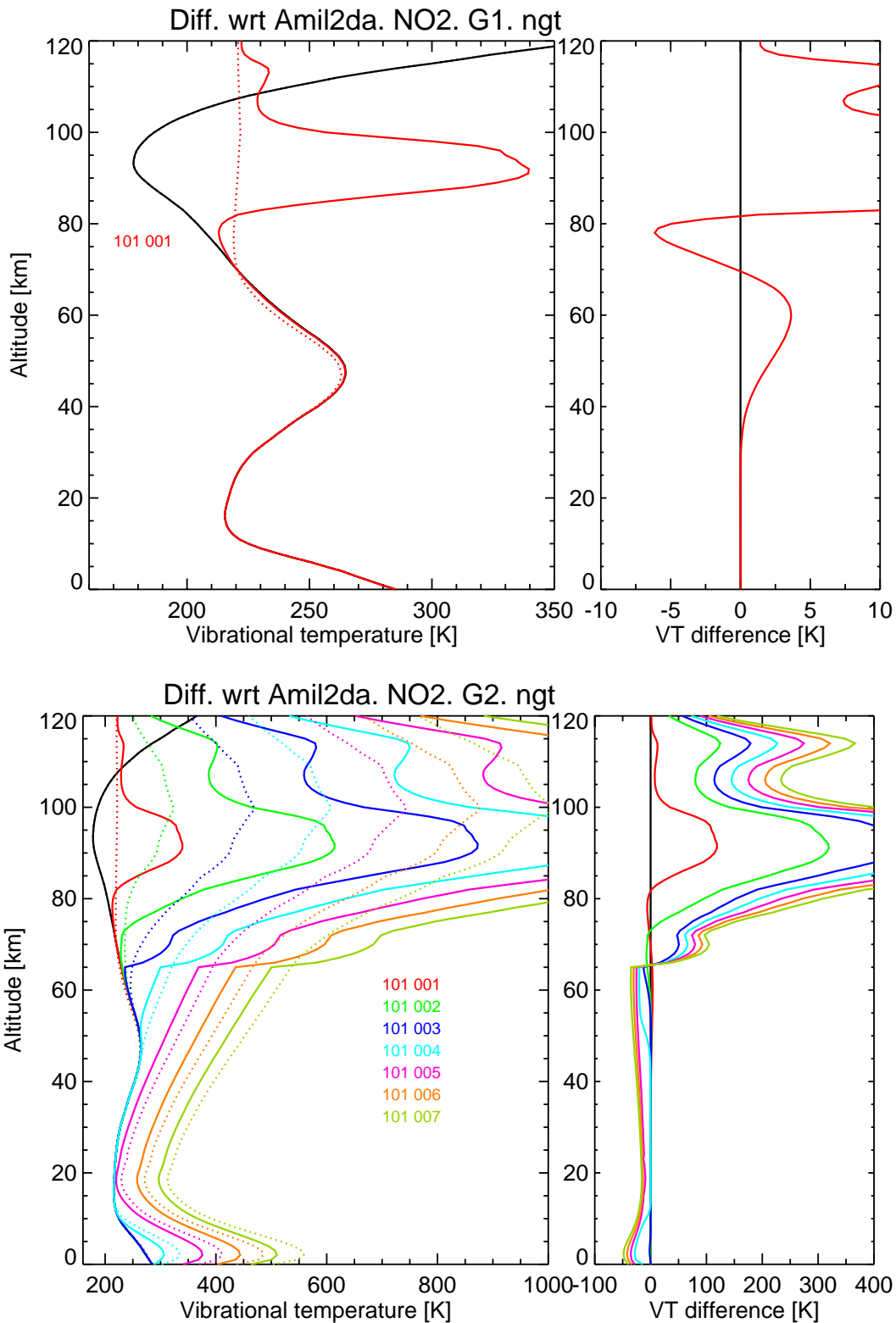


Figure 135: Differences in vibrational temperatures w.r.t. previous version (AMIL2DA) for the NO₂ levels, for reference atmosphere #2, night. Solid: this study; dash: AMIL2DA. Right panels: this study–AMIL2DA.

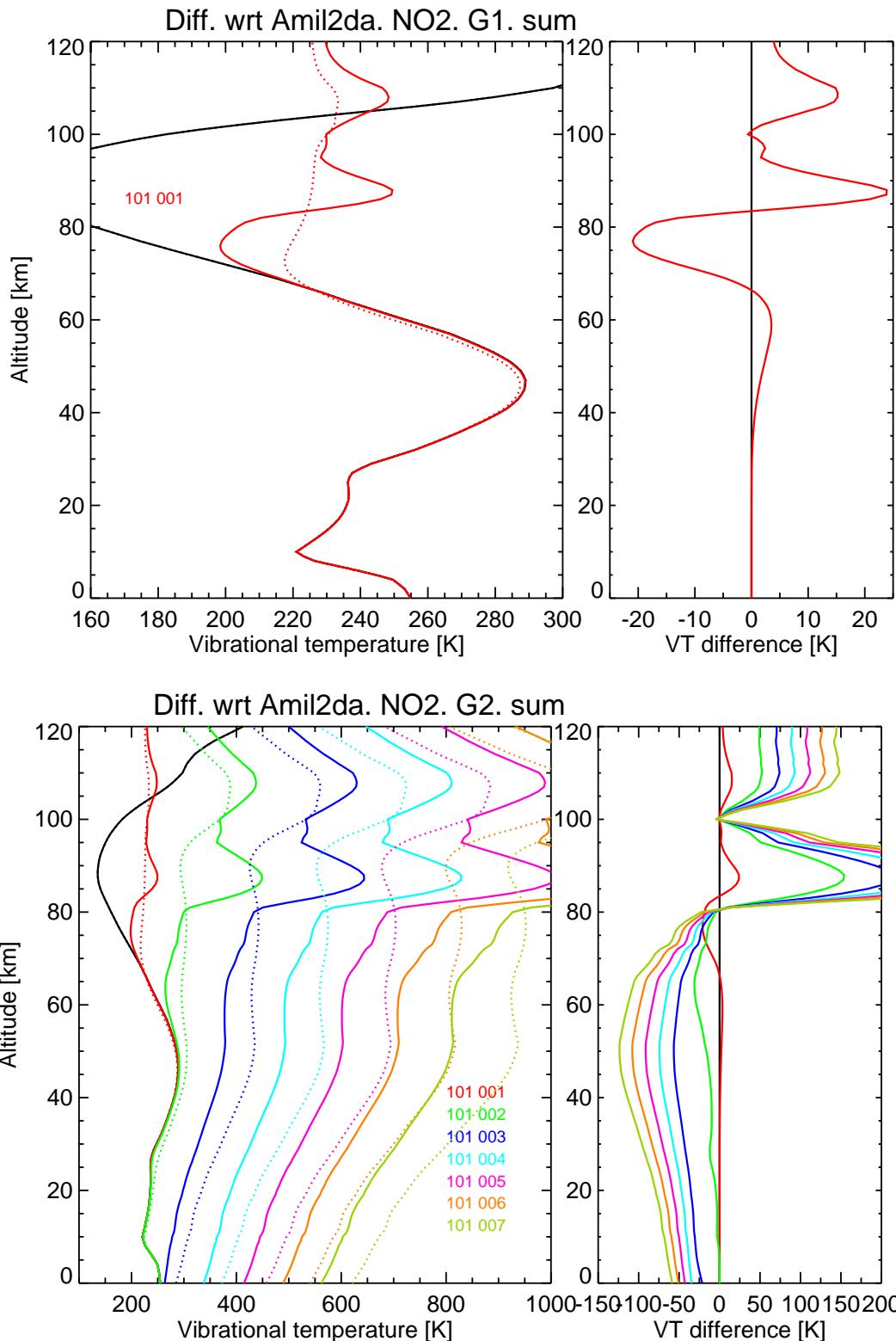


Figure 136: Differences in vibrational temperatures w.r.t. previous version (AMIL2DA) for the NO₂ levels, for reference atmosphere #3, summer. Solid: this study; dash: AMIL2DA. Right panels: this study–AMIL2DA.

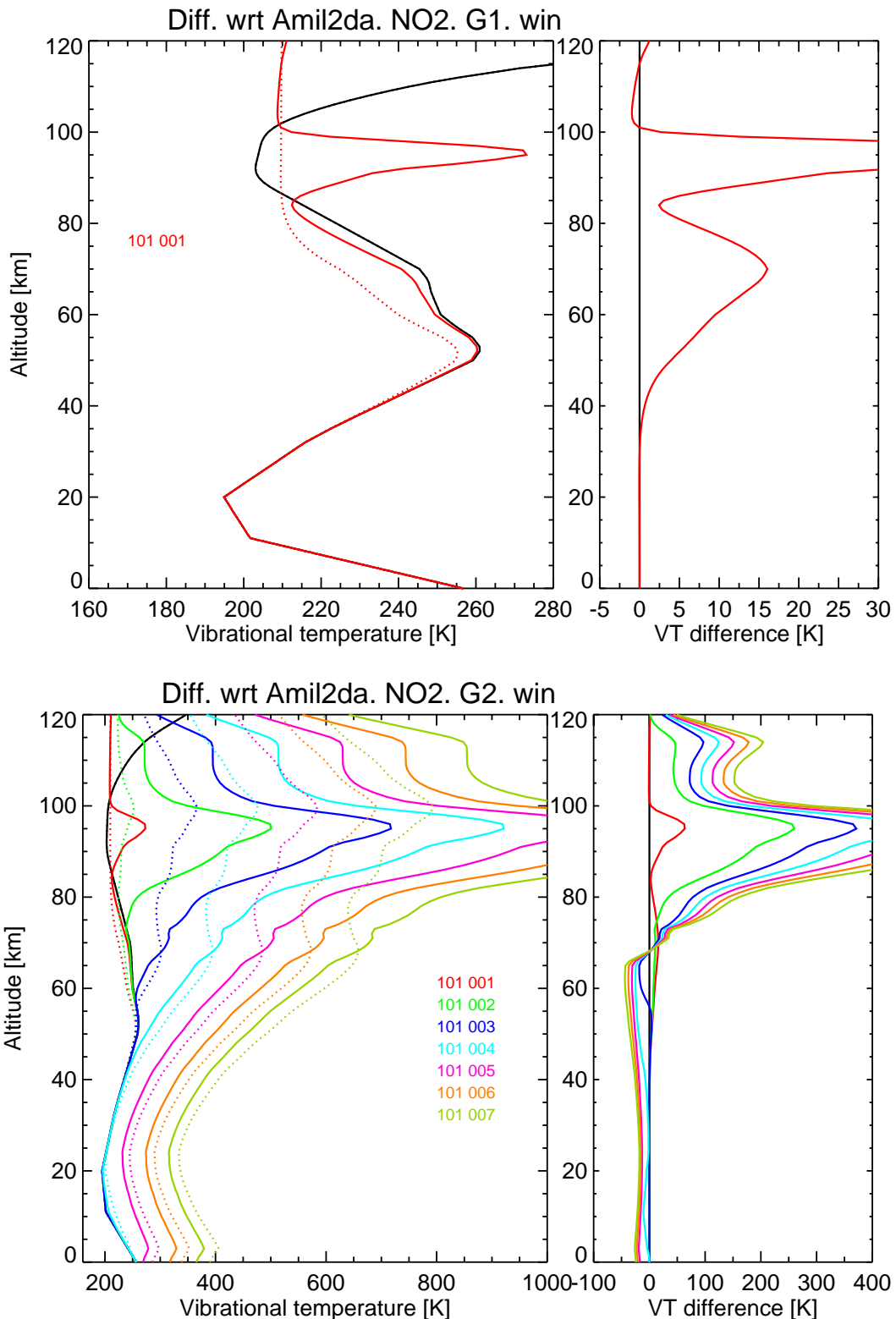


Figure 137: Differences in vibrational temperatures w.r.t. previous version (AMIL2DA) for the NO₂ levels, for reference atmosphere #4, winter. Solid: this study; dash: AMIL2DA. Right panels: this study–AMIL2DA.

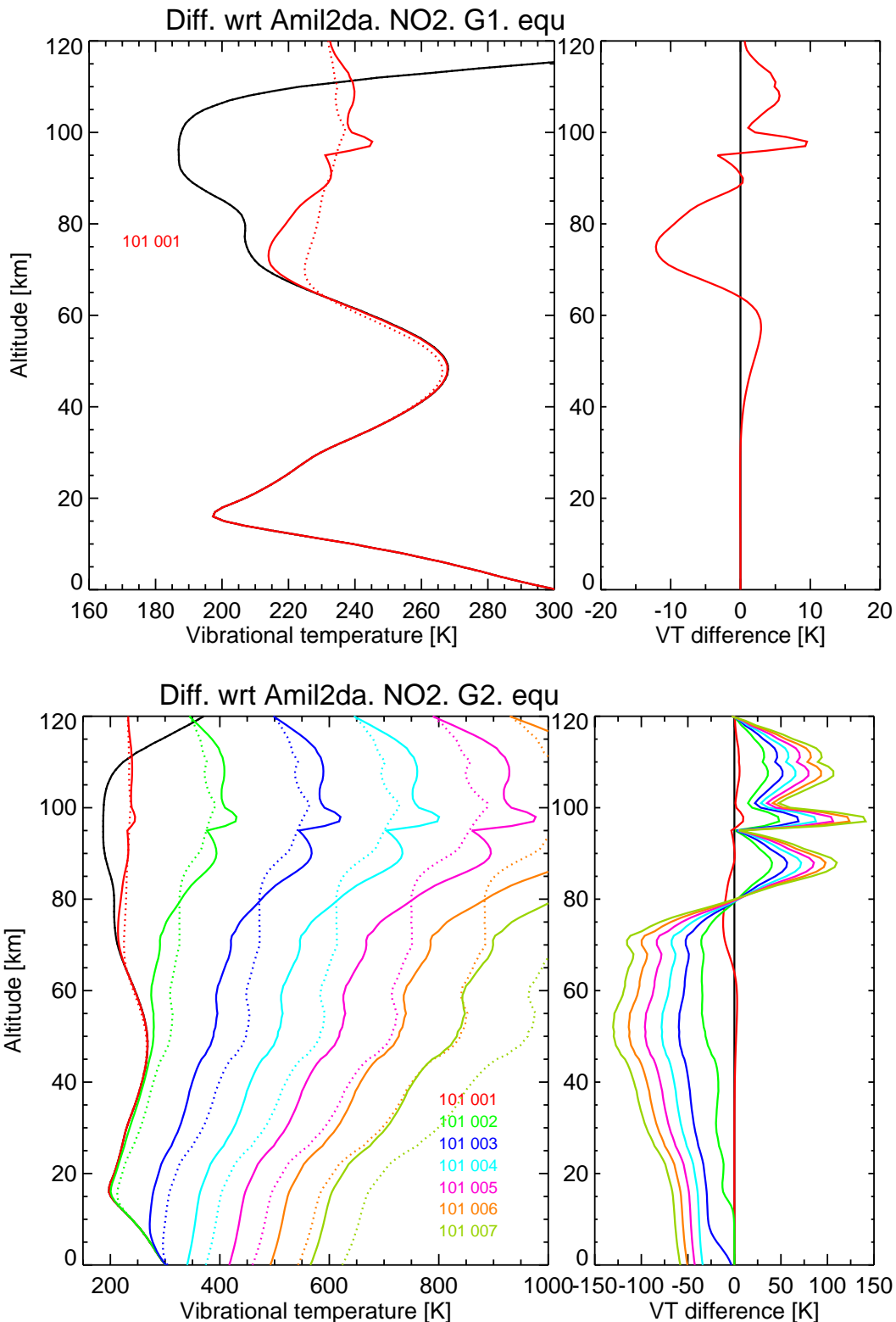


Figure 138: Differences in vibrational temperatures w.r.t. previous version (AMIL2DA) for the NO₂ levels, for reference atmosphere #5, equator. Solid: this study; dash: AMIL2DA. Right panels: this study–AMIL2DA.

3.10 HNO₃

The major improvement in the HNO₃ non-LTE model is a more accurate calculation of the radiative transfer. This lead to significant changes in the populations but limited to the non-LTE region in the upper mesosphere.

Figures 139-143 show the vibrational temperatures for the HNO₃ energy levels.

Figures 144-148 show the differences in the vibrational temperatures for the NO₂ energy levels with respect to previous (AMIL2DA) version.

The major differences are caused by the more accurate radiative transfer excitation included in this study (in particular the consideration of a tropospheric upwelling flux) causing, in general, larger vibrational temperatures in the non-LTE region.

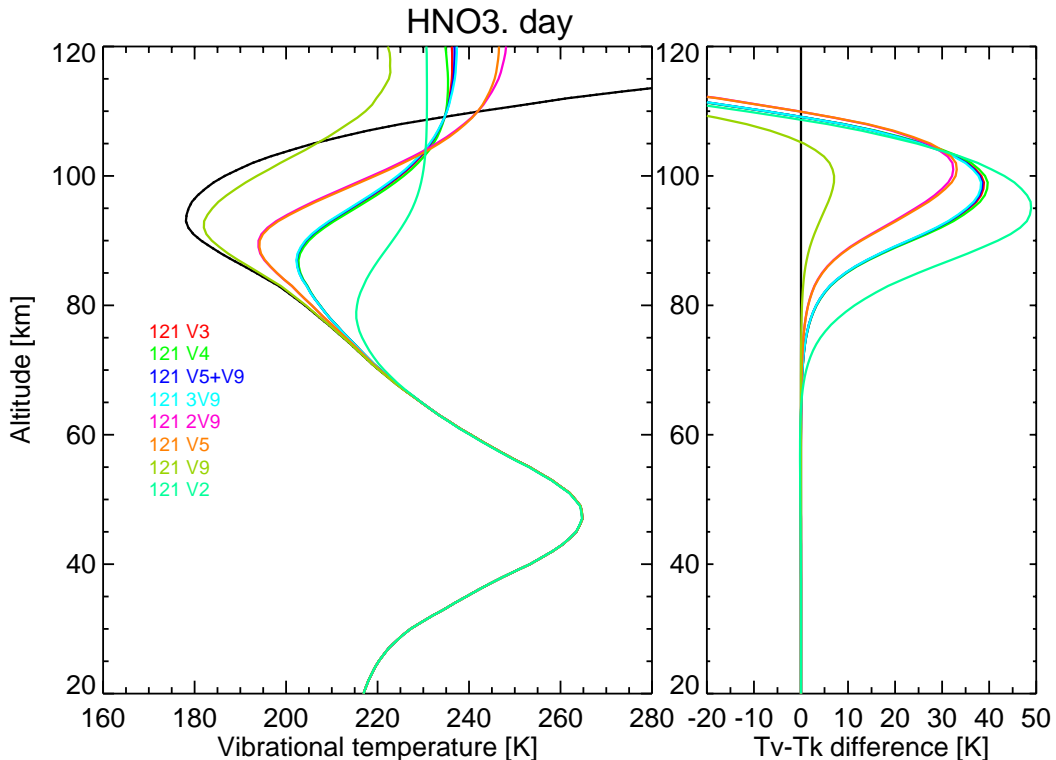


Figure 139: Vibrational temperatures for HNO₃ levels, for reference atmosphere #1, day.

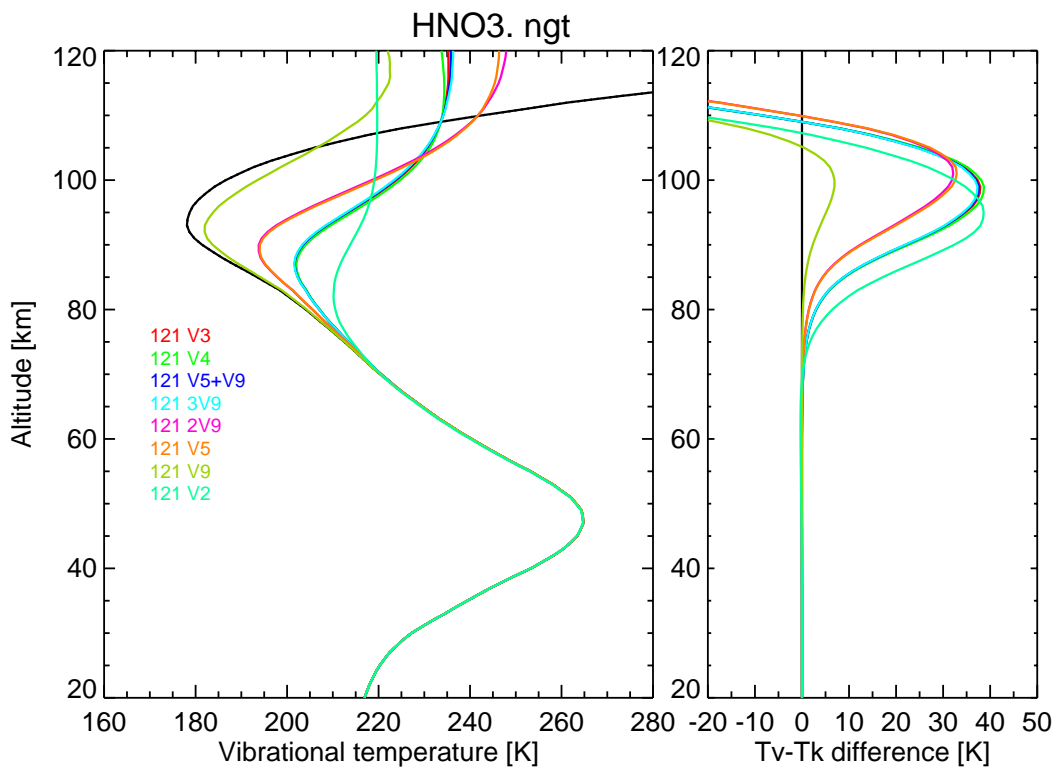


Figure 140: Vibrational temperatures for HNO₃ levels, for reference atmosphere #2, night.

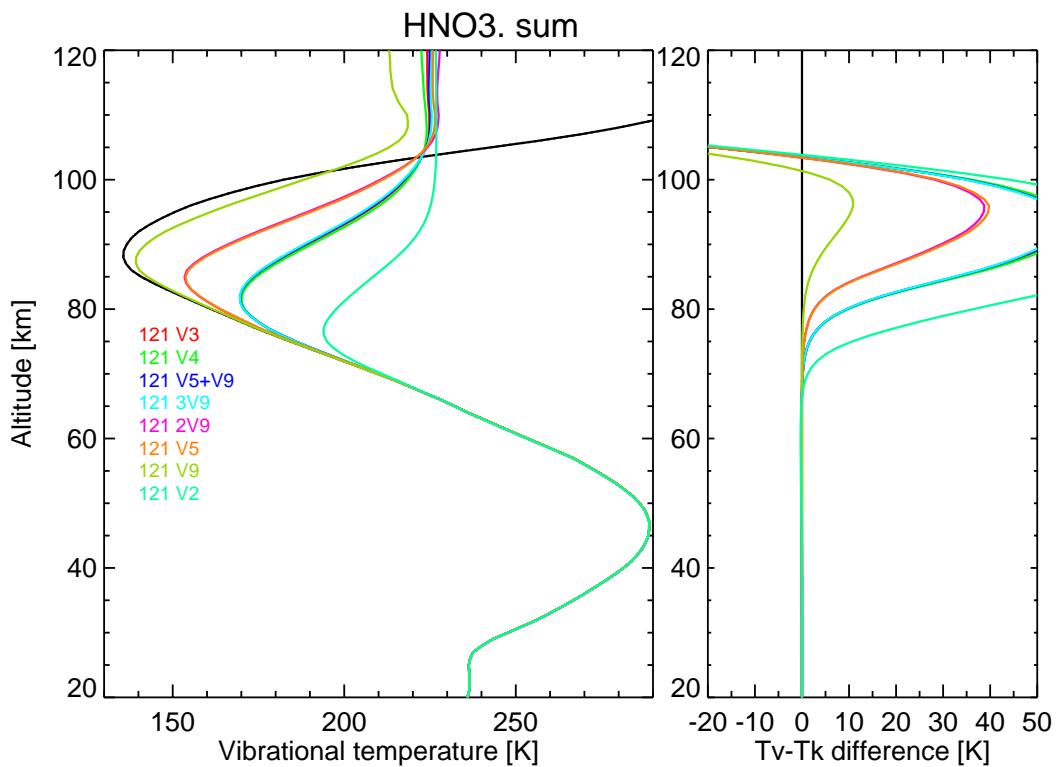


Figure 141: Vibrational temperatures for HNO₃ levels, for reference atmosphere #3, summer.

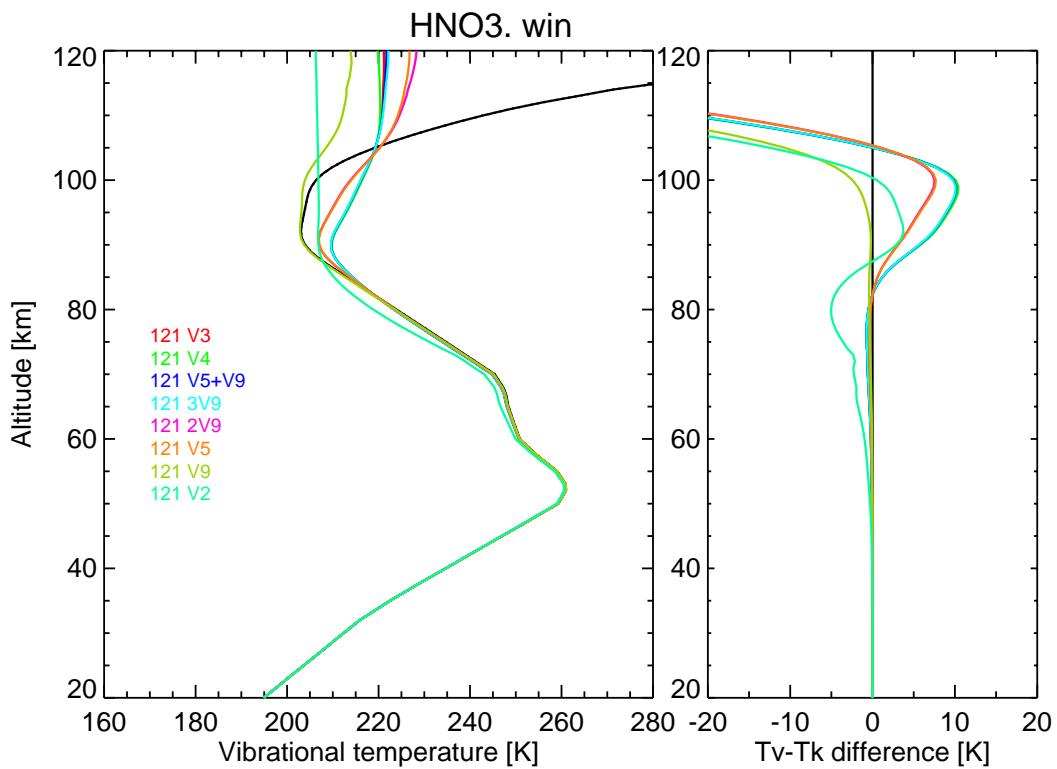


Figure 142: Vibrational temperatures for HNO₃ levels, for reference atmosphere #4, winter.

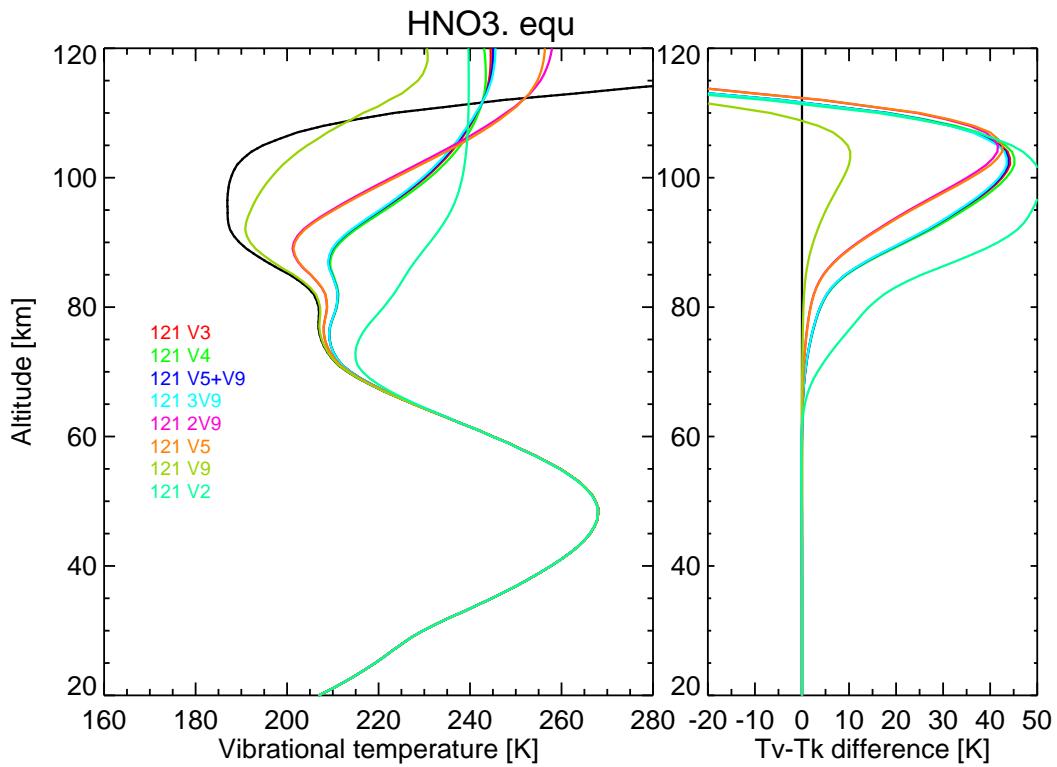


Figure 143: Vibrational temperatures for HNO₃ levels, for reference atmosphere #5, equator.

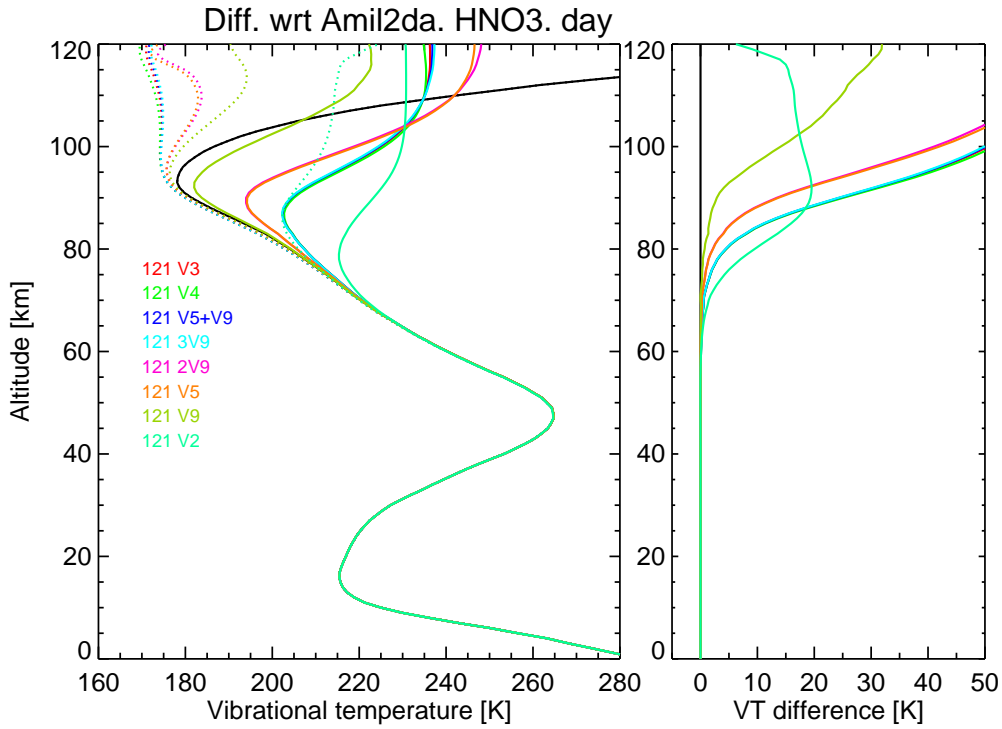


Figure 144: Differences in vibrational temperatures w.r.t. previous version (AMIL2DA) for the HNO₃ levels, for reference atmosphere #1, day. Solid: this study; dash: AMIL2DA. Right panels: this study–AMIL2DA.

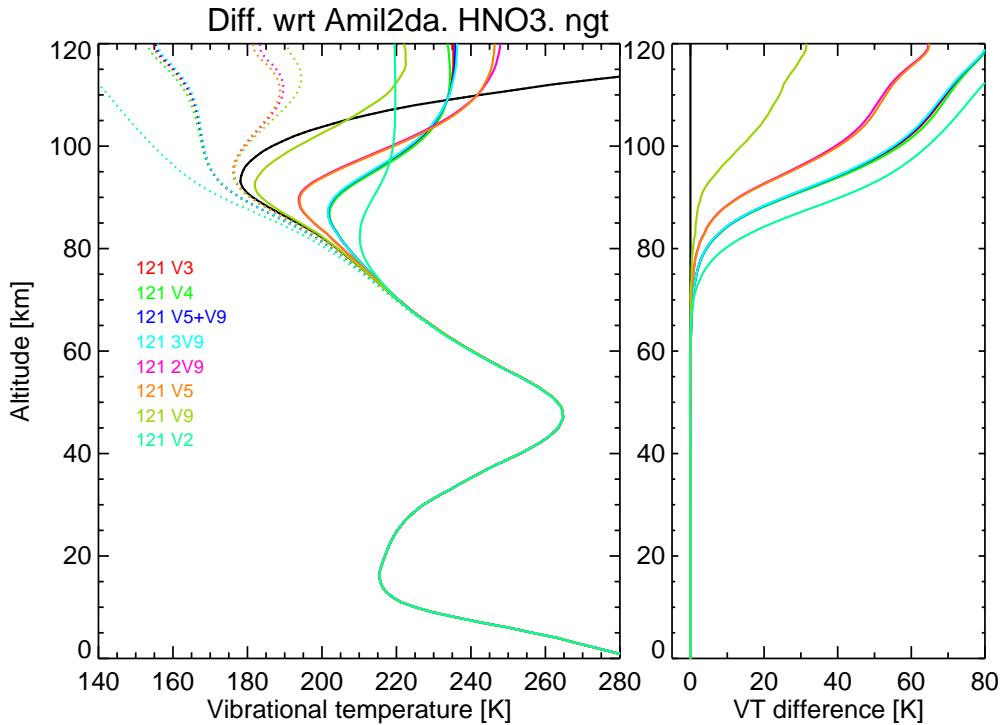


Figure 145: Differences in vibrational temperatures w.r.t. previous version (AMIL2DA) for the HNO₃ levels, for reference atmosphere #2, ngt. Solid: this study; dash: AMIL2DA. Right panels: this study–AMIL2DA.

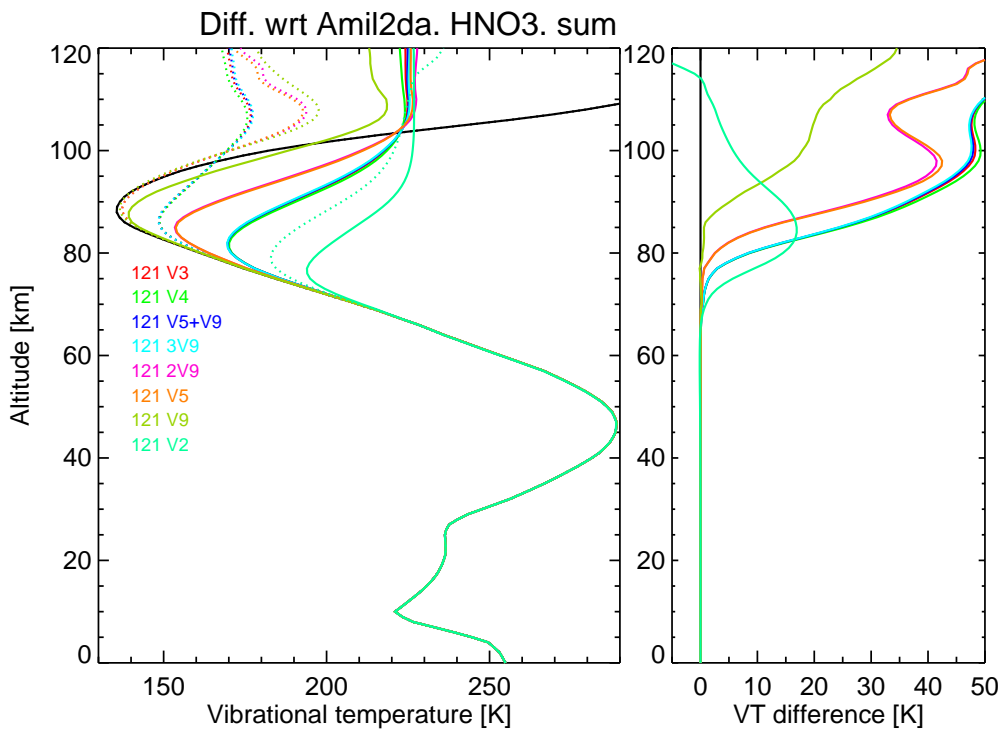


Figure 146: Differences in vibrational temperatures w.r.t. previous version (AMIL2DA) for the HNO₃ levels, for reference atmosphere #3, summer. Solid: this study; dash: AMIL2DA. Right panels: this study–AMIL2DA.

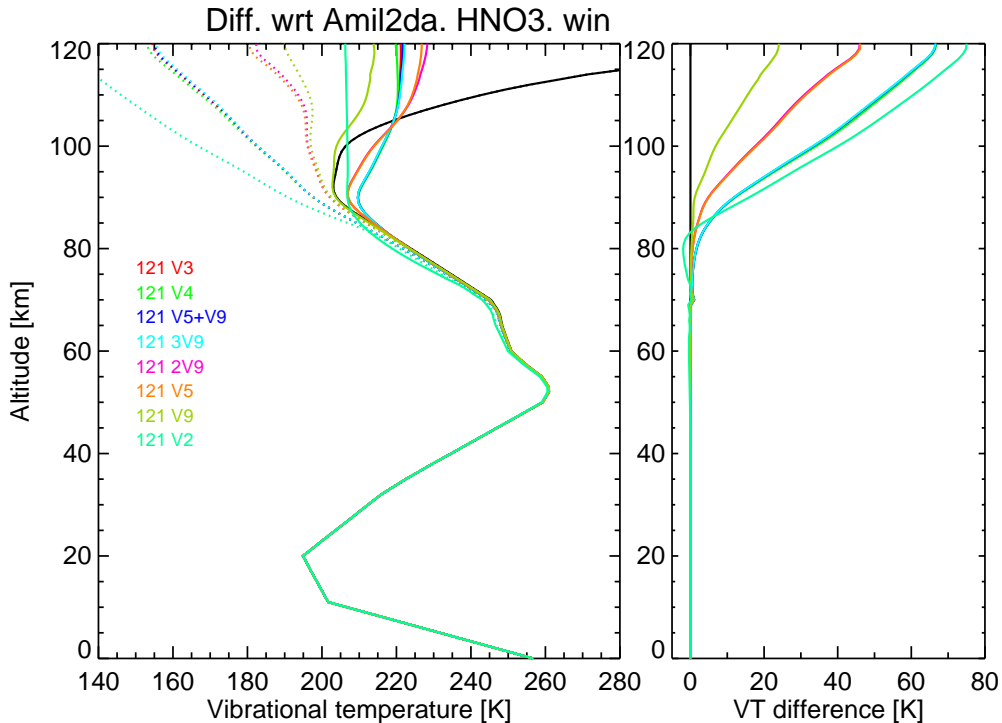


Figure 147: Differences in vibrational temperatures w.r.t. previous version (AMIL2DA) for the HNO₃ levels, for reference atmosphere #4, winter. Solid: this study; dash: AMIL2DA. Right panels: this study–AMIL2DA.

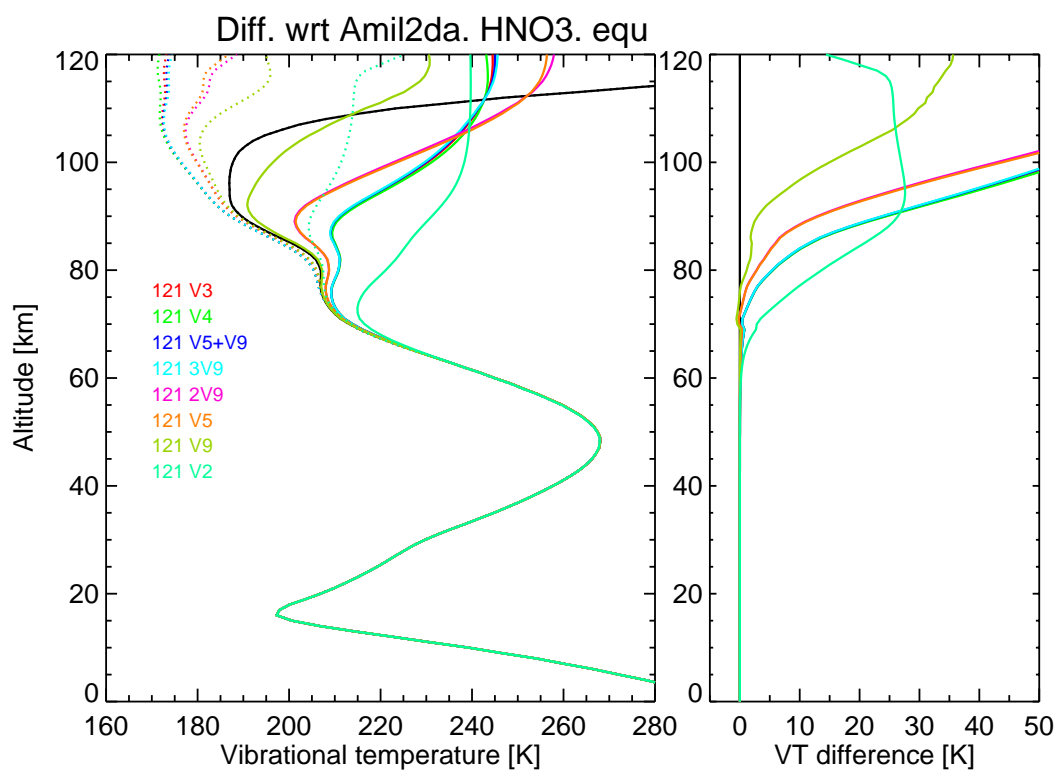


Figure 148: Differences in vibrational temperatures w.r.t. previous version (AMIL2DA) for the HNO₃ levels, for reference atmosphere #5, equator. Solid: this study; dash: AMIL2DA. Right panels: this study–AMIL2DA.

3.11 OH

The non-LTE model for the OH($v=1-9$) levels has not changed. The differences obtained in the vibrational temperatures of the OH($v=1-9$) levels are caused by the different abundances included now for O₃ and H.

Figures 149-153 show the vibrational temperatures for the OH(v) vibrational energy levels with spin=1/2 for the 5 reference atmospheres. We have treated the two OH spin populations in the same way as for NO (see Sec. 3.8).

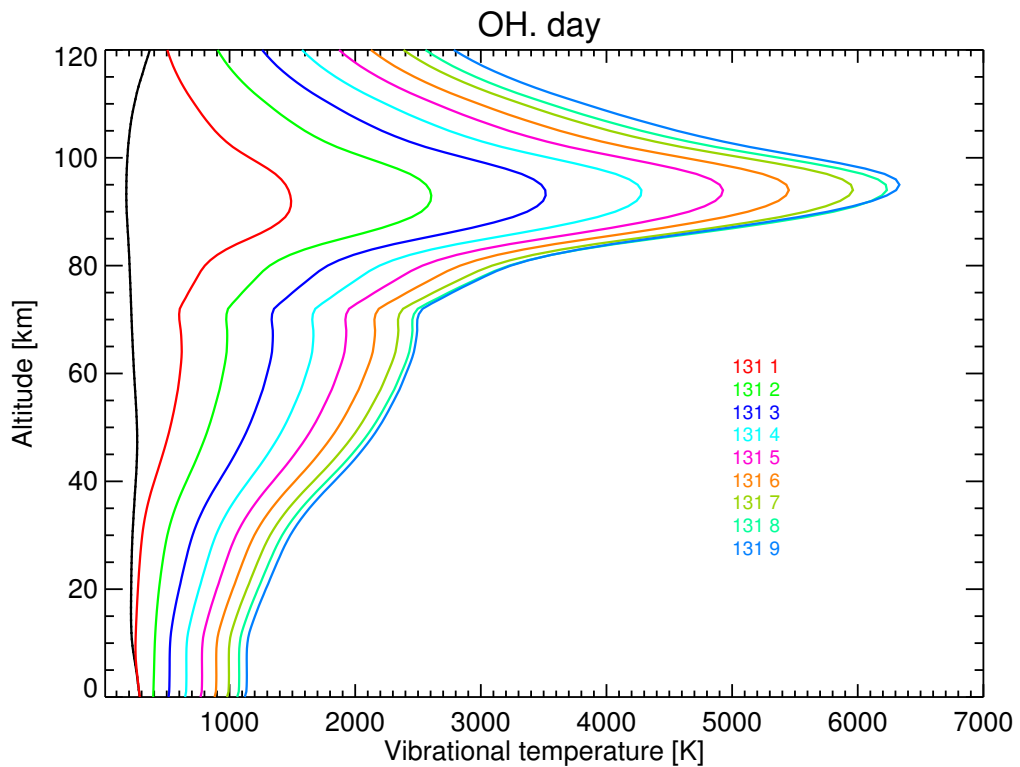


Figure 149: Vibrational temperatures for OH levels, for reference atmosphere #1, day.

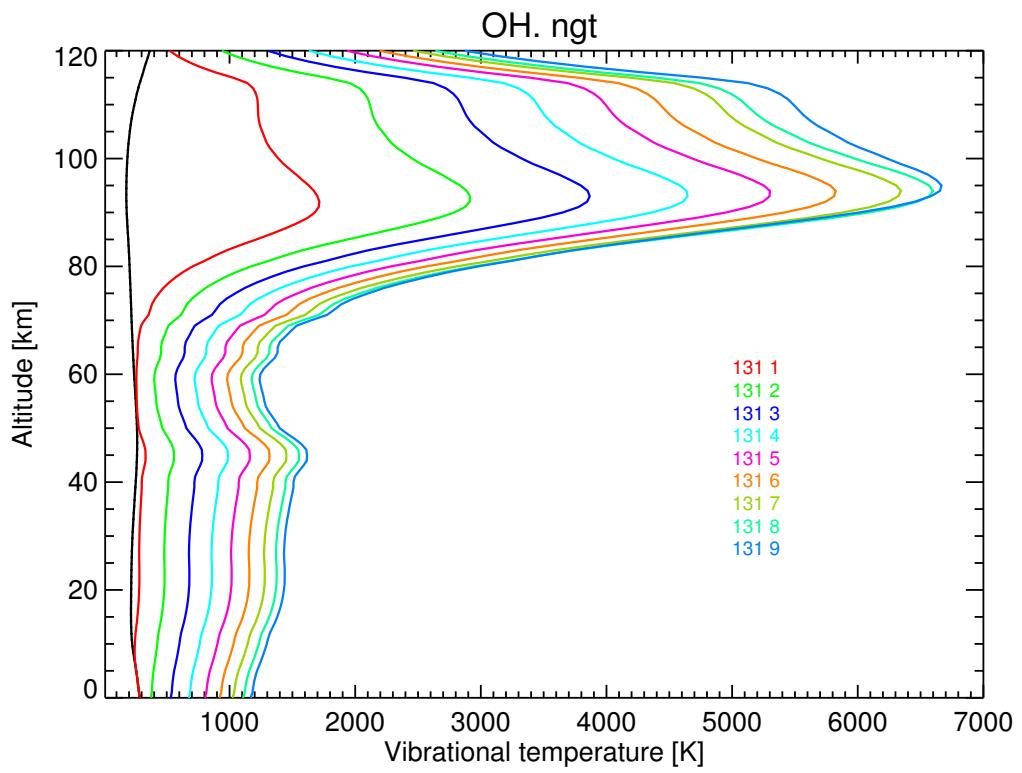


Figure 150: Vibrational temperatures for OH levels, for reference atmosphere #2, night.

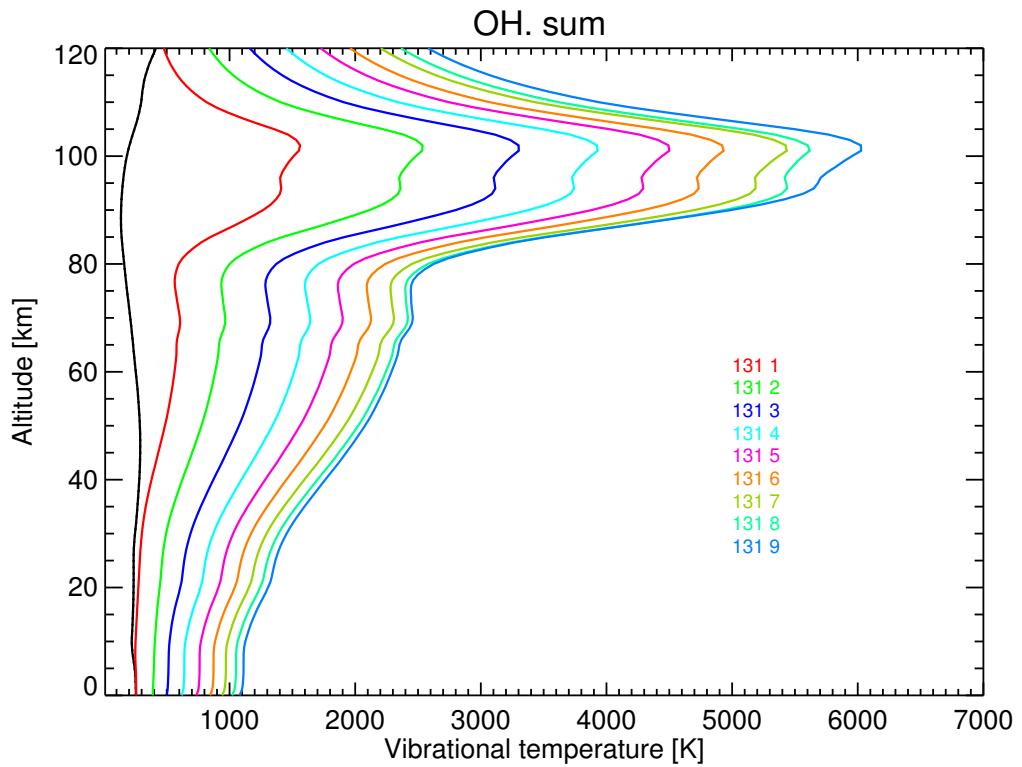


Figure 151: Vibrational temperatures for OH levels, for reference atmosphere #3, summer.

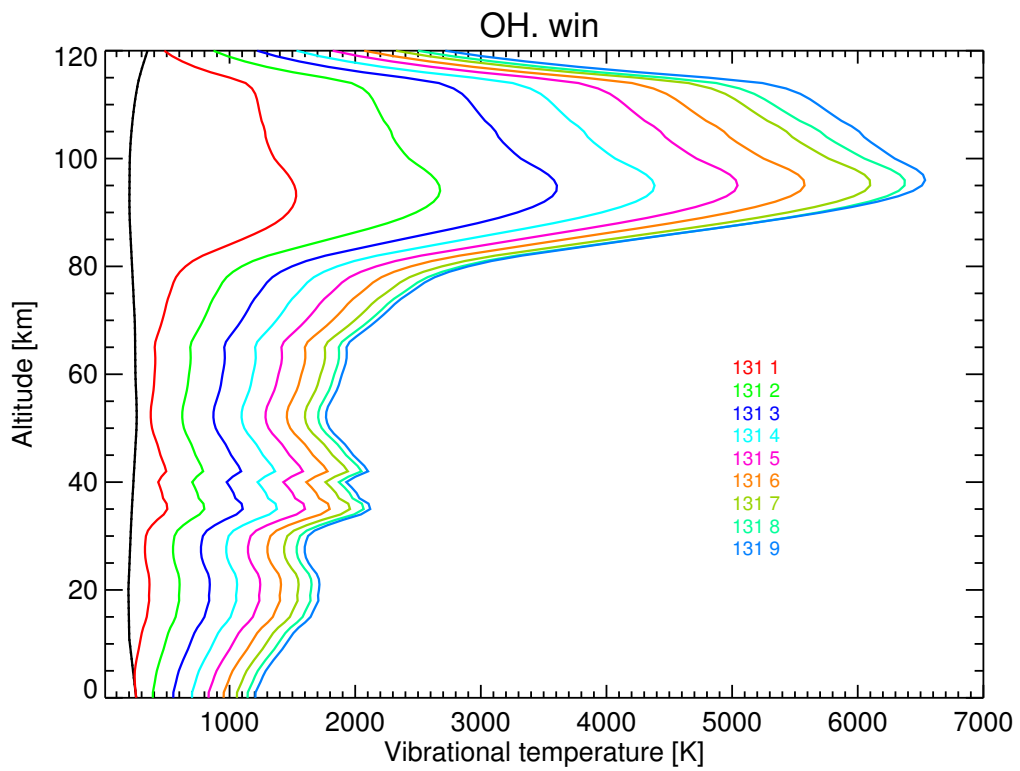


Figure 152: Vibrational temperatures for OH levels, for reference atmosphere #4, winter.

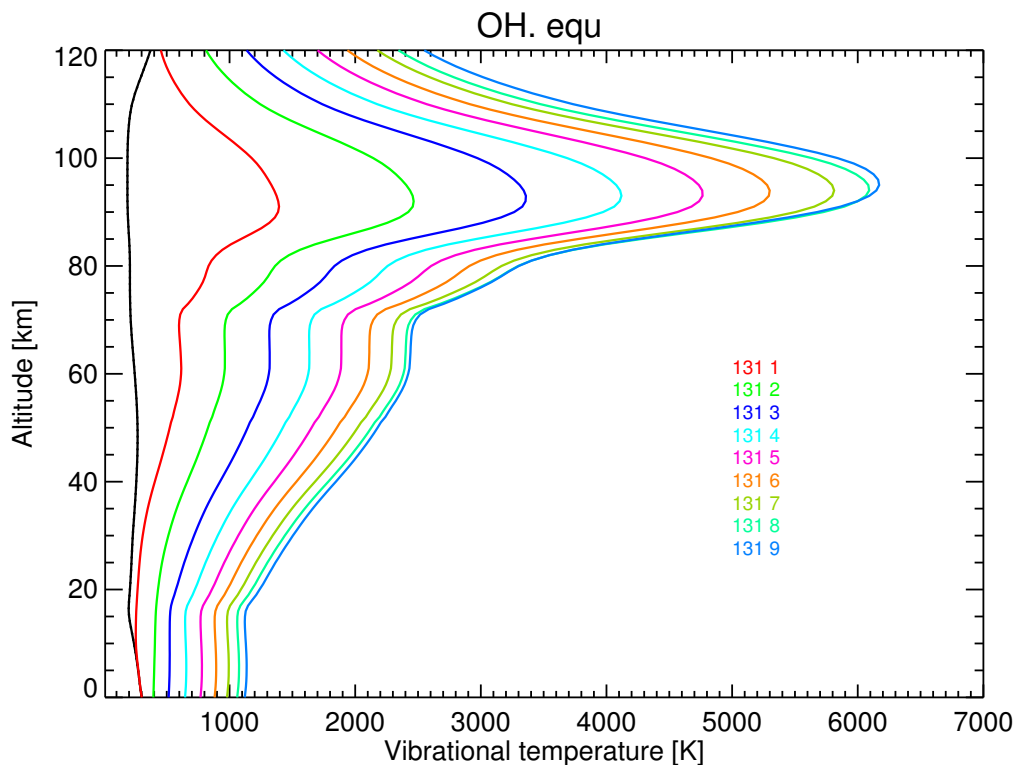


Figure 153: Vibrational temperatures for OH levels, for reference atmosphere #5, equator.

3.12 HCN

A new model for the HCN vibrational populations has been developed. Table 6 lists the energy levels for which we have calculated vibrational temperatures, and Table 7 the collisional processes incorporated into the model.

In the Earth atmosphere, the most important collisional processes are 3 and 4, which transfer energy from the v_3 states excited by absorption of sunlight, and 1: the quenching of v_2 .

Radiative transitions included are:

- The $010 \rightarrow 000$, and $001 \rightarrow 000$ bands have been treated with Curtis matrix in the range 10-200 km, and with line-by-line calculation of upwelling tropospheric flux generated at 0-10 km.
- For all other transitions a constant tropospheric ($T_{eff}=T_{surface}$) and solar (top of the atmosphere) fluxes were assumed.

Figures 154-158 show the vibrational temperatures for the HCN energy levels. The non-LTE effects in the (010-000) band, used for HCN retrieval, are completely negligible below about 80 km. For higher energy levels the non-LTE effects are important, particularly during illuminated conditions, but they do not affect the potential MIPAS retrieval of HCN.

Table 6: HCN energy levels for which vibrational temperatures are calculated.

No.	HITRAN ID	Level	Energy, cm ⁻¹
1	2	0110	713.4590
2	3	0200	1411.4130
3	4	0220	1427.6300
4	5	1000	2096.8456
5	6	0310	2113.4080
6	7	0330	2144.9300
7	8	1110	2806.1777
8	9	0400	2797.9686
9	10	0420	2814.1400
10	11	1200	3500.9244
11	12	1220	3517.0957
12	13	2000	4173.0259
13	14	0001	3311.4772
14	18	2110	4878.4052
15	19	0111	4005.6290
16	22	2200	5569.1995
17	23	2220	5585.3709
18	25	0201	4684.1056
19	26	0221	4699.8000
20	27	1001	5393.7621
21	32	1111	6083.4250
22	36	1201	6758.4860
23	37	1221	6774.6573
24	38	0002	6519.6040
25	44	0440	2862.6540

Table 7: Collisional processes included for HCN.

No.	Process	Rate	Reference
1	$\text{HCN}(v_1, v_2, v_3) + \text{M} \rightarrow \text{HCN}(v_1, v_2-1, v_3) + \text{M}$	$1. \times 10^{-12}$	Srinivasan et al. (2008) (rate for Kr, scaled by 0.3 to account for the k001(Kr)/ k001(M) ratio from Arnold and Smith (1981)).
2	$\text{HCN}(v_1, v_2, v_3) + \text{M} \rightarrow \text{HCN}(v_1-1, v_2+3, v_3) + \text{M}$	2.7×10^{-14}	Srinivasan et al. (2008): rate for Kr, scaled by 0.3 to account for the k001(Kr)/ k001(M) ratio and divided by 2 (goes to 03^30 and 03^00).
3	$\text{HCN}(v_1, v_2, v_3) + \text{O}_2 \rightarrow \text{HCN}(v_1+1, v_2+2, v_3-1) + \text{O}_2$	6.7×10^{-16}	Hastings et al. (1991) (di- vided by 2: goes to 02^00 and 02^20).
4	$\text{HCN}(v_1, v_2, v_3) + \text{N}_2 \rightarrow \text{HCN}(v_1+1, v_2+2, v_3-1) + \text{N}_2$	1.2×10^{-14}	Hastings et al. (1991) (di- vided by 2: goes to 02^00 and 02^20).
5	$\text{HCN}(v_1, v_2, v_3) + \text{HCN} \rightarrow \text{HCN}(v_1, v_2-1, v_3) + \text{HCN}$	4.0×10^{-12}	Garvey et al. (1977).
6	$\text{HCN}(v_1, v_2, v_3) + \text{HCN} \rightleftharpoons \text{HCN}(v_1+1, v_2+1, v_3-1) +$ $\quad \quad \quad + \text{HCN}(010)$	2.4×10^{-12}	Hastings et al. (1991)
7	$\text{HCN}(v_1, v_2, v_3) + \text{N}_2 \rightarrow \text{HCN}(v_1-1, v_2, v_3) + \text{N}_2$ (1)	5.0×10^{-15}	Same value as for CO+N ₂ (similar energy gap).

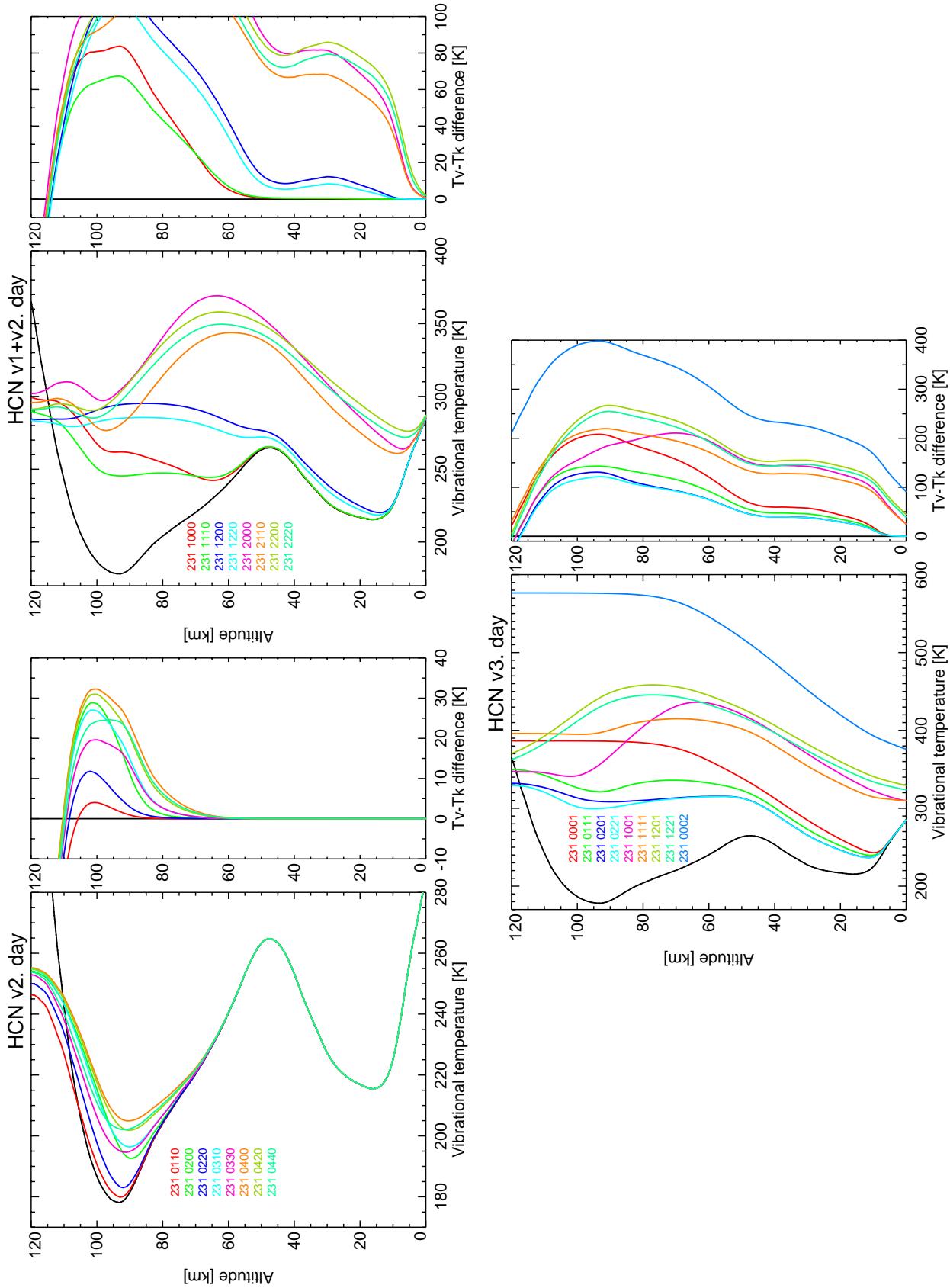


Figure 154: Vibrational temperatures for HCN levels, for reference atmosphere #1, day.

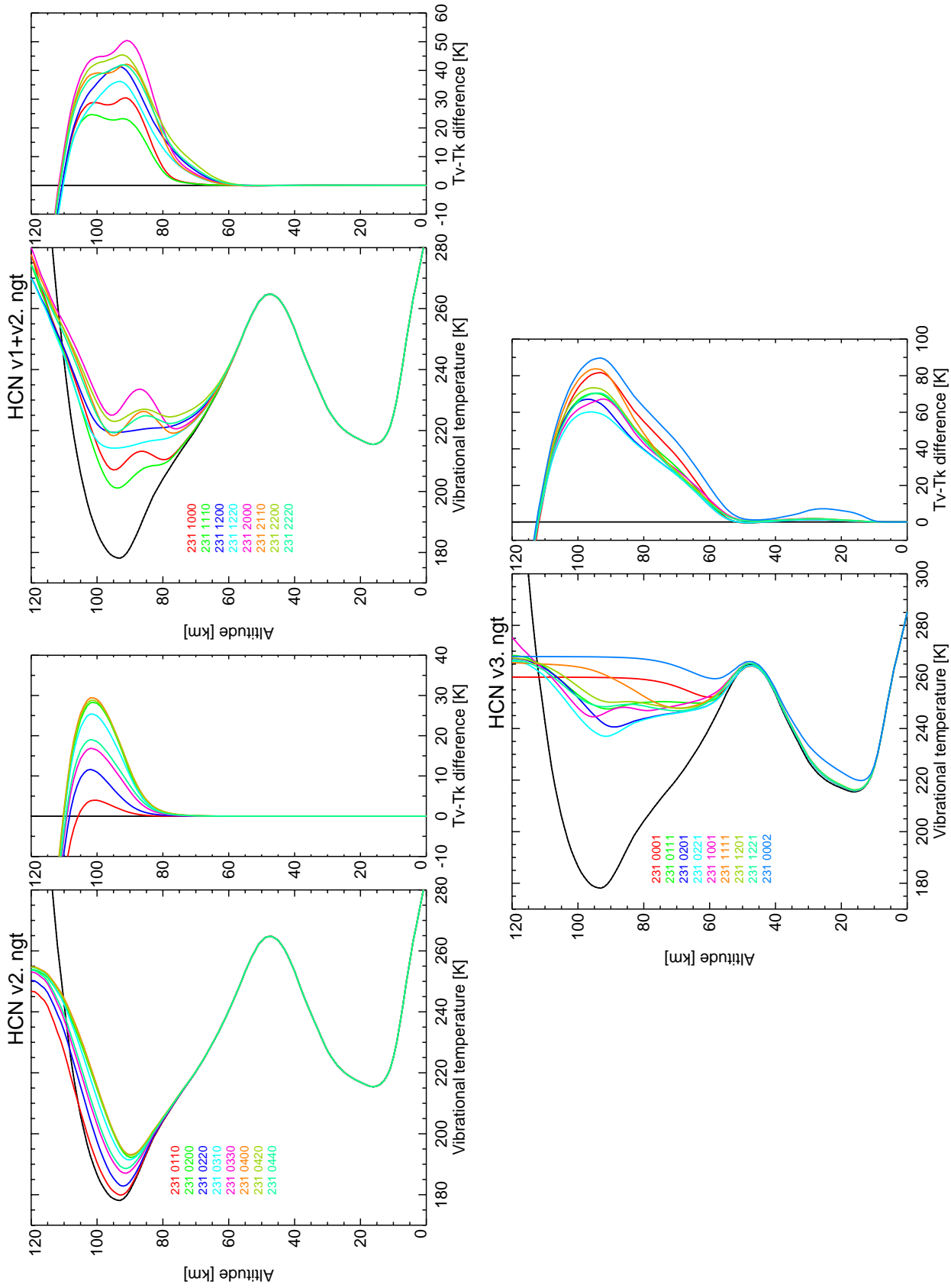


Figure 155: Vibrational temperatures for HCN levels, for reference atmosphere #2, night.

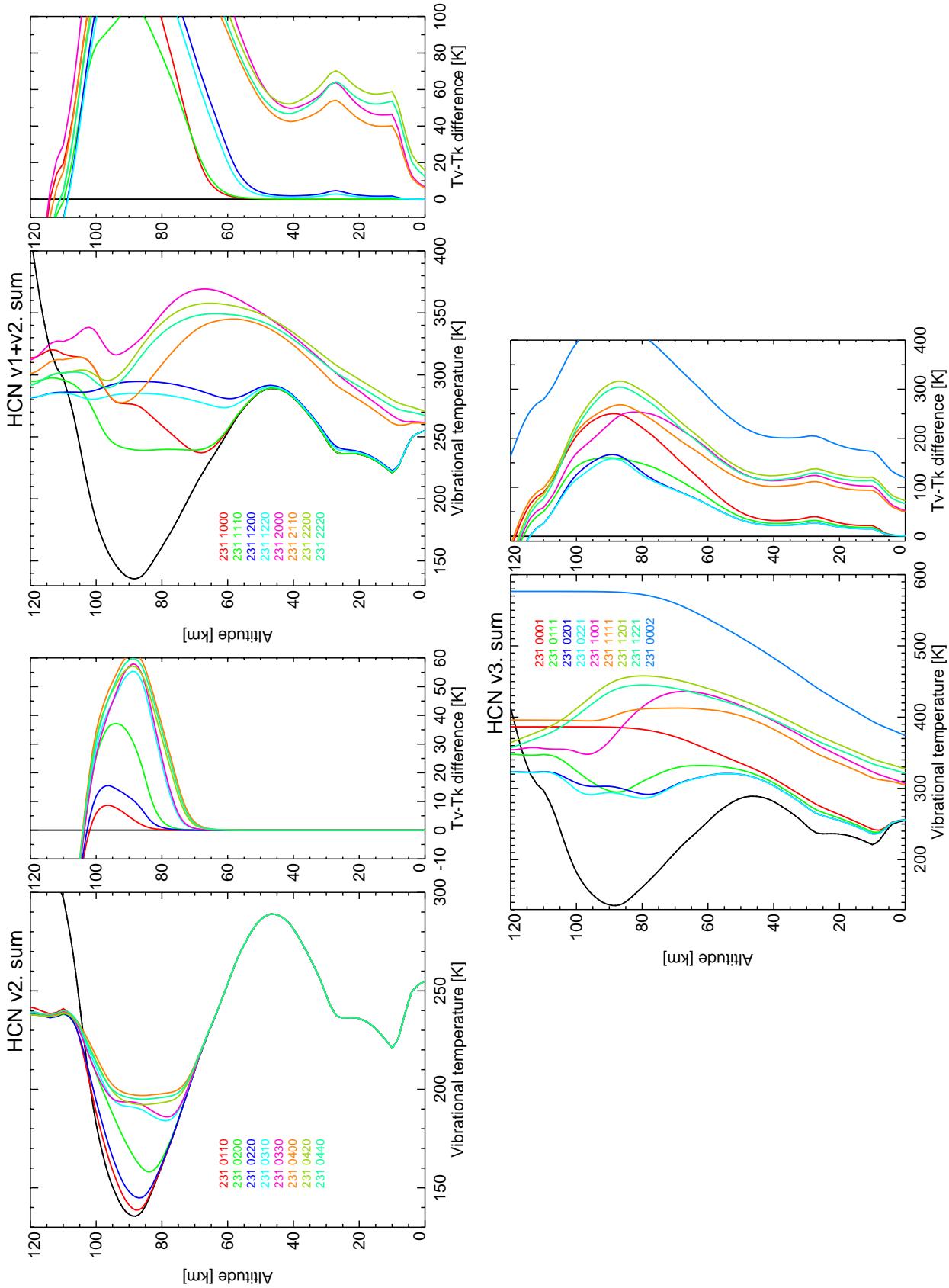


Figure 156: Vibrational temperatures for HCN levels, for reference atmosphere #3, summer.

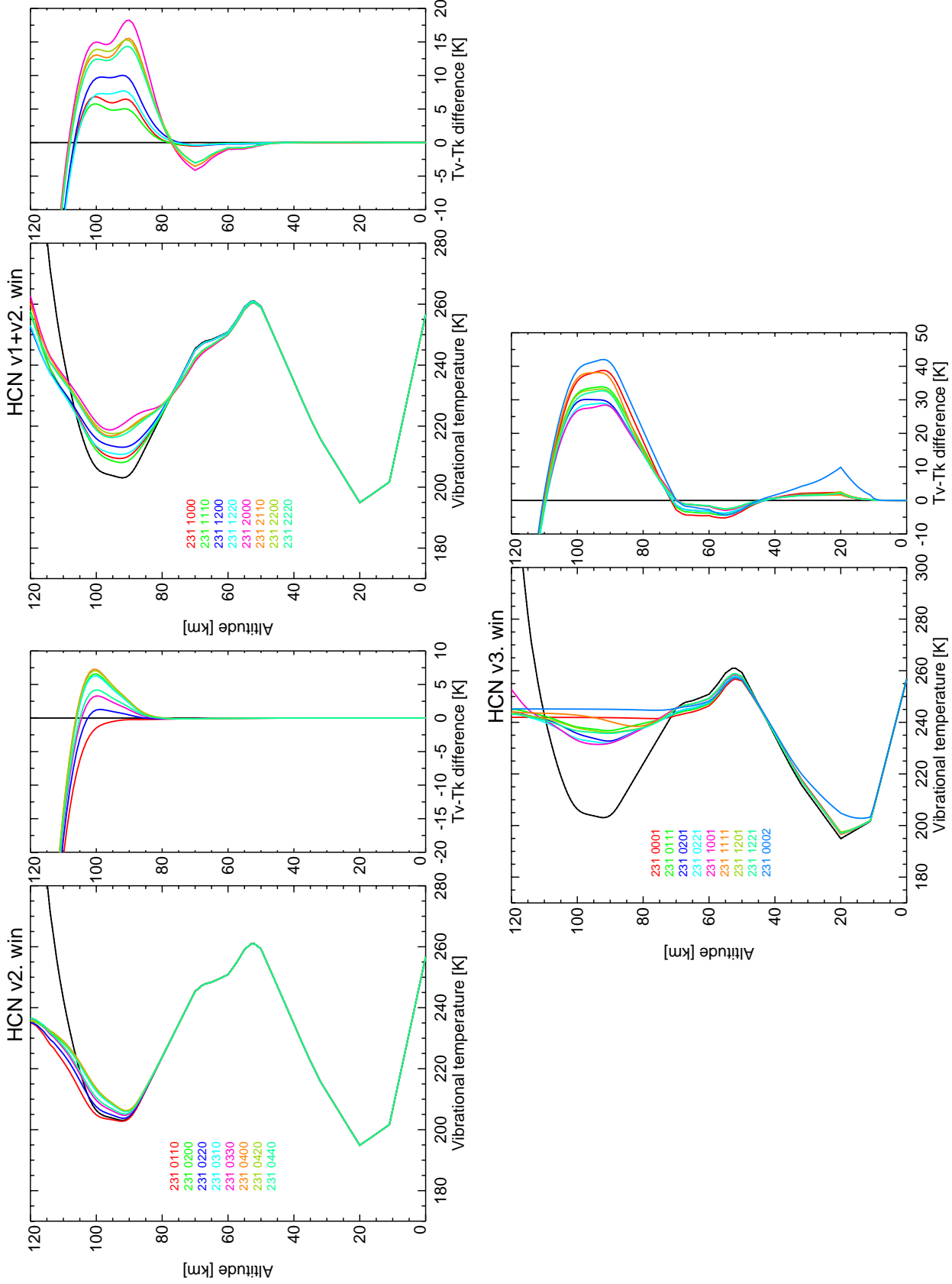


Figure 157: Vibrational temperatures for HCN levels, for reference atmosphere #4, winter.

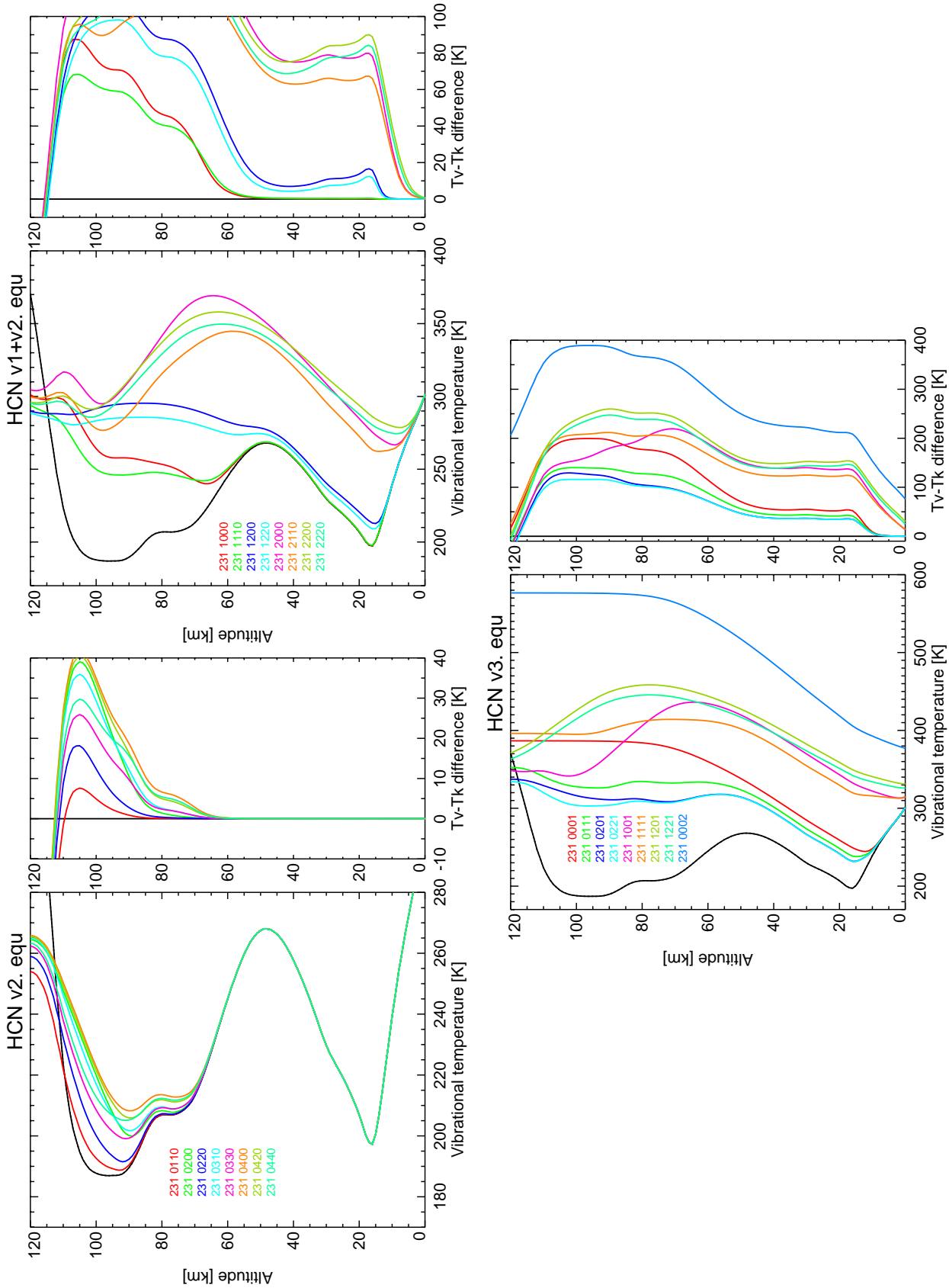


Figure 158: Vibrational temperatures for HCN levels, for reference atmosphere #5, equator.

4 Summary and Conclusions

- CO₂, O₃, and NO₂(00v₃) vibrational temperatures have changed significantly, although not for all levels.
- CO: small (but significant) changes in vibrational temperatures and in the spectra.
- H₂O-CH₄ vibrational temperatures show some minor changes (although the rates for the involved processes have changed significantly).
- CH₄ high-energy levels have largely changed (due to more accurate radiative transfer) but limited to the non-LTE region. We expect small changes in the spectra.
- N₂O and HNO₃ VTs have significantly changed because of the more accurate radiative transfer but limited to the non-LTE region (at high altitudes). We expect small changes in the spectra.
- NO exhibits very small changes.
- OH also exhibits very small changes, only those introduced by the IG O₃ and H profiles.
- A new model has been developed for HCN. The predicted non-LTE effects for the (010-000) band, used for HCN retrieval, below 80 km is negligible. The higher energy levels exhibit large deviations from LTE during illuminated conditions but do not have any impact on the HCN retrieval and the effects on the spectra are expected to be very small.

References

- Anderson, S. M., F. S. Klein, and F. Kaufman, *J. Chem. Phys.*, **83**, 1648, 1985.
- Arnold and Smith, J Chem. Soc Faraday Trans 2, 77, 861, 1981.
- Bass, H.E.: Vibrational relaxation in CO₂-O₂ mixtures, *J. Chem. Phys.*, **58**, 4783, 1973.
- Bohn, B., A. Doughty, G. Hancock, E. L. Moore and C. Morrell, Vibrational relaxation of NO(v=1-3) and NO₂(0,0,1) with atmospheric gases, *Phys. Chem. Chem. Phys.*, **1**, 1833-1842, 1999.
- Boursier, C., J. Ménard, and F. Ménard-Bourcin, Vibrational Relaxation of Methane by Oxygen Collisions: Measurements of the Near-Resonant Energy Transfer between CH₄ and O₂ at Low Temperature, *J. Phys. Chem. A*, **111**, 7022–7030, doi: 10.1021/jp072377y, 2007.
- Clarmann, v. T., Dudhia, A., Echle, G. et al. (1998) “Study on the simulation of atmospheric infrared spectra”, *ESA Final Report*, ESA CR12054/96/NL/CN.
- Copeland, R., Measurement Of Oxygen Vibrational Relaxation Rate Constant With Oxygen Atoms At Low Temperature, Final Report MP 08-069, January 2009.
- Dang, C., J. Reid, and B. K. Garside, Dynamics of the CO₂ upper laser level as measured with a tunable diode laser, *App. Phys. B*, **31**, 163–172, 1983.
- Edwards, D. P., G. Zaragoza, M. Riese and M. López-Puertas, Evidence of H₂O nonlocal thermodynamic equilibrium emission near 6.4 μm as measured by cryogenic infrared spectrometers and telescopes for the atmosphere (CRISTA 1), *J. Geophys. Res.*, **105**, 29003, 2000.

- Fischer, H., M. Birk, C. Blom, B. Carli, M. Carlotti, T. von Clarmann, L. Delbouille, A. Dudhia, D. Ehhalt, M. Endemann, J.-M. Flaud, R. Gessner, A. Kleinert, R. Koopmann, J. Langen, M. López-Puertas, P. Mosner, H. Nett, H. Oelhaf, G. Perron, J. J. Remedios, M. Ridolfi, G. P. Stiller, and R. Zander, ‘MIPAS: an instrument for atmospheric and climate research’. *Atmos. Chem. Phys.* **8**, 2151–2188, 2008.
- Funke, B. and López-Puertas, M., “Non-LTE vibrational, rotational, and spin state distribution for the NO($v=0,1,2$) states under quiescent conditions”, *J. Geophys. Res.* **105**, 4409, 2000.
- Funke, B., Martín-Torres, F.J., López-Puertas, M., Höpfner, M., Hase, F., López-Valverde, M. A., and García-Comas, M., A generic non-LTE population model for MIPAS-ENVISAT data analysis, vol. 4, abstracts of the Contributions of the European Geophysical Society, Nice, France, 21–26 April 2002, CD-ROM, ISSN:1029–7006, 2002.
- Funke, B., et al., Retrieval of stratospheric NOx from 5.3 and 6.2 μm nonlocal thermodynamic equilibrium emissions measured by Michelson Interferometer for Passive Atmospheric Sounding (MIPAS) on Envisat, *J. Geophys. Res.*, 110, D09302, doi:10.1029/2004JD005225, 2005.
- Funke, B., M. López-Puertas, D. Bermejo-Pantaleón, T. von Clarmann, G. P. Stiller, M. Höpfner, U. Grabowski, and M. Kaufmann, Analysis of nonlocal thermodynamic equilibrium CO 4.7 μm fundamental, isotopic, and hot band emissions measured by the Michelson Interferometer for Passive Atmospheric Sounding on Envisat, *J. Geophys. Res.*, 112, D11305, doi:10.1029/2006JD007933, 2007.
- Garcia, R.R., and S. Solomon, A new numerical model of the middle atmosphere 2. Ozone and related species, *J. Geophys. Res.*, 99, 12937–12951, 1994.
- García-Comas, M., M. López-Puertas, B. T. Marshall, P. P. Wintersteiner, B. Funke, D. Bermejo-Pantaleón, C. J. Mertens, E. E. Remsberg, L. L. Gordley, M. G. Mlynczak, and J. M. Russell III, Errors in Sounding of the Atmosphere using Broadband Emission Radiometry (SABER) kinetic temperature caused by non-local-thermodynamic-equilibrium model parameters, *J. Geophys. Res.*, 113, D24106, doi:10.1029/2008JD010105, 2008.
- Gardner, J. L., M. López-Puertas, B. Funke, S. M. Miller, S. J. Lipson, and R. D. Sharma, Rotational and spin-orbit distributions of NO observed by MIPAS/ENVISAT during the solar storm of October/November 2003, *J. Geophys. Res.*, 110, A09S34, doi:10.1029/2004JA010937, 2005.
- Gardner, J. L., B. Funke, M. G. Mlynczak, M. Lopez-Puertas, F. J. Martin-Torres, J. M. Russell III, S. M. Miller, R. D. Sharma, and J. R. Winick, Comparison of nighttime nitric oxide 5.3 μm emissions in the thermosphere measured by MIPAS and SABER, *J. Geophys. Res.*, 112, A10301, doi:10.1029/2006JA011984, 2007.
- Garvey et al., *J. Chem. Phys.* 66, 3189, 1977.
- Gil-López, S., Determinación del ozono atmosférico de las medidas de MIPAS/Envisat, Ph.D. Univ. of Granada, 2006.
- Hastings et al., *J. Chem. Phys.* 78, 3893, 1991.
- Huestis, D. L., Vibrational energy transfer and relaxation in O₂ and H₂O, *J. Phys. Chem. A*, 10.1021/jp054889n, 2006.

- Huddleston, R. K., and E. Weitz (1981), A laser-induced fluorescence study of energy transfer between the symmetric stretching and bending modes of CO₂, *Chem. Phys. Lett.*, **83**, 174-179.
- Kalogerakis, K. S., R. A. Copeland, and T. G. Slanger, Measurements of the rate coefficient for collisional removal of O₂(X³Σ_g⁻, v = 1) by O(³P), *J. Chem. Phys.*, **123**, 194303, 2005.
- Kaufmann, M., S. Gil-López, B. Funke, M. García-Comas, M.E. Koukouli, M. López-Puertas, N. Glatthor, U. Grabowski, M. Höpfner, G.P. Stiller, T. von Clarmann and M. Riese, vibrationally excited ozone in the middle atmosphere, *J. Atmos. Solar-Terr. Phys.*, doi:10.1016/j.jastp.2005.10.006, **68**, 202–212, 2006.
- Kaye, J. A., and J. B. Kumer, Nonlocal thermodynamic equilibrium effects in stratospheric NO and implications for infrared remote sensing, *Appl. Opt.*, **26**(22), 4747-4754, 1987.
- Kutepov, A. A., A. G. Feofilov, B. T. Marshall, L. L. Gordley, W. D. Pesnell, R. A. Goldberg, and J. M. Russell III, SABER temperature observations in the summer polar mesosphere and lower thermosphere: Importance of accounting for the CO₂ v₂ quanta V-V exchange, *Geophys. Res. Lett.*, **33**, L21809, doi:10.1029/2006GL026591, 2006.
- López-Puertas, M., G. Zaragoza, B. J. Kerridge and F.W. Taylor, Non-local thermodynamic equilibrium model for H₂O 6.3 and 2.7 μm bands in the middle atmosphere, *J. Geophys. Res.*, **100**, 9131–9147, 1995.
- López-Puertas, M., Zaragoza, G., López-Valverde, M.A. and Taylor, F.W. (1998a) “Non-LTE atmospheric limb radiances at 4.6μm as measured by UARS/ISAMS I. Analysis of the daytime radiances”, *J. Geophys. Res.* **103**, 8499.
- López-Puertas, M., Zaragoza, G., López-Valverde, M.A. and Taylor, F.W. (1998b) “Non-LTE atmospheric limb radiances at 4.6μm as measured by UARS/ISAMS. II. Analysis of the daytime radiances”, *J. Geophys. Res.* **103**, 8515.
- López-Puertas, M. and F. W. Taylor, *Non-LTE Radiative Transfer in the Atmosphere*, World Scientific Publishing Co., River Edge, N.J., 2001.
- López-Puertas, M., et al. Advanced MIPAS Level 2 Data Analysis (AMIL2DA), Project EVG1-CT-1999-00015, Report on the Climatology of Vibrational Temperatures, March 2002.
- López-Puertas, M., B. Funke, S. Gil-López, M.L. Koukouli, and M. Kaufmann, Presentation at QWG #4, Paris, July 2004.
- López-Puertas, M., M. García-Comas, B. Funke, R.H. Picard, J.R. Winick, P.P. Wintersteiner, M.G. Mlynczak, C.J. Mertens, J.M. Russell III and L.L. Gordley, Evidence for an OH*(v) excitation mechanism of CO₂ 4.3-μm nighttime emission from SABER/TIMED measurements, *J. Geophys. Res.*, **109**, D09307, doi:10.1029/2003JD004383, 2004b.
- López-Puertas, M., M.E. Koukouli, B. Funke, S. Gil-López, N. Glatthor, U. Grabowski, T. von Clarmann, G. P. Stiller, Evidence for CH₄ 7.6 μm non-local thermodynamic equilibrium emission in the mesosphere, *Geophys. Res. Lett.*, **32**, L04805, doi:10.1029/2004GL021641, 2005.
- López-Puertas, M., B. Funke, S. Gil-López, M.Á. López-Valverde, T. Clarmann, H. Fischer, H. Oelhaf, G. Stiller, M. Kaufmann, M.E. Koukouli and J.-M. Flaud, Atmospheric non-Local Thermodynamic Equilibrium Emissions as Observed by the Michelson Interferometer for Passive Atmospheric Sounding (MIPAS), *C. R. Physique*, **8**, 848–863, doi 10.1016/j.crhy.2005.07.012, 2005b.

- López-Puertas, M., B. Funke, D. Bermejo, M.L. Koukouli, Non-LTE Studies using Equivalent Latitudes for H₂O(v_1), N₂O(v_3), and CO₂ (10 μm), López-Puertas, M., B. Funke, S. Gil-López, M.L. Koukouli, and M. Kaufmann, Presentation at QWG #10, ESRIN, 13-14 June 2006a.
- López-Puertas, M., et al. NLTE in MIPAS CO₂ 10 μm using equivalent latitudes, 22 Nov 2006, unpublished, 2006b.
- López-Puertas, M., B. Funke, D. Bermejo-Pantaleón, T. von Clarman, G. P. Stiller, U. Grabowski, and M. Höpfner, Evidence for N₂O ν_3 4.5 μm non-local thermodynamic equilibrium emission in the atmosphere, *Geophys. Res. Lett.*, 34, L02825, doi:10.1029/2006GL028539, 2007.
- Madronich, S., and S. Flocke, The role of solar radiation in atmo-spheric chemistry, in *Handbook of Environmental Chemistry*, edited by P. Boule, pp. 1–26, Springer, New York, 1998.
- Marsh, D. R., S. C. Solomon, and A. E. Reynolds (2004), Empirical model of nitric oxide in the lower thermosphere, *J. Geophys. Res.*, 109, A07301, doi:10.1029/2003JA010199.
- Minschwaner, K., and D. E. Siskind (1993), A New Calculation of Nitric Oxide Photolysis in the Stratosphere, Mesosphere, and Lower Thermosphere, *J. Geophys. Res.*, 98(D11), 20,401–20,412.
- Orr and Smith, *J. Phys. Chem.*, 91, 6106-6119, 1987.
- Picone, J., A. Hedin, D. Drob, and A. Aikin, NRLMSISE-00 empirical model of the atmosphere: Statistical comparisons and scientific issues, *J. Geophys. Res.*, 107(A12), 1468, doi:10.1029/2002JA009430, 2002.
- Rothman, L. S., R. B. Wattson, Ronald Gamache, John W. Schroeder, and Andrew McCann, HITRAN HAWKS and HITEMP: high-temperature molecular database, *Proc. SPIE* 2471, 105, DOI:10.1117/12.211919, 1995.
- Sander, S.P. et al. (2006), Chemical kinetics and photochemical data for use in stratospheric modeling, Evaluation Number 15, <http://jpldataeval.jpl.nasa.gov>, JPL Publ., 06-2.
- Seeber, K. N., Radiative and collisional transitions between coupled vibrational modes of CO₂, *J. Chem. Phys.*, 55, 5077-5081, doi:10.1063/1.1675625, 1971.
- Shved, Kutepov and Obigalov (1998), *J. Atmos. Sol. Terr. Phys.*, 60, 289-314.
- Solomon, S., and R.R. Garcia, On the distribution of long-lived tracers and chlorine species in the middle atmosphere, *J. Geophys. Res.*, 89, 11633–11644, 1984.
- Srinivasan et al. *J. Chem. Phys.*, 129, 074309, 2008.
- Stiller, G. P., von Clarman, T., Funke, B., Glatthor, N., Hase, F., Höpfner, M., and Linden, A.: Sensitivity of trace gas abundances retrievals from infrared limb emission spectra to simplifying approximations in radiative transfer modelling, *J. Quant. Spectrosc. Rad.*, 72, 249-280, 2002.
- Tobiska, W.K, T. Woods, F. Eparvier, R. Viereck, L. Floyd, D. Bouwer, G. Rottman, and O.R. White, "The SOLAR2000 empirical solar irradiance model and forecast tool," *J. Atm. Solar Terr. Phys.*, 62, 1233-1250, 2000.
- Toselli, B., T. Walunas, and J. Barker, Time dependent thermal lensing measurement of V-T energy transfer from highly excited NO₂, *J. Chem. Phys.*, 92(8), 4793–4804, 1990.

Yankovsky, V. A. and R. O. Manuilova, Model of daytime emissions of electronically-vibrationally excited products of O_3 and O_2 photolysis: application to ozone retrieval, *Ann. Geophys.*, **24**, 2823–2839, 2006.

Zaragoza, G., M. López-Puertas, A. Lambert, J. J. Remedios and F. W. Taylor, Non-local thermodynamic equilibrium in H_2O $6.9\ \mu m$ emission as measured by the improved stratospheric and mesospheric sounder, *J. Geophys. Res.*, **103**, 31, 293-31, 308, 1998.

Zhou, D. K., M. G. Mlynczak, M. López-Puertas and G. Zaragoza, Evidence of non-LTE effects in the mesospheric water vapour from spectrally-resolved emissions observed by CIRRIS-1A, *Geophys. Res. Lett.*, **26**, 67-70, 1999.